ELECTROCHEMICAL REDUCTION OF CARBON DIOXIDE

TO HYDROCARBONS

BY

SK SAFDAR HOSSAIN

A Dissertation Presented to the

DEANSHIP OF GRADUATE STUDIES

KING FAHD UNIVERSITY OF PETROLEUM & MINERALS

DHAHRAN, SAUDI ARABIA

In Partial Fulfillment of the
Requirements for the Degree of

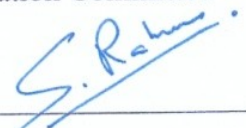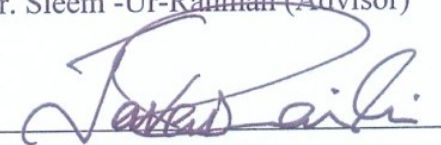# DOCTOR OF PHILOSOPHY

In

CHEMICAL ENGINEERING

DECEMBER 2011

KING FAHD UNIVERSITY OF PETROLEUM & MINERALS
DHAHRAN 31261, SAUDI ARABIA
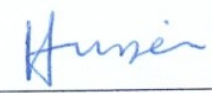
DEANSHIP OF GRADUATE STUDIES

This dissertation, written by **SK Safdar Hossain** under the direction of his dissertation advisor and approved by his dissertation committee, has been presented to and accepted by the Dean of Graduate Studies, in partial fulfillment of the requirements for the degree of **DOCTOR OF PHILISOPHY IN CHEMICAL ENGINEERING**.
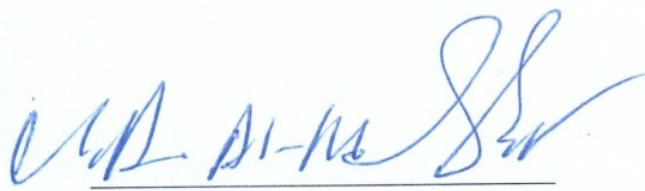
Dissertation Committee

_____
Dr. Sleem -Ur-Rahman (Advisor)

_____
Prof. S. M. Javaid Zaidi (Co-Advisor)

_____
Dr. Shakeel Ahmed (Member)

_____
Prof. Ibnelwaleed A. Hussein (Member)

_____
Prof. S. Basu (Member)

_____
Dr. Usamah Al-Mubaiyedh
(Department Chairman)

_____
Dr. Salam A. Zummo
(Dean of Graduate Studies)

Date_____ 29/5/12 _____

ii

Dedicated to
my beloved parents, family and teachers

ACKNOWLEDGEMENTS

"In the name of Allah, The Most Gracious and The Most Merciful"

TABLE OF CONTENTS

LIST OF TABLES

LIST OF FIGURES

THESIS ABSTRACT (ENGLISH)

NAME : SK SAFDAR HOSSAIN

TITLE : ELECTROCHEMICAL REDUCTION OF CARBON DIOXIDE TO
    HYDROCARBONS

MAJOR : CHEMICAL ENGINEERING

DATE : DECEMBER, 2011

Electrochemical reduction of carbon dioxide (ERC) is an elegant method to abate global warming by chemically fixing a major green house gas (GHG), carbon dioxide (CO_2). Major synthesis products include economically attractive chemicals like methanol, formic acid methane and ethylene etc. Various aspects of ERC, like thermodynamics, kinetics and mechanism (s), have been extensively studied in past two decades in both aqoues and non-aqueous medium. The process requires an efficient catalyst and energy because very CO_2 being a very stable molecule and its slow electroreduction kinetics. Moreover, reduction products strongly depend on electro-catalyst and electrical potentials used. In both aqueous and non aqueous environments, even at higher over potentials, the yield and selectivity towards desired products is still relatively low. The major bottle neck is believed to be the low solubility of carbon dioxide in electrolyte and slow kinetics leading to low current density and high overpotential at which this reaction proceeds. Moreover, typically, ERC proceeds concomitantly with hydrogen evolution which, in turn, further limits the overall efficiency of the process.

Focus of this work was on the development of nano electrocatalysts and a gas phase reactor system for ERC. In this work, in the first part copper, ruthenium, palladium and

iron supported on carbon nanotubes (CNTs) were synthesized by incipient impregnation and deposition-precipitation method. The synthesized catalysts were characterized for their morphology and structure by XRD, SEM, TEM, BET and XPS. The results shows that the above mentioned metals in the nano scale were successfully mounted on the support. These catalysts were tested in a half cell to quick evaluation of their electrocatalytic activity and then membrane electrode assembly (MEA) was made using the optimum catalyst to further test their activity in a continuous solid polymer electrolyte (SPE) reactor.

The second part involved the synthesis of titanium oxide nanotubes (TNTs) and its utilization as catalyst support. Copper, ruthenium, palladium and iron supported on TNT catalysts were prepared. These catalysts were characterized for their morphology and structure. Electro-catalytic activities are evaluated in a half cell as well as in H-type Pyrex cell by linear sweep voltammetry (LSV) and chronoamperometry methods (CA). The products were analyzed by gas chromatography equipped with flame ionization detector (FID) and thermal conductivity detector (TCD). Then the optimum catalyst was used to prepare MEA using nafion as proton conducting membrane to test the optimum catalyst in a continuous SPE reactor under varied process parameters. Methanol, methane, and ethylene were detected as major products.

DOCTOR OF PHILOSOPHY

KING FAHD UNIVERSITY OF PETROLEUM & MINERALS

DHAHRAN, SAUDI ARABIA

THESIS ABSTRACT (ARABIC)

الاسم: سافدار حسين

عنوان الرسالة : الكهروكيميائية على تخفيض نسبة ثاني أكسيد الكربون إلى المحروقات

الرئيسية: الهندسة الكيميائية

التاريخ: ديسمبر 2011

هو أسلوب رائع لتخفيف ظاهرة الاحتباس الحراري عن طريق تحديد كيميائيا رئيسي للغاز البيت الأخضر (غازات). المنتجات الرئيسية وتشمل تركيب المواد الكيميائية مثل جذابة اقتصاديا، CO_2الدفيئة)، وثاني أكسيد الكربون (، مثل حركية، الديناميكا الحرارية وآلية ERCوالميثانول الميثان حمض الفورميك والاثيلين إلخ جوانب مختلفة من والمتوسطة غير مائي. هذه aqoues(آليات)، وتمت دراسة على نطاق واسع في العقدين الماضيين في كل من electroreduction جدا كونه جزيء مستقرة جدا وحركية لها CO_2 العملية تتطلب حافزا كفاءة وطاقة لأن بطيئة. وعلاوة على ذلك، ومنتجات تعتمد بشدة على تخفيض الحافز الكهربائي وإمكانات الكهربائية المستخدمة. في البيئات المائية على حد سواء وغير مائي، حتى في أعلى أكثر من امكانات، والغلة والانتقائية نحو المنتجات المطلوبة لا تزال منخفضة نسبيا. ويعتقد ان عنق الزجاجة الرئيسي ليكون ذوبان منخفضة من غاز ثاني أكسيد ارتفاع في overpotentialالكربون في حركية المنحل بالكهرباء وبطيئة مما أدى إلى كثافة التيار المنخفض و العائدات بالتزامن مع تطور الهيدروجين والتي، ERCالعائدات التي تي رد الفعل هذا. وعلاوة على ذلك، وعادة، بدورها، ويحد من زيادة الكفاءة الكلية للعملية.

نانو ومفاعل مرحلة نظام الغاز لهيئة الإنصاف electrocatalystsوكان التركيز في هذا العمل على تطوير والمصالحة. في هذا العمل، في الجزء الأول من النحاس، الروثينيوم والبلاديوم والحديد المعتمدة على أنابيب الكربون النانوية (تشارك المركز الوطني) تم توليفها من قبل التشريب الأولية وطريقة ترسب-هطول الأمطار. النتائج تظهر أن XPS، الرهان و TEM، SEM، XRDتميزت المحفزات توليفها لمورفولوجيا وبنيتها بواسطة شنت بنجاح المعادن المذكورة في الجدول نانو على الدعم. وقد تم اختبار هذه المواد الحفازة في زنزانة نصف تقييم

) باستخدام العامل المساعد الأمثل MEA ومن ثم تم تجميع غشاء القطب (electrocatalyticسريع لنشاطهم

) المفاعل.SPEلاختبار المزيد من نشاطهم في المنحل بالكهرباء البوليمر الصلبة المستمر (

) واستخدامها في تقديم الدعم الحفاز. TNTsالجزء الثاني ينطوي على تركيب الأنابيب النانوية أكسيد التيتانيوم (

وأعدت والنحاس، والروثينيوم والبلاديوم والحديد معتمدة على المواد الحفازة تي ان تي. وتميزت هذه المحفزات

نوع من Hالمورفولوجيا وبنيتها. ويتم تقييم الأنشطة الكهربائية الحفاز في خلية 2/1 وكذلك في الخلية بيركس

voltammetry) الاجتياح الخطي LSV وطرق chronoamperometry) (CA وقد تم تحليل هذه .(

TCD) والحرارية للكشف عن الموصلية (FIDالمنتجات من قبل اللوني للغاز مجهزة مكشاف تأين الاشتعال (. ثم

كما بروتون إجراء غشاء لاختبار nafionتم استخدام المحفز الأمثل لإعداد الشرق الأوسط وأفريقيا باستخدام

المستمر تحت معلمات عملية متنوعة. تم الكشف عن والميثانول، والميثان، والاثيلين SPEمحفز الأمثل في مفاعل

والمنتجات الرئيسية.

دكتوراه في الفلسفة

جامعة الملك فهد للبترول والمعادن

الظهران بالمملكة العربية السعودية

CHAPTER 1

INTRODUCTION

1.1   Carbon Dioxide and Environment

Carbon dioxide (CO_2) is an essential component of earth's ecosystem. It is important to animals and plants alike. It is produced by various anthropogenic activities and used mainly by plants in photosynthesis [1]. Until recently, the CO_2 concentration was steady in the ecosystem at around 300 ppm as the CO_2 emission and its utilization was in balance. However, concentration of CO_2 has increased alarmingly in last few decades. In fact, it has risen from 280 parts per million (ppm) before the industrial revolution to 382 ppm in 2010, an increase of more than 40%. This is mainly due to excessive amount of CO_2 being released to the atmosphere [2, 1]. Figure 1-1 shows how the concentration of CO_2 has increased in the atmosphere over the years[2].

One direct consequence of increased CO_2 concentration is the phenomenon of global warming. Evidence that human activities are causing the planet to warm up is now equivocal according to the Intergovernmental Panel on Climate Change (IPCC)[3]. Greenhouse gases (GHG) are responsible for the global warming which trap solar radiation on its surface. Water vapor (H_2O), carbon monoxide, methane, nitrous oxide and ozone are well known green house gases. But, carbon dioxide has been considered as the main gas responsible for the greenhouse effect and accounts for about 55% of the anthropogenic greenhouse effect [3, 4]. Adverse impacts of global warming include

rising sea levels, disappearance of some of the islands, occurrence of extreme weather, and climate change[5, 6].

Carbon Dioxide Concentration
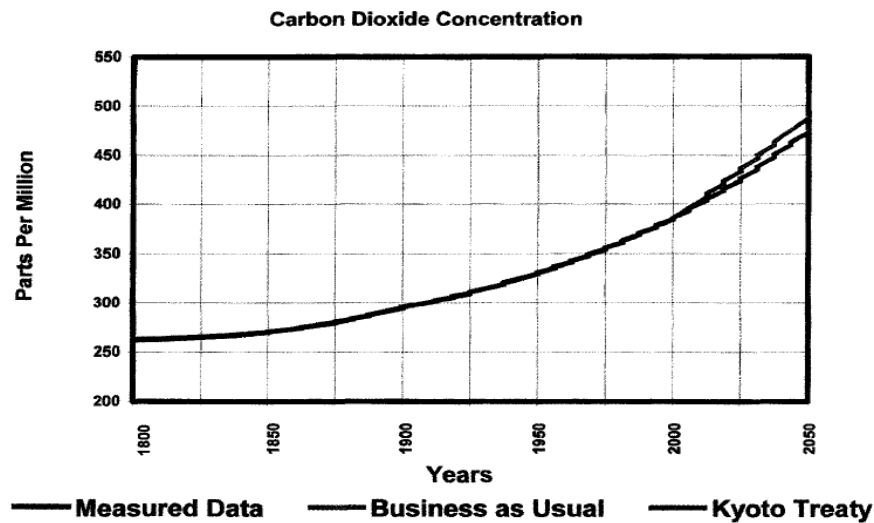
Figure 1-1: Average global carbon dioxide concentration in atmosphere over past thousand years

The sources of CO_2 emissions can be categorized into three divisions. They are stationary, mobile and natural sources. Stationary sources include power plants and house hold applications whereas mobile sources are mainly related to the transport. The main natural source of CO_2 is related to the decomposition of carbonate minerals. Energy generation (either as process heat or as electricity) by the direct combustion of fossil fuels remains the most sought energy generation method. Fossil fuels (coal, oil, and natural gas) are consumed in the residential, commercial, industrial, and transportation sectors with the last two of which are the largest contributors to the CO_2 emissions. Global energy demand is all set to surge to new level as the global population is increasing at a high rate coupled with desire for better living standard. This increased demand of energy will be met by burning more and more fossil fuels as contribution from renewable sources of energy (solar, wind and hydrothermal) still remains disappointingly low[2]. Figure 1-2 shows the world total energy sources in 2010. In 2010 energy supply by power

source was oil 33.5%, coal 26.8%, gas 20.8% (fossil 81%), renewable (hydro, solar, wind, geothermal power and bio fuels) 12.9%, nuclear 5.8% and other 4%. Oil was the most popular energy fuel [7, 2]. Oil and coal combined represented over 60% of the world energy supply in 2010. It is certain that fossil fuels, coal and oil, will remain popular as predicted in many scenarios by International Energy Agency (lEA). From the International Energy Outlook 2010, with society's current level of energy consumption and high standards of living, world total energy consumption will increase by 49 % from 495 quadrillion Btu (2007) to 739 quadrillion Btu (2035) [8]. Almost all models predict that greenhouse emission will increase. In 2010, total emission of carbon dioxide was 30,398 million tonnes whereas in 2002, it was 22690 million tonnes. There was a decline in the emissions in 2009 because of economic recession [2]. This economic recession produced a small decline of about ten million metric tons per year in net emissions [8]. Total emissions in 2012 are predicted to be 44% above the Kyoto target whereas in 2020 this will be 62% above the target [2, 9]. Thus, global warming could become more and more severe in future unless something substantial is done now to limit the CO_2 concentration[5].
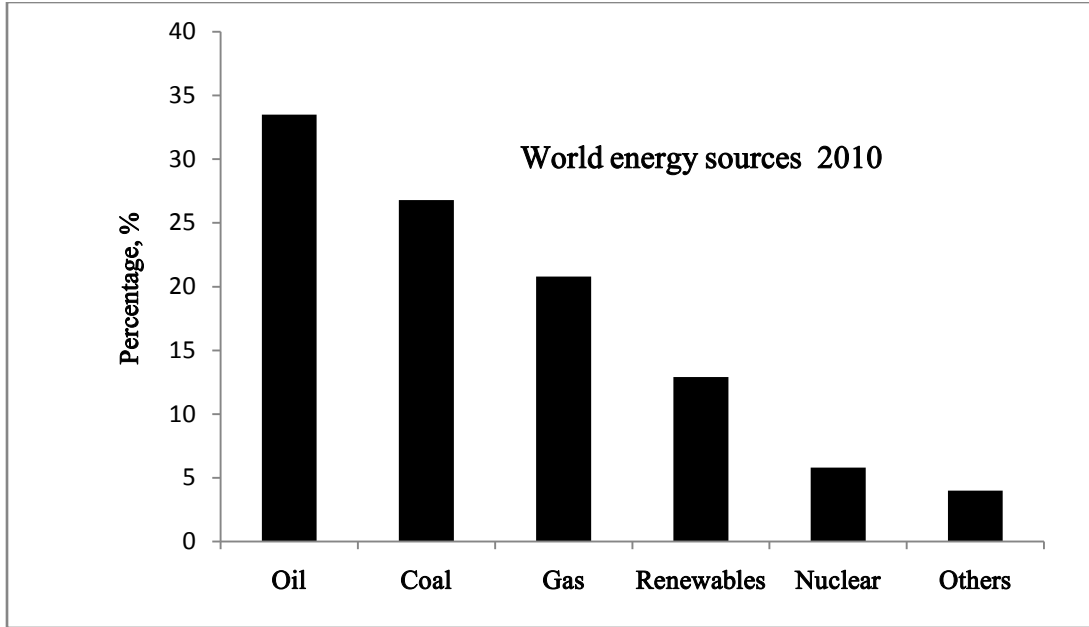
Figure 1-2: World energy distribution by source

Breakdown of the CO_2 production rate for various fuels is shown in Table 1.1 [2]. It is evident from the table that coal produces highest amount followed by oil and gas.

Table 1-1:Carbon dioxide emission from fossil fuel[2]

Fuels	Grams per kilowatt hour
Natural Gas	190
Gasoline	250
Oil	260
Coal	430

Table 1-2 shows a typical composition of flue gas from combustion of fossil fuel with CO_2 contributing 10%[1].

Table 1-2:Composition of typical flue gas from combustion of fossil fuel[1]

Composition, volume %				
CO_2	H_2O	N_2	O_2	NO_2
10	20	69	1	0.001

Recently, more and more stringent federal laws are coming into existence on CO_2 tolerance and industrial complexes as well as automobile manufacturers are under enormous pressure to curb their CO_2 emission and to use eco-friendly fuels and processes. Kyoto protocol and its subsequent amendments is one such attempt [10, 11]. To meet stringent climate change targets, such as stabilizing CO_2 concentrations below 350 ppm, or limiting the global temperature rise to $2^{\circ}C$ above pre-industrial levels requires drastic CO_2 reductions of 60–80% in 2050 compared to 1990 emissions, which is a daunting challenge [4]. This will require a portfolio of technologies and mitigation activities across all sectors such as improving energy efficiency, carbon capture and storage (CCS) and the use of renewable energies or nuclear power. Deep cuts in emission will also be required in the transport sector. Implementing CO_2 emissions reduction measures in the transport sector is often accompanied by the co-benefits of reducing traffic congestion and/or improving air quality [4, 6, 1].

The CO_2 emission reduction strategies can be divided into five broad categories

    a) Control of energy consumption

    b) Use of renewable energies

    c) Enhancement of natural sequestration

    d) Use of nuclear energy

    e) Management of fossil fuel energies including:

-Change in the fossil energy mix

-CO_2 capture and sequestration

-Conversion of CO_2 to useful products

1.2 CO_2 Conversion and Utilization

Recently global emphasis has been laid on the use of renewable energy (Solar, hydrothermal, tidal, etc) as an alternate source of energy because fossil fuels are limited and generate CO_2. However, even after continued effort to adopt renewable energy, their contribution in meeting global energy demand remains insignificant compared with the fossil fuels[2, 12, 11]. As a consequence, CO_2 will continue to be accumulated in atmosphere leading to more severe global warming. However, CO_2 is turning image recently and there are increasing attempts to consider it a resource and business opportunity rather than a waste with a cost of disposal. Carbon sequestration and storage (CSS) has been planned extensively in the last five years[13]. However, accidents such as 'Lake Nayos' where 1700 people died as carbon dioxide leaked from a naturally occurring sequestration site, has raised question regarding is environmental impact [4]. Therefore, it becomes imperative not only to sequester carbon dioxide but to utilize it by converting it to useful products. Increasing amount of low cost and nearly pure carbon dioxide is available now from plants for CSS. Carbon dioxide can, potentially, be used in varieties of applications. It can be used as feedstock for manufacturing chemicals. Apart from chemical utilization, CO_2 can be directly used in applications such as carbonated beverages, fire fighting, secondary oil recovery and supercritical extraction [9, 14].

Chemical utilization of CO_2 to manufacture fuels and other chemicals is regarded as one of the most attractive ways of CO_2 mitigation [4, 15, 1]. Carbon dioxide will be the

6

feedstock of nearly zero (or even negative) cost for conversion to fuels and chemicals. CO_2 has always attracted the greatest interest, as nature uses this compound successfully to as a synthetic building block in photosynthesis-the basis of life on earth. Moreover, the carbon reserves on our planet in the form of CO_2 and carbonates and are for all practical purposes inexhaustible, exceeding the carbon content of the deposits of fossil materials many times over [14]. In addition, the chemical conversion of CO_2 is of great interest because it can mitigate CO_2 emission and at the same time utilize the cheap and abundant CO_2 as a carbon source for the manufacture of the fuels or other useful chemicals, thus adding value to the CO_2 disposal [9]. From the safety aspects also, CO_2 is an ideal raw material. Carbon dioxide can be used as a reactant or co-feed in various non-catalytic chemical processes and heterogeneous or homogeneous catalytic processes. Thus, transformation of CO_2 into organic compounds is a promising long-term objective as it could allow the preparation of fuels and chemicals from cheap and abundant carbon source[9]. The main products of CO_2 conversion must be fuels to reduce CO_2 emission significantly and to create great economic value, although some of them (methanol, ethanol, etc.) could be considered in the double role of fuel and chemical[16].

Other factors stimulating the interest in CO_2 chemical conversion is the presence of many emissions for which CSS option is not suitable: distance from safe sequestration site, dilute concentration of CO_2 in emitting gas, and small- medium size sources[4]. Therefore, a chemical recycling of CO_2 may significantly contribute to reduction of its emissions only when the products of ERC are components for the fuel pool. Consumptions of the fuels are much higher than the use of the chemicals as such.

The synthesis of urea from ammonia and carbon dioxide, and the production of salicylic

acid from phenol and carbon dioxide are good examples of the large-scale production processes where CO_2 is utilized as a raw material. These are some of the possible ways to expand the utilization of carbon dioxide in chemical industry[14].

Chemical utilization of CO_2 has been a major research focus for scientists since 1970's. Bandi et. al. argued that producing carbon-based liquid energy carriers from CO_2 is more attractive than that producing liquid hydrogen, due to the easier and less expensive handing of the carbon-based fuels and their higher energy density relative to hydrogen [17]. Frese et. al. proposed the electrochemical synthesis of fuels from captured CO_2 using renewable energy (wind, solar ,etc.) and the storage of the fuels within the existing infrastructure for transportation applications[18]. Therefore, CO_2 conversion can be positioned as step for CO_2 recycling and resource conservation.

Carbon dioxide is very stable, as illustrated by its standard free energy of formation (ΔGo = -394.359 kJ/mol)[9]. Carbon dioxide is the most oxidized form of carbon, and therefore the only chemical transformation at "normal" energies is to reduce it. It has low reactivity because of its linear structure, but there are many pathways for its activation, in particular using homogeneous or heterogeneous catalysts. But it is necessary to overcome a thermodynamic barrier associated with its activation. For this reason, external energy required and providing the energy for the reaction is the critical aspect in evaluating the alternative routes for CO_2 conversion[19].

In general, there are four main approaches to chemically utilize CO_2 are:

1. To use high-energy starting materials such as hydrogen, unsaturated compounds, small-membered ring compounds, and organometallic.

2. To choose oxidized low-energy synthetic targets such as organic carbonates.

3. To shift the equilibrium to the product side by removing a particular compound.

4. To supply physical energy such as light or electricity.

Various methods have been proposed to convert CO_2 to useful chemicals. In the past century, researchers have focused on investigating different pathways to convert carbon dioxide to valuable products such as hydrocarbons and alcohols. Most of the processes are still subject of research in the laboratory, and very few have reached large-scale production [1, 4, 20]. An array of chemicals can be manufactured from CO_2 using these methods. It can be used as the whole molecule in reactions, and it can be used as a carbon source or as an oxygen source [21]. Figure 1-3 shows various pathways for production of industrially important chemicals starting from CO_2.
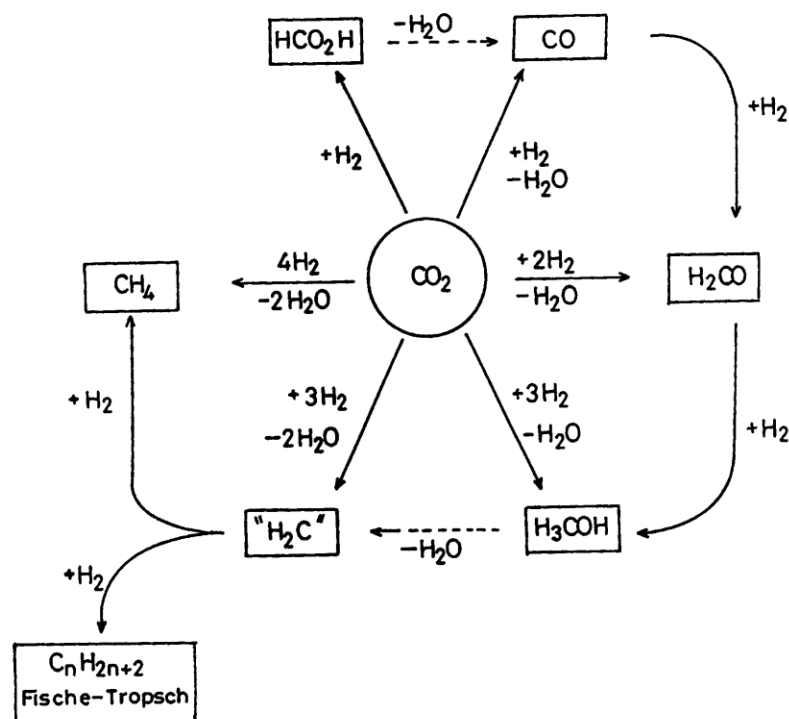
Figure 1-3: Various Reduction Pathways for CO_2 for Industrially Important Products

Hydrogenation of carbon dioxide has been intensively studied and has shown promising results in pilot plants; however, high temperature and high pressure conditions, in addition to high consumption of hydrogen, make this process less efficient [22]. Other attractive method is the carbon dioxide reforming[23]. High temperature, high pressure coupled with expensive catalysts limits it application in industrial scale. The conversion of carbon dioxide at room temperature and atmospheric pressure using solar light or electrical energy are more attractive routes. Photocatalysis uses semiconductor to promote reactions in the presence of light radiation. Photocatalytic method is quite popular and has been a major research area [24-31]. Formic acid, methane, methanol, and ethanol are common products of the photo electrochemical reduction of carbon dioxide at metal/oxide electrodes; however, the quantum efficiency and production rate are very

10

low. A recent innovation in conversion of carbon dioxide has been developed via aqueous electrocatalytic reduction [32].

Other important promising methods are briefly discussed below.

2.1   Radiochemical Method

$$CO_2+H_2O \quad \begin{array}{c} \nearrow HCOOH \\ \\ \searrow HCHO \end{array} \quad \quad (1)$$
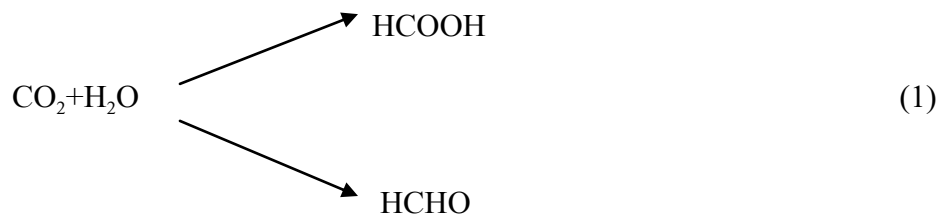
Radiochemical conversion used radiation to excite the CO_2 for the reaction. The use of non-fossil fuel energy, i.e., nuclear energy might be attractive point of this method .This is a relatively new research area. First report was in 1960, with less than 10 papers published by 2011[1].

2.2   Thermo chemical Method

Thermo chemical conversion covers a vast range of reactions of CO_2 to organic or inorganic products [9, 1]. It requires high temperature for CO_2 bond breaking. Only few examples are provided here, among which the productions of carbon monoxide, methanol and urea have been industrialized [1, 9].

.

$$2Mg + CO_2 \rightarrow 2MgO + C \tag{2}$$

$$CO_2 + C \rightarrow 2CO \tag{3}$$

$$CO_2(g) + xH_2(g) \rightarrow CH_3OH, CH_4, C_2H_5 \tag{4}$$

$$CO_2 + CH_4 \rightarrow 2CO + 2H_2 \tag{5}$$

$$CO_2(g) + 2NH_3 \rightarrow H_2NCONH_2 + H_2O \tag{6}$$

The chemistry of thermo-chemical reduction of CO_2 is briefly introduced here to show the comparison between thermo-chemical reduction and electro-chemical reduction of CO_2. There are two main thermo-chemical processes that use CO_2 to produce new chemicals and fuels as a potential means of mitigating CO_2 emissions [9, 1].

2.3   Hydrogenation

$$CO_2 + 3H_2 \rightarrow CH_3OH(l) + H_2O(l) \qquad \Delta G^0_{298} = -9.2 \times 10^3 \text{ kJ kmol}^{-1} \tag{7}$$

$$\Delta H^0_{298} = -131.2 \times 10^3 \text{ kJ kmol}^{-1}$$

$$CO_2(g) + 4H_2 \rightarrow CH_4 + 2H_2O(l) \qquad \Delta G^0_{298} = -130.8 \times 10^3 \text{ kJ kmol}^{-1} \tag{8}$$
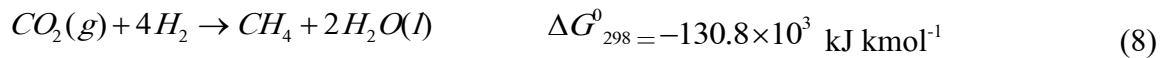
$$\Delta H^0_{298} = -252.9 \times 10^3 \text{ kJ kmol}^{-1}$$

The exothermic hydrogenation of CO_2 to produce methanol or methane, as shown in reaction 7 or 8 is thermodynamically feasible at standard conditions and 298 K but requires a high pressure (1-5 MPa) and temperature (500-800 K) to maintain useful conversion and reaction rate. The major problem with the hydrogenation of CO_2 is not the process itself but rather the availability of H_2. If the purpose of this process is to limit the emissions of CO_2 to the atmosphere then the hydrogen must be produced without

emissions of CO_2, by using renewable energy sources like nuclear, hydro or solar.

2.4   Methane Reforming

Methane reforming with CO_2 to produce synthesis gas is represented by reaction 10 and some of the parallel or consecutive reactions are shown by reactions 11 and 12:

$$CO_2 + CH_4 \rightarrow 2CO + 2H_2 \qquad \Delta G^0{}_{298} = 288.0 \times 10^3 \text{ kJ kmol-1} \qquad (9)$$

$$\Delta H^0{}_{298} = 261.0 \times 10^3 \text{ kJ kmol-1}$$

$$CO_2 + C \rightarrow 2CO \qquad \Delta G^0{}_{298} = -120.0 \times 10^3 \text{ kJ kmol-1} \qquad (10)$$

$$\Delta H^0{}_{298} = -172.4 \times 10^3 \text{ kJ kmol-1}$$

$$CH_4 \rightarrow C + 2H_2 \qquad \Delta G^0{}_{298} = +50.0 \times 10^3 \text{ kJ kmol-1} \qquad (11)$$
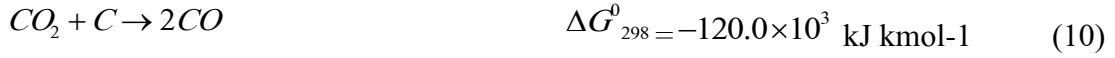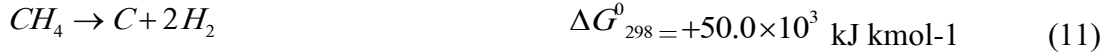
$$\Delta H^0{}_{298} = +74.9 \times 10^3 \text{ kJ kmol-1}$$

The high standard free energy change of reaction (9) dictates a high operating temperature to obtain a favored equilibrium and useful conversion for the reforming process, i.e. 900 - 1200 K. Also, the thermodynamically highly favored formation of coke (reactions (10) and (16)) deactivates the catalyst [23, 19]. Therefore, the challenges for this process are to achieve it under an input energy as low as possible to avoid secondary generation of CO_2, and to develop catalysts that are not prone to coking (noble metals) and more stable over time.

2.5   Photochemical Method

$$CO_2 + H_2O \rightarrow CO, HCHO, HCOOH \tag{12}$$

Photochemical conversion has been used to successfully convert CO_2 to methanol and methane [33]. In these method photo catalysts like Titania and tungsten oxides are used along with light or laser to energize the CO_2 molecule and subsequently convert it to products. Izumi has published an excellent review article on this subject [34]. Performance of any photocatalytic conversion of CO_2 depends on the reaction conditions, such as the incident/absorbing light intensity from the sun or a simulated solar light source, and the photocatalyst used. Although promising, but till date high conversion is yet to be achieved [33, 34].

2.6   Electrochemical Method

$$CO_2 + xe^{-1} + xH^+ \xrightarrow{\quad eV \quad} CO, HCOOH, CH_4, (HCOOH)_2 \tag{13}$$
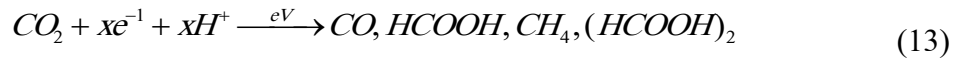
The electrochemical conversion of CO_2 has attracted a lot of research effort, which is introduced below in section 1.4 and elaborated in the coming sections as this is topic of the present work.

2.7   Biochemical Method

$$CO_2 + 4H_2 \xrightarrow{\quad bacteria \quad} CH_4 + 2H_2O \tag{14}$$
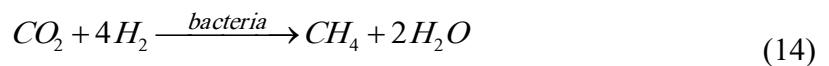
This biomethanation process has been carried out in a laboratory fixed-bed reactor (ca. 50 cm^3) to generate CH_4 at 80 % of the theoretical conversion with a space-time yield of ca. 5 m3 STP m^{-3} h^{-1} [13, 9]

2.8   Photoelectrochemical Method

$$CO_2 + 2e^- + 2H^+ \xrightarrow{\quad hv + eV, Semicondutcor \quad} CO + H_2O \qquad (15)$$
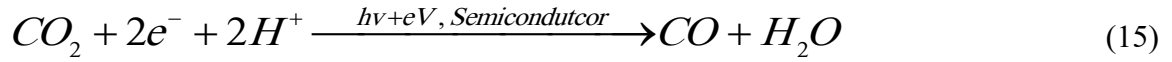
Photo-electro-chemical conversion is the electrochemical conversion that uses light (such as sunlight) as the energy input and a semi-conductor (e.g. SiC, GaP, ZnTe) as the cathode [35].With the photoelectrochemical approach, the solar harvesting process is incorporated into the electrochemical systemic this can be done without sacrificing the performance of the electrochemical and light-harvesting systems, there could be benefits in terms of cost and space saving[31].

1.3   Challenges for CO_2 Utilization

The costs involved for CO_2 capture from a manufacturing process, its separation and purification from the gaseous mixture, and energy requirements for CO_2 conversion are some of the main challenges being faced for the CO_2 utilization [1, 4]. Moreover, the amount of CO_2 has increased and will continue to increase. Thus, the need for the introduction of the new technologies and the change of infrastructure are desired. The rate at which these new technologies would be developed is also an equally important issue compared to the development of these technologies. The important issue would be how to introduce new technology in a small scale and then get them to grow into widespread commercial use. No single new technology will solve the entire problem. There should be an emergence of a number of promising new technologies that could contribute to the carbon dioxide emission reductions. All of them will have to overcome

challenges of economics, performance, and associated environmental impacts. Performance, cost, safety, regulatory compliance, and low environmental impacts are some of the barriers identified to be able to make a new technology into widespread commercial use. For example, consider the case of separation and sequestration of carbon dioxide from large combustion facilities. Among the critical design considerations is whether to combust in air or in oxygen. In either case, procedures must be designed to remove oxygen from air or to remove carbon dioxide from flue gas [12]. Additional procedures are needed to compress the carbon dioxide to high pressure in order to move it elsewhere and dispose it for long periods of time. Introduction of new technology solutions require extensive research and development to identify the current barriers, as well as finding solutions that improve performance, cost, safety, environmental acceptability, and consumer acceptability.

1.4　Electrochemical Reduction of Carbon dioxide

Electrochemical reduction of carbon dioxide (ERC) provides means to convert greenhouse carbon dioxide gas to produce diverse attractive chemicals and fuels like methanol, formic acid, and other hydrocarbons by using electricity as source of energy[36]. Products of the ERC include formic acid, methanol, methane, ethylene and carbon monoxide with product distribution strongly dependant on the electrocatalyst and the potential. This process is attractive because it can be carried out at room temperature and low pressure. However, to compete with alternative processes successfully, carbon dioxide reduction must take place at low potential with high efficiency and selectivity at high current densities. The process requires electrocatalyst or cathode material to carry out the reaction at low overpotential and with high current density.

16

Most of the reduction reaction of CO_2 occurs in the potential range in which hydrogen evolution reaction (HER) due to hydrolysis of water occurs [37]. So, there is always competition between CO_2 and HER, especially in the aqueous media, which results in low current efficiency in ERC. There are several ways of suppressing HER, including choosing the electrocatalyst with high overpotential for hydrogen evolution and affinity for CO_2 and operating at high CO_2 pressure and to use solid polymer electrolyte membrane reactor to increase the availability of CO_2 at the electrocatalyst. Traditionally most of the CO_2 reduction research has been carried out in aqueous media. Solubility of carbon dioxide in is very small (0.03 M) in aqueous and non aqueous electrolytes. Due to this mass transfer resistance the resultant current remains very low even at the most active electrocatalyst. These issues can be addressed by using highly efficient electrocatalyst and efficient electrochemical reactor design.

Electrochemical reduction of carbon dioxide has been carried out on a variety of electrode surfaces, including most of the metals in the periodic table, a number of alloys, metal oxides and chemically modified electrodes[38, 20, 39-41, 16, 42-49, 9]. Among all the electrode materials, copper, both metallic and in oxides form, is the most promising electrode material as it offers medium hydrogen overvoltage and production of more reduced form of carbon dioxide (methanol, ethane, methane, and ethylene). Copper metal, copper oxide and cuprous oxide and modified copper oxides have been studied extensively. The electrodes, in the form of high purity (e.g. 99.9 wt%) foil, plate, rotating disc, a bundle of wires, a bed of particles, tubes, mesh or GDE, are most intensively studied [32, 9].

1.5 Motivation for Current Work

Supporting the active metals (Cu, Fe, Pd, & Ru) on high surface area supports like carbon nanotubes (CNTs) and titania nanotubes (TNTs) is expected to increase the current density and lower the overpotential required. This is due to the fact that the reaction is a multistep reaction involving adsorption of carbon dioxide as an intermediate step. Therefore, increasing the surface area is expected to have positive impact on the process. Various binary combinations of metal are anticipated to impart synergic effect and may lead to increased activity of the catalyst. These supported metal electrocatalysts can be conveniently used in solid polymer electrolyte membrane (SPE) reactor which operates in gas phase. With the absence of any mass transfer limitation in SPE reactor in comparison with aqueous electrolyte can enhance the current density.

1.6 Organization of the Thesis

The goal of this study is to synthesize CNTs and TNTs supported Cu, Fe, Ru, and Pd in single as well as in binary combination and to evaluate these catalysts in a continuous solid polymer electrolyte membrane reactor.

Chapter 1 introduces several processes for carbon dioxide utilization such as hydrogenation, photo electrochemical reduction and electrochemical reduction. Catalytic hydrogenation reaction for methanol synthesis requires high temperature and pressure conditions, whereas photoelectrochemical and electrochemical reduction processes offer convenient ways to reduce carbon dioxide to hydrocarbons and oxygenates at mild

conditions. While carbon dioxide electrochemical reduction has been proven to primarily yield methane and ethylene at metallic copper.

Chapter 2 focuses on the thermodynamics, kinetics of the electrochemical reduction of carbon dioxide. A detailed account of the electrocatalysts used till the time of this thesis write up is provided along with major electrochemical reactor schemes used. Major issues related to large scale implementation of the process is discussed in details. A brief description of TNTs and CNTs are provided to familiarize the reader as they were used as catalyst support. Various methodologies of membrane electrode assembly (MEAs) are compared and the most optimum methodology is indicated in the section 2.8.

Chapter 3 describes all the experimental details of the studies conducted in this work. Firstly, the methodology of purification and functionalization of CNTs are given. Afterwards, various methods of catalysts synthesis for low metal loading as well as high metal loadings have been discussed in detail. The synthesis procedure of TNTs from anatase powder is provided along with methodologies to prepare TNT supported high metal loading catalysts. A brief description of the characterization techniques that has been used in this work is provided. Experimental details of the electrocatalytic activity testing set up for liquid electrolyte phase and the SPEs in gas phase are provided in detail in section 3.7. MEA fabrication technique is explained in details in section 3.8.

Chapter 4 describes the relationship between surface chemistry and catalyst performance via characterization. All the physical characterization results are provided to evaluate the

morphology and other physical properties of the catalysts synthesisized. These results showed that nano scale electrocatalyst were prepared. The electroactivity of the catalysts are discussed in detail, and the relationship between both the physical as well chemical properties of electrocatalysts has been correlated with their electro catalyticactivity. The novel supports like CNTs and TNTs imparted positive effect on the catalyst properties. It is essential to construct a better catalyst design which allows a stable reaction with high catalytic activity and selectivity, as well as reproducible results.

Chapter 5 provides major conclusions and future recommendations.

CHAPTER 2

LITERATURE REVIEW

2.1   Electrochemical Reduction of Carbon dioxide (ERC)

The electro-reduction of CO_2 is of great interest in the fields of theoretical and applied electrochemistry, as reflected in the number of papers on ERC published since 1982, i.e. 441. The incentive for this application is that it needs carbon dioxide and water to produce very high value products like methanol, ethanol, methane, ethylene, with product distribution completely tunable by selecting the electrocatalysts and operating potential. However, the key argument against ERC is that, if electricity came from the combustion of fossil fuels, the electric energy used in such a process would increase CO_2 emissions. Therefore, ERC will have a future only when it can be carried out with high efficiency on an industrial scale and renewable energy is adopted as the source of electricity. The electroreduction of carbon dioxide has been studied since the late 19th century. Majority of the previous work has focused on the electro-catalysis and mechanistic aspects of CO_2 reduction, with experiments carried out in the batch mode in small (e.g. 1 x 10^{-4} m^2) electro-chemical cells (or half-cells) under conditions that are unlikely to sustain a practical process[50]. There are several issues in the research of ERC that should be dealt with in the development of a process that will be interesting at the industrial scale (with reproducibility, long-term stability, high efficiency, low cost and so on)[32]. Different aspects of the electrochemical reduction of carbon dioxide will be discussed in details…..

2.2   ERC: Stoichiometry, Thermodynamics, Mechanism and Kinetics

2.2.1   Thermodynamics of ERC

The thermodynamic requirements for various CO_2 reduction reactions should be considered because it plays a major role in the conversion and selectivity for the process. The equilibrium redox potentials of the various couples involving CO_2 and its reduction potentials are given in Table 2-1. Equilibrium potentials of CO_2 reduction are not very negative as compared with that of HER in the aqoues electrolyte solutions[51]. For example, electrochemical reduction of CO_2 to $HCOO^-$ in aqueous solution is given below together with standard electrode potential at pH 7.0 at $25°C$ with respect to standard hydrogen electrode (NHE)[52].

$$CO_2 + H_2O + 2e^- = HCOO^- + OH^- \quad \text{(-0.61V vs. NHE at \textbf{pH} 7.0)} \quad (2.1)$$

:
Table 2-1: CO_2 reduction reactions [52]

Reaction	E^0/V (NHE) 298K at pH=7
$2H^+ + 2e^- = H_2$	-0.414
$CO_2 + H^+ + 2e^- = HCOOH$	-0.61
$CO_2 + 2H^+ + 2e^- = CO + H_2O$	-0.52
$CO_2 + 4H^+ + 4e^- = HCHO$	-0.48
$CO_2 + 6H^+ + 6e^- = CH_3OH + H_2O$	-0.38
$CO_2 + 8H^+ + 8e^- = CH_4 + H_2O$	-0.24

The CO_2 reduction in aqueous media involves H_2O and OH^-, and the equilibrium potential varies in accordance with pH of the electrolyte. Equilibrium potential vs. pH relations (Pourbaix diagram) can be constructed on the basis of thermodynamic data, as shown in Figure 2-1 as an example for formation of HCOOH from CO_2[53]. Figure 2.1 is the Pourbaix diagram for carbon dioxide showing the equilibrium reduction potentials as a function of pH. As shown from the potentials, nature of the reduction product has a strong influence on its thermodynamic accessibility from CO_2. Particularly important is the number of electrons involved in the reduction processes. As expected, the redox potentials become less and less negative as the reactions involves multi electronic pathways. The potentials required for reduction is not much high but in practical , CO_2 reduction does not take place easily, and the actual electrolysis potentials required are much more negative in most cases than the equilibrium ones. The reason is that the intermediate species CO^-_2, formed by an electron transfer to a CO_2 molecule, proceeds as the first step at highly negative potential, such as -1.9 V vs. SHE[35]. This makes the mono-electron reduction mechanism highly unfavorable. Depending on the electrode material used and the experimental conditions adopted', different products of CO_2 reduction could be obtained[54].

Electro-chemical reduction of CO_2 is an attractive way to convert CO_2 because of the following advantages over thermo-chemical methods: (1) water is the proton source; (2) high equilibrium conversion at ambient temperature; (3) pure oxygen is produced as a by-product [55, 35]. Carbon dioxide can be electrochemically reduced to a wide range of end products. However, the extent to which any of these reactions occurs depends, regardless of their equilibrium potential values, on the electrode kinetics and conditions of the

23

particular system [56].
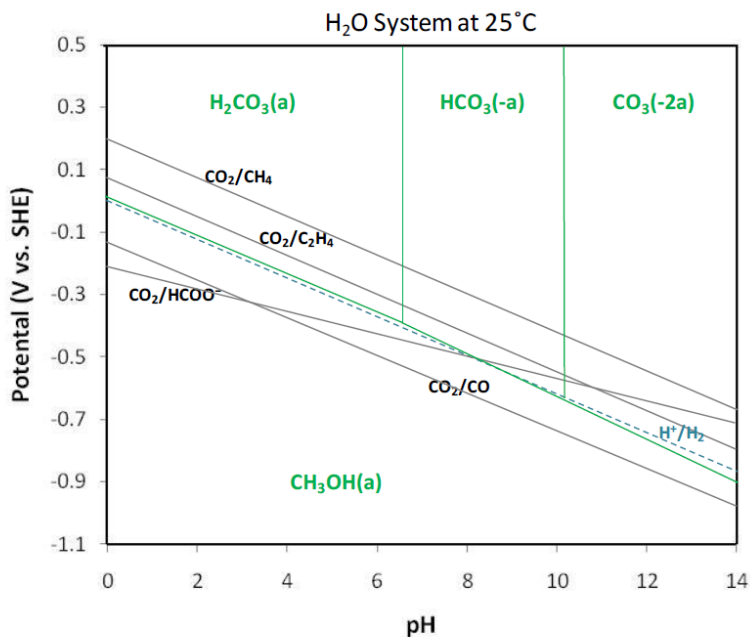
Figure 2-1: Pourbaix Diagram for Carbon Dioxide Reduction Reaction at 25°C

2.2.2 Mechanisms of Electrochemical Reduction of CO_2

A number of research groups have dedicated their efforts to fundamental studies of the mechanisms of ERC on a variety of electrode surfaces[57]. The reaction pathways and resulting product distributions can be very complex, because they not only are related to the energies of adsorption of a whole range of possible species, including reactants, intermediates and products, but also depend on the electro-catalyst, the electrolyte and the cathode potential. The detailed mechanistic pathways for each product are not clear at present, and in many cases several different schemes have been proposed. Figure 2-2 shows the most commonly proposed pathways for ERC to formate (formic acid), methane and ethylene [58-61].
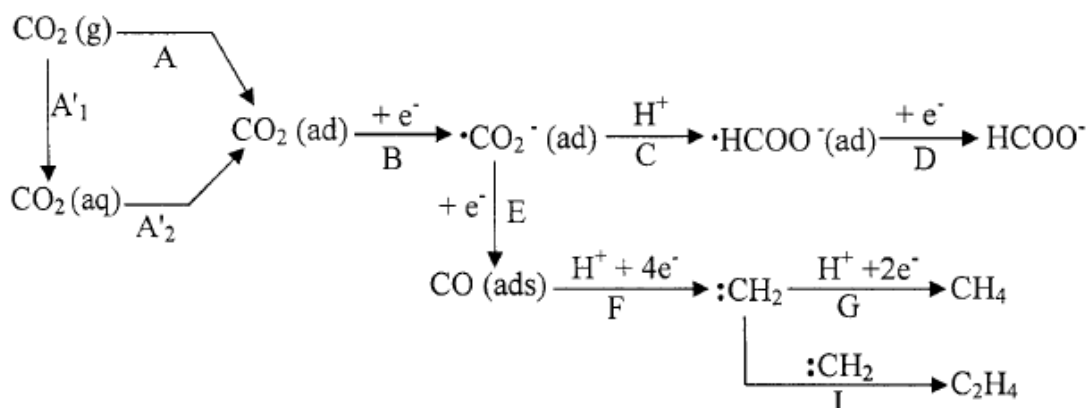
Figure 2-2: Mechanistic Pathways Commonly Proposed for ERC

Step A, the adsorption of CO_2 onto the electrode surface was suggested by some researchers [38] to be a prerequisite to CO_2 reduction. In some aqueous systems an intermediate hydration step (stepA'$_1$) is required before adsorption (step A'$_2$) occurs. In this case, the low solubility of CO_2 in water, i.e. 0.070 M at STP conditions, will limit the availability CO_2 (aq) and thus limit the CO_2(ad) concentration at the cathode sites, especially when CO_2 reacts competitively to give HCO_3^- and / or CO_3^{2-} in alkaline solution. The use of gas phase flow should overcome this limitation by allowing the formation of CO_2 (ad) directly from the gaseous state (step A) [56], and catalysts that have high affinity to CO_2 or low activation energy for adsorbing CO_2 should help to raise the concentration of CO_2(ad). In addition, ways of increasing CO_2 solubility can be useful in aqueous systems, such as operating under high pressure / or low temperature, using additives to enhance the solubility of CO_2.

Step B is the one electron reduction of CO_2 (ad) to the intermediate radical $\cdot CO_2$', whose standard redox potential is about -1.9 V (SHE) [35, 62, 38, 63]. It is seen from Table 2-1

that the overall standard redox potentials for ERC are in the same range as that for the reduction of protons to H_2 (E^o = zero V (SHE)), which indicates that ERC is not thermodynamically much more difficult than hydrogen evolution. However, ERC is kinetically suppressed because of the high energy intermediate radical $\cdot CO_2^-$ and the involvement of multi-electron transfer, i.e. 2 electrons for $HCOO^-$ (step B - C - D) and 8 electrons for CH_4 (step B - E - F - G).

2.2.3   Kinetic Consideration

The kinetic information/data on ERC is sparse and difficult to summarize because of the variety of approaches and experimental conditions. Therefore the kinetic information is given here in a "list form". It has to be noted that the reaction kinetics depend on many interacting factors, so results obtained by one researcher under his conditions might not apply under other conditions.

(l) Frese calculated the exchange current density for step B of Figure 2 (the formation of $\cdot CO_2^-$ radical) at 100 kPa (abs) and 298 K in CO_2 saturated aqueous solution (~0.036M) to be 4.8 x10-7 kA m^{-2} [44, 45, 64].

(2) Frese et al studied the kinetics with a copper foil electrode at 273 and 295 K using two separate electrode pretreatments to remove the oxide layer, i.e. 10 wt % HCI and 10 wt% HNO_3 [38]. The kinetic information is listed in Table 2-2

Table 2-2: Kinetic inFormation of Carbon Dioxide reduction to CH4 on Cu foil Cathode at Ambient Pressure. Catholyte = 0.5 M KHCO$_3$ at pH =7.6[21].

Temp. (K)	Pretreatment	Tafle slope V/decade	Jo kAm^{-2}	Highest CE	CE*at -1.46V (SHE)
273	10 wt % HCl	0.539	NA	NA	47
295	10 wt % HCl	0.11	1.94×10^{-7}	50	20
295	10 wt %HNO3	0.17	NA	32	NA

* CE is the "current efficiency" which is one of the performance indicators for electro-chemical processes.

(3) Gupta et al reported the exchange current densities for ERC to formate at 293K in (0.95 M KCI+0.05 M NaHCO$_3$) on In, Hg and Sn respectively as: $1 \times 10^{-7}, 1 \times 10^{-10}$, 1×10^{-8} kAm^{-2} [65].

2.3 Major Issues Related to ECR

2.3.1 Mass Transfer Constraint

For industrial electro-chemical processes, the superficial current density and current efficiency should be respectively at least 1 kA m^{-2} and 50 %. However, the relatively low solubility of CO$_2$ in aqueous solutions (ca. 70 mM at STP), coupled with the CO$_2$ (aq)/HCO$_3$/ CO equilibria, creates a mass transfer constraint on the reduction of CO$_2$ that limits the primary current density to a maximum value of the order 0.1 kA m^{-2} under the typical laboratory reaction conditions (one phase flow, 2-D cathode) with 100 kPa (abs) CO$_2$ pressure at 298 K. Several devices have been suggested to relieve the CO$_2$ mass transfer constraint, including operation at super-atmospheric pressure and/or sub-ambient

27

temperature, using a gas-diffusion cathode (GDE) or using a fixed-bed cathode while providing a "3-phase interface" for the reaction by sparging the cathode chamber with CO_2 gas [66-73] .

2.3.2 Reactor Capacity

Apart from the constraint of the CO_2 mass transfer limiting current density, a practical reactor for ERC must be able to handle volumetric gas feed rates in the order of 1 m^3 STP per hour per kA [21]. With the possible exception of gas diffusion systems (GDE's) most electrochemical reactors, and particularly those used by previous investigators of ERC, are not capable of handling high gas loads at the gas space-velocity (GSV) required of an industrial process (e.g. 100 to 1000 h^{-1} at STP)[21].

2.3.3 Lack of Engineering Research

The research of ERC is still at a stage of fundamental investigations on mechanisms and kinetics using tiny electrodes (e.g. 1 x 10^{-4} m^2) with little consideration of the possibility for practical application. Research on the engineering aspects of ERC should be initiated to bridge the gap between the previous laboratory work and industrial reality. Such engineering research includes the design and scale-up of continuous electro-chemical reactors, together with the conception, design and economic projections for complete ERC processes. At the time of writing this report (December 2011) only five articles have appeared that describe the electro-reduction of CO_2 in a continuous reactor. Akahori et al., who are apparently the first to report continuous operation, used a lead wire bundle cathode in a flow by reactor with a cation membrane separator[74]. This reactor obtained a formate current efficiency near 100 % with single-phase flow of a CO_2 saturated

catholyte solution at 1.4 ml min^{-1} and current about 0.02 kA m^{-2}). The second source is a recent communication [66, 75]. The third and the latest one is. by Delacourt et al. [70].

2.4   Electrocatalysts for ERC

An elctrocatalyst participates in an electron transfer reaction (at an electrode) and facilitates acceleration of a chemical reaction. Both the electron transfer and chemical kinetics must be fast for an efficient electrocatalyst. Additionally, an optimal electrocatalyst must display a good thermodynamic match between the redox potential (E^0) for the electron transfer reaction and chemical reaction that is being catalyzed. These factors can be optimized by chemical tuning of the electrocatalyst. Electrocatalyst are typically screened for their redox potential, current efficiencies, electron transfer rate and chemical kinetics in order to determine the best overall catalyst [76, 77, 15]. In the general sense, electrocatalyst are electron transfer agents that ideally operate near the thermodynamic potential of the reaction to be driven, E^0 (products/substrates). Thus, electrocatalyst offer critical solutions to lowering the over potentials, improving selectivity, and increasing the reaction kinetics of carbon dioxide conversion. If the reduction of carbon dioxide to liquid fuels is to be accomplished through electrochemical means, the deployment of efficient elctrocatalyst will be essential for the development of practical industrial processes. Direct electrochemical reduction of carbon dioxide on most electrode surfaces requires large overvoltages which consequently lowers the conversion efficiency. The overvoltage is the difference between the applied electrode potential, $V_{applied}$, and E^0(products/substrates), at a given current density. Both thermodynamic and kinetic considerations are important here. Clearly, in order to minimize overvoltages, catalysts need to be developed that have formal potentials, E^0 ($Cat^{n+/0}$) well matched to E^0(products/substrates), and appreciable rate constants for the chemical reduction of

29

substrates to products at this potential. In addition, the heterogeneous rate constant for reduction of the elctrocatalyst at the electrode must be high for Vapplied near E^0 $(Cat^{n+/0})$[78-81, 9, 82, 83].

In the mechanism of reduction of CO_2, it is observed that, on one hand, CO_2 competes with hydrogen for electrons and on the other hand, most of the reduction requires protons. Therefore, the problem is twofold: to transfer the electrons to CO_2 instead of protons, and after forcing them not to go to the protons, to liabilize CO_2 sufficiently to receive them. In electrochemical terms, the reduction of CO_2 can e catalyzed either positively, in the sense that the overpotential is decreased, and/or the current increased, or it can be catalyzed negatively, in the sense that competing reactions are discouraged. Thus, ERC needs both protons and electrons, and therefore hydrogen evolution must be discouraged. The nature of electrodes not only affects the yields, but also the distribution of products. One of the methods is to employ electrodes with high hydrogen overpotential.

All the electro reduction techniques need to overcome the difficulty of finding electrodes with both a high electrocatalytic activity and a satisfactory lifetime. Studies on the electrocatalysts for reduction of carbon dioxide began more than a century ago with high hydrogen overpotential metals and alloys. In 1904, Coehn and Jahn used zinc, amalgamated zinc and amalgamated copper cathode to electrolytically reduce carbon dioxide in aqueous $NaHCO_3$ and K_2SO_4 solutions, in which formic acid was the only product [84]. Fischer and Prziza ran electrolytic reduction reactions of carbon dioxide that had been dissolved under pressure[85]. Once again, formic acid was the only product and copper plated with amalgamated zinc electrodes were reported to be the most

efficient. Finally, minimal amounts of methanol were obtained with Pb electrodes in K_2SO_4 and $(NH_4)_2SO_4$ electrolyte. In 1969, Paik et al. reduced carbon dioxide on the mercury electrode in buffered neutral and acidic aqueous solutions by means of steady state polarization techniques, cathodic galvanostatic charging techniques, and current efficiency determinations[86]. The only reduction product in neutral solution was formic acid; while in the acid solution, both formic acid and hydrogen were formed. However, these early papers show that with mercury as the cathode, the current efficiency was high at initial stages, and then fell rapidly with time. Ultimately, Udupa et al. investigated the electrolytic reduction of carbon dioxide at a rotating amalgamated cathode to improve and maintain high current efficiency so that formate could be built up without loss in current efficiency[87]. In 1977, Russell et al. attempted to electrochemically reduce carbon dioxide to methanol through intermediate reactions because conditions for a direct conversion could not be achieved [88]. Formic acid was reduced from carbon dioxide in a neutral electrolyte on a mercury electrode; however, it could not be further reduced to methanol due to the limited potential region. Fortunately, formaldehyde could be reduced to methanol at a current density of $10 mAcm^{-2}$. In 1982, Hori et al. studied the effect of electrolyte in carbon dioxide electrolytic reduction on a mercury electrode by investigating different aqueous solutions of $NaHCO_3$, NaH_2PO_4, Na_2HPO_4, $NaCl$, $NaClO_4$, Na_2SO_4, $LiHCO_3$, and $KHCO_3$ as well as their combination [89].

Similar studies were continued on different metal electrodes with the hope of finding the optimal catalysts for the process. In 1983, as part of a program to study the conversion of inorganic substances into fuels, Canfield and Frese investigated the reduction of carbon dioxide to methanol, formaldehyde and methane on n and p-GaAs, and p-InP

semiconductor electrodes[90]. The highest current achieved was around 400 μAcm^{-2}. In 1985, Frese and Leach chose ruthenium electrode because ruthenium was known at that time for being active in the gas phase conversion of carbon dioxide to methane at low temperature[64]. The reaction yielded carbon monoxide, methane, and a small amount of methanol. Even though the reaction was stable, current density was less than $0.4mAcm^{-2}$. Frese et. al. also tried molybdenum electrodes in 0.2 M Na_2SO_4 electrolyte (pH = 4.2) to convert carbon dioxide to methanol at good selectivity and yield under appropriate conditions[91]. It was shown that the Faradaic efficiency depends on several factors such as chemical surface pretreatment and voltage cycling pretreatment. In voltage cycled electrodes, carbon dioxide rapidly converted to methanol at up to 37 % faradaic efficiency; however, cycled electrodes were also subject to molybdenum corrosion. During the same period, Hori et. al. succeeded in electrochemically reducing carbon dioxide to hydrocarbons at several metal electrodes in an aqueous bicarbonate solution (0.5-1.0 M $KHCO_3$) with a high current density (5.0-5.5 mA cm^{-2}) [40]. Cd, In, Sn, and Pb electrodes mainly produced formate. Ag and Au yielded majority of CO. Ni and Fe exclusively produced H_2, with trace amount of CO and CH_4. Only Cu cathode produced significant amount of CH_4. The copper electrodes were pretreated by etching in 7% HNO_3 aqueous solution; however, little difference in Faradaic efficiency of CH_4 formation was observed. In addition, the presence of oxygen in the electrolyte remarkably enhances the CH_4 production. After successfully producing methane from copper electrodes, in 1986, Hori et al. continued their studies using copper electrode in an aqueous bicarbonate solution at a low temperature with a current density of 5 mA cm^{-2}. The Faradaic efficiency of methane formation was about 65 % at 0°C and dropped with an increase in temperature, whereas that of ethylene formation rose up to 20 % at 40 °C.

By 1987, Cook et al. were able to improve the efficiency of methane and ethylene production using in situ electrodeposited copper layers on a glassy carbon electrode[48]. At 8.3 mAcm^{-2}, the carbon dioxide reduction reached almost 100% current efficiency. At 25 mAcm^{-2}, the overall current efficiency for carbon dioxide reduction was 79 %. These yields were by far the highest Faradaic efficiency and current density yet reported for the carbon dioxide reduction reaction. A systematic rule for the electrocatalytic reduction of carbon dioxide on metal surfaces was suggested. Azuma and colleagues measured the reduction products on 32 types of metals in aqueous $KHCO_3$ solution at low temperature (0°C) and discussed the reduction mechanism [59] (Table 2-3 and Table 2-4).

Table 2-3: Typical Current Efficiencies (%) for CO_2 Reduction Products at -2.2 V vs. SCE (193°C) in a CO_2 Saturated 0.05 M $KHCO_3$ Aqueous. (Reprinted from [59])

Metal	T °C	CH_4	CO	C_2H_4	C_2H_6	HCOOH	H_2	Sum
Cd[a]	0	0.015	3.7	0.002	0.00056	55.9	35.7	95
	20	0.0073	1.8	0.001	0.00040	35.5	63.2	100
In[a]	0	0.001	3.0	0.00035	0.0006	70.0	25.0	98
	20	0.050	14.7	0.0046	0.0067	33.3	56.5	105
Sn	0	0.65	1.4	0.068	0.44	28.5	67.5	99
	0	0.84	0.35	0.95	0.69	5.2	94.9	102
Pb[a]	0	0.39	0.12	0.008	0.0014	16.5	82.9	100
	20	0.06	0.10	0.001	0.0003	9.9	93.3	103
Tl	0	0.20	0.16	0.003	0.0010	53.4	46.2	100
Hg	0	0.0004	0.20	t	t	90.2	9.5	100
	20	0.0035	0.64	0.0002	0.00006	87.6	7.9	96
Zn	0	0.23	9.8	t	nm	19.5	68.1	98
Pd[a]	0	0.083	11.6	0.011	0.014	16.1	73.3	101
	20	0.31	3.2	0.061	0.078	8.6	90.3	103
Ti	0	t	13.5	t	nm	5.2	69.4	83
Ni	0	0.71	21.0	0.069	0.18	13.7	61.7	97
	20	0.13	0.60	0.010	0.021	0.10	98.8	100
Ag	0	1.4	40.7	0.0052	0.013	20.5	32.6	95
	20	1.1	30.0	0.0090	0.0027	16.0	50.0	98
Au	0	t	16.9	t	nm	10.3	73.4	101
Cu	0	24.7	16.5	6.5	0.015	3.0	49.3	100
	20	17.8	5.4	12.7	0.039	10.2	52.0	98
C	0	0.11	t	0.0064	0.0070	0.31	92.5	93
Al	0	0.012	t	0.00022	0.00040	0.78	95.7	96
Si	0	0.025	0.08	t	t	1.6	102.2	104
V	0	0.02	1.3	t	nm	2.6	91.9	96
Cr	0	0.74	0.49	0.050	0.18	0.15	92.2	94
Mn	0	1.5	0.34	0.093	0.29	0.03	90.9	93
Fe	0	0.07	2.2	t	nm	1.1	89.8	93
Co	0	0.13	0.47	0.0057	0.032	0.85	92.9	94
Zr	0	0.49	0.42	0.021	0.055	t	99.9	101
Nb	0	0.16	0.46	0.0088	0.042	0.03	97.3	98
Mo[a]	0	0.010	t	0.00028	0.0015	0.21	99.9	100
	20	0.031	0.02	0.00077	0.0057	0.19	98.6	99
Ru	0	0.043	0.65	t	t	0.08	99.1	100
Rh	0	0.031	2.5	0.00067	0.0036	1.35	99.3	103
	20	0.053	0.66	0.0030	0.011	2.4	99.3	103
Hf	0	0.0046	1.14	0.00027	0.0010	0.35	99.2	101
	20	0.0073	0.08	0.00057	0.0005	0.21	100.9	101
Ta[b]	0	0.0015	0.09	0.0015	0.0002	t	100.7	101
	20	0.0039	t	0.0039	0.0001	t	102.2	102
W[a]	0	0.015	0.06	0.0043	0.0022	1.3	96.3	98
	20	0.055	0.21	0.0022	0.010	2.6	96.9	100
Re[a]	0	0.044	t	0.00022	0.0056	2.0	99.0	101
	20	0.038	t	0.00024	0.0048	1.4	95.3	97
Ir	0	0.051	0.53	0.0035	0.0072	1.0	98.8	100
	20	0.086	t	0.0057	0.015	0.58	100.3	101
Pt	0	0.29	1.2	t	nm	5.5	92.6	100

[a] At −2.0V vs. SCE.
[b] At −2.8V vs. SCE.
t : trace.
nm: not measured.

34

Table 2-4:Typical Current Efficiencies (%) for Hydrogen Evolution (η[H2]) and total CO_2 (η[CO2]) on Various Metal Electrodes and the Distribution (%) into CO (FCO) and HCOOH (FHCOOH) and Hydrocarbons (FCxHy) at 0.05M $KHCO_3$, 0°C, -2.2 Vvs. SCE. (Reprinted from [59])

Electrodes	$\eta(H_2)$	$\eta(red-CO_2)$	F_{CO}	F_{HCOOH}	F_{CxHy}	Note
Cd	35.7	59.6	6.2	93.8	t	−2.0V
In	25.0	73.0	4.1	95.9	t	−2.0V
Sn	67.5	31.1	4.5	91.8	3.7	
Pb	82.9	17.0	0.7	96.9	2.4	−2.0V
Tl	46.2	53.8	t	99.8	t	
Hg	9.5	90.4	0.2	99.8	t	
Zn	68.1	29.5	33.2	66.0	0.8	
Pd	73.3	27.8	41.7	57.9	0.4	−2.0V
Ti	69.4	18.7	72.2	27.8	t	
Ni	61.7	35.7	58.9	38.4	2.7	
Ag	32.6	62.6	65.0	32.7	2.2	
Au	73.4	27.2	62.1	37.9	t	
Cu	49.3	50.7	32.5	5.9	61.5	
C	92.5	0.43	t	71.5	28.5	
Al	95.7	0.79	t	98.4	1.6	
Si	102.2	1.7	4.77	93.8	1.5	
V	91.9	3.9	33.2	66.3	0.5	
Cr	92.2	1.6	30.4	9.3	60.2	
Mn	90.9	2.3	15.1	1.3	83.6	
Fe	89.8	3.4	65.3	32.6	2.1	
Co	92.9	1.5	31.6	57.1	11.3	
Zr	99.9	0.99	42.6	t	57.4	
Nb	97.3	0.70	65.6	4.3	30.1	
Mo	99.9	0.22	t	94.7	5.3	−2.0V
Ru	99.1	0.77	84.1	10.4	5.6	
Rh	99.3	3.9	64.3	34.7	0.9	
Hf	99.2	1.5	76.2	23.4	0.4	
Ta	100.7	0.30	29.7	t	70.3	−2.8V
W	96.3	1.4	4.3	94.1	1.6	−2.0V
Re	99.0	2.0	t	97.6	2.4	−2.0V
Ir	98.8	1.6	33.3	62.8	3.9	
Pt	92.6	7.0	17.2	78.7	4.1	

t: trace.

Out of 32 metals (including Cd, In, Sn, Pb, Tl, Hg, Zn, Pd, Ti, Ni, Ag, and Au) Cu showed relatively high total current efficiencies for carbon dioxide reduction. Only copper was able to produce hydrocarbon efficiently, while other metals yield primarily formic acid. Based on this dependence of reduction products on various metals, a periodic table for carbon dioxide reduction was developed which suggested a systematic rule for the electrochemical reduction of carbon dioxide on transition metal surfaces (Figure 2-3). Heavy transition metals in the IIB, IIIB, and IVB groups reduced carbon dioxide to formate. Some of VIII and IB metals are effective for carbon monoxide

production. Copper is located between these two groups and is selectively active toward carbon dioxide reduction to hydrocarbons. Similarly, in 1992, Bandi et al. had already discovered a relationship between the metals' positions in the periodic table and their ability to chemisorb carbon monoxide dissociatively, the initial step for hydrogenation to methanol [92].
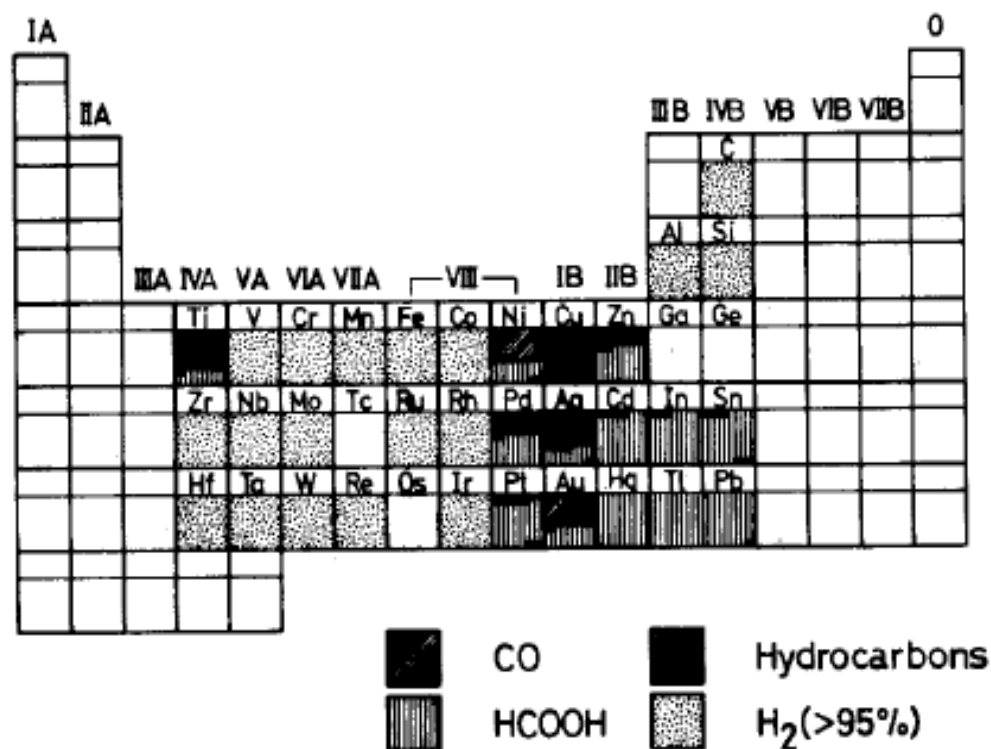
Figure 2-3: Periodic Table for CO_2 Reduction products at -2.2V vs. SCE in Low Temperature 0.05 M $KHCO_3$ Solution reprinted from [59]

However, at present, there is no consensus on the molecular mechanism of the metal electrodes and their properties toward electrocatalytic activities and selectivities for carbon dioxide reduction.

With the discovery of copper as an active catalyst for carbon dioxide reduction to hydrocarbons, electrocatalytic research has moved to a higher level. Kaneco and

coworkers have done a series of experiment in this field using copper in different electrolytes to produce formic acid, methane, ethylene and carbon monoxide with increasing Faradaic efficiency [93-103, 26, 104, 29, 105]. Frese et. al. studied the electrochemical reduction of carbon dioxide to methane on copper foil electrodes in 0.5 M $KHCO_3$, pH 7.6. The highest methane formation rates at 22 ℃ and 0 ℃ were 8 x10^{-5} and 1.1x10^{-4} mol cm^{-2} h^{-1} at current densities of 17 and 23 mAcm$^{-2,}$ respectively [45]. The results showed that the catalytic properties of copper depended on its physical form and method of preparation. Polishing the copper surface helped achieve the highest methane formation rates. Cleaning copper with HCl was preferred over HNO_3 cleaning. In this experiment, copper foil was oxidized by oxygen in air prior to carbon dioxide reduction to form a visible layer of CuO and Cu_2O on copper surface. After HCl cleaning, all the oxides were dissolved to form cuprous chloride complex ions. The Cu^+ in the Cu_2O was stabilized and prevented from disproportionating to Cu^0 and Cu^{2+}. It was concluded that HCl removed the oxides without precipitation of metallic copper, which was known to deactivate the catalyst surface[106].

Understanding the characteristics of metal surfaces would be beneficial to recognizing the carbon dioxide reduction reaction mechanism. Even though it is known that copper is the vital active catalyst component, the active sites and orientation are still a topic of debate. Carbon dioxide was electrochemically reduced at Cu (100), Cu(110) and Cu (111) electrodes at constant current density of 5 mAcm^{-2} in 0.1 M $KHCO_3$ at ambient temperature[107]. Ethylene was favorably produced on Cu (100), while Cu (111) yielded mostly methane. Terunuma et al. studied the relationship between hydrocarbon production in the electrochemical reduction of carbon dioxide and the characteristics of

the copper electrode by conducting various pretreatment methods on copper [79]. A copper metal surface is easily contaminated with organic compounds due to its high affinity for absorbed oxygen. Surfaces with copper oxide to some extent demonstrated much higher activity for hydrocarbon production. The Cu_2O site has a stronger activity for the reduction of protons than the Cu site. In the experiment, the Cu site was responsible for the physical adsorption of carbon dioxide to form carbon monoxide as a first step. The heat of adsorption of carbon monoxide on Cu_2O is larger than that on metallic Cu, and the Cu_2O site is more favorable to the adsorption of carbon monoxide than the Cu site. Therefore, controlling the number of Cu (I) sites is very important in enhancing the selectivity and productivity towards methanol formation.

There are good reasons to expect Cu^+ ions in the Cu_2O to be the active site for methanol production from electrochemical reduction of carbon dioxide. Recently, Chang et al. have investigated the electrochemical reduction of carbon dioxide by Cu_2O catalyzed carbon cloths and concluded that methanol was the only product. It was indicated that Cu^+ is directly involved in the catalytic actions to promote carbon dioxide compositions[37]. Frese et al. have observed the carbon dioxide reduction to methanol at several oxidized copper electrodes including anodized copper foil, copper foil thermally oxidized in air, and air oxidized copper electrodeposited on anodized or air oxidized Ti foil at 22 $°C$ [44]. The highest methanol rate obtained was 1 $\times 10^{-4}$ mol cm^{-2} h^{-1} from anodized copper foil in 0.5 M $KHCO_3$. The current density was as high as 33 mA cm^{-2}. While copper oxides show the greatest yields and efficiencies, a more fundamental question regarding oxidized Cu electrodes centers on their formal reduction potentials relative to CO_2. The formal potential for CO_2 reduction to CH_3OH occurs 20 mV positive of the SHE, while

38

copper oxides are reduced at more positive potentials. Further, several CO_2 reduction studies suggest an initial step requiring CO which has a formal potential of – 0.103 V (SHE) [16, 108, 109]. Copper is considered unique among metals with both intermediate hydrogen overpotentials and carbon monoxide adsorption allowing further reduction to hydrocarbons. The first pathway in the system is the formation of both formate and carbon monoxide. As the potentials become more negative, carbon monoxide and formate suppress hydrogen evolution. At potentials more negative than –1.25 V (SHE), carbon monoxide is further converted to ethylene at first, and methane becomes dominant after –1.35 V (SHE). Understanding how equilibrium potentials affect the activity and selectivity of the reaction might be helpful in determining the reaction mechanism.

Metal electrodes are divided into four groups shown in Table 2-5 according to the nature of the main products and representative results on solid metal electrodes are listed in Table 2-6.Basically in literature following type of electrocatalysts are used:

- Bulk metal

- Modified metal

- Metal alloys

- Semi-conductors

- Metal- oxides

- Transition Metal-complexes

Copper has been the most studied electrode both in metallic as well as oxide form [110]. ECR has been tries on ruthenium oxide coated diamond electrodes were used by Spataru et al and showed that conductive metallic oxides are promising elctrocatalyst for ECR

and allows higher reduction products to be obtained [80]. The main products obtained in acidic and neutral media were formic acid and methanol with product efficiencies 40 and 7.7 %, respectively. Komatsu et. al. prepared Cu-solid polymer electrolyte composite electrodes and application to gas-phase electrochemical reduction of CO_2[111].

ECR on ruthenium electrode deposited onto poly crystalline gold support was used by Schrebler et al and their main product was CO (87%) and H_2 (13%)[82]. Qu et al prepared ruthenium oxide & titanium oxide nanotubes composite electrode and tested for their catalytic properties and the current efficiency for conversion of CO_2 to methanol was up to 60.5 % on RuO_2/TiO_2 nanotubes modified Pt electrodes. Compared with RuO_2 and RuO_2/TiO_2 nano-particles composite electrodes, RuO_2/TiO_2 composites modified Pt electrode had the higher activity for the electrochemical reduction to methanol [112].

Mitrovski et al synthesized and characterized novel catalysts, ones that showed exceptional selectivity towards the carbon-dioxide reduction reaction (practically 100 %). These catalysts were based on tin and tin modified thin-film gold electrodes. Three types of electrodes were fabricated (electrodeposited tin, spontaneously deposited tin on gold and electron-beam deposited gold) and their electrochemical activity was studied by monitoring the carbon-dioxide reduction polarization curves using linear sweep voltammetry[113].

Table 2-5: Various products from metal electrodes

Groups	Metals	Products
A	Cu	Hydrocarbons and alcohols
B	Au, Ag, Zn, Pd, and Ga	Carbon monoxide
C	Pb, Hg, In, Sn, Bi, Cd, and Tl	Formate/formic acid
D	Ni, Pt, Fe, Co, Rh, Ir, and W	Multi-products; only exhibit useful catalytic activities at high pressure and low temperature

Even though the effort to put everything together is still tremendous and requires substantial time commitment, with human intelligence, electrochemical reduction of carbon dioxide at industrial scale will no longer be an unrealistic dream

Table 2-6: Representative results of ERC at flat solid metal electrodes[21].

Electrode	Ag	In	Cu	Ag	Cu	Sn
Electrolyte	$KHCO_3$	$KHCO_3$	$KHCO_3$	KOH	$TBABF_4$	K_2CO_3
Solvent	H_2O	H_2O	H_2O	CH_3OH	CH_3OH	H_2O
T (K)	298	298	273	248	298	298
P (kPa)(abs)	3000	6000	100	100	4000	100
Product	CO	*$HCOO^-$	CH_4	CO	CO	*$HCOO^-$
CE (%)	76	108**	65	90	87	75
PCD^{***} (kA m^{-2})	1.51	2.15	0.10	0.18	2.88	0.20
$E_{cathode}$(V SHE)	NA	NA	-1.39	-5.76	-1.50	-1.66
Reference	Hara 1995	Todoroki 1995	Hori 1986	Kaneco 1998	Saeki 1995	Ito 1975

Note:$TBAF_4$ (Tertiarybutylammonium tetraflouroborate)

*Formic Acid was claimed to be the product here-but since pH>6 the actual product is the formate ion.

**108% CE was obtained by summation of the partial CE's obtained by product analysis.

***PCD is the partial current density.

2.5 Supported Electrocatalysts

Most important criteria for selection of any porous support material for electrochemical application are surface area and electrical conductivity. Electrodes require an electrically conductive material to provide a conductive path for the electrons to travel from the reaction site to the current collector. Often, the electrocatalyst serves the dual purpose of facilitating the electrochemical reaction and transporting the electrons. However, when the electrocatalyst is a precious metal such as platinum, it is advantageous to support it on

a conductive substrate such as carbon. This enables the expensive electrocatalyst to be highly dispersed, thus minimizing the amount of precious metal without sacrificing catalytic activity. Dispersion of precious metals onto inexpensive supports is the same approach used in heterogeneous catalysts for non-electrochemical reactions. In these cases though, the support is often an insulating metal-oxide material that has high surface area and promotes catalytic activity (i.e., enhanced catalyst-support interactions). In electrochemical applications (e.g., proton exchange membrane fuel cells), the typical support material is carbon due to its high surface area and high electron conductivity rather than any enhanced catalyst-support interactions. However, carbon-supported electrodes that operate at voltages above ~0.9 V in the presence of water are known to undergo carbon corrosion. Corrosion of the support can create a loss of electrical contact with the catalyst particle, thus decreasing the performance of the cell.

Yamamoto et al examined the electroreduction of CO_2 on metals (Fe, Ni, Cu, and Pd) electrocatalysts supported on activated carbon fibers, which contain slit-shaped pores with widths on the orders of 2 nm. These catalysts exhibited relatively high selectively (faradaic efficiency = 67%) and high partial current density (~ $63mAcm^{-2}$). Much lower activities were observed for the same types of metal catalysts supported on non – activated carbon fibers. The enhancement of CO_2 reduction selectivity with the micro support is thought to involve a nanospace effect at ambient pressures. The CO_2 reduction mechanism on Ni is proposed to involve an absorbed CO_2- CO_2^- adduct, which is known to exist on (110) surface[114].

 Whipple et al studied electrochemical reduction of CO_2 on carbon-supported Ru–Pd in

microfluidic. The use of gas diffusion electrodes enables better control of the three-phase interface where the reactions take place. Furthermore, the versatility of the microfluidic reactor enabled rapid evaluation of catalysts under different operating conditions. Operating at acidic pH resulted in a significant increased the performance: faradaic and energetic efficiencies of 89 and 45%, respectively, and current density of 100 mA/cm^2[115].

Gangeri et al used Pt/CNT and Fe/CNT electrocatalysts to convert carbon dioxide to liquid fuels, particularly iso-propanol. Fe/CNT showed a better behavior than Pt/CNT, although a faster deactivation. The main reason of deactivation was believed to be the cross-over of the electrolyte, particularly of K ions. They react with iron particles and cause their dissolution and migration. In the case of Pt/CNT there is no, or minor, dissolution of metal, but potassium covers the Pt particles and/or induce deactivation. It is shown, however, that the electrolyte was necessary to simulate the half-cell of the full photoelectrocatalytic device, while in the latter no electrolyte is needed, being the protons and electrons produced by water splitting. The elimination of the electrolyte probably could eliminate or significantly reduce a main cause determining the observed fast deactivation [116]. Other important studies are carried out by Subramaniam et. al. [117],Narayanan et. al. [118] and Delacourt et al [70].

2.5.1   Carbon Nanotubes (CNTs)

Among the different types of supports used in heterogeneous catalysis, carbon materials attract a growing interest due to their specific characteristics which are mainly: (i) resistance to acid/basic media, (ii) possibility to control, up to certain limits, the porosity and surface chemistry and (iii) easy recovery of precious metals by support burning resulting in a low environmental impact. Several reviews dealing with this subject have been published[119, 120]. Recently, new carbon forms like graphite nanofibers (GNF) or monofilaments and carbon nanotubes (CNT) have generated an intense effervescence in the scientific community. They exhibit fascinating and useful properties. Among these materials, carbon nanotubes represent the most striking example. Carbon nanotubes (CNTs) were discovered in 1991 by Sumio Iijima while studying the surfaces of graphite electrodes used in an electric arc discharge[121]. Since then, there have been great improvements in their synthesis techniques, which can now produce reasonably pure nanotubes in good quantities.

CNT have since then become one of the most active fields of nanoscience and nanotechnology due to their exceptional properties that make them suitable for many potential applications as polymer reinforcements for composites or breakthrough materials for energy storage, electronics and catalysis. Of course, such a promising material attracts the interest of industrial groups that foresee a high economical impact in the near future. Currently, one of the main challenges is the low cost, industrial scale production of nanotubes that might be achieved by exploiting chemical vapor deposition (CVD) processes.

CNTs are considered to be excellent candidates for many potential applications, including but not limited to: catalyst and catalyst supports, composite materials, sensors and actuators, field emitters, tips for scanning probe microscopy, conductive films, bio-nanomaterials, energy storage media and nanoelectronic devices. Application of CNT in the field of catalysis as new class of catalyst supports has already been investigated and preliminary results have been already reviewed[122, 123]. Excellent reviews on the use of CNT as fuel cells electrodes [124] or supported catalysts for fluid phase reactions are available[125].

It is the structure, topology and size of nanotubes that make their properties exciting compared to the parent, planar graphite-related structures, such as are for example found in carbon fibers. The uniqueness of the nanotube arises from its structure and the inherent subtlety in the structure, which is the helicity in the arrangement of the carbon atoms in hexagonal arrays on their surface honeycomb lattices. The helicity (local symmetry), along with the diameter (which determines the size of the repeating structural unit) introduces significant changes in the electronic density of states, and hence provides a carbon nanotubes can be divided essentially into two categories: SWNT and MWNT as displayed in Figure 2-4. Figure 2-4 illustrates the morphology of the single wall carbon nanotubes and multi wall carbon nanotubes. Ideally, single-wall carbon nanotube are made of a perfect graphene sheet, i.e. a poly aromatic mono-atomic layer made of an hexagonal display of sp^2 hybridized carbon atoms that genuine graphite is built up with, rolled up into a cylinder and closed by two caps (semi-fullerenes). The internal diameter of these structures can vary between 0.4 and 2.5 nm and the length ranges from few

microns to several millimeters. The MWNT can be considered as concentric SWNT with increasing diameter and coaxially disposed. The number of walls present can vary from two (double wall nanotubes to several tens, so that the external diameter can reach 100 nm. The concentric walls are regularly spaced by 0.34 nm similar to the inter graphene distance evidenced in turbo-stratic graphite materials. It is worth to note that residual metallic particles coming from the production process can be found in the inner cavity of MWNT. The main difference between nanotubes and nanofibers consists in the lack of a hollow cavity for the latter.. In short they are classified as either (a) "single-walled" tubes (SWCNTs, 0.7 < d < 2 nm), which consist of a single layer of graphene sheet seamlessly rolled into a cylindrical tube, or (b) multiwalled CNTs (MWCNT, 1.4 < d < 150 nm), which comprise multiple concentric tubes separated by about 0.34 nm.
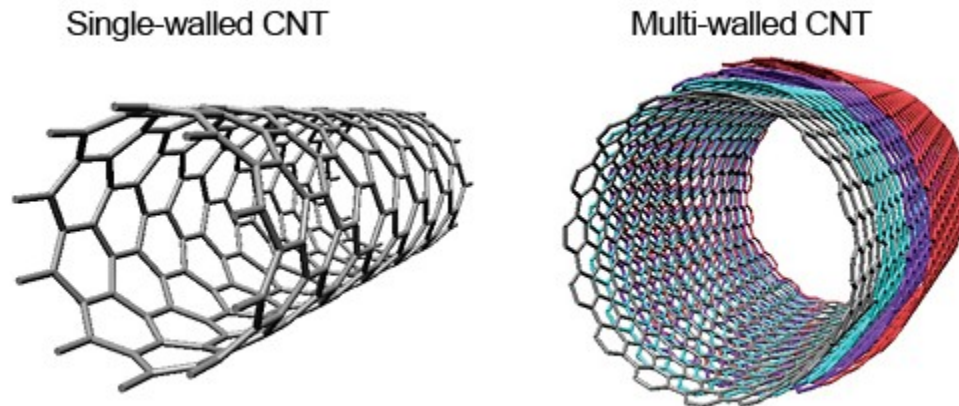
Figure 2-4: Different Types of CNTs [126]

Exhaustive studies concerning electronic properties of both SWCNT [127] and MWCNT[128], are available in the literature. In the case of SWCNT, studies have demonstrated that they behave like pure quantum wires (1D-system) where the electrons

are confined along the tube axis. Electronic properties are mainly governed by two factors: the tube diameter and the helicity, which is defined in which the graphene layer is rolled up (armchair, zigzag or chiral). In particular, armchairs SWCNT are metallic and zigzag ones display a semi-conductor behavior. This curvature of the graphene sheet induces strong modifications of the electronic properties and a comparison to graphite shows a modification of the pi-electron cloud. These theoretically predicted electronic properties are often drastically modified by the presence of defects such as pentagons, heptagons, vacancies or impurities[129]. In addition, production techniques do not currently allow a selective production of one specific type of SWCNT and the final purity of the obtained material, i.e. after purification steps, is far from being perfect.

Studies on MWCNT's electronic properties have revealed that they behave like an ultimate carbon fiber [128] : at high temperature their electrical conductivity may be described by semi-classical models already used for graphite, whereas at low temperature they reveal 2D-quantum transport features. A fine prediction of the electronic properties is even more difficult than in the case of SWCNT due to two main factors: the rolling up of the graphene layers can vary along the different walls of a single MWCNT and the higher complexity of the structure will increase the possibility of the presence of defects.

When used in catalysis, these conductive supports present clear differences with respect to activated carbon, and a recent theoretical study related to the interaction of transition metal atoms with CNT and graphite indicates major differences[130]. It has been demonstrated that the binding sites are depending on the structure of the support: the studies conducted over nickel show that the most stable anchoring sites vary sensibly between graphite and SWCNT due to the different curvature of the surfaces where the

active species can be deposited. The curvature also affects significantly the values of magnetic moments on the nickel atoms on the nanotube's wall and the charge transfer direction between nickel and carbon can be inverted. Therefore, the possibility of peculiar metal–support interaction has to be taken into account.

In general, CNTs possess large specific surface areas due to their hollow geometry, while their structural integrity and chemical inertness support relatively high oxidation stability. Other advantages include their exceptional physical properties, which have been are summarized in Table 2-7 in comparison with graphite[131] .

Considering the advantageous properties of CNT and GNF as supports discussed previously several studies have been carried on different catalytic reactions. Particularly, a lot of attention has been dedicated to liquid-phase reactions with MWCNT and GNF supported catalysts; indeed, their high external surface and their mesoporosity should allow significant decreases on mass-transfer limitations when compared to activated carbon. It is also relevant that very few studies dealing with SWCNT supported catalytic systems have been reported, due either to their microporosity or to the fact that it is still very difficult to obtain large enough quantities of pure material to conduct catalytic studies[126].

Table 2-7: Summary of Physical Properties of CNTs in Comparison with Graphite[131]

Property	SWCNT	MWCNT	Graphite
specific gravity (g/cc)	0.83	<1.8	2.26
Surface area	400–900	200-400	700-1200
Electrical resistivity	5-50 $\mu\Omega$ cm	5-50 $\mu\Omega$ cm	50 $\mu\Omega$ cm (in plane)
Thermal conductivity	3000 W m^{-1} K^{-1}	3000 W m^{-1} K^{-1}	3000 W m^{-1} K^{-1} (in plane) 6 W m^{-1} K^{-1} (c-axis)
Elastic modulus	~1.4 TPa	~0.3-1 TPa	1 TPa (in plane)

2.5.2   Titania Nanotubes (TNT)

Titanium oxide (TiO_2) is an n-type semiconductor and a typical photocatalyst, attracting much attention from both fundamental and practical viewpoints. Popular types of TiO_2 are anatase, rutile and their mixture, Degussa® (P-25). It has been used for long in many industrial areas including environmental purification, antibacterial, solar cells, gas sensors, pigments and cosmetics [132, 133]. Specially, over the past decades, nanosize materials derived from TiO_2 like Titania nanotubes have extensively been investigated for vast applications, including solar cells/batteries, electroluminescent hybrid devices, photocatalysis, heterogeneous catalysis and electrocatalysis owing to their superior chemical and physical characteristics compared with conventional titanium oxides.

Moreover, the discovery of carbon nanotubes intrigued the intensive researches of one-dimensional nanostructures, such as nanotube, nanorod, nanowire, and nanobelts. TiO_2-based nanotubes, therefore, attracted extensive and engrossing interest, in spite of its crystalline structure still being controversial. TiO_2-based nanotubes with high specific

surface area, ion-changeable ability, and photocatalytic ability have been considered for extensive applications.

Nanoscaled TiO_2 is also widely used as the support of catalysts for the catalytic combustion of methane or sewage disposal [134, 135]. These properties are definitely dependent on its physical and chemical characteristics such as crystal structure, morphology and surface structure. The nanotube structure of TiO_2 seems to increase the dispersion of active materials and consequently results in the enhancement of capacitance. The tubular structure enhances the aspect ratio which favors the diffusion of reacting species. The large BET surface area, high stability and homogenous size distribution are helpful to increase the gas/liquid interfacial area. Therefore, as a support it can improve the catalytic activity for a certain reaction by increasing the surface area [136, 133]. However, TiO_2 nanotube is not very suitable for using as the support alone for the electrocatalysts because of its poor conductivity. Ways to increase the electrical conductivity are the metallization of the TNTs[137] and doping TNTs with suitable non-metals [138].

Titania nanotubes of different geometrical shapes and microstructures have been fabricated by various methods, like sol–gel, anodization, electrodeposition, sonochemical deposition, or other methods involving the chemical treatment of fine titania particles[139]. Referring to Hoyer et al TiO_2 nanotubes with diameters of 70–100 nm were produced through a sol–gel processing[140]. Imai et al.[141] fabricated titanium oxide nanotube arrays by anodic oxidation. Here the nanotubes had an inner diameter of 100 nm and the length of 200 nm. Kasuga et al.[142, 143] reported the first evidence that

titanium oxide nanotubes with the diameter of 8 nm and length of 100 nm could be obtained via chemical treatment. When TiO_2-SiO_2 powder produced by the sol-gel method was treated with an aqueous solution of 10 M NaOH for 20 h at 110°C and then treated with HCl aqueous solution and distilled water, nanotubes (anatase phase) with an inner diameter of 5 nm, an outer diameter of 8 nm, and a length of 100 nm were obtained. The nanotubes were also produced when TiO_2 granules (P-25, Nippon Aerosol, containing crystalline phases of anatase and rutile) were used as the raw material. Process for the synthesis of TNT is outlined in the Figure 2-5. Recently, it is shown that for TiO_2 nanotubes produced by the method of alkali hydrothermal treatment, the possible mechanisms of nanotube formation is based on the key stage of wrapping of intermediate multilayered titanate nanosheets. The driving force for wrapping is considered to be the mechanical stress arising during crystallization /dissolution.
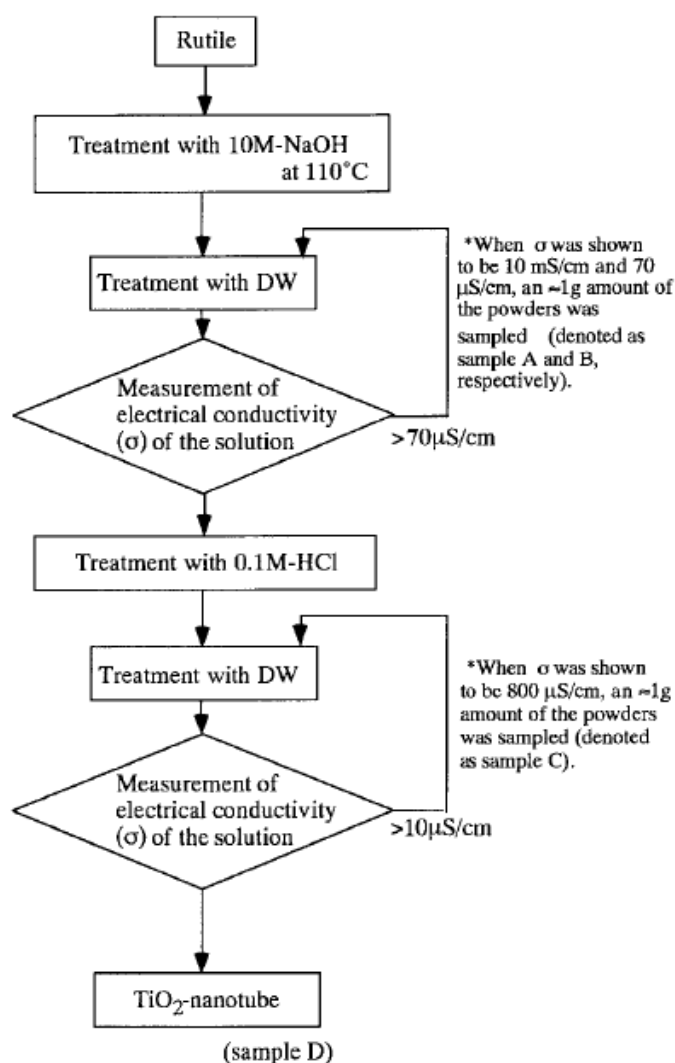
Figure 2-5: Preparation of Titania nanotubes from rutile adapted from Kasuga [143].

2.6 Electrochemical Reactors

The limiting problem with the electrochemical reduction of CO_2 is the low solubility of CO_2 in aqueous solution which limits the current density to 0.2 kAm^{-2} [144] and catalyst poisoning owing to solvent or electrolyte impurities. It required very high potential for

the reaction to take place. In other words, the reaction has high over potential. Efficient electrocatalyst are required to decrease the overpotential of the reaction. Several studies have been done on the electrocatalyst required for the electrochemical conversion of carbon dioxide at low overpotential and high current density. Other problem is that the solubility of the carbon dioxide is as low as 30 mM at 1 atm at room temperature, restricting the availability of carbon dioxide at the electrode. Thus, significant mass transfer resistance is encountered for the reaction to occur in an aqueous solution which considerably reduces the current density. Under moderate experimental conditions, the highest current density is limited to 20 mA/cm^{-2} or so for formation of CO or HCOO$^-$ for example. Such a low transport process must be improved by any means, if the reduction is utilized for a practical process. There have been several approaches to alleviate this problem of mass transfer limitation. Application of high pressure, non-aqueous electrolyte, using rotating electrode gas diffusion electrode and solid polymer electrolyte have already been employed in a good effect to alleviate the mass transfer related problem [87]. However, none of the method provides a satisfactory way of increasing the rate of mass transport of carbon dioxide to the electrode. Plausible methods are to operate the reaction at high pressure and to carry out the reaction in gas phase. In this section, various approaches to reactor design used in the literature for the electrochemical reduction of carbon dioxide are discussed.

Gas-diffusion electrode (GDE) is a porous composite electrode developed for fuel cell technology, usually composed of Teflon bonded catalyst particles and carbon black. The GDEs have been applied to CO_2 reduction by many workers, successfully enhancing the rate of the process.

Polytetrafluoroethylene (PTFE)–bonded gas diffusion electrodes were developed for overcoming the mass transport limitations in hydrogen-Oxygen fuel cells. These electrodes are both porous and hydrophobic and have structures which not only allows extensive utilization of the electrocatalyst but increase the three phase interface between gas, electrode, and electrolyte, the region in the electrode where the reaction proceeds. Hence they are capable of operating at high current densities at atmospheric pressure. Despite their well known use in fuel cells, they have not been extensively employed in other applications where maximum current density is severely limited by the low solubility of the gas in electrolyte.

The very first use of GDE for Carbon dioxide reduction was by Mehmood et al in 1987. Mehmood et al. carried out the electrochemical reduction of carbon dioxide to formic acid at lead, indium, and tin-impregnated, PTFE bonded, carbon gas diffusion electrodes in aqueous, acidic medium. Lead-impregnated electrodes operated at 115 mAcm^{-2} in an aqueous acidic electrolyte (pH 2) selectively produced formic acid with a current efficiency of nearly 100% at IR-corrected potential of approximately –1.8 V versus saturated calomel electrode (SCE). Electrodes impregnated with either indium or tin produced formic acid at rates comparable with those containing lead. However, in addition to formic acid, small quantities of carbon monoxide were also produced and the simultaneous production of hydrogen by the reduction of water was more significant. Thus, it was inferred that the electrocatalytic activity for the electrochemical reduction of carbon dioxide to formic acid is lead>indium ~tin[145].

Mehmood et al. used polytetrafluoroethylene-bonded, carbon gas-diffusion electrodes, prepared with carbon impregnated with metal phthalocyanine, for the electrochemical reduction of carbon dioxide in aqueous, acidic solution. High rates of reduction of carbon dioxide to carbon monoxide were demonstrated at electrodes impregnated with cobalt (II) phthalocyanine. In contrast, formic acid, and not carbon monoxide, was produced at low rates at electrodes impregnated with manganese, copper or zinc phthalocyanine. This marked variation in reaction product on changing the central metal ion of the organometallic complex is rationalized in terms of a reaction mechanism involving, as the first step, the electrochemical reduction of cobalt (II) to cobalt (I)[146].

Cook et al in 1987 published first of a series of papers on electrochemical reduction of carbon dioxide. In 1987, they reported the electrochemical reduction of carbon dioxide to methane using cold-rolled B370 CU cathodes(99.9%) in carbon dioxide saturated 0.5 M $KHCO_3$, at high current densities (Upto $38mA/cm^2$) where faradaic efficiencies of 33% were observed. In another work, copper was in situ deposited on glassy carbon electrodes which resulted into both high current density and faradaic efficiencies [147].

Furuya et al in 1989 used porous carbon gas-diffusion electrodes modified by 17 kinds of different metal phthalocyanines were used as electrocatalysts for the electrochemical reduction of carbon dioxide. The distribution and current efficiencies of the electrolysis products depend strongly on the nature of the central metal coordinated to the phthalocyanine. In the case of metal phthalocyanines with transition metals of Group VIII, the main electrolysis product was carbon monoxide: A current efficiency of ca. 100% was observed on Co and Ni phthalocyanines. On the other hand, formic acid was formed mainly on metal phthalocyanines with Sn, Pb or In, which belong to Group IIIB

or **IVB**. The highest current efficiency of ca. 70% was observed on Sn phthalocyanine around -1.6 V. In the case of Cu, Ga and Ti phthalocyanines, methane was the main product, the highest current efficiencies being 30–40%[148].

Cook et al in 1990 achieved a faradaic efficiency of 71.3% for gas phase reduction to gaseous hydrocarbon at current efficiency greater than 0.5 mA/cm^2 using electrolyte gas diffusion electrode[149].

Shwartz et al in 1993 tried Electrochemical reduction of CO_2 under ambient conditions to methanol, ethanol, and n-propanol is reported at perovskite-type A~.sA~.2CuO$_4$ (A = La, Pr, and Gd; A' = Sr and Th) electrocatalysts when incorporated into gas diffusion electrodes. In the absence of copper at the perovskite B lattice site, no activity was found. This investigation resulted in the identification of electrochemical conditions whereby perovskite-type electrocatalysts could achieve cumulative Faradaic efficiencies for CO_2 reduction to methanol, ethanol, and n-propanol up to 40% at current densities of 180 mA/cm^2[150].

These closely related observations imply that copper purity and morphology will be crucial for promoting high rate and efficient carbon dioxide reduction.

Sakata et al. employed GDEs purchased from Tanaka Noble Metal Co. under elevated pressure. The GDE, loaded with Pt catalyst, can reduce CO_2 at elevated pressure higher than 5 atm in 0.5 M KHCO$_3$, whereas the GDE scarcely reduces CO_2 at 1 atm. GDE without Pt catalyst is not active under 20 atm, and only HER takes place. Under 20 atm, CO_2 is reduced mainly to CH$_4$ with the current density of 600 mA cm^{-2} with the faradaic efficiency of ca. 50% for total CO_2 reduction at -1.93 V vs. Ag/AgCl. They further

studied Fe, Pd and Ag. The problem with regard to the transport process may be solved by some modified CO_2 reductions, such as electrolysis under high pressure[59, 151] gas diffusion electrode[146], and metal- coated ion exchange membrane electrode (occasionally called "solid polymer electrolyte" or SPE) [144, 47, 152-154, 111]. Among these devices SPE is a safe technology, employed under atmospheric pressure [144]. Ion-exchange membrane coated with porous catalyst metal can provide gas phase electro-reduction of carbon dioxide. The use of ion-exchange membrane as electrolyte medium is convenient so as to limit cross over, resulting in a decrease in current efficiency of the electrochemical cell. The SPE electrodes were applied to CO_2 reduction as previously reported by some workers.

There are two components of such SPEs. The ion-conducting membrane and elctrocatalyst coating. Issues related with the design and selection of an efficient elctrocatalyst for ECR has already been discussed in the previous sections (2.1 & 2.3). In this section mainly the membrane base will be discussed.

Polymer electrolyte membrane (PEM) is recognized as the key element for an efficient ERC system. There are basically two types of membranes used for ERC applications. One is cation exchange membranes (CEM) and anion exchange membrane (AEM). Recently, proton conducting per fluorinated ionomers based DuPont Nafion® has been used as a membrane material. Although many new membranes have been tried with the PEM fuel cells, no other membrane has been tested in ERC.

Maeda and co-workers used a cation exchange membrane (CEM) (Nafion 315) coated

with Au as the electrode metal. The reaction product was CO, but the current density of CO_2 reduction was much lower than that obtained by a conventional electrolysis using an Au plate electrode. The low current density is probably due to poor electric contact of Au particles on the SPE electrode [155].

DeWulf et al prepared a Cu SPE electrode using a CEM (Nafion 115). Their measurements of CO_2 reduction with 1 mM H_2SO_4 as the electrolyte solution (counter solution) gave a total current efficiency of 19% as a maximum with much lower partial current than the value obtained by a bulk Cu metal electrode. Nafion was in contact with an aqueous solution of H_2SO_4 at the anode side, and increasing the concentration of H_2SO_4 led to the decrease of the Faradaic efficiency for CO_2 [152].
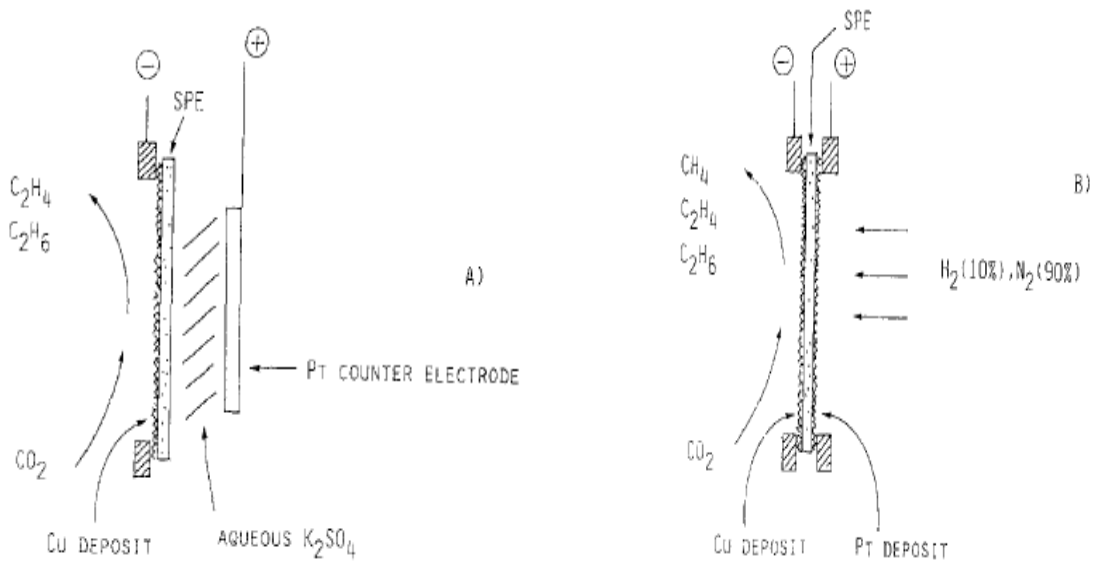
Figure 2-6:Schematic of the Solid polymer electrolyte cell with (A) aqueous electrolyte (B) hydrogen in anode side [149]

Cook et al. reported CO_2 reduction with a Cu-deposited CEM (Nafion 117). The maximum current .density was 0.30 kAm^{-2}, and the current efficiency of C_2H_4 formation was less than 6.5%. They also investigated various metals containing Ag as the electrode metal of SPE . They reported that none of the electrode metals they tested showed high electrocatalytic activity for CO_2 reduction [149]

Komatsu et al. compared Cu-coated SPEs prepared from a cation exchange membrane (Nafion 117) and an anion exchange membrane (Selemion AMV).This was the first time AEM was used for ERC applications. They showed that the maximum partial current density of CO_2 reduction was less than ca. 0.013 $kA\ m^{-2}$for both SPE electrodes with the electrolyte solution of 0.5 M K_2SO_4. The major reaction product was C_2H_4 for the SPE with the AEM, and HCOOH for the SPE with the CEM. The SPE from Nafion 117 formed C_2H_4 as the product with the maximum partial current 0.02 $kA\ m^{-2}$at -1.8 V vs. SCE. Both the SPE retained stable electro activity in CO_2 reduction for 5 h [111].

Kunugi and Yumiyama also reported CO_2 reduction at Bi-coated SPE electrodes. The product from CO_2 was mainly HCOOH with slight amount of CO. The maximum partial current density of CO_2 reduction was 0.18 $kA\ m^{-2}$at -1.9 V vs. SCE [144].Hori and co-workers used Silver-coated ion exchange membrane electrodes (SPE) were prepared by electroless deposition of silver onto ion exchange membranes. The SPE electrodes were used for CO_2 reduction with 0.2 M K_2SO_4 as the electrolyte with a platinum plate (Pt) for the counter electrode. In an SPE electrode system prepared using Nafion-117 as cation exchange membrane (CEM), the surface of the SPE was partly ruptured during CO_2 reduction, and the reaction was rapidly suppressed. SPE electrodes made of an anion

exchange membrane (Selemion AMV). (SPE/AEM) sustained reduction of CO_2 to CO for more than 2 h, whereas, the electrode potential shifted negatively during the electrolysis. The reaction is controlled by the diffusion of CO_2 through the metal layer of the SPE electrode at high current density. The partial current density of CO_2 reduction by SPE/AEM amounted to 0.60 kA m^{-2} i.e. three times the upper limit of the conventional electrolysis by a plate electrode [144].

Delacourt and co-workers in their work to produce syngas from ERC proposed four different cell configurations each employing pure unsupported silver (Ag) as cathode catalyst and unsupported Pt-Ir as anode catalyst both anodes and cathodes were designed so that the loading of catalyst in the catalyst layer was close to 8–10 mg/cm^2. The catalyst layer had fixed proportion with acetylene black carbon and a polymer. (the selection of which depends on the cell configuration) In the first configuration the electrochemical reactor was operated similar to the fuel cell type configuration. For the cation exchange membrane (CEM) (Nafion-117), a 5 wt % solution of perflourosulfonic acid–poly tertaflouroethylene co-polymer was used. No gaseous CO_2 reduction product was detected and current efficiency for hydrogen was 100% at a current density of 0.2 kA m^{-2}. The reason cited was that the acidity of the Nafion membrane is likely to shift the cathode selectivity towards hydrogen evolution. In the buffer-layer type cell a buffer layer of aqueous $KHCO_3$ was introduced between cathode catalyst and CEM. This layer of thickness 800 μm is made of an inert support (glass fibers) impregnated with an aqueous $KHCO_3$ solution (0.5 mol/L).A large increase in the selectivity for the CO evolution over the fuel cell configuration was observed, with a CO efficiency of 82% and H_2 efficiency of 10-15% was observed. In the cell structure with anaion exchange membranes (AEM),

polyethersulfone based membrane was used as AEM. Although the current efficiency for CO was very low compared to the buffer layer configuration, is still larger greater than the fuel cell like configuration. The final configuration was to use Nafion membrane in the K^+ form and therefore, aqueous solutions containing potassium ions needed to be circulated at both electrodes. KOH and $KHCO_3$ were used as anolyte and catholyte respectively. The CO efficiency was around 40 % [70].

Although strictly speaking not lying in the category of SPE, yet some relevant works were done using membrane as an integral part of the ERC system. Those works are summarized in the Table 2-8.

Li and co-workers reported the investigation of ERC in a continuous rector with co-current flow of reactant gas and catholyte liquid through a flow-by 3D cathode of 30# mesh tinned-copper. Although they did not use SPE but they used Nafion 450 as cation exchanged membrane separator [21]. Subramanian et al. employed filter press type membrane flow reactor at constant current density for electrochemical conversion of CO_2 to formate. For this purpose they used Nafion 961 and Nafion 430.Maximum current efficiency of 93% for formate formation was obtained [117].

Whipple et al studied electrochemical reduction of CO_2 on carbon-supported Ru–Pd in microfluidic. The use of gas diffusion electrodes enables better control of the three-phase interface where the reactions take place. Furthermore, the versatility of the microfluidic reactor enabled rapid evaluation of catalysts under different operating conditions. Operating at acidic pH resulted in a significant increased the performance: faradaic and

energetic efficiencies of 89 and 45%, respectively, and current density of 100 mA/cm^2[115].

Table 2-8: Membranes Used for ERC.

Membrane/Catalyst	Major product	Refrence
Nafion-117+Cu	Methane, Ethylene, Ethane.	[153]
Nafion®417 and Nafion®117 Ni,Ru,Rh,Pd,Ag,Re,Os,Ir,Pt,and Au	Various products	[47]
Nafion 315+Au	CO	[155]
Nafion 117 and an anion exchange membrane +Cu	C_2H_4 for the SPE with the AEM. HCOOH for the SPE with the CEM.	[111]
Bi-coated	HCOOH	[144]
(Nafion 117) and an anion exchange membrane+ Ag	CO	[144]
Nafion-117 as CEM Nafion-117 in the K$^+$ form. polyethersulfone based membrane as AEM	CO+H$_2$	[70]

Many electrochemical cell designs for ERC have been described in the literature. The earlier ones used in ERC were mainly H-type electrolytic cells with flat metal electrodes. Later many modifications appeared

Li et al. described the ERC in a laboratory bench scale continuous reactor with co-current flow of reactant gas and catholyte liquid through a flow by 3D cathode of 30 $^\#$ mesh tinned copper factorial and parametric experiments were carried out in this apparatus with the variables: current (1–8 A), gas phase CO_2 concentration (16–100 vol.%) and operating time (10–180 min), using a cathode feed of $[CO_2 + N_2]$ gas and 0.45 M $KHCO_3$(aq) with an anolyte feed of 1 M KOH (aq), in operation near ambient conditions (ca.115 kPa (abs), 300 K). The primary and secondary reactions here were respectively the reduction of CO_2 to formate ($HCOO^-$) and of water to hydrogen, while up to ca. 5% of the current went to production of CO, CH_4 and C_2H_4 kWh/kmol, space-time yield of $HCOO^- = 2\times10^{-4}\text{-}6\times10^{-4} \text{kmol/m}^3 s$, conversion of CO_2 = 20–80% and yield of organic products from CO_2 = 6–17% [75].

In a recent article by Delacourt et al. described four alternate cell designs for ECR to mainly produce methanol via syngas ($CO+H_2$) at room temperature (25 degree centigrade). The design was based on the technology very close to that of proton exchange membrane fuel cells (PEMFC).The electrodes used were gas diffusion electrodes so as to achieve high current densities. A cell configuration involving proton-exchange membrane (Nafion) was shown to be unfavorable for ERC. When a design based on insertion of pH-buffer layer (aqueous $KHCO_3$) between the silver-based cathode catalyst layer and the Nafion membrane allows for a great enhancement of the cathode selectivity for CO_2 reduction to CO [ca. 30 mA/cm^2 at a potential of -1.7 to -1.75 V vs SCE (saturated-calomel reference electrode). A CO/H_2 ratio of 1/2, suitable for methanol synthesis, is obtained at a potential of ca. -2 V vs SCE and a total current density of ca. 80 mA/cm^2. An issue that has been identified is the change in product selectivity upon

long-term electrolysis. Results obtained with two other cell designs are also presented and compared [70].

2.7 Electrode Design

Due to the low solubility of CO_2 in aqueous solution the current density of ERC is typically limited by the mass transfer of CO_2 from the bulk catholyte to the electrode surface. In this context, various types of 3-D electrode with three-phase (G/L/S) operation have been used for ERC. They are introduced in the following paragraphs:

2.7.1 Gas Diffusion Electrode (GDE's)

Gas diffusion electrodes, based upon PTFE (polytetrafluoroethylene) as a binder, have been developed to overcome mass transport limitations with gaseous reactants in fuel cells. When employed in ERC, GDE's operated in batch mode, provided much higher superficial current densities than those obtained with 2-D metal plate electrodes [71, 156, 157]. For example, Hara et al. obtained a current density of ERC of about 1.51 kA m^{-2} with a CE of 76 % for CO at 3000 kPa (abs) with Ag wire cathode (1.6 x10^{-5} m^2 geometric surface area) in 1995[41], then achieved a superficial current density of 2.58 kA/ m^2 and a CE of 86 % for ERC at 2000 kPa (abs) with Pt-GDE cathode (1 x10^{-4} m^2 geometric surface area) in 1997[157]. Mahmood et al. reported nearly 100% current efficiency using Pb, In and Sn impregnated GDE's for ERC to produce formic acid in a pH range of 1-5, a current density of 1.15 kA m^{-2} at ambient pressure and temperature, with a sodium sulfate catholyte whose pH was adjusted by sulfuric acid[71]. Again simultaneous reduction of carbon dioxide and nitrogen dioxide was examined by using gas diffusion electrode with Cu, Ag, and Au catalysts. The maximum efficiency of urea

formation at Cu, Au, and Ag were observed to 37%, 26% and 38% in the range of -0.75 to -3.0 V (SHE), respectively [83].

2.7.2 Fixed-bed Electrode

The ERC was carried out by Koleli et al. in 2004 [158] in an undivided fixed bed reactor where Pb and Sn granules (1 mm and 3 mm diameter, respectively) were placed at the bottom of the reactor as cathode material. Batch mode operation was employed with CO_2 gas bubbling up through the bed under ambient conditions. Only one product, formic acid, was supposedly produced, with the maximum current efficiency of 90% at a superficial current density of 0.008 kAm^{-2}. A subsequent publication [117] describes a similar fixed-bed batch reactor, with pressure and temperature respectively up to 50 bar and 353 K, in which CO_2 was reduced to formic acid with a current efficiency about 90 % at a superficial current density of 0.02 kAm^{-2}, The actual product was probably potassium formate, since HCOOH (pKa = 3.8 at 298 K) should not exist at significant concentration in the catholyte used (0.5 M $KHCO_3$ (pH 6-8) and 0.2 M K_2CO_3 (pH 11-12).

2.7.3 Mesh Electrode

Yano et al. performed ERC in a batch reactor at the 3-phase (G/S/L) interface on Cu and Pt mesh electrodes [73, 159] at ambient pressure and temperature. In this system CO_2 was supplied to the electrode from the gas phase by bubbling CO_2 through the mesh, aiming to maintain a high concentration of CO_2 at the cathode surface. The maximum total CE of 83 % for ERC (10 products) was obtained with Cu mesh at a superficial current density

of about 0.05 kAm^{-2}, using a catholyte of 0.5 M KCl +HC1, whose initial pH was 2.2 [159].

2.7.4   Electrolyte for ERC.

Because of the influence of the solvent on the nature of the products, there have been two main routes for CO_2 electro-reduction based on whether the catholyte is aqueous or non aqueous. Aqueous media have long been a popular selection for ERC research because the water provides a proton source, and aqueous electrolytes have typically much higher electric conductivity than that of non-aqueous electrolytes. A lot of studies have been done in aqueous media on almost all the electrodes described in Section 2.4, with a variety of electrolytes (see Section 2.4). The solubility of CO_2 in aqueous electrolytes is relatively low but can be increased by organic additives. Kneko et al. reported that by adding 10 vol % propylene carbonate into an 0.5 M KC1 catholyte, the maximum total current efficiency of ERC (multi-products) was increased from 50 to 75 % as a result of enhanced CO_2 solubility[97].

Non-aqueous media present certain advantages for CO_2 reduction, namely, higher CO_2 solubility than that in water, the suppression of H_2 evolution, and the possibility to work at low temperature, e.g., below the freezing point of water. The DMF (N, N-dimethyl formamide), DMSO (dimethyl sulfoxide) or AN (acetonitrile) are some of the solvents for non-aqueous media [83]. But the most potentially useful results have been reported in methanol with various solid metal electrodes [160, 68, 161]. Methanol has been industrially used as a physical absorber of CO_2 (the Rectisol method). Until 1998, more than 70 large-scale plants for the Rectisol process had been established [17]. Thus, the

study on CO_2 reduction in methanol provides valuable information on the direct utilization of the industrial methanol-based CO_2 absorber medium as the solvent for the electro-reduction process. Although the main products from CO_2 reduction in non-aqueous media have been found to be quite similar to those in aqueous media, i.e., carbon monoxide, oxalic acid and formic acid, the reaction mechanisms can follow pathways different from those in aqueous media[162]. The electrolytes used in non-aqueous system are different from those in aqueous media. KOH and $TBABF_4$ (tetrabutylammonium tetrafluoroborate) were both employed as the electrolyte for non-aqueous media, but the latter was more frequently used.

The electrolyte (catholyte) composition affects the solubility of CO_2, the electrode double-layer, the specific adsorption of reactants and intermediate species, and thus the product distribution and current efficiency of ERC[38]. A variety of combinations of alkali metal cations and various anions, such as PO_4^{-3}, HCO_3^-, SO_4^{--}, ClO_4^-, HPO_4^- have been used as the electrolyte in aqueous media for ERC. As for the effect of cations, Hori et al. [163] report that the formate current efficiency increases in the sequence Li<Na+<K+ on Hg, but the reverse sequence is observed by Ito et al. [63] on an In cathode. With respect to the electrolyte anions some authors imply a unique role for carbonate/bicarbonate [63, 83] while others Hori et al [164] claim that among carbonate, phosphate, acetate and borate the partial current for formate production is independent of the buffer anion on Hg and In cathodes. Analogous cation and anion effects on reaction selectivity are observed in the electro-reduction of CO_2 to CO and hydrocarbons on copper [163].

Apart from the effects of the electrolyte, the effects of the composition and pH of the electrolyte have been studied. Most authors prefer $KHCO_3$ (ca. 0.5 M) with pH 6-8[68, 41] but others have excellent results in Na_2SO_4 at pH 2 [71]and some claim good current efficiency in a catholyte of K_2CO_3, whose normal pH would be near 12 [158].

2.7.5 Pressure, Temperature and Current density

Operating ERC at high pressure takes advantage of the increased solubility of CO_2 in aqueous solution. Some sources indicate that the rate for reaction is nearly independent of CO_2 pressure but most workers show that larger current densities for ERC are achieved with increasing pressure, reflecting a reaction order near 1 with respect to CO_2 (aq) [41].

The effect of temperature is not consistent in the literature of ERC, probably due to the fact that increasing temperature lowers the solubility of CO_2 while raising the exchange current densities for the cathode reactions. One source [165] shows a twenty fold increase in current density as the temperature rises from 275 to 333 K, without comment on the selectivity. Another [158] shows a monotonic increase in formate faradic efficiency on Pb, with increasing temperature (298 - 353 K), while a third [68] indicates a parabolic effect of temperature on a Pb cathode, together with monotonic decrease in formate CE on In and Sn over the range 293 - 373 K.

Increasing current density typically lowers the CE of ERC by an effect that may be attributed mainly to CO_2 concentration polarization. However some data on Sn as well as results from experiments on Pb at 5000 kPa (abs) CO_2 pressure imply a parabolic dependence of formate CE on current density with a maximum CE at about -1.5 V(SHE)[158].

69

2.8   Membrane Electrode Assembly (MEA)

The MEA is heart of any electrochemical system, where the electrochemical reactions take place either to generate electrical power in PEMFC or for carrying out reaction by applying power in solid polymer electrolyte membrane reactor (SPE). A typical MEA consists of two gas diffusion layers (GDLs), two dispersed catalysts layers, and a membrane. Each component of an MEA performs unique role. The GDLs have many roles to play. As the name implies, the main purpose of the GDL is to distribute the reactants from flow channels uniformly along the active surface of the catalyst layer. In addition, the GDL ensures proper transport of the liquid product, electron and heat. The GDL assists in water management by allowing an appropriate amount of water to reach, and be held at the membrane for hydration on the anode side, especially if the anode has is dry gas in fuel cell. While on the cathode side, the water that forms must be easily repelled from the catalyst surface to prevent flooding. If water collects near, or in, the catalyst layer, a large fraction of the catalyst will not be utilized. Typically, PTFE is applied through various methods to the GDL in order to manage water. However, PTFE is not an electric conductor and reduces the porosity, which hinders the transport of the reactant gases. Thus, appropriate amount of PTFE should be used carefully. The GDL provides the electrical contact between the current collector bipolar plates and the catalyst layers. Thus, a thin GDL with a high conductivity is desired for electrical efficiency. Furthermore, the GDL serves as the base substrate for the deposition of the catalyst layer or forms a protective layer over the very thin layer of the catalyst.

The GDLs are usually constructed from porous carbon paper, or carbon cloth, with a

thickness in the range of 100-300 μm. The in plane and the through plane resistivities of

the commercial GDLs are in the range of 25-100 mΩcm^{-2} and 6-20 mΩcm^{-2} respectively[166]. The in-plane and the through–plane resistances depend on the microstructure of the GDL. The in-plane resistance affects the reactions uniformity while the through-plane resistance dictates the cell resistance. To improve the mass transport, GDLs can be made more porous at the cost of increased electrical resistance. Critical parameters that affect the performance of the GDLs include the PTFE content, thickness, pore size distribution and microstructure.

The performance of an MEA depends critically on the activity of the anode and cathode electro catalysts. The procedure and method for the preparation of the MEA play an important role in the distribution, efficiency and electrocatalytic activity of the electrocatalysts, with direct consequences to the SPE reactor.

2.8.1 Conventional Method of MEA Preparation

A mixture was prepared consisting of Pt/C catalyst, solvent (mixture of water and iso-propanol) and Nafion (5 wt % solution from DuPont). The ratio of Pt/C to Nafion is kept around 7:3. An Ink was prepared and painted on the uncatalysez gas diffusion electrode and sintered in a vacuum oven at 90°C for 30 min. The catalyst loading was obtained by weighing the MEA before and after applying the catalyst ink and drying in the oven. The MEA was fabricated by uniaxially hot pressing the anode and the cathode onto a pre-treated Nafion 115 (in H$^+$ form) at 130°C for 2 min [167] .
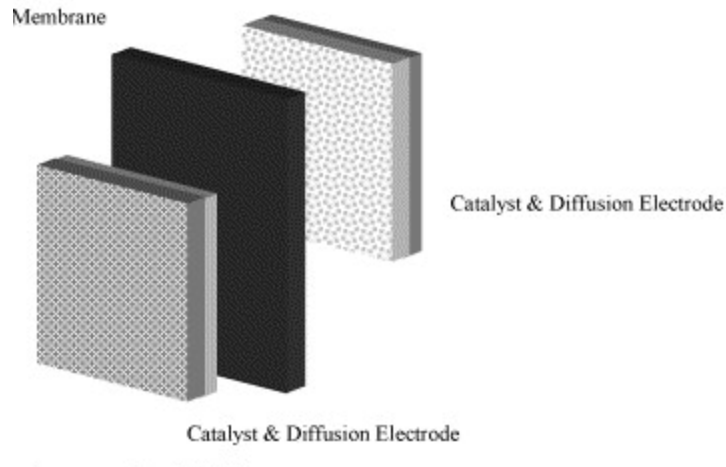
Figure 2-7: Conventional method of MEA fabrication

2.8.2 Decal Transfer Method of MEA Preparation

Song et al. (2005) studied the effect of electrode preparation procedure, the structural properties of membrane electrode assembly (MEA), and investigated how this affects the performance of DMFC[14]. Commercial Pt-Ru anode catalyst and Pt cathode catalyst was used. They prepared the MEA using decal transfer method (DTM). It was found that catalyst ink preparation and high temperature transfer process are the key factors affecting the particle size of Pt black catalyst. It was also found that the maximum power density of the single DMFC using a MEA fabricated by DTM, when air is used as oxidant, is more than two times greater than that of the cell using conventionally prepared MEA, and more than three times greater than when pure oxygen is used as oxidant. Using DTM method of catalyst layer deposition, one can obtain better mass transfer due to thinner catalyst layer. The method of incorporating catalyst layer on the membrane, in this case Nafion 115, by Decal transfer process is explained as follows.

72

The pretreatment of Nafion$^®$115 is accomplished by successively boiling the membrane in 5 % H_2O_2, deionized water, 0.5 MH_2SO_4, and then the deionized water again, for one hour each. The Nafion$^®$115 membranes in the H^+ form is converted to Na^+ form by slightly boiling them in 0.5 M NaOH aqueous solution, deionized water for one hour each. Catalyst ink was prepared by wetting the calculated amount of catalysts with water, followed by dispersing the catalysts ink in ethanol and finally adding the calculated amount of 5% Nafion solution. The soluble Nafion is converted into the Na^+ form by adding an appropriate amount of NaOH aqueous solution. The solution is well stirred in ultrasonic bath, and mechanical stirring is also done. Appropriate amount of anode and cathode inks are then uniformly sprayed by a spray gun to teflon decal blank with a given area. The catalyst coated membrane (CCM) is obtained by transferring the catalyst films from the Teflon films to the membrane by preheating at 160-120°C for 1 minute to remove water from the electrolyte membrane and then hot pressing at 160-200°C and 100 psig for 1.5 minute. Finally, the complete protonation of the CCM is obtained by immersing the CCM it in 1 N H_2SO_4 aqueous solution for 2 hours and then rinsing it in the deionized water for 1 hour at 80°C. The CCM is then sandwiched between diffusion layer and inserted into the SPE reactor [14].
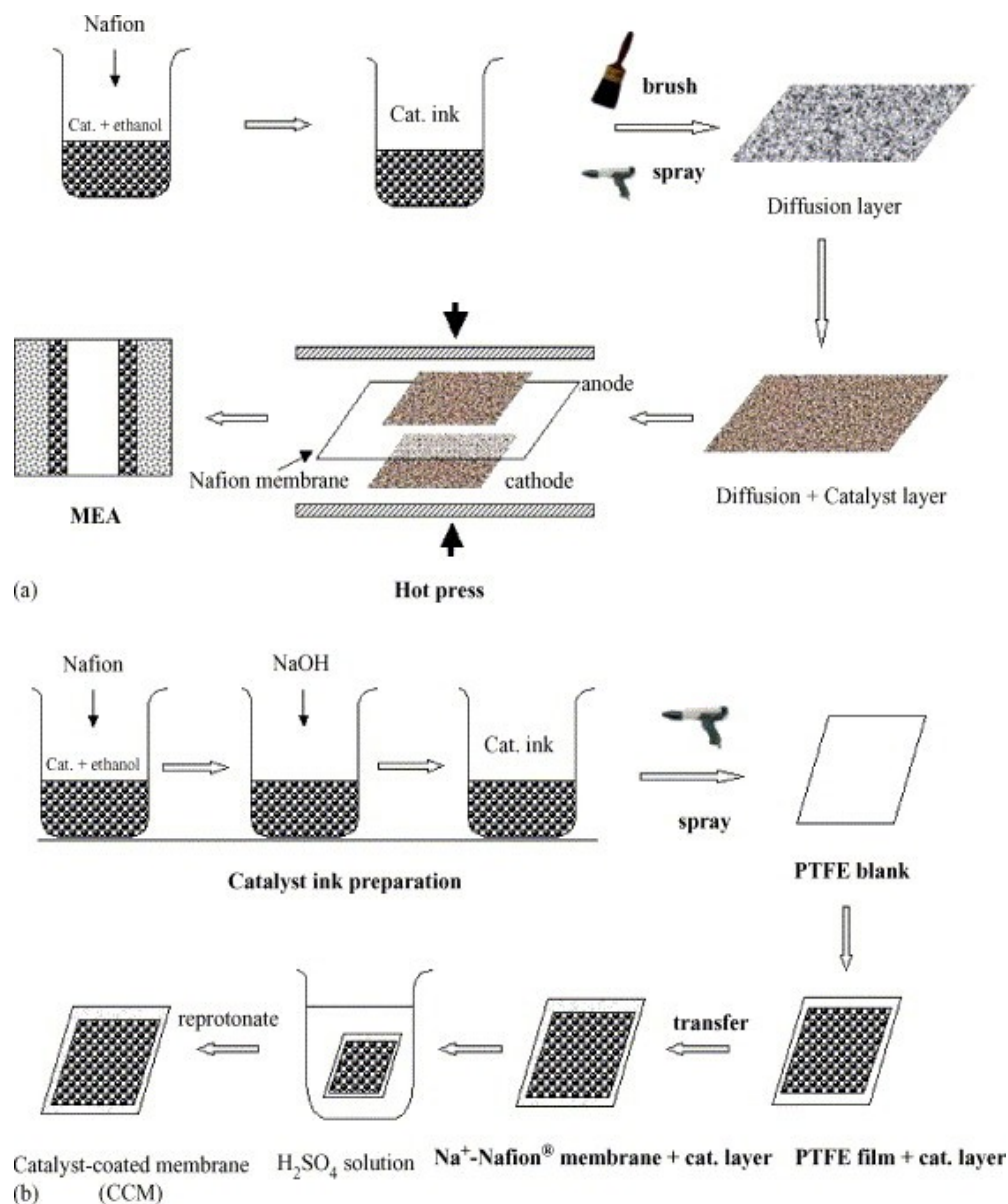
Figure 2-8: The schematically detailed electrode preparation procedure of the conventional method and the typical decal transfer method.

2.8.3 MEA Preparation by Modified Film Method

Xiong and Manthiram prepared high performance membrane electrode assemblies with ultra low Pt loading by a modified thin film method [167]. Commercial Pt/C (20 wt .% Pt on carbon Alfa Aesar). Nafion® solution (5 wt. % solution from Dupont) and deionized

water was mixed to prepare the catalyst ink. The ratio of Pt/C to Nafion® was 7:3 as this represents the best performance as reported in the literature[168] . To prevent any catalyst burning that may occur when the catalyst was added, these were first wetted with small amount of deionized water.

Then Nafion® solution was added in proper ratio and stirred for a few minutes. This was diluted with some deionized water followed by ultrasonic blending for 40 minute, and stirring for 30 minute thereafter. This gave a viscous mixture in which the solid material did not separate from liquid easily. This prepares the catalyst ink which had to be kept under continuous stirring before applying onto Nafion®115 membranes. The Nafion® membrane were pretreated with 5% H_2O_2 solution for 1 hour and then in 0.2 M NaOH solution. Then this was washed with deionized water and dried under vacuum at 60°C for about 15 minute. Then the catalyst ink was applied on the Nafion® membrane by painting a layer on its one side. This was followed by heating under vacuum at 80°C for 1 hour to dry the ink. Then the opposite side of the membrane was also coated in the same manner to get the anode and the cathode with the electrolyte membrane in between. No other organic solvent was used in this method of MEA preparation as this causes swelling effect. The catalyst loading were obtained by weighing the MEA before and after applying the catalyst ink and drying in the oven. The catalyzed membranes were then hydrated and made into protonic form by immersing them into light boiling 0.5 M H_2SO_4 for about 2 hour. Uncatalyzed gas diffusion electrodes were used diffusion backing for the thin film catalyst layer. So this method of MEA preparation was simpler and more and more economical with Pt loading at both the electrodes to be as low as 0.05 mg/cm^2.

2.8.4   Other Methods of MEA Preparation

Chen et al studied a manufacturing process for electrocatalyst layers [169]. Systematic study was done for an optimum performance of MEA in a DMFC by controlling each physical parameter such as electrocatalyst loading at each electrode, electrocatalyst compositions, and layer thickness, and varying the methanol concentration. The anode ink was made by mixing 40 % wt. %Pt-20 % wt. Ru catalyst supported on carbon black, with 60 wt. % Pt-30 wt. % Ru catalyst and a fixed amount of 5 wt.% Nafion$^®$ solution. The cathode ink was prepared by mixing 60 wt. % Pt/carbon black, 100 wt. % water, and a fixed amount of 5 wt. % Nafion$^®$ solution. These were vigorously stirred to give paste or catalyst ink to be applied on the Nafion$^®$117 membrane. A thin layer electrode was applied on each surface of the membrane by screen painting with the prepared catalyst, after cleansing the membrane. Then the MEA consisting of the electrocatalyst layers, the membrane were hot pressed at 120°C, and 5-30 kg/cm^2 for 2 minutes, the electrode area of the MEA was 4 cm^2. The assessment of the optimum content of the electrocatalyst loading was done by varying the Pt loading at the cathode, keeping the Pt-Ru loading at the anode constant, and vice versa. On testing these MEAs it was found that the power density is more influenced by Pt loading than by Pt-Ru loading. Also the increase in electrocatalyst concentration may slightly increase power density, but considerably decrease the specific power density for a given layer thickness. The maximum power density declined as the methanol concentration was increased from 3 to 9 wt. % at low Pt loading. The curve gently falls with increasing methanol concentration and then turn upward when Pt loading is raised from 1.2 to 4.0 mg/cm^2 and then 10.5 mg/cm^2.

Kim et al. prepared a novel structure of membrane electrode assembly for direct methanol fuel cells [170]. He studied composite membranes with low methanol crossover and diffusion with hydrophilic nano-particles for use in the MEA structure. The catalysts used were Pt-Ru, with surface area of 80 m^2/g on the anode side, and Pt, with surface area of 20 m^2/g on the cathode side. The polymeric membrane of 50μm was prepared by solution casting method. The catalyst layer was prepared by squeezing method. The catalyst were first mixed with deionized water, followed by addition of iso-propanol and Nafion $^®$ solution (5 wt. %). The slurry was sonicated for 120 minutes after mechanical stirring. The slurry ink was coated on the catalyst support layer made of Toray plain paper. The loading of Pt-Ru and Pt on the catalyst support were 8 mg/cm^2. Nano silica of 4-5 nm and ordered mesoporous silica (OMS) of 300 nm in size with 10-20 nm pores were used as constituents of diffusion layers. The anode diffusion layers was sprayed on the carbon backing layer with nano-silica particles and the polyvinyl fluoride (PVDF) mixtures whose weight ratio was 7:3. Mixture of carbon particles (Vulcan XG72) and polytetrafluoroethylene (PTFE) was first sprayed on the carbon backing layers with the loading of 2 mg/cm^2 carbon base for the cathode diffusion layer. Then these mixtures were sprayed on the anode and the cathode diffusion layer. The backing layer was SGL plain paper and Toray$^®$ 090 (40 wt. % PTFE) is used as the cathode backing layer. The layers were hot pressed for 1 min at 1 ton and then 3 min at 2.2 tonnes at 125°C. The water back diffusion through the membrane can be enhanced by hydrophilic anode diffusion layer and hydrophobic cathode diffusion layer. Now the water concentration at the cathode can be decreased by making cathode diffusion layer hydrophilic. Therefore, the cathode diffusion layer should be both hydrophilic and hydrophobic. Taking this conflict into consideration, Kim et al used two sub layers as cathode diffusion layer. The

first layer was hydrophobic to decrease hydraulic pressure through the membrane, and then second layer is hydrophilic which would decrease water concentration.
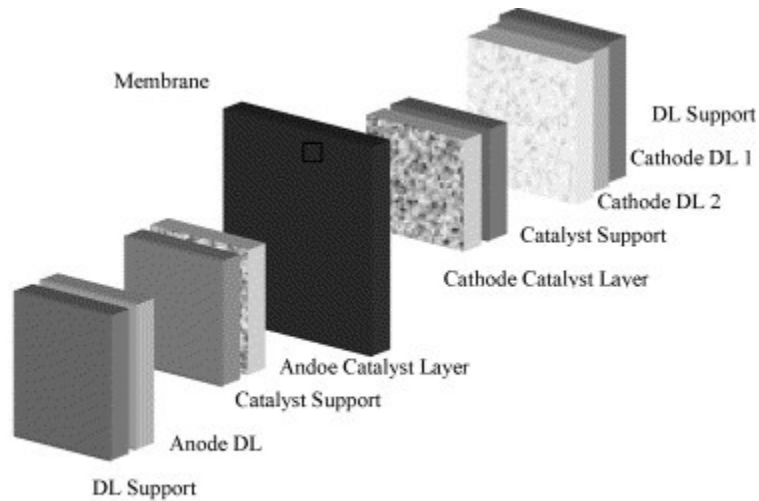
Figure 2-9: Novel Method of MEA Structure

Li et al. described a method MEA preparation. They used carbon electrodes with 2 mg/cm^2 Pt (20 wt. % Pt/VXC72) from the electrochem Inc. (USA). After the electrodes were cut into desired size, ionomers dispersion on its surface was done with the help of Nafion (5%) dispersion type of DE-521. This type of dispersion contains 5 wt. % polymer content, around 45% water and balance organic content. Then it was dried for 2 h at 80°C. The ionomer dispersion coating on the electrodes was about 0.8 mg/ cm^2. Ionomer dispersion was also done on the PEM and then dried at room temperature for 30 minutes. The MEAs were then pressed at 110°C under 8 MPa for 3 minutes [171].
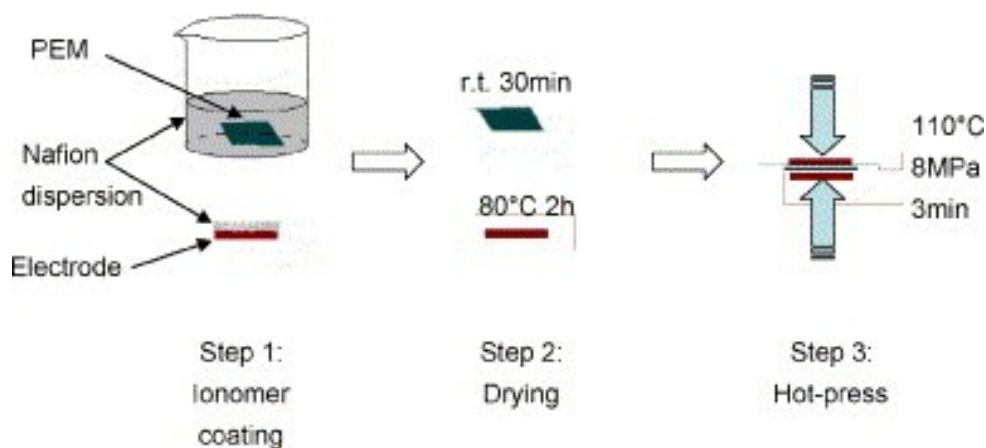
Figure 2-10: Novel method of MEA Preparation

2.9   Catalyst Activity Evaluation

Reaction rates for these processes can be estimated from the steady-state limiting current in cyclic voltammetry, or by rotating disk voltammetry studies of the heterogeneous electron transfer kinetics. The electro catalytic activity can be observed easily in cyclic voltammetry (CV). In a CV under a dry inert atmosphere, an elctrocatalyst should show a reversible redox couple. Upon addition of CO_2, the diffusion limited current should increase significantly, while the potential shifts anodically, and the reversibility in the return oxidation wave is lost due to the chemical reaction between CO_2 and the electrocatalyst.

2.10 Research Objective

The objective of this dissertation work is to develop new catalysts and design of a solid polymer electrolyte membrane reactor for electrochemical reduction of carbon dioxide (ERC).

1. To functionalize multi-wall carbon nanotubes (CNT) and synthesize Titania nanotubes (TNT) support material.

2. To characterize the prepared support materials using SEM, FTIR, TEM, XRD and BET.

3. To synthesize ERC electrocatalyst using active metal species Cu, Ru, Pd and Fe deposited on CNT and TNT support.

4. To characterize the as synthesized catalyst by SEM, TEM, XRD, FTIR and BET.

5.   To study the electrocatalytic activity of the electrocatalysts using linear sweep voltammetry (LSV) and chronoamperometry (CA).

6. To design a SPE system for ERC.

7. To evaluate the performance of new catalyst in SPE for ERC.

2.11 Strategies and Scope of the Present Work Objective

The reviewed literature shows the amount of work done in this area has been tremendous and has recently picked up more pace reflected by the surge in the number of publications. The research of ERC is still at a stage of fundamental investigations on mechanisms and kinetics using tiny electrodes (e.g. 1×10^{-4} m^2) with little consideration of the possibility for practical application. From the detailed literature review it is evident that there is a lot of R&D has been done in this area and lot more to be done on ERC to bring it to practical application. Such work embraces stepping form the small batch cells to a continuous reactor. The reported literature has in depth information about the elctrocatalyst and its impact on ECR research on the engineering aspects of ERC should be initiated to bridge the gap between the previous laboratory work and industrial reality. The general objective of the proposed work is to develop a new system for ECR that can provide both acceptable efficiency and the possibility for practical application in a continuous industrial process for production of hydrocarbons (such as methanol and methane). Our purpose in this research are twofold, one to come up with a novel elctrocatalyst for ECR and then design a continuous solid polymer electrolyte reactor to remove the mass transfer limitation to increase the current density from the common range of 0.01 -0.02kA/m^2 to 1kA/m^2. This research will aim to achieve high conversion of CO_2 at high energy efficiency at high selectivity of the desired product. The main underlying philosophy of this work is to reduce CO_2 with high selectivity, high energy efficiency, and high reactivity.

CHAPTER 3

EXPERIMENTAL METHODS

From the critical analysis of the literature, it has been found that the active metals, support materials and morphology determine the activity of the electrocatalyst as well as product selectivity for ERC. Moreover, the reactor system also has impact on the current efficiency as mass transfer plays an important role. To achieve the stated objectives of this research work, experiments were designed and performed. In this chapter, experimental procedure for catalysts synthesis and their physical as well as electrochemical characterization are discussed in details.

3.1 Materials

Copper nitrate trihydrate, copper acetate monohydrate, ruthenium chloride, palladium chloride, iron nitrate monohydrate and sodium hydroxide were purchased from Merck®, Germany. Unfunctionalized 95% pure CNT was purchased from Cheap Tubes Inc.®. Titanium oxide, in anatase form, was provided free of cost as compliment from Crystal Global®, France. Nafion® membrane and 5 % Nafion® solution were purchased from Sigma Aldrich®, analytical grade sodium bicarbonate was purchased from VWR® international. All other solvents were purchased from Sigma Aldrich®. All chemicals were used as received, without any further treatment. Deionized water purified by Millipore® water purification system was used in all experiments.

3.2 Support Materials Preparation & Treatment

Carbon nanotubes (CNT) and Titania nanotubes (TNT) have been used a support materials for the catalysts synthesized in this work. In the following section, their synthesis and treatments are discussed one by one.

3.2.1 CNT: Purification & Functionalization

CNTs used in this research were supplied by Cheap Tubes Inc. CNTs were produced by combustion chemical vapor deposition (CCVD) and acid purified. Characterization of these as received CNTs was conducted using scanning electron microscopy (SEM), transmission electron microscopy (TEM), raman spectroscopy and thermogravimetric analysis (TGA).

TGA was used to track weight loss with increasing temperature of the sample placed on a sensitive microbalance located inside a furnace where gases are allowed to flow. The furnace was programmed to heat to 80°C at a rate of 10°C/minute in an air environment, held for 30 minutes then ramped to 900°C at 10°C/minute.

Pristine CNTs have too little anchor points in form of defects and functional groups to make attachment with the metal particles. Therefore the surface activation step to create surface active sites is essential in order to improve the dispersion of catalyst metals on the CNT surface. The aromatic conjugate ring structure of the CNT surface can be modified by an oxidation process of extremely aggressive reagents (HNO_3 or H_2SO_4 or a mixture of two), resulting in some functional groups on the CNT surface such as hydroxyl (–OH),

carboxyl (–COOH) and carbonyl (–C=O) [172, 131]. These surface functional groups roughly have a site ratio of 4(–OH): 2(–COOH):1(–C=O) [172]. These groups are expected to facilitate the chemical interaction between the anchoring catalyst metal ions and the modified CNT surface.

The as received CNTs were functionalized using the acid treatment as shown in the Figure 3-1. Figure 3-1 shows that after acid treatment carboxyl acid groups are attached to the side walls of the otherwise bare CNT which is devoid of any anchoring points. One gram carbon nanotube was added into the mixed acid of 60 ml concentrated sulfuric acid (98%) and 180 ml strong nitric acid (65%) and the mixture was boiling refluxed for 12 hours. After being air pump filtered, washed copiously with distilled water the product was dried at 120°C in air overnight. The obtained product was the acid treated functionalized carbon nanotube. Figure 3-2 describes the acid functionalization process.
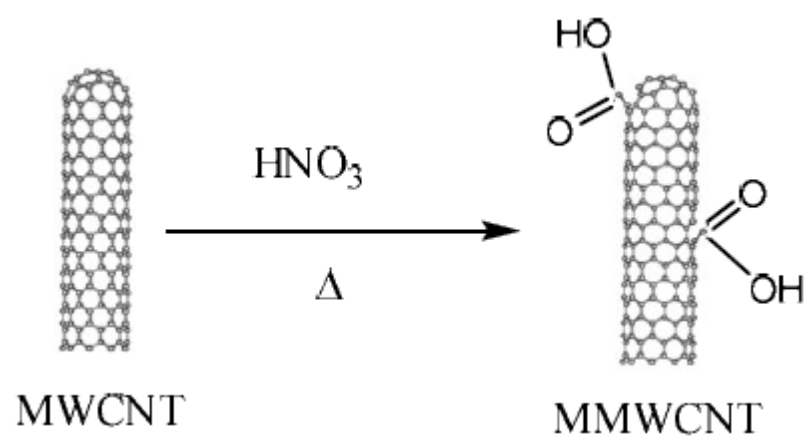
Figure 3-1: Functionalization of Carbon NT

```
┌─────────────────────────────────────────┐
│   As-received CNTs+ (HNO₃+H₂SO₄)         │
└─────────────────────────────────────────┘
                    │
                    ▼
┌─────────────────────────────────────────┐
│       Refluxed at 80°C for 24 hours      │
└─────────────────────────────────────────┘
                    │
                    ▼
┌─────────────────────────────────────────┐
│          Centrifuged and washed          │
└─────────────────────────────────────────┘
                    │
                    ▼
┌─────────────────────────────────────────┐
│       Dried in oven at 100°C overnight   │
└─────────────────────────────────────────┘
                    │
                    ▼
             Functionalized CNTs
```

As-received CNTs+ (HNO_3+H_2SO_4)

Refluxed at 80°C for 24 hours

Centrifuged and washed

Dried in oven at 100°C overnight

Functionalized CNTs
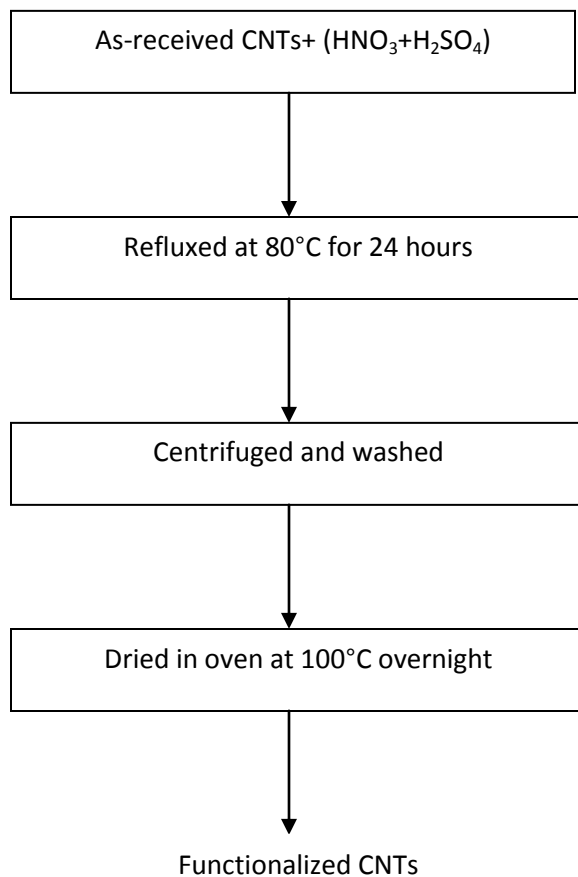
Figure 3-2: Carbon Nanotubes Functionalization Procedure

3.2.2 Titania Nanotubes: Synthesis

Titania nanotubes were prepared with titanium oxide in anatase form as starting material. Some amount of 10 molar sodium hydroxide solution was taken in a Teflon beaker and heated till 120°C. At 120°C, 2 grams of anatase was added to it with vigorous mixing. The solution was refluxed at 120°C with vigorous stirring for 48 hours. The white slurry was first treated with 200 ml with 5% HCl solution at 60°C with stirring and then with deionized water till neutralization. This white powder is calcined at 450°C to get the desired titania nanotubes with desired morphology. The synthesis procedure is shown in Figure 3-3.

```
┌─────────────────────────────────────────────┐
│ 50 ml 10 M NaOH taken in a teflon beaker     │
│                                              │
└─────────────────────────────────────────────┘
                      │
                      │  Heated till 120°C
                      ▼
┌─────────────────────────────────────────────┐
│            Anatase powder added              │
└─────────────────────────────────────────────┘
                      │
                      │  Refluxed for 48 hours at 120°C
                      ▼
┌─────────────────────────────────────────────┐
│    Centrifuged and washed with 5% HCl and    │
│                   water                      │
└─────────────────────────────────────────────┘
                      │
                      ▼
┌─────────────────────────────────────────────┐
│       Dried in oven at 100°C overnight       │
└─────────────────────────────────────────────┘
                      │
                      ▼
┌─────────────────────────────────────────────┐
│          Calcined at 450°C for 3 hours       │
└─────────────────────────────────────────────┘
                      │
                      ▼
```

Titania nanotubes (TNT)

Figure 3-3: Synthesis of Titania Nanotubes

3.3 Electrocatalyst Synthesis

In this work, electrocatalysts were prepared with copper, ruthenium, palladium, and iron as active metals with carbon nanotubes (CNT) and titania nanotubes (TNT) were used as support material. Supported metal catalysts both in singl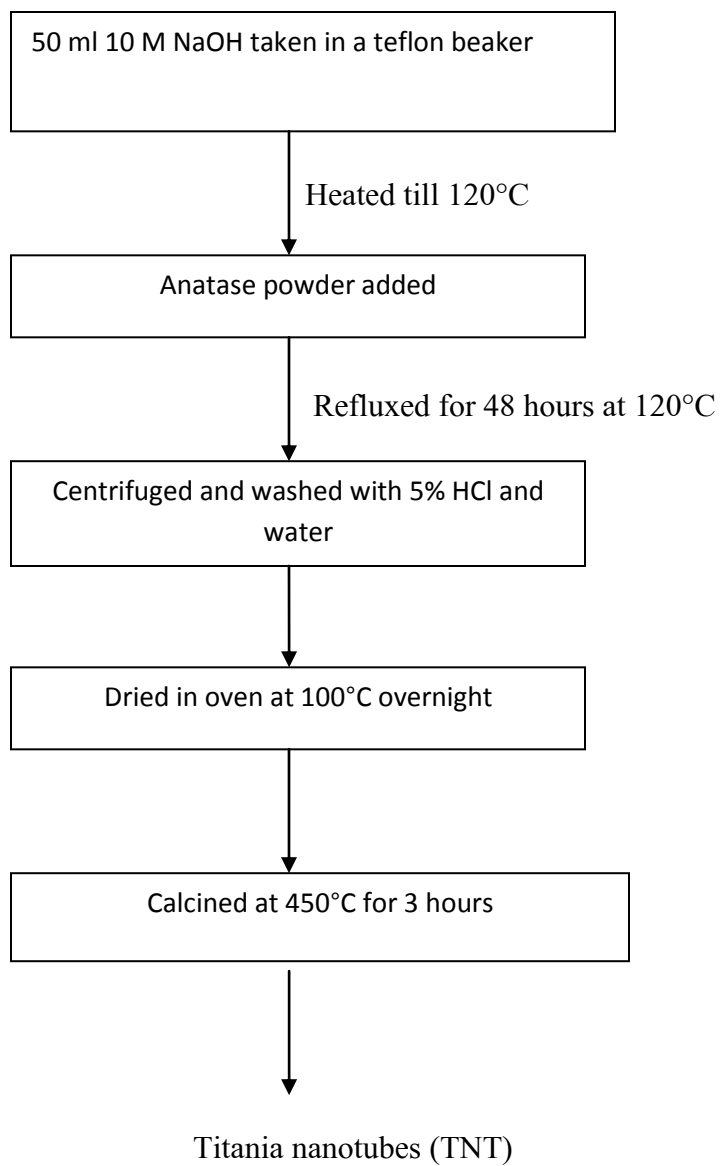e as well as in bimetallic form were prepared. Since a range of catalysts was prepared in this work, a number catalyst synthesis procedure was tried. After many trials, finally following methods of catalyst synthesis were selected for the synthesis. Following sections give detail account of the various synthesis procedures used in the catalyst synthesis

3.3.1 Incipient Wetness Impregnation Method

Generally catalysts with metal loading up to 20% are prepared by standard incipient impregnation method [173]. In this method, appropriate metal salt, used as precursor, was dissolved in deionized water. Volume of water was taken as the pore volume of the CNT. The metal salt solution was added drop wise to the support material. After evaporation of water, the impregnated sample was dried at 110°C overnight, and calcined at appropriate temperature to decompose the metal precursor in an argon flow in a tubular furnace to avoid burning of the carbonaceous support material. For TNT calcination was performed in air. The calcined samples were finally reduced in 100 ml/min 10% H_2/ Argon flow for 4 hours. In the reduction step, metal oxide produced in the calcination step was reduced by H_2 to form metal supported catalyst. For preparing bi-metallic catalyst, a similar approach called sequential impregnation method was used. In this method first a metal was impregnated by above mentioned method, and then the sample was again impregnated with another metal. Schematic synthetic procedure is shown in the Figure 3-4.
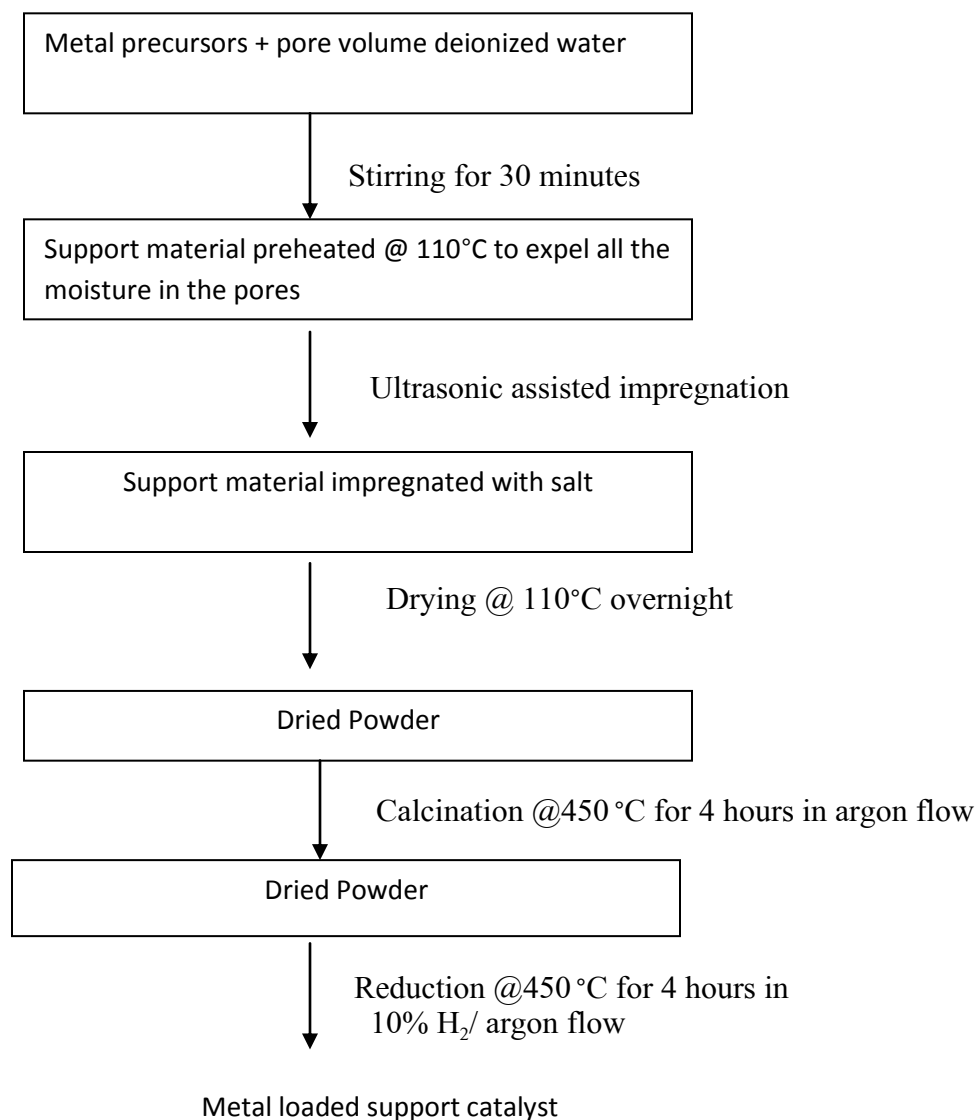
```
┌─────────────────────────────────────────────┐
│ Metal precursors + pore volume deionized water │
└─────────────────────────────────────────────┘
                      │
                      │  Stirring for 30 minutes
                      ▼
┌─────────────────────────────────────────────┐
│ Support material preheated @ 110°C to expel all the │
│ moisture in the pores                        │
└─────────────────────────────────────────────┘
                      │
                      │  Ultrasonic assisted impregnation
                      ▼
┌─────────────────────────────────────────────┐
│ Support material impregnated with salt       │
└─────────────────────────────────────────────┘
                      │
                      │  Drying @ 110°C overnight
                      ▼
┌─────────────────────────────────────────────┐
│ Dried Powder                                 │
└─────────────────────────────────────────────┘
                      │
                      │  Calcination @450 °C for 4 hours in argon flow
                      ▼
┌─────────────────────────────────────────────┐
│ Dried Powder                                 │
└─────────────────────────────────────────────┘
                      │
                      │  Reduction @450 °C for 4 hours in
                      │  10% H₂/ argon flow
                      ▼
            Metal loaded support catalyst
```

Reduction @450 °C for 4 hours in $10\%\ H_2$/ argon flow

Figure 3-4: Incipient Wetness Method for Synthesis of Metal Supported Catalyst

3.3.2 Homogeneous Deposition Precipitation

In a typical synthesis procedure, required amount of metal salt, used a precursor, was added in a constant stirring suspension made by suspending appropriate amount of preheated support in 200 ml deionized water. The suspension was sonicated for 1 hour to make a homogenous suspension. The resulting suspension was, then, heated with vigorous stirring. When the suspension temperature reaches 90°C, 30 ml of 0.42 M aqoues urea solution was added dropwisely. Then the suspension was maintained at 90°C with vigorous stirring for deposition to take place. At 90°C, hydrolysis of urea takes place at slow rate so the hydroxyl ions slowly react with metal ion resulting in the precipitation as metal hydroxide. The disposition process was allowed for 8 hours. After deposition, the slurry was cooled to room temperature, centrifuged, thoroughly washed with deionized water and dried at 110°C for 5 hours. The powder was calcined at appropriate temperature in argon flow in a tubular furnace. The calcined samples were finally reduced in 100 ml/min 10% H_2/ Ar flow for 4 hours. This method was specifically used for synthesizing catalyst with metal loading higher than 20%. Synthesis procedure for bimetallic catalyst was similar. Required salts were added to suspension and rest of the procedure was similar. Schematic procedure of the synthesis is shown in Figure-3-5.
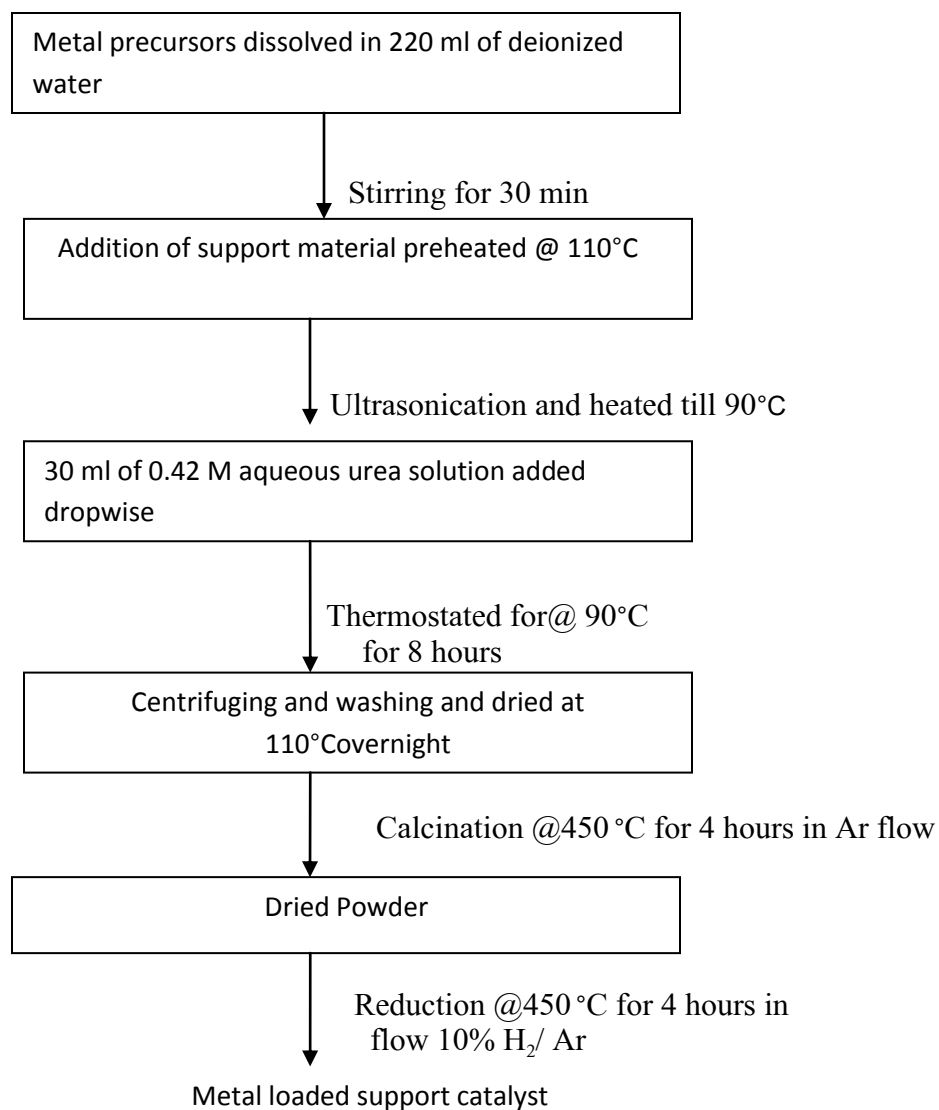
```
┌─────────────────────────────────────────────┐
│ Metal precursors dissolved in 220 ml of deionized │
│ water                                         │
└─────────────────────────────────────────────┘
                    │
                    │  Stirring for 30 min
                    ▼
┌─────────────────────────────────────────────┐
│ Addition of support material preheated @ 110°C │
│                                               │
└─────────────────────────────────────────────┘
                    │
                    │  Ultrasonication and heated till 90°C
                    ▼
┌─────────────────────────────────────────────┐
│ 30 ml of 0.42 M aqueous urea solution added   │
│ dropwise                                      │
└─────────────────────────────────────────────┘
                    │
                    │  Thermostated for@ 90°C
                    │       for 8 hours
                    ▼
┌─────────────────────────────────────────────┐
│ Centrifuging and washing and dried at         │
│ 110°Covernight                                │
└─────────────────────────────────────────────┘
                    │
                    │  Calcination @450 °C for 4 hours in Ar flow
                    ▼
┌─────────────────────────────────────────────┐
│ Dried Powder                                  │
└─────────────────────────────────────────────┘
                    │
                    │  Reduction @450 °C for 4 hours in
                    │   flow 10% H₂/ Ar
                    ▼
        Metal loaded support catalyst
```

Figure 3-5 Homogenous Deposition Precipitation Method for Synthesis of Metal Supported Catalyst

3.3.3 Borohydride Reduction Method

Borohydride reduction method is standard method for synthesis of fuel cell electrocatalysts. In this method, support material was dissolved in 30 ml deionized water and sonicated for about an hour. Then the precursor solution was added dropwise to the suspension. The resulting suspension was firs sonicated and then mechanically stirred for 3 hours. Then, appropriate amount of sodium borohydride dissolved in deionized water was added dropwise amid stirring. The suspension was stirred for 10 hours. The synthesis was carried out at room temperature. Then the solid material was recovered by centrifuge, washed with water several time and dried at 80°C in a vacuum oven. Synthesis procedure is shown in Figure 3-6

```
┌────────────────────────────────────────────────────┐
│ Support material preheated suspended in 30 ml       │
│ deionized water                                     │
└────────────────────────────────────────────────────┘
                         │
                         │   Ultrasonicated for 1 hour
                         ▼
┌────────────────────────────────────────────────────┐
│ Precursor solution added drop                       │
│                                                     │
└────────────────────────────────────────────────────┘
                         │
                         │   Stirred for 3 hours
                         ▼
┌────────────────────────────────────────────────────┐
│ Sodium borohydride solution added dropwise          │
│                                                     │
└────────────────────────────────────────────────────┘
                         │
                         │   Stirred for 3 hours
                         ▼
┌────────────────────────────────────────────────────┐
│ Centrifuged, washed with water                      │
│                                                     │
└────────────────────────────────────────────────────┘
                         │   Dried@80°C
                         ▼
                Metal loaded catalyst
```
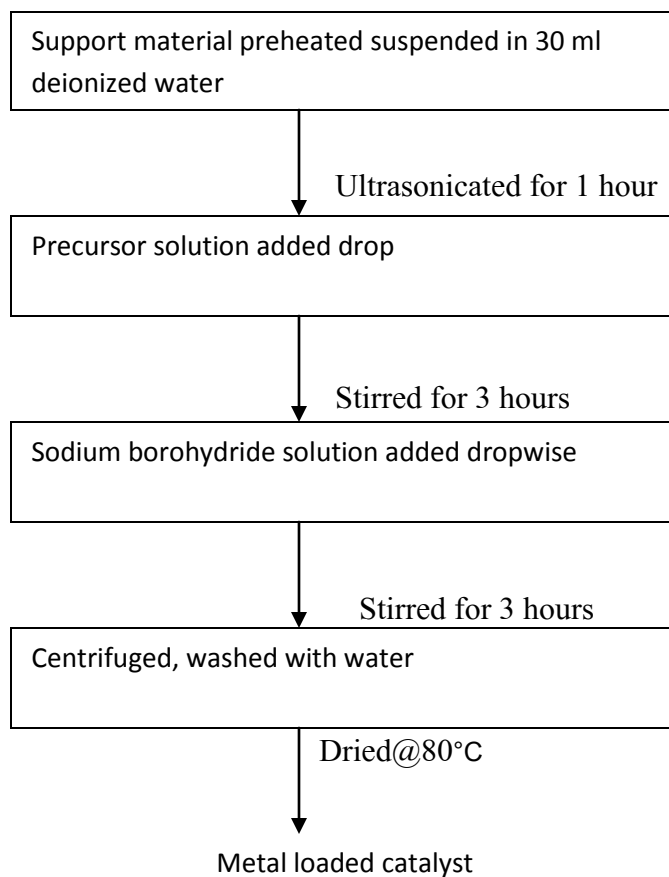
Figure 3-6: Borohydride Reduction Method for Synthesis of Metal Supported Catalyst

3.4 Carbon Nanotubes Based Electrocatalysts

CNT was used as support material to synthesize copper, ruthenium, palladium and iron supported catalysts. Single metal as well as binary catalysts were synthesized. Because a range of catalysts was prepared in this work, a number catalyst synthesis procedure was tried. Details of the catalysts as well as their synthesis method are summarized in the Table 3-1. As a general rule, catalysts up till 20 wt % loading were synthesized by incipient impregnation method whereas homogenous deposition precipitation method was used for higher loading.

Table 3-1: Catalyst Synthesized in this Work and Their Synthesis Procedure

Catalyst Sample	Synthesis method
Copper loaded on CNT	
10%Cu/CNT	Incipient impregnation method
20%Cu/CNT	Incipient impregnation method
30%Cu/CNT	Homogeneous deposition precipitation
40%Cu/CNT	Homogeneous deposition precipitation
50%Cu/CNT	Homogeneous deposition precipitation
60%Cu/CNT	Homogeneous deposition precipitation
Copper, Ruthenium loaded on CNT	
20%Ru/CNT	Borohydride reduction Method
5%Cu5%Ru/CNT	Incipient impregnation method
10%Cu10%Ru/CNT	Homogeneous deposition precipitation
20%Cu20%Ru/CNT	Homogeneous deposition precipitation
30%Cu30%Ru/CNT	Homogeneous deposition precipitation
Copper, Palladium loaded on CNT	
20%Pd/CNT	Borohydride Reduction method
5%Cu5%Ru/CNT	Wet impregnation method
10%Cu10%Ru/CNT	Homogeneous deposition precipitation
20%Cu20%Ru/CNT	Homogeneous deposition precipitation
30%Cu30%Ru/CNT	Homogeneous deposition precipitation
Copper, Iron loaded on CNT	
20% Fe/CNT	Incipient impregnation method
5%Cu5%Fe/CNT	Incipient impregnation method
10%Cu10%Fe/CNT	Homogeneous deposition precipitation
20%Cu20%Fe/CNT	Homogeneous deposition precipitation
30%Cu30%Fe/CNT	Homogeneous deposition precipitation

3.5 Titania Nanotubes Based Catalyst

TNT was used as support material to synthesize copper, ruthenium, palladium and iron supported catalysts. Single metal as well as binary catalysts were synthesized. Because a range of catalysts was prepared in this work, a number catalyst synthesis procedure was tried. Detailed description of the catalyst prepared and their synthesis procedure are mentioned in the Table 3-2. As a general rule, catalysts up till 20 wt % loading were synthesized by incipient impregnation method whereas homogenous deposition precipitation method was used for higher loading.

Table 3-2: Electrocatalyst prepared supported on TNT and their synthesis procedure

Catalyst Sample	Synthesis method
Copper loaded on TNT	
5%Cu/TNT	Incipient impregnation method
10%Cu/CNT	Incipient impregnation method
20%Cu/CNT	Homogeneous deposition precipitation
Copper, Ruthenium loaded on TNT	
5%Cu5%Ru/TNT	Incipient impregnation method
10%Cu10%Ru/TNT	Homogeneous deposition precipitation
20%Cu20%Ru/TNT	Homogeneous deposition precipitation
Copper, Palladium loaded on TNT	
5%Cu5%Ru/TNT	Wet impregnation method
10%Cu10%Ru/TNT	Homogeneous deposition precipitation
20%Cu20%Ru/TNT	Homogeneous deposition precipitation
Copper, Iron loaded on TNT	
5%Cu5%Fe/TNT	Wet impregnation method
10%Cu10%Fe/TNT	Homogeneous deposition precipitation
20%Cu20%Fe/TNT	Homogeneous deposition precipitation
30%Cu30%Fe/TNT	Homogeneous deposition precipitation

3.6   Physical Characterization of the catalyst

The support materials as well as the synthesized elctrocatalyst were characterized for their morphology which includes particle size and is dispersion, composition, and surface area and pore volume. These properties reveal very important features of the catalysts and bear direct relationship with their activity. In this work following techniques have been used for characterization:

    A.   X-Ray Diffratogram (XRD)

    B.   Thermo Gravimetric Analysis (TGA)

    C.   Fourier Transform Infrared Spectroscopy (FTIR)

    D.   Scanning Electron Microscopy (SEM)

    E.   Transmission Electron Microscopy (TEM)

    F.   Surface area and Pore Volume

    G.   X-Ray Photoelectron Microscopy (XPS)

3.6.1   X-Ray Diffratogram (XRD)

X-ray diffraction is the most of the widely used technique to characterize materials. It is a non-destructive technique that reveals the detailed information about the chemical composition and the crystalline phase of synthesized materials. Higher amount of crystalline materials mean higher active surface are and thus the enhanced catalytic Activity. The XRD patterns were obtained from 2-theta scanning diffractometer. It scanned from 4 to 80°. The obtained XRD patterns were compared with the patterns of International Center Diffraction Data (ICDD) or formerly known as Joint Committee on Powder Diffraction Standards (JCPDS).

Fine powdered samples were spread onto a glass slide using double sided sticky tape and X-ray diffractograms were collected using a Smart Lab (9kW) Rigaku XRD X-ray diffraction X-ray diffractometer, with a diffraction angle range $2\theta = 20–80°$ using Cu Kα radiation. From the resulting diffratogram the crystallite size (d, nm) was estimated using the Scherrer equation

$$d = \frac{0.9\lambda}{\beta\cos\theta}$$

(3.1)

where λ is the X-ray wavelength (1.54°A), $\boldsymbol{\theta}$ is the Bragg angle of the peak of interest and $\boldsymbol{d}$ is the line broadening measured from the increased peak width at half height through a Gaussian fit obtained from Origin plotting software. The analysis was done by PDXL software which uses database provided by ICDD.

3.6.2 Scanning Electron Microscopy (SEM)

Scanning Electron microscopy is a powerful visualization tool for the investigation of catalyst morphology including particle size, pore size, structure, surface characteristics and dispersion of impregnated metals on the catalyst support. EDX was carried out to find out the composition of the catalyst.

The morphologies of the support and catalysts were investigated by using a scanning electron microscope (JEOL JSM-6460LV) operated at 20 KV equipped with energy dispersive X-ray (EDX).

3.6.3 Transmission Electron Microscopy (TEM)

TEM is used to examine the structure, composition, or properties of a specimen in submicroscopic detail. One can see objects to the order of a few Angstrom (10^{-10} m). Using TEM offers the advantage of increased magnification and resolution. The TEM passes an accelerated electron beam through a thin sample (50-300°A). Some of the electrons are scattered by the atoms in the sample. A phase distortion is created, resulting in a phase contrast that is used to create the image. The TEM enables the operator to see the "inside" of the sample rather than the surface.

In this work TEM was done at King Abdullah Institute of Nanotechnology (KIAN) at king Saud University. TEM images were obtained with ultra-high resolution FETEM (JEOL, JEM-2100F) at an accelerating voltage of 200 kV.

The sample for both TEM and SEM was prepared by one milligram of pre reduced catalyst was sonicated in 10 ml of ethanol for 30 minutes and then a drop of the suspension was placed on a an aluminum foil which was mounted on the sample holder by means of a double sided adhesive tape. In order to facilitate charge transfer for titania based catalysts, a thin gold film is deposited on the sample using plasma deposition. No such coating was used for CNT.

3.6.4 Thermo Gravimetric Analysis (TGA)

Thermogravimetric analysis or thermal gravimetric analysis (TGA) is a type of testing performed on samples that determines changes in weight in relation to change in temperature. Such analysis relies on a high degree of precision in three measurements:

weight, temperature, and temperature change. Approximately 5 mg of sample was placed into an aluminum sample pan for TGA using an empty aluminum pan as a reference. All TGA were recorded on a Shimadzu TGA-60 between 25°C and 800°C at the default ramp rate of 10°C/min under an argon atmosphere. TGA was used to find the optimum calcination temperature of the supported catalyst materials as well the metal loading on the catalyst for CNT based catalysts.

.

3.6.5   Fourier Transform Infrared Spectroscopy (FTIR)

Infrared radiation interacts with chemical bonds to cause stretches, bends and various other atomic vibrations. For a vibration to give rise to absorption of infrared radiation, it must cause a change in the dipole moment of the molecule. The larger this change the more intense the absorption band will be. FTIR spectra were measured in transmittance mode on a Perkin-Elmer FC-16 FTIR spectrometer. Spectra were taken by making pellet of different powder samples with potassium bromide (KBr). Around 4-5 mg of sample was mixed with approximately 200 mg of KBr to prepare the pellets. The spectrum for each pellet was taken with the above-mentioned spectrometer using 16 scans per sample at a resolution of 4 cm^{-1} over the range 4000 – 400 cm^{-1}

3.6.6   Surface Area & Pore Volume

Surface area and pore volume were evaluated by the Brunauer, Emmett and Teller (BET) analysis of the support and the synthesized catalysts was carried out using Micromeritics model ASAP 2010. Physical adsorption was done at liquid nitrogen temperature of 77K. In this method the amount of nitrogen at the equilibrium and at the normal boiling point (-195.8°C) is measured over a range of nitrogen pressure below one atmosphere. In

essence, the Langmuir adsorption isotherm is extended to apply to multilayer adsorption, arriving at the following equation called Brunauer-Emmet-Teller.

$$\frac{p}{v(p_0 - p)} = \frac{1}{V_m C} + \frac{(c-1)p}{c V_m p_o}$$ …………………………………………………… (3.2)

Where p_0 is the saturation or vapor pressure, V_m is the volume of monolayer of the adsorbed gas and c is a constant for the particular temperature and gas-solid system.

3.6.7 X-ray Photoelectron Spectroscopy (XPS)

X-ray Photoelectron Spectroscopy is a surface sensitive analytical technique, which is applied to determine the chemical composition of a sample surface (including the identification of (traces of) impurities). This method is based on the energy measurement of an ejected electron. As demonstrated in the scheme in figure 3-6, the process is initialized by excitation of the sample via X-ray treatment or an electron beam. This leads to the emission of a photoelectron (core electron). Since in case of XP spectroscopy characteristic X-rays are used, the ejected photoelectron has a well-defined element-characteristic binding energy E_b. The electrons and their kinetic energies, E_k, are detected with an electron energy analyzer. The binding energy can then be calculated according to equation 3.3.

$$E_k = h\nu - E_b - \Phi$$ …………………………………………………………….…… (3.3)

There $h\upsilon$ is the excitation energy and Φ is the spectrometer work function. In addition to the elemental analysis (element specific binding energy of photoelectrons) information about the chemical state (oxidation state) of the elements can be extracted from the chemical shift of the binding energy of the photoelectron. After creating a core hole and

emission of a photoelectron, the surface atom remains in an excited state. This surface atom returns to a less excited state by the decay of an electron from an energetically higher shell into the core hole. The energy from this transition is emitted either as an (characteristic) X-ray photon (fluorescence energy $h\nu_f = E1s - E2s$).

Core level photoelectron spectra were collected on a VG scientific ESCALAB MKII spectrometer equipped with a dual aluminum-magnesium anode X-ray gun and a 150-mm concentric hemispherical analyzer using $AlK\alpha$ ($h\nu$=1486.6 eV) radiation from an anode operated at 130W.
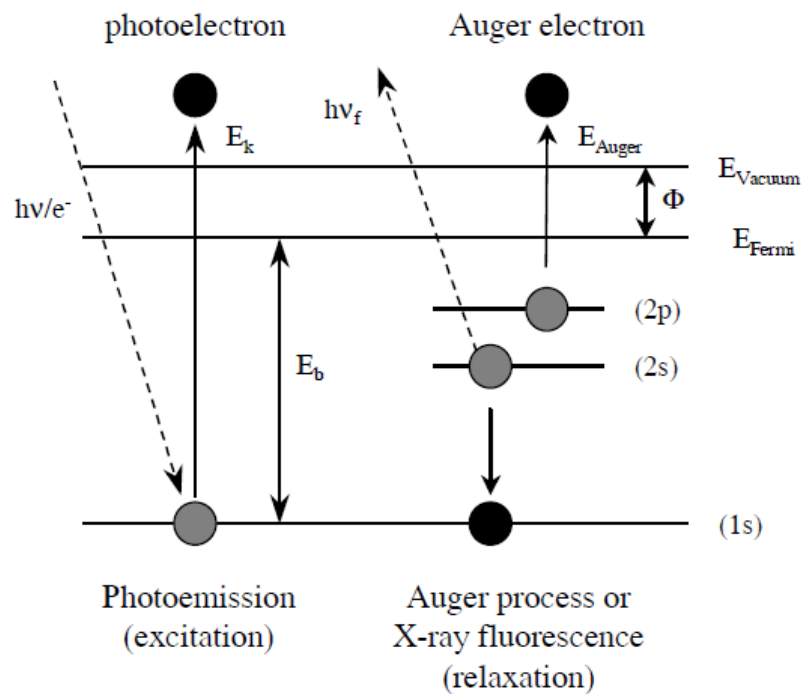
Figure 3-7: Photoemission Process in XPS

3.7 Electrocatalytic Activity Characterization

3.7.1 Half Cell

Catalytic activities of the as prepared catalysts were determined by linear sweep voltammetry (LSV) and chronoamperometry (CA). Electrochemical studies were carried out in a conventional indigenously made H-type cell (0.5 dm^3) with anode and cathode compartments separated by proton conducting Nafion-117® membrane. The compartments were separated to prevent the cathode and anode products being mixed. Catalyst ink prepared by ultrasonicating 50 mg of the prepared catalysts along with iso-propanol and 0.82 ml of 5% Nafion solution for 30 minutes. The catalyst ink was brush painted on Toray® carbon paper. The catalyst coated (or uncoated) carbon paper and platinum mesh were used as working electrode and counter electrode respectively. Active surface area of working electrode and counter electrode were 1.0 cm^2 and 8.0 cm^2 respectively. Standard calomel electrode (SCE) was used as the reference electrode in all the experiments. Schematic of the set-up is shown in Figure 3-8. A 0.5 molar aqueous solution of sodium bicarbonate was used both as catholyte and anolyte. Firstly, the catholyte solution was purged with high purity nitrogen for 30 minutes at 50 ml/minute and, then with high purity (99.998%) carbon dioxide at 100 ml/min for 1 hour each. The pH of the catholyte before and after CO_2 purging was measured to be 8.67 and 7.38, respectively. Purging CO_2 for longer duration did not change the pH which clearly shows that one hour purging with CO_2 was enough to saturate the catholyte. Linear sweep voltammetry was carried out from 0 to -3 V with scan rate of 25 mV/s and chronoamperometry at -1.7 V for 6000 seconds. All electrochemical experiments were performed with PGSTAT 302 (Eco Chemie, Netherlands) using Nova ® software.
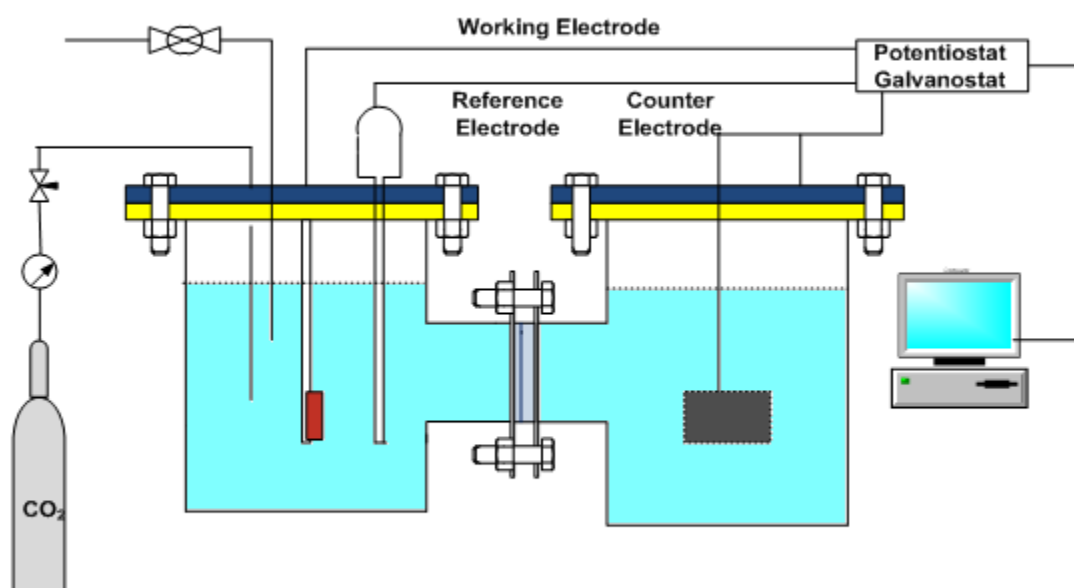
Figure 3-8: Schematic Diagram of Half Cell Assembly

3.7.2 Solid Polymer Electrolyte (SPE) Reactor

Research grade (99.999%) CO_2 was passed through a hydrocarbon trap to remove any trace hydrocarbon present in the reactant gas stream. The flow rate of the gas was 20 ml/minute. Gas flow was controlled by a mass flow controller. The tubing for the line is ¼ inch (63.5 mm). A dew point humidifier with gas heating was installed in the line to humidify the CO_2 gas flow. A hygrometer was installed in the line after the humidifier to measure the moisture content & temperature of the gas stream. This humidified CO_2 gas was fed to the cathode side of the cell. After this, a pressure gauge was installed to continuously monitor the inlet gas pressure to the electrochemical reactor. The issuing gas from the reactor was first passed through a water trap to remove any moisture. On this line a pressure gauge & temperature indicator was installed to monitor the pressure and temperature of the product gas. A back pressure regulator was used to regulate the pressure in the system. The line between the back pressure regulator and the electrochemical cell was heated electrically and insulated to keep the products in vapor phase. In between the back pressure regulator and electrochemical cell, a sampling point for gas chromatography is provided by a ball valve. Figure 3-9 shows the schematic diagram of the experimental set up.

Another flow loop was to use a water tank of 5 L and a peristaltic pump was used to deliver water at 20 ml/minute. To accurately monitor the water flow rate a mass flow controller was installed in the line. The tubing used for this was ¼ inch. This delivers water to the anode of the sides of the electrochemical reactor.

The electrochemical reactor cell is similar to systems to that are used for fuel-cell studies.

Figure 3-10 shows the actual experimental set up after fabrication of the individual parts. The electrochemical cell is shown in the Figure 3-11. The cell is to be composed of two blocks in which channels have been machined and are used as current collectors as well as to feed gaseous (humidified carbon dioxide) or liquid (water) reactants to the cathode and anode respectively. The cathode block was made of graphite treated to make it nonporous. Because it was anticipated that graphite could be oxidized upon electrolysis at the anode, polytetrafluoroethylene (PTFE) was chosen as material for the anode block. The flow pattern was same as that in the fuel cell. A platinum screen placed between the PTFE block and the electrode was to be used as current collector. It was connected to the external circuit by means of a platinum wire through the PTFE block. The membrane-electrode assembly (MEA) was placed between the two blocks. The active area for cell sought was 25 cm^2. The whole sandwich is to be placed between two aluminum/stainless steel frames with eight bolts of diameter (1/4 inch) 0.635cm fastened. Two stainless steel plates or aluminum plates (15 cm × 10 cm × 2 cm) were used as back plates to provide mechanical strength just like fuel cells, the anode and cathode had channels for reactants and products. In short, the cell was essentially fuel cell hardware with PTFE anode. All other features were unchanged.
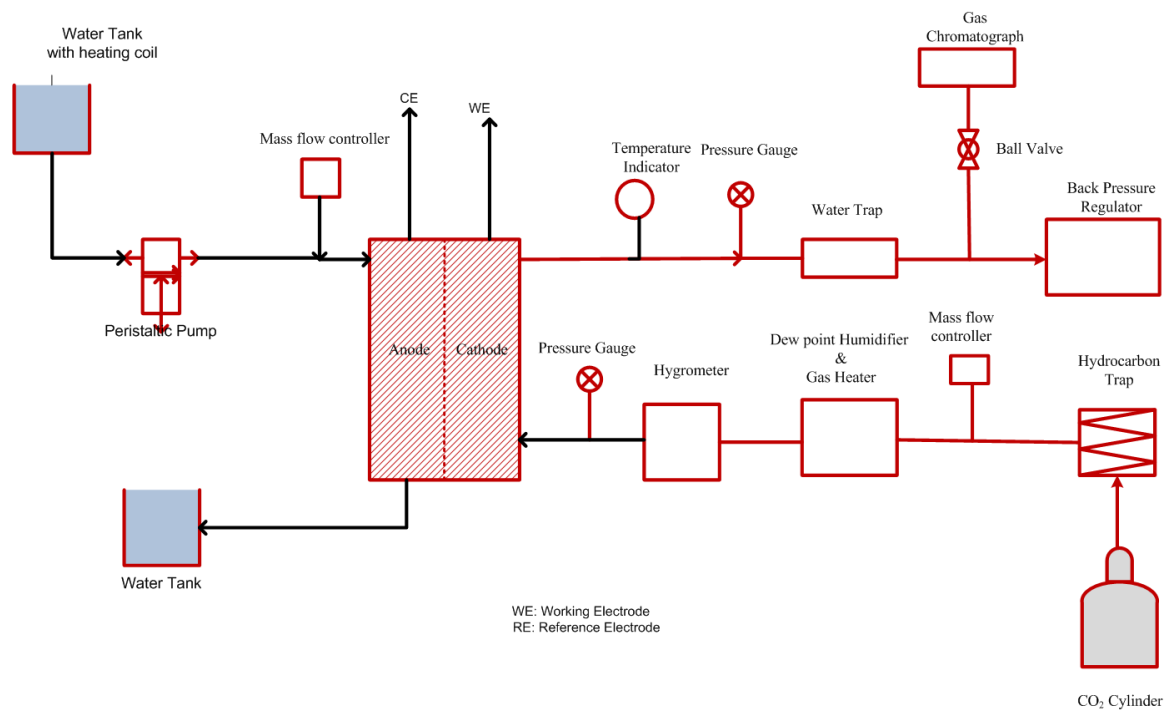
Figure 3-9: Experimental Setup for SPE Reactor System

Figure 3-10: Experimental Setup for SPE Reactor System

Figure 3-11: Electrochemical Reactor Cell

3.8 MEA Fabrication

Commercial Nafion®117 membrane was used as proton exchange membrane to prepare MEAs. The membranes were cut into appropriate sizes and pre-treated to exchange the Na^+ cations with H^+ ions in the membrane. The pretreatment procedure is shown in Figure 3-12.

For the catalyst slurry, catalyst loading of 4 mgcm^{-2} and 2 mgcm^{-2} for cathode (the prepared catalyst samples to be tested) and anode (60% Pt-Ru/C) were used respectively. To determine the amount of catalyst and Nafion that will give the corresponding metal loading, the following relationship is used:

$$m_{catalyst+support} = \frac{(2\sigma_{catalyst} \times A_{active})}{f_{catalyst}} \quad \ldots\ldots\ldots\ldots\ldots\ldots\ldots\ldots\ldots\ldots\ldots\ldots \text{(3.3)}$$

Where $\sigma_{catalyst}$ is the catalyst loading (mgcm^{-2}), A_{active} is the active surface area for the catalyst deposition (cm^2) and $f_{catalyst}$ is the fraction of the metal species in the catalyst. In In order to determine the required amount Nafion solution (which serves as the binder), the following expression is used:

$$m_{Nafion} = \frac{\left(f_{Nafion} \times m_{catalyst+support} \times \left(\frac{1}{0.05}\right)\right)}{1 - f_{Nafion}} \quad \ldots\ldots\ldots\ldots\ldots\ldots\ldots\ldots\ldots \text{(3.4)}$$

The prepared catalyst slurry was then coated with on both the sides of the membrane and GDLs and sandwiched together. After drying, the MEAs were hot-pressed in a Carver press at 130°C and 2000 psi for 5 minutes.

```
┌─────────────────────────────────────┐
│   As- received Nafion® Membrane      │
└─────────────────────────────────────┘
                  │
                  │  Cut into appropriate sizes
                  ▼
┌─────────────────────────────────────┐
│   Washed with deionized water & boiled │
│   in 5 wt. % H₂O₂ for 1 hour         │
└─────────────────────────────────────┘
                  │
                  ▼
┌─────────────────────────────────────┐
│   Flushed several times with         │
│   deionized water                    │
└─────────────────────────────────────┘
                  │
                  ▼
┌─────────────────────────────────────┐
│   Flushed several times with         │
│   deionized water                    │
└─────────────────────────────────────┘
                  │
                  ▼
┌─────────────────────────────────────┐
│   Boiled in 0.5 M H₂SO₄ solution for 1 │
│   hour to exchange Na⁺ with H⁺       │
└─────────────────────────────────────┘
                  │
                  ▼
┌─────────────────────────────────────┐
│   Rinsed with deionized water and    │
│   stored in deionized water          │
└─────────────────────────────────────┘
```
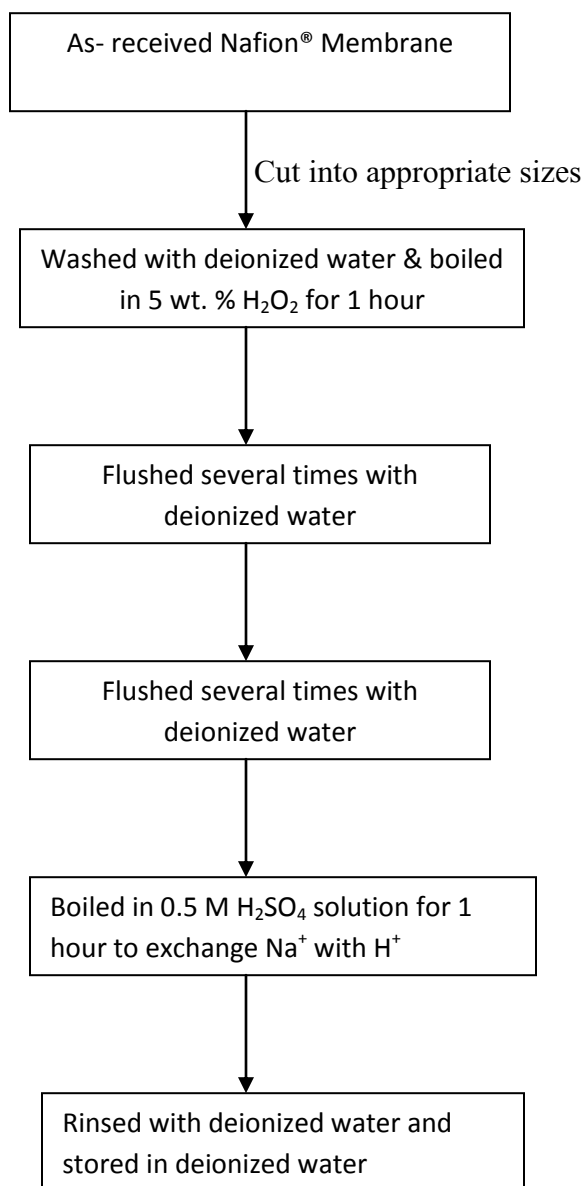
Figure 3-12: Nafion® Pre-treatment for MEA Fabrication

CHAPTER 4

RESULTS AND DISCUSSION

All the electrocatalysts synthesized in this work were mentioned in the Table 3-1 & 3-2 along with their composition. In the following sections, their physical as well as electrochemical characterizations are discussed in detail.

4.1 Carbon Nanotubes (CNTs) Supported Catalysts

In this section, physical characterization results of the single and binary electrocatalysts supported on CNTs are presented and discussed, and later, their catalytic activities for electrochemical reduction of CO_2 are discussed. Four different types of electrocatalysts have been used: Cu/CNT, Cu-Ru/CNT, Cu-Pd/CNT and Cu-Fe/CNT as mentioned in Table 3-1 in the previous chapter.

4.1.1 Copper Supported on CNT

In the following sections, the synthesized copper metal supported on CNTs have been explored for their morphology and electrocatalytic activity for ERC.

A.   Physical Characterization

Scanning electron microscopy (SEM) was carried out to ascertain the morphology and dispersion of metals on the support. Figure 4-1 shows the SEM image of the functionalized CNT. Characteristic uniform tubular nanostructure of the CNT can be observed in the micrograph. Average diameters of the nanotubes are found to be in few

nanometers and length up to few microns. There are large empty spaces in between the entangled tubes. Figure 4-2 shows the morphology of the catalyst with 10 wt % copper loading on CNT. For 10%Cu/CNT, the copper particles are uniformly distributed on the nanotubes support with absence of any visible agglomeration. As the copper loading was increased, the copper particle grew in size as evident from the comparison of SEM micrographs of 10% and 20% Cu/CNT (Figure 4-2 & 4-3), but the copper particles remains homogenously coated on the surface of the CNT. However, as the copper loading is increased to 40%, agglomeration starts to appear and, very large agglomerated copper particles are formed as evident in the micrographs shown in Figure 4-4 & 4-5. Figure 4-6 shows the particles distribution in case of 60 % copper loading. Large agglomerations can be clearly spotted. These findings were confirmed by particle size estimated from XRD. Energy-dispersive X-ray spectroscopy (EDX) was performed to find out the composition of the catalysts. Figure 4-7 shows the EDX spectra of 30 % copper loaded CNT catalysts. Very strong peak of carbon is observed along with peaks of copper and oxygen. Oxygen peak arises as a result of acid functionalization of the pristine CNT. Therefore, it can be inferred from this observation that acid group was indeed created on the CNT. Presences of copper peaks indicate that copper has been successfully mounted on the CNTs.
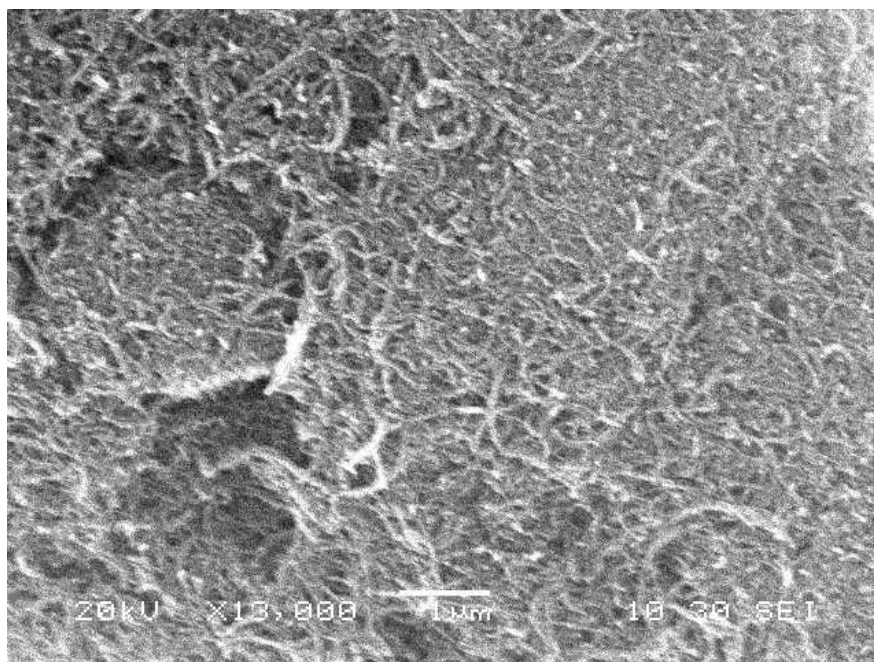
Figure 4-1: SEM Image of Functionalized Single Wall Carbon Nanotubes (CNTs)
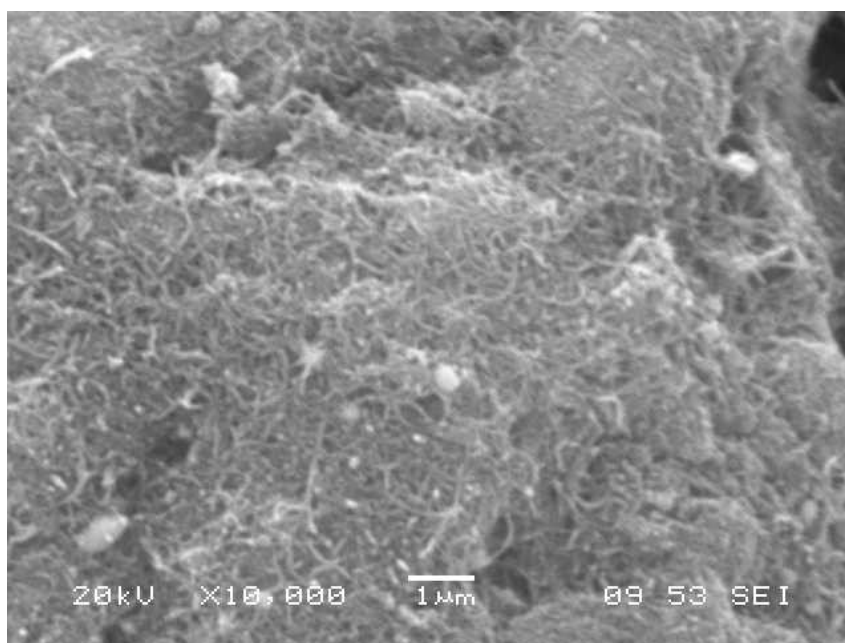
Figure 4-2: SEM Image of 10% Cu/CNT
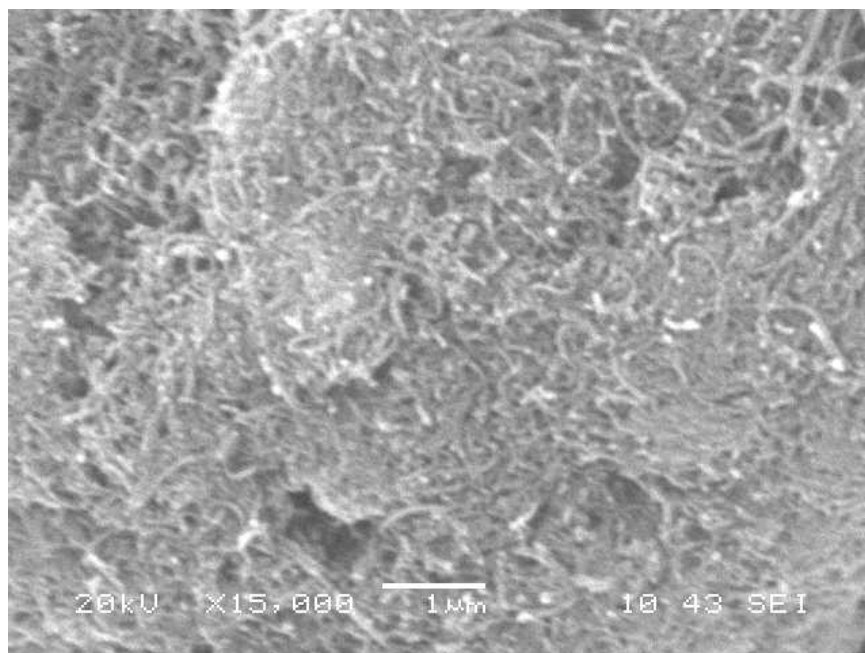
Figure 4-3: SEM image of 20% Cu/CNT
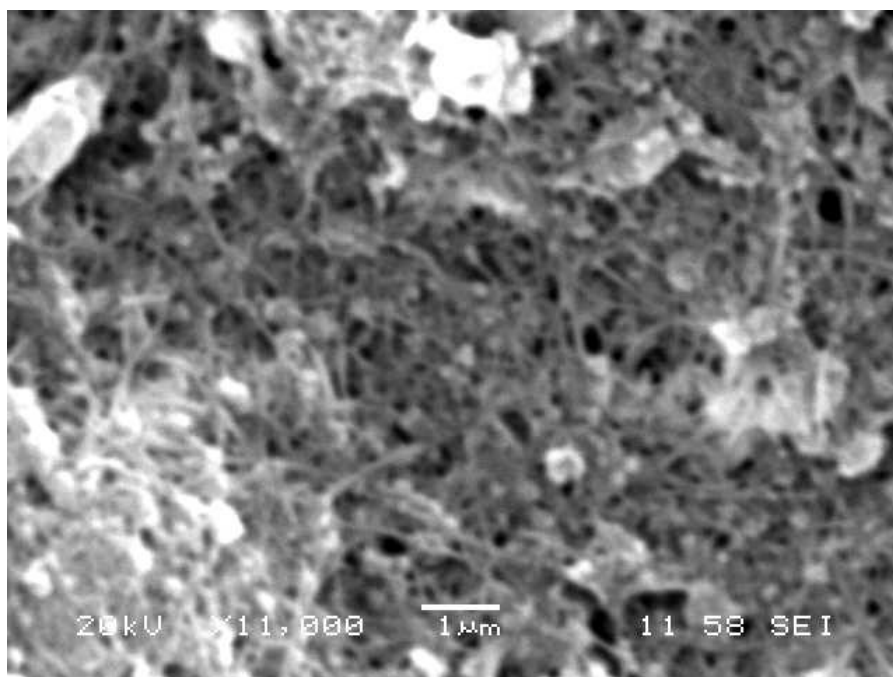
Figure 4-4: SEM Image of 30% Cu/CNT
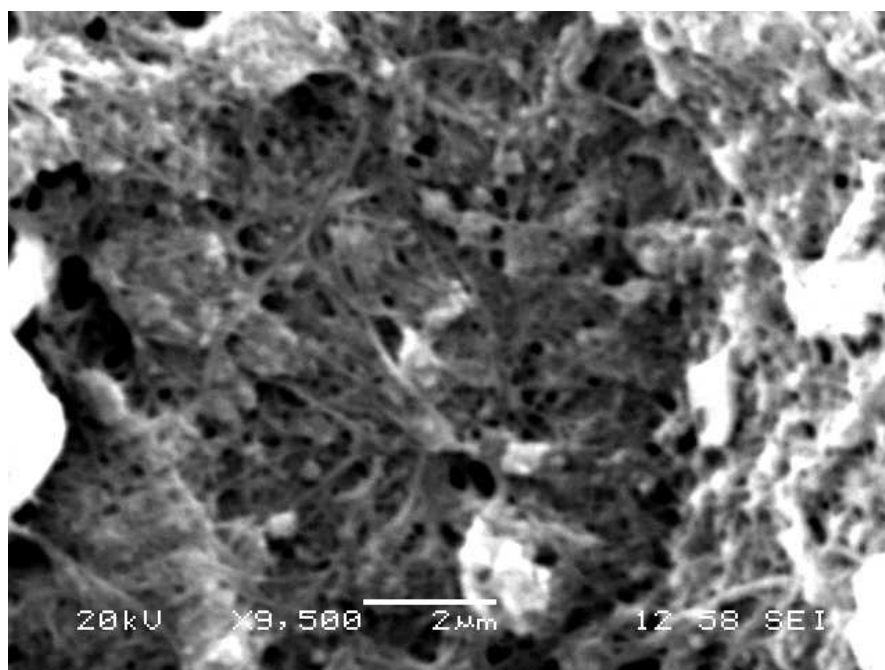
Figure 4-5: SEM Image of 40% Cu/CNT
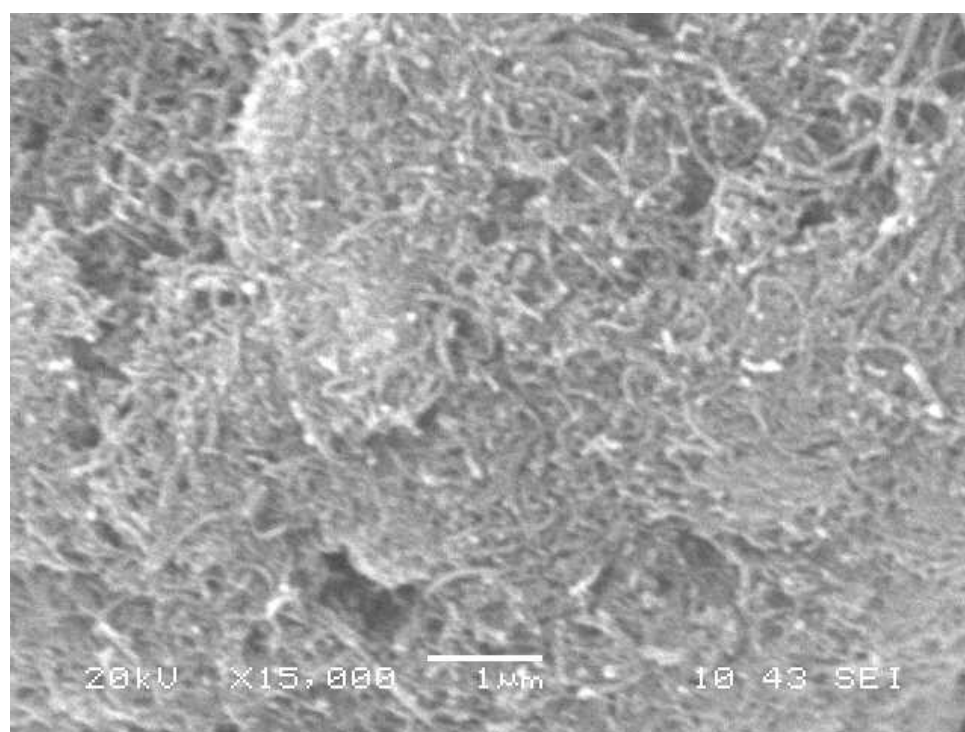
Figure 4-6: SEM Image of 60% Cu/CNT
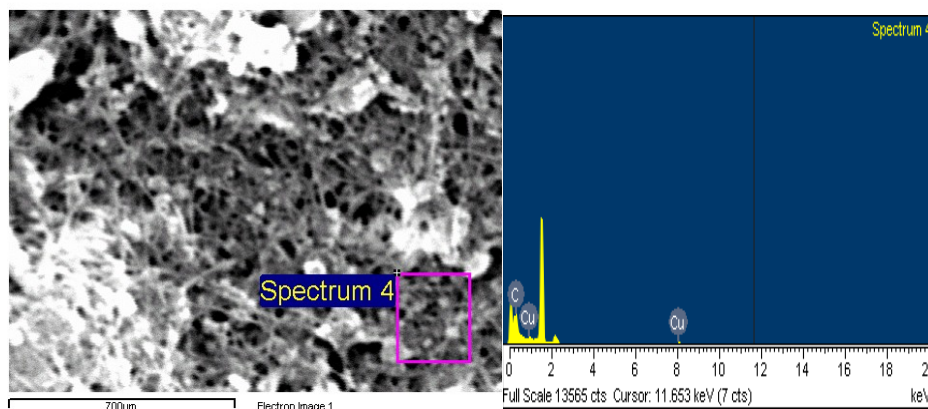
Figure 4-7: SEM-EDX Image of 30% Cu/CNT

The X-ray diffraction (XRD) analysis was carried out to investigate the structure of the Cu-based catalysts supported on carbon nanotubes (CNT) for different metal loading conditions. Figure 4-8 shows the XRD pattern for the different catalyst samples with different copper metal loading. It can be observed that the purified CNTs shows characteristic peaks at $2\theta = 26.18$ °, and 43.18 ° which were due to the diffractions of the (002) and (100) planes of graphite-like tube-wall of the CNTs. For all the other copper metal supported catalysts, in addition to the characteristic CNT peaks, diffraction peaks of zero valent copper phase of (111), (200) and (220) at $2\theta = 43.23°$, 50.10°, 73.97° respectively, were identified. This shows that copper was successfully deposited on CNTs by the homogenous deposition precipitation method. By comparing the peak intensities of the patterns for different copper loadings, the higher loading catalysts showed stronger peak intensity than the low loading catalysts. This revealed that bigger

117

the copper particles supported on CNT, the stronger is the XRD pattern. The mean Cu particle size was determined from the analysis of characteristic Cu (111) peak corresponding to diffraction angle equal to 43.23. The mean particle sizes of Cu were estimated by analyzing the broadening of the strongest (111) diffraction peak by using Scherrer equation (Equation 3-1). Results of the analysis of XRD pattern are summarized in Table 4-1. As can be seen in the Table 4-1, with increasing Cu loading from 10% to 60%, the size of the copper particles increased significantly from 3.5 nm to around 60 nm, indicating the formation of larger sized aggregate in the case of the higher Cu loading. This result corroborates the results obtained from SEM analysis.
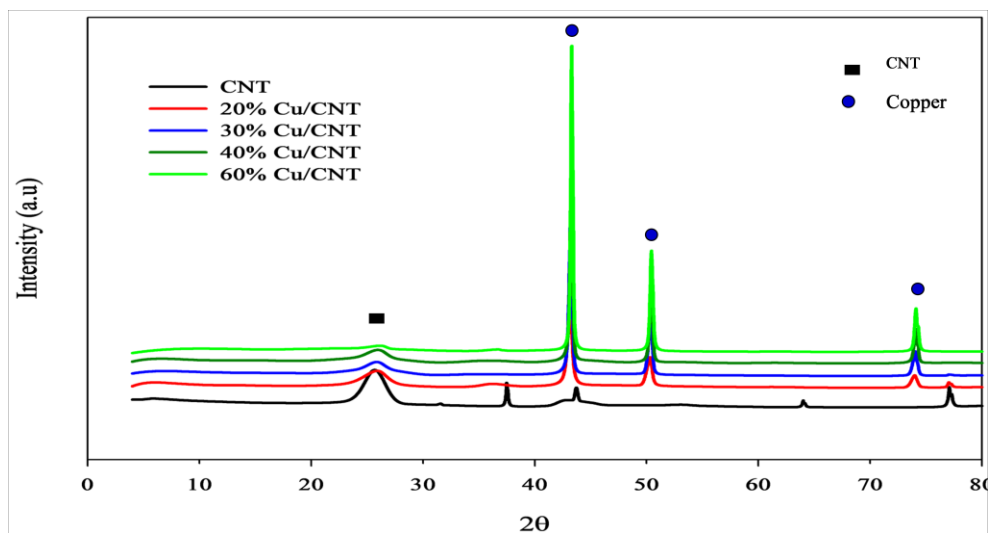
Figure 4-8: XRD Pattern of Cu/CNT catalysts with Different Cu Loading Amount

Table 4-1: XRD data Analysis Results for the Cu/CNT Catalysts

Catalyst Sample	FWHM (degree)	Crystal size (nm)	d_{hkl} (A^0)
Functionalized CNT	NA	NA	NA
10% Cu/CNT	2.32	3.83	0.21
20% Cu/CNT	2.1	19.7	0.35
30% Cu/CNT	1.8	56.6	0.38
40% Cu/CNT	1.77	59.0	0.31
60% Cu/CNT	1.83	53.9	0.36

Transmission electron microscopy (TEM) was carried out to find the size and morphology of the copper particles deposited on CNT. The TEM image of the functionalized CNT is shown in Figure 4-8. It shows that CNT has characteristic tube like structure with tube diameter in the range 4-10 nm which is consistent with the supplier specifications. The tubes were found to be entangles together. Figures 4-9 through 4-12 show the TEM images of the copper loaded CNT. It is evidently seen that the copper nano particles are homogeneously coated on the surface of CNTs and intimately attached to the CNTs. For 10% Cu loading, the particles are found to be in the range of 3-5 nm whereas for 20% loading, the particle sizes are found to be in the range 15-20 nm. These observations are in good agreement with the particle size estimated from XRD analysis.

Figure 4-9: TEM Image of Pure CNT
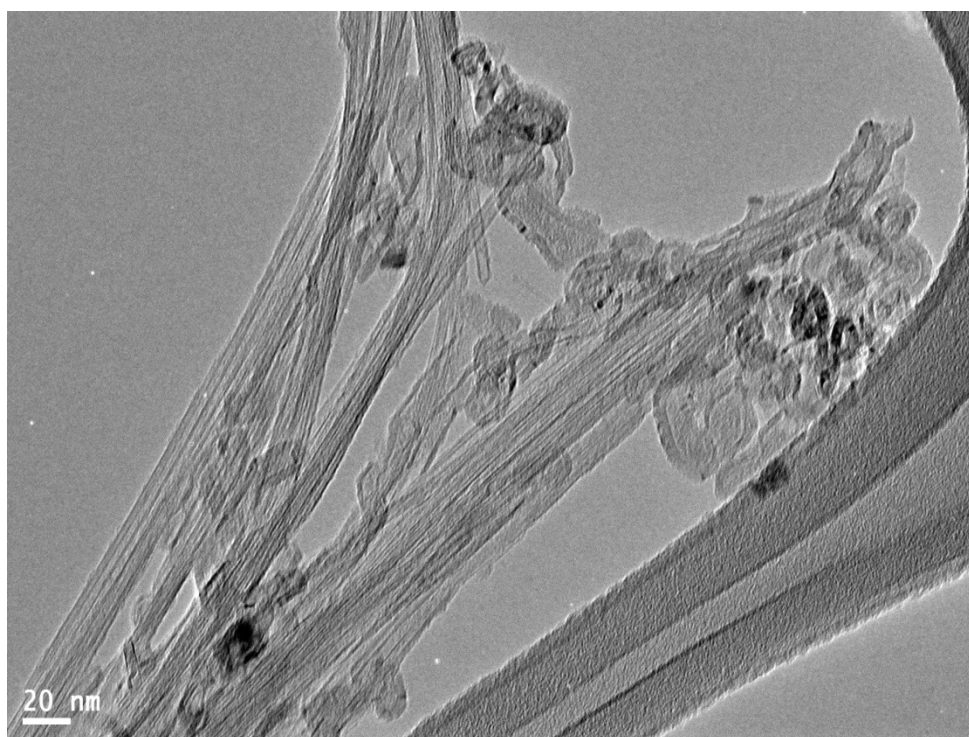
Figure 4-10: TEM Image of 10%Cu/CNT
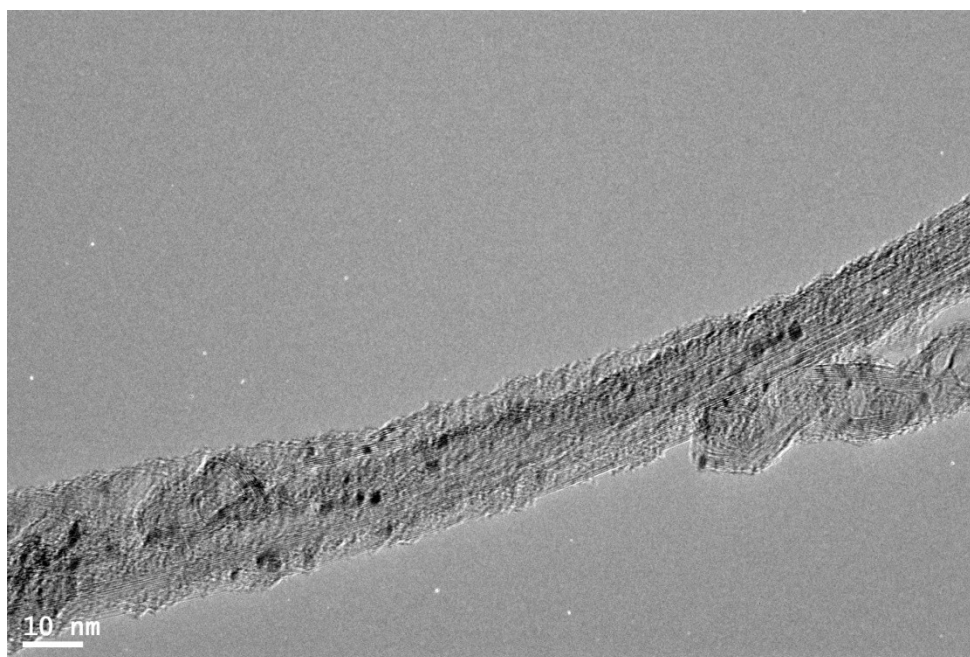
Figure 4-11: TEM Image of 10% Cu/CNT
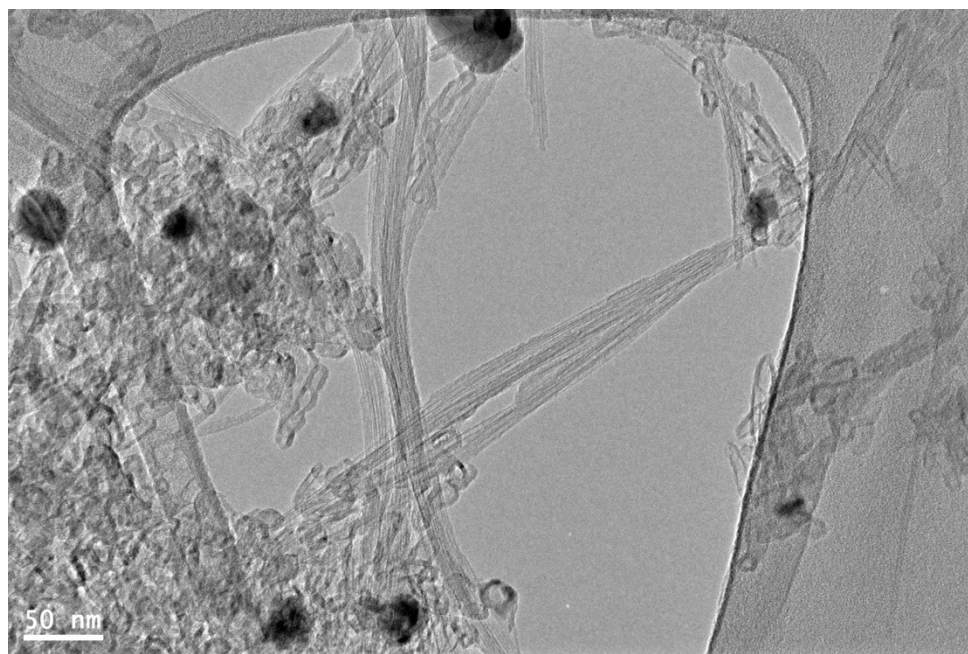
Figure 4-12: TEM Image of 20% Cu/CNT

X-ray photoelectron spectroscopy (XPS) was performed to acquire information about the chemical state of the copper deposited on the surface of the support. Figures 4-13 through 4-13 show the XPS spectra of 30 % Cu/CNT catalyst. Spectrum in Figure 4-13 shows a strong carbon peak of C1s at 284 eV which shows the pyrolytic carbon substrate CNT. Figures 4-14 & 4-15 show XPS spectra at medium and high binding energies. There are strong Cu peaks of Cu2p3, Cu2p1/2, O1s at about 929.46, 955 and 525.86 eV respectively. These results show that copper in metallic form has been successfully deposited on CNT.
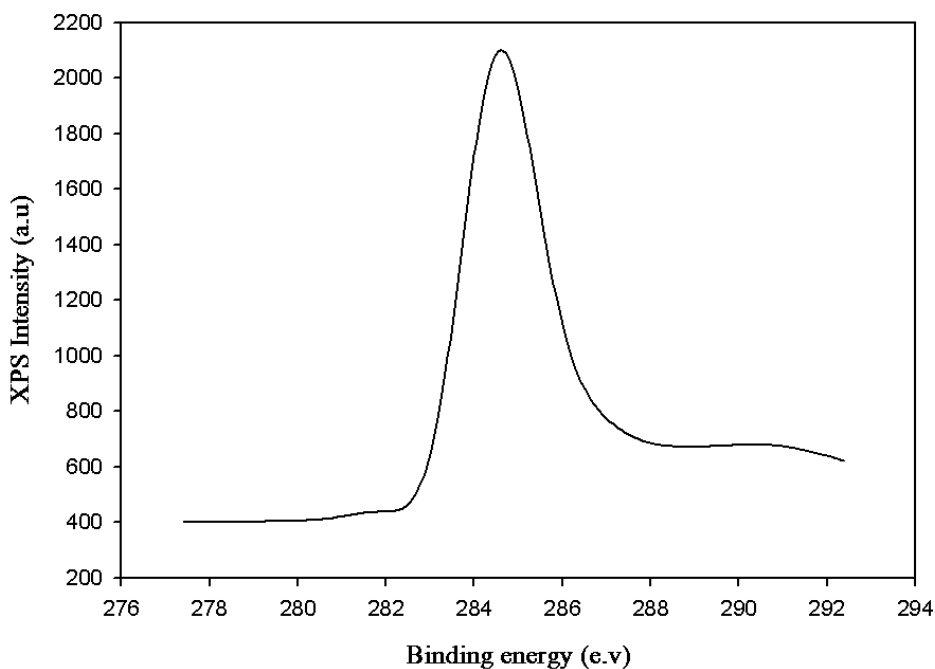
Figure 4-13: XPS Spectrum of 30% Cu/CNT at Low Binding Energy
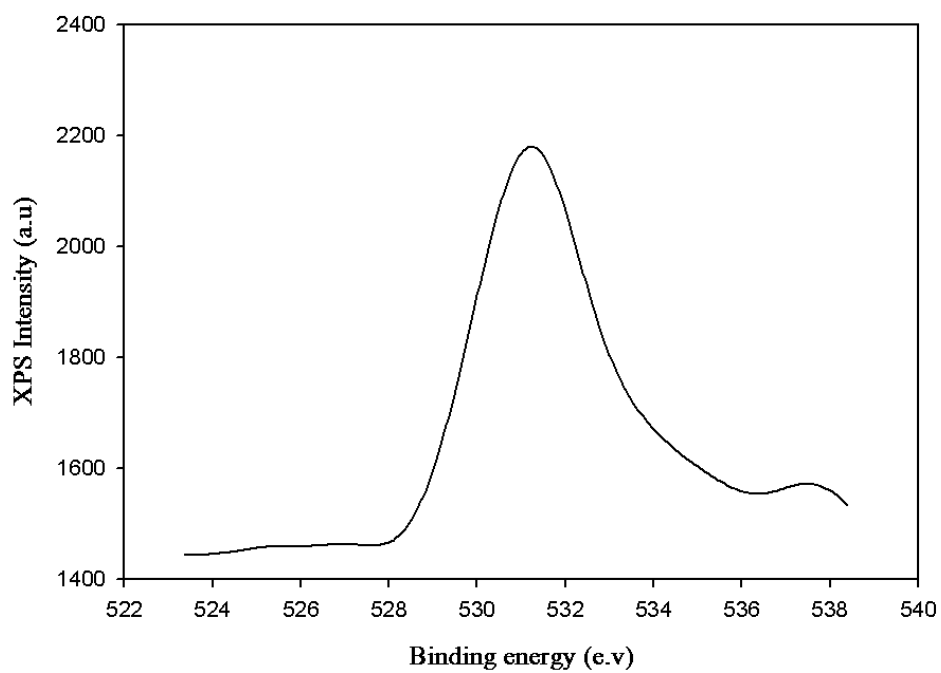
Figure 4-14: XPS Spectrum of 30% Cu/CNT for Medium Binding Energy
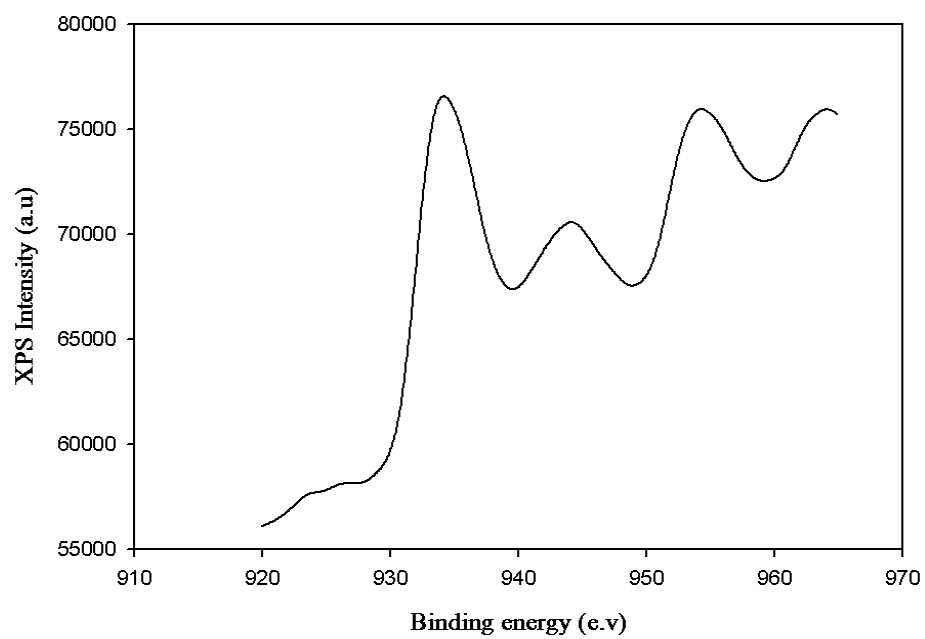
Figure 4-15: XPS Spectrum of 30%Cu/CNT for High Binding Energy

Nitrogen adsorption and desorption experiments were carried out to ascertain the surface area, types of pore and the total pore volume of the catalysts. Figure 4-16 shows the N_2 adsorption-desorption isotherms for the pristine CNTs. The figure shows that the isotherms show a typical type IV adsorption model according to the IUPAC classification. This isotherm shows a hysteresis loop which indicates the presence of pores in the mesoporous range. As can be seen from the Figures 4-16 & 4-17 that the amount of nitrogen adsorbed in case of functionalized CNT is higher than the unfunctionalized CNT. It can be inferred from these observations that acid treatment of the pristine CNTs increases the surface area. In fact, upon acid treatment for the purpose of purification and functionalization, the specific surface area increased from 236 to 365 m^2/g. This is due the fact that acid treatment generates more functional groups and opens up the tube ends and generate defect on the sidewalls of the CNTs thereby increasing the surface area. Figures 4-18 & 4-19 show the adsorption isotherms for 10 and 30 wt % copper supported on CNT. Loading copper decreases the surface area and pore volume of the catalyst. The results are summarized in Table 4-2. It can be observed that in the Table 2 that the surface area for 60% Cu loading decreased to121 m^2/g compared to the functionalized pure CNTs 365 m^2/g. This decreased is due to the pore blocking of the CNTs by the copper particles, and with increase in loading, the pores become more and more inaccessible for adsorption. The BET surface areas for the CNTs-supported Cu catalysts range from 357 to 121.6 m^2/g. The averaged crystallite size of Cu supported on CNTs (estimated on the basis of TEM image) ranges from 3.8 to 59 nm, which depends on the copper loading content. As increasing the copper content of the CNTs supported copper catalysts, both the BET surface areas and the pore volume decreased,

124

accompanied with the increase of the size of the copper particles. Generally, the decrease of the copper dispersion or the increase of the particle size will lead to the decrease of the catalyst activity. The above results indicate that, the changes of the catalyst properties induced by altering the copper loading contents would cause significant influence on the electrocatlytic activity of the prepared catalysts.
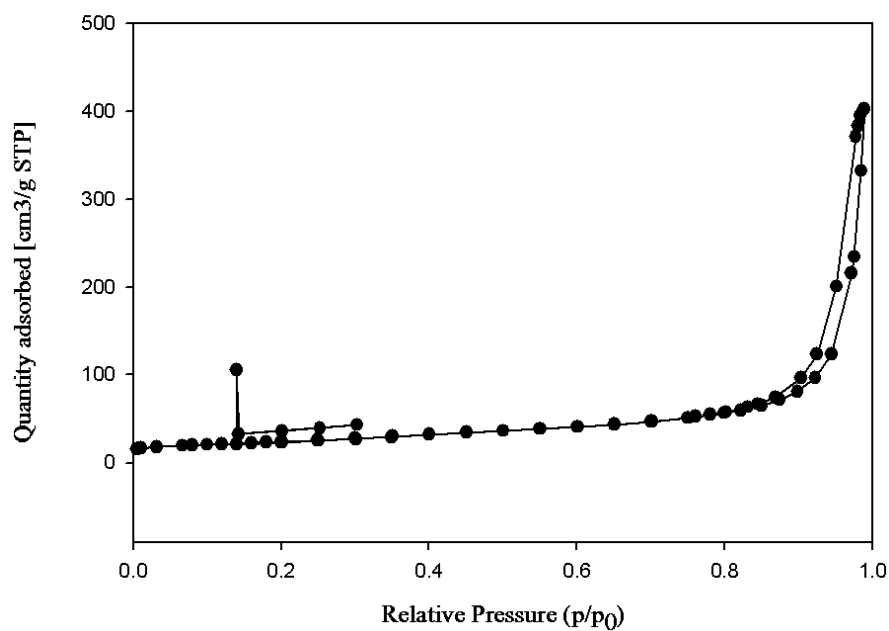
Figure 4-16: N_2 Sorption Isotherm for as-received CNT

125
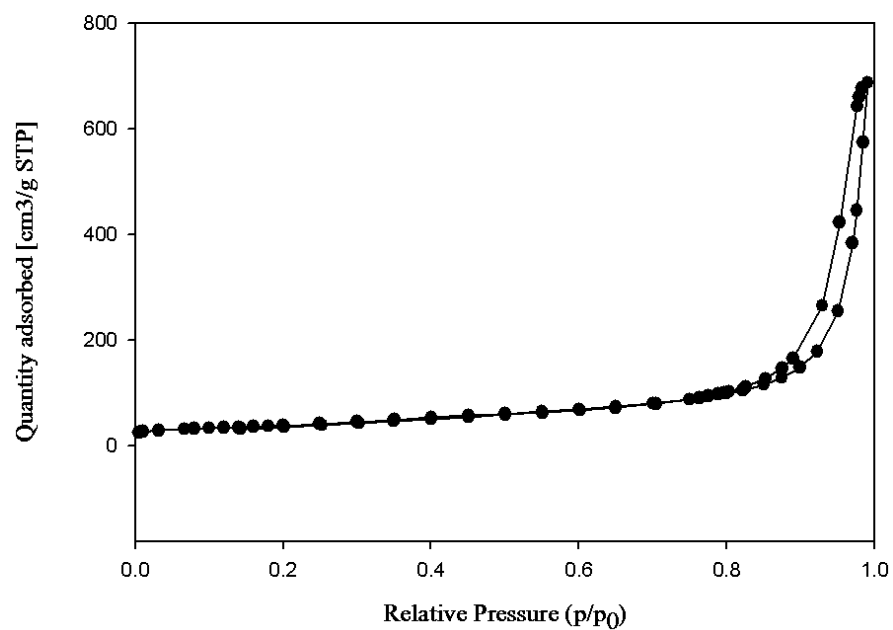
Figure 4-17:N_2 Sorption Isotherm for Functionalized CNT
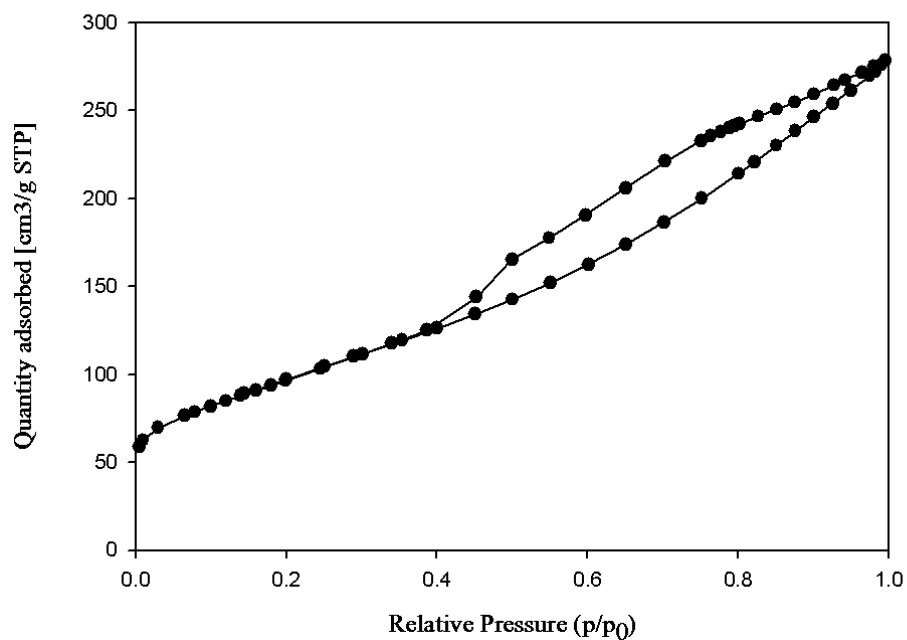
Figure 4-18:N_2 sorption Isotherm for 10% Cu/CNT
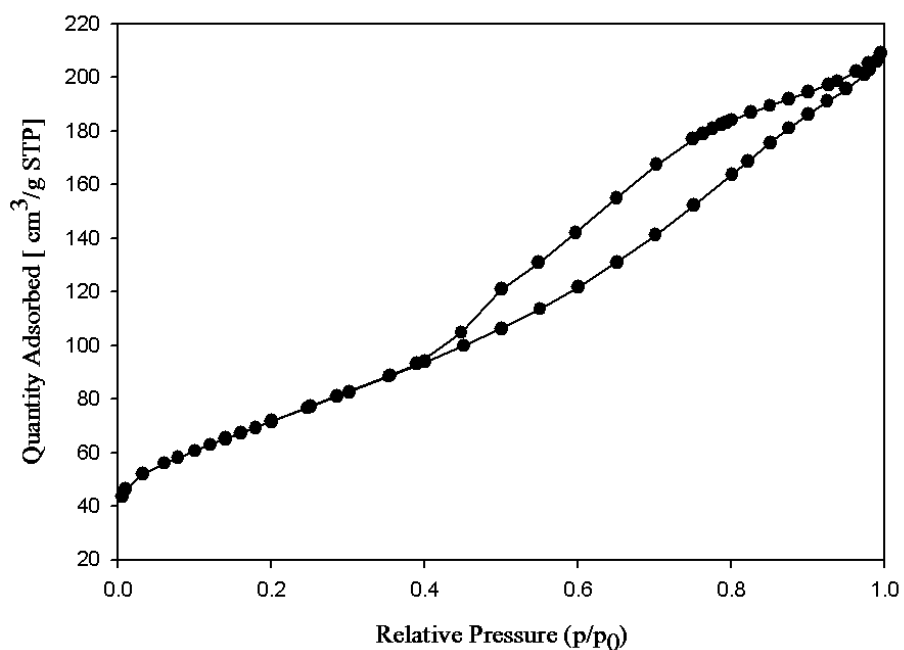
Figure 4-19: N_2 Sorption Isotherm for 30 % Cu/CNT

Table 4-2: BET Surface Area and Pore Volume

Sample	Surface area m²/g	Pore volume cm³/g
Pristine SWCNT	220	0.32
Functionalized SWCNT	365	0.56
10%Cu/CNT	347	0.41
20%Cu/CNT	339	0.40
30% Cu/CNT	257	0.31
40% Cu/CNT	180	0.26
60%Cu/CNT	121	0.20

The type and density of the functional groups attached to the carbonaceous support material bear significant influence on its suitability for use as a support material for the preparation of ERC electrocatalyst. These functional groups provide attachment sites for

the foreign particle on otherwise inert CNTs. In addition, availability of more functional groups implies more sites where active elements can be anchored. This is particularly important for the cases where high metal loading is desired. FTIR spectra gives idea about the nature of the functional groups attached to a particular support material.

FTIR spectra of functionalized CNTs is shown in Figure 4-20.The peaks which are identified at 1360, 1710 and 3402cm^{-1} characterize C-O, C=O and O=H bonds in the functionalized CNTs. Another absorption peak is evident in Figure 4-20 at 3441cm^{-1} and at 1385cm^{-1} that correspond to the hydroxyl bands (-OH). Peaks at 1710 and 3450cm^{-1} can be attributed to acidic groups like carboxyl, phenol and lactol. Peak at 1576cm^{-1} assigns C=C bond in CNTs. These observations show that the acid groups were successfully introduced in the CNT. IR spectra of 20% Cu/CNT in Figure 4-21 shows peak, apart from characteristic functionalized CNT peaks, at around 650 cm^{-1} indicating the formation of Cu-C bond in the prepared catalyst. Similar observations were made by Wang et al. [171].
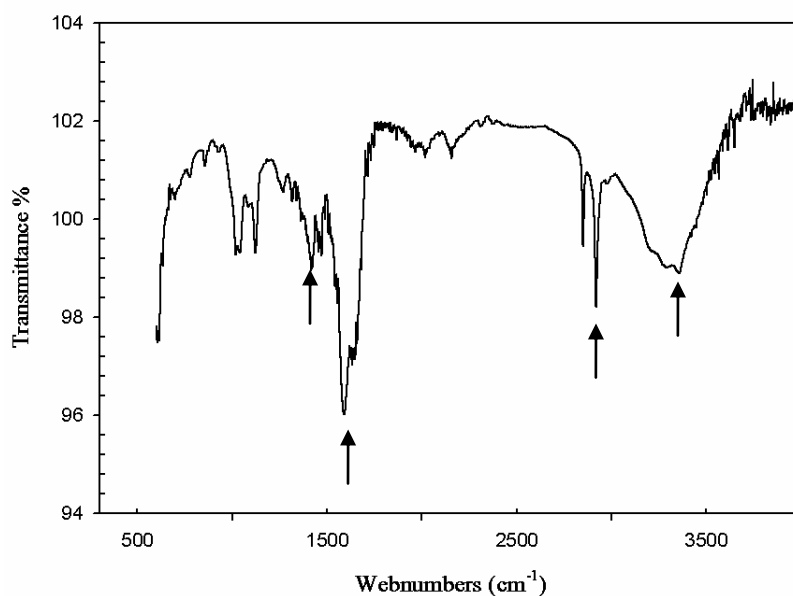
Figure 4-20: IR spectra of Functionalized CNT
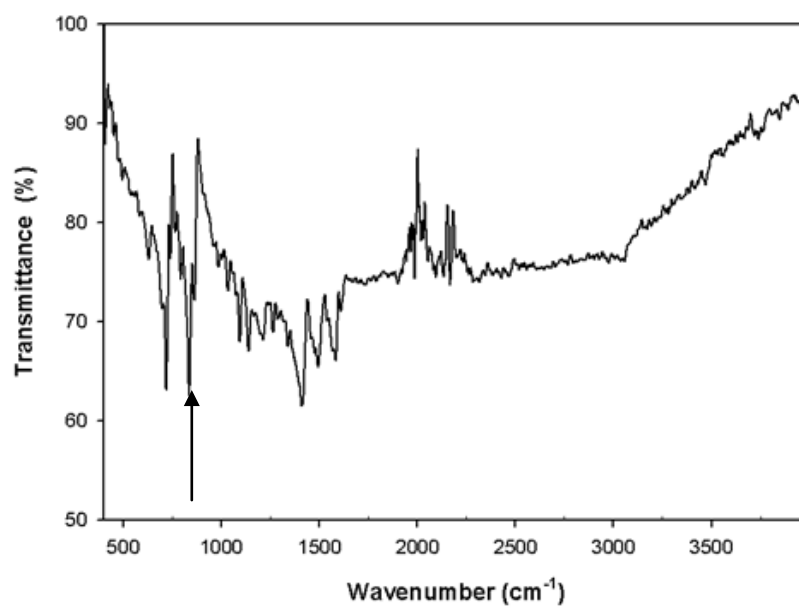
Figure 4-21: IR spectra of 20% Cu/CNT

B.   Electrochemical Performance

Linear sweep voltammetry (LSV) and chronoamperometry (CA) were carried out to assess the electrocatalytic activities of the prepared catalysts. Figure 4-22 shows the LSV curves in the 0 to -3.0 V range for 10%Cu/CNT coated on carbon paper in 0.5 M $NaHCO_3$ under nitrogen and carbon dioxide saturation. Under both the scenario, after the onset potential (i.e., the potential at which current is more than 1 m AmA), there exists a linear relationship in the current and potential for rest of the scan range with the absence of any evident cathodic reduction peak. No visible change in the electrode was observed in the potential range used in the experiment. This shows that the support material is stable under the testing condition. Hydrogen evolution reaction (HER) as a result of water electrolysis occurs in aqueous 0.5 M $NaHCO_3$ solution under N_2 and CO_2 saturation. In absence of CO_2, entire current is due to production of hydrogen by HER. But under CO_2 saturation, two competing reactions occur; CO_2 reduction and H_2 evolution reaction. The HER is an undesirable reaction and consumes electrical energy that is meant for ERC. Under the nitrogen saturation, the current density is found to be 0.0045 A/cm^2 whereas under CO_2 saturation, it shows current density of 0.008 A/cm^2 at - 1.5 V. Difference in current density for the two cases arises from the CO_2 reduction which takes place under CO_2 saturation This confirms that copper effectively catalyses the ECR. Cathodic current obtained in our studies is much higher than the results reported in the available literature [52, 108, 44, 174] This increase in current could be due to the excellent activity of the highly dispersed copper particles on high surface area CNT (400m^2/g). Similar results were obtained by Yamamoto et al. on porous activated carbon [114]. The observed higher current with CO_2 saturated solution is in line with some of the findings that are available

in the open literature [80, 161, 174, 107]. However, there are some reports suggested that the amount of current obtained from the CO_2 is lower than that in the N_2 saturated solution [148, 108]. This observation shows that although CNT catalyses HER but copper is not active towards it from the catalysts systems in these studies. This showed that the CNT supported copper catalysts exhibited good catalytic activity with highly dispersed active sites. Cathodic current obtained in the present study is higher than the results reported in the available literature [52, 108, 44, 174] This increase in current could be due to the excellent activity of the highly dispersed copper particles on high surface area CNT which posses higher electrical conductivity as well [126].

In order to study the effect of Cu content on the ERC and the optimum loading, we prepare catalysts with different metal loading on CNT from 10 to 60%. Figure 4-23 shows the effect of copper loading on the current–potential curve. In theory, the catalytic activity increases with the metal content in the catalyst. More active sites provide better probability of reactants reacting. Therefore, cathodic current was found to increase with increase in copper loading till 20 wt %. However, with further increase in loading, as shown in Figure 4-23, the current eventually starts decreasing. For example, currents for 10% Cu/CNT and 20% Cu/CNT at -1.5 V were 0.004 A/cm^2 and 0.0175 A/cm^2 respectively. At the same potential, 30% Cu/ CNT showed 0.012 A/cm^{2}A current$A$) and, further increase in loading has no impact on the current. The results are summarized in Table 4-3 and shown in Figure 4-24. Similar observation was made by Lee et al. in ERC copper loaded gas diffusion electrode [175]. This can be explained by the TEM and XRD of the catalyst. Beyond 20% Cu loading the size of the particles increased coupled with active sites become increasingly inaccessible for the reactant due to the reduced surface

area and micropore sizes because of pore blocking and agglomeration of the copper particles. Therefore, the optimum loading for the CNT catalyst prepare by homogeneous deposition and precipitation is 20%.
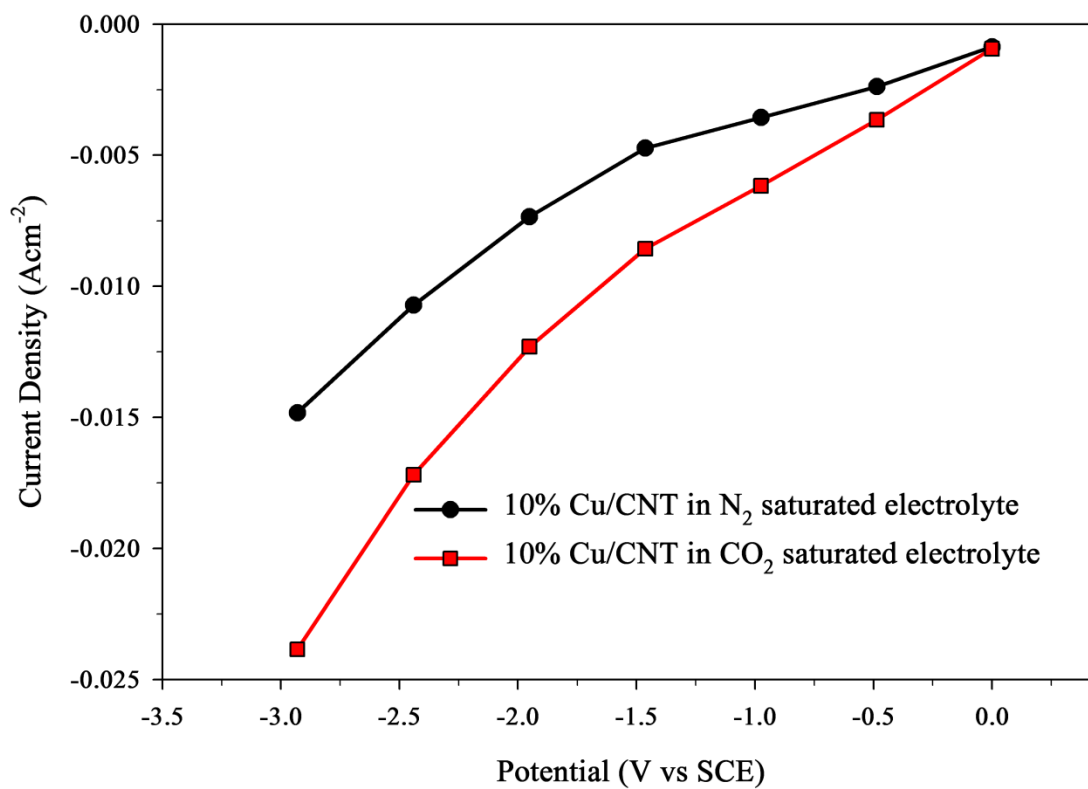
Figure 4-22: Linear Sweep Voltammetry Results for 10%Cu/CNT under N_2 and CO_2 Saturation
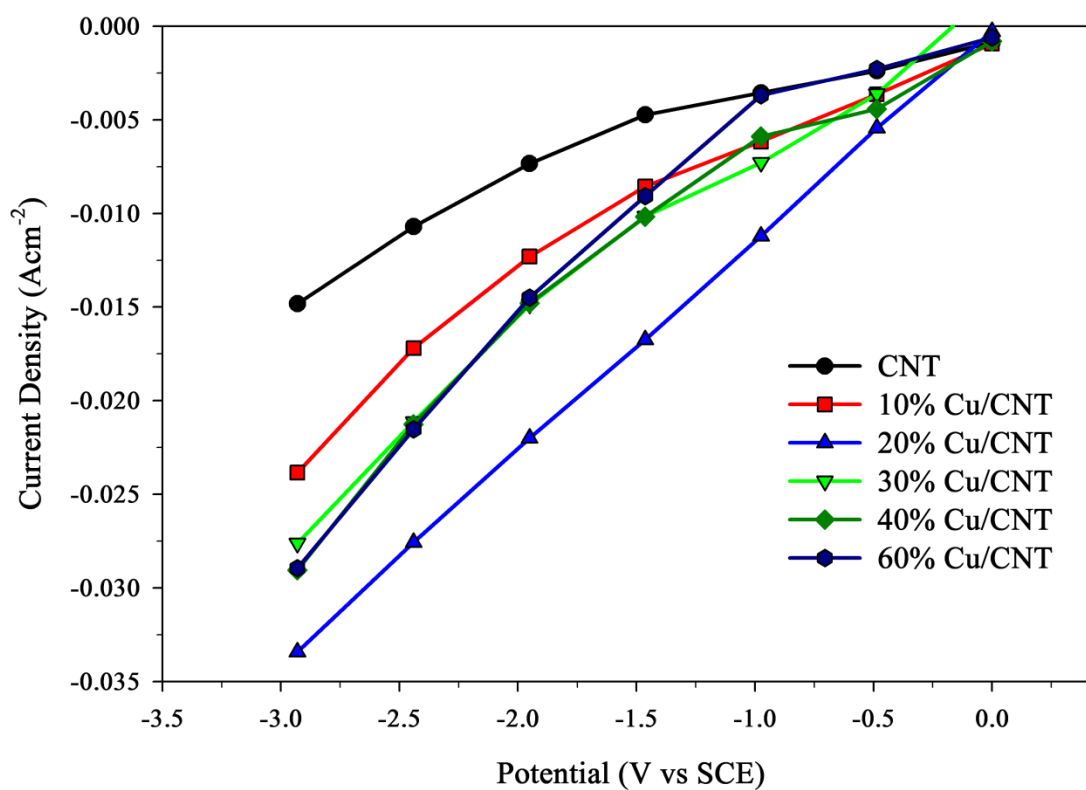
Figure 4-23: Linear Sweep Voltammetry Results for Copper Supported on CNT in CO2 saturated

Table 4-3:: Linear Sweep Voltammetry Analysis Results for the Cu/CNT Catalysts

Catalyst Sample	Current Density (mA/cm^2)
Functionalized CNT	-5
10% Cu/CNT	-14
20% Cu/CNT	-31
30% Cu/CNT	-16
40% Cu/CNT	-16
60% Cu/CNT	-20
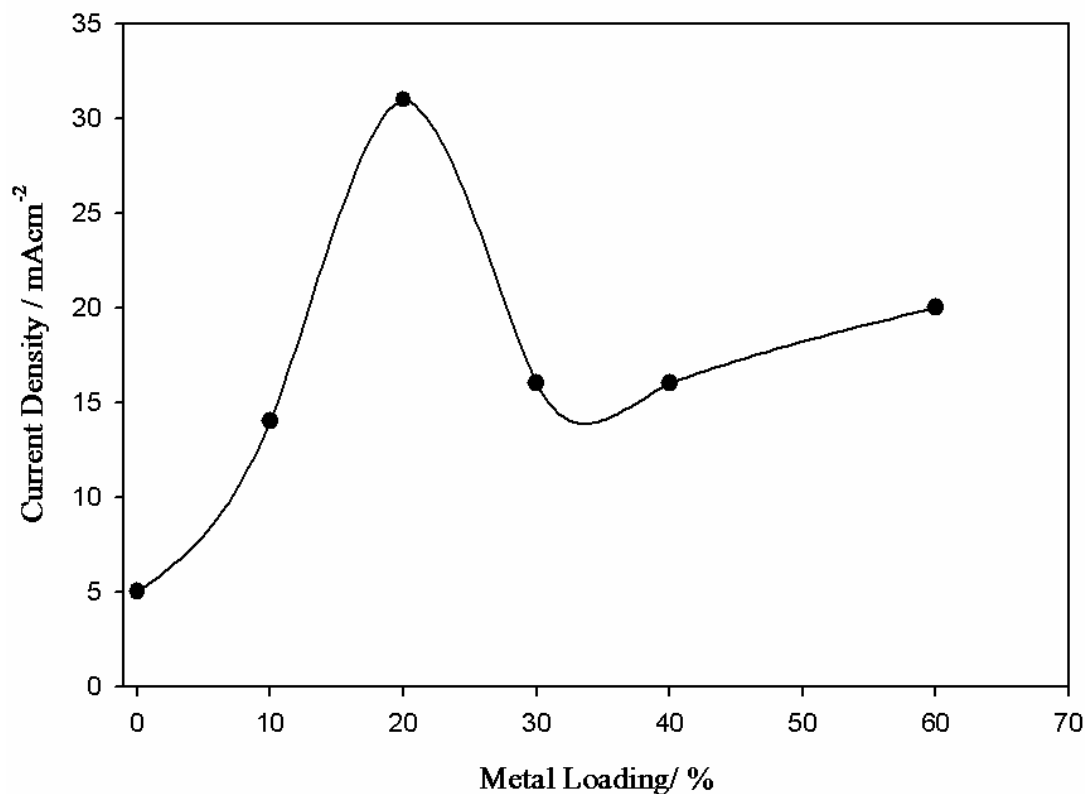
Figure 4-24: Cathodic Current Density at Different Copper Loading for the Cu/CNT Catalysts

For example, current density for CNT and 10%Cu/CNT at -1.5 V were -5 and -14 mA/cm^2 respectively. At the same potential, 20%Cu/CNT showed -31mA/cm^2 current. Starting from CNT, effect of adding copper is manifested in terms of *A)* increased catalytic activity, hence, high current density. However, with further increase in loading to 30%, current decreases to -16 mA/cm^2. This is due to the fact that the fact that effect of adding copper is masked by the increased particle size and poor distribution of copper in the CNT as shown by SEM and XRD results. For 60 % copper loading, current density is observed to be higher than 30% but lower than 20 % loading. This could be due to the favorable effect imparted by the increased amount of copper metal in the catalyst but low surface area and poor distribution of metal prohibits its effective utilization. Similar

134

observation was made by Lee et al. in ERC copper loaded gas diffusion electrode [175]. Therefore, it is concluded that 20% Cu loading on CNT is the optimum loading.

To study the long term performance of the catalyst, potentiostatic electrolysis was carried out at -1.7 V for 6000s. Results are shown in Figure 4-24. The current of the ERC increases with increase in copper loading till 20% and, then decreased with further increase in copper content till 60% loading at which catalytic activity was recovered. This is in consistence with the results from the LSV. The result shows that copper supported on CNT is catalytically active for at least 6000 s.
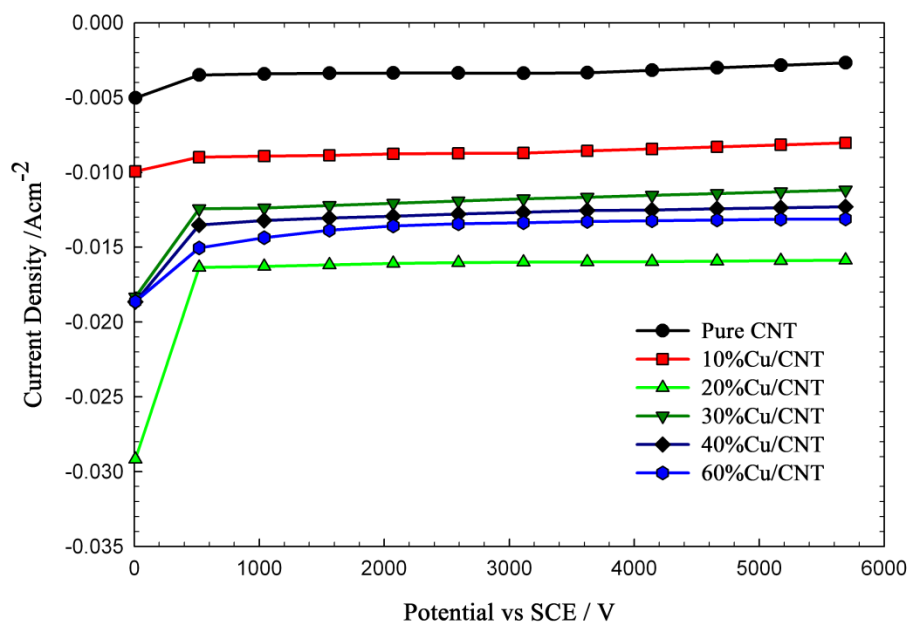
Figure 4-25: Chronoamperometry of Copper supported CNT

Methanol concentration in the catholyte was measured by GC equipped with FID. Prior to the analysis, methanol was extracted in diethyl ether. Faradaic efficiency for methanol production was measured by the following formula:

$$FE = \frac{nFm}{It}$$ …………………………………………………………….(4-1)

Where **n** is number of electrons involved in the reaction to produce the product and it is six for methanol production. **F** is the Faraday's constant and **m** is moles of product formed. **I** is the total current in ampere and **t** is the time in seconds. Figure 4-25 shows the faradaic efficiency of methanol production as a function of potential. The potential of -1.7 V is observed to be the potential at which maximum FE of 38.4%.
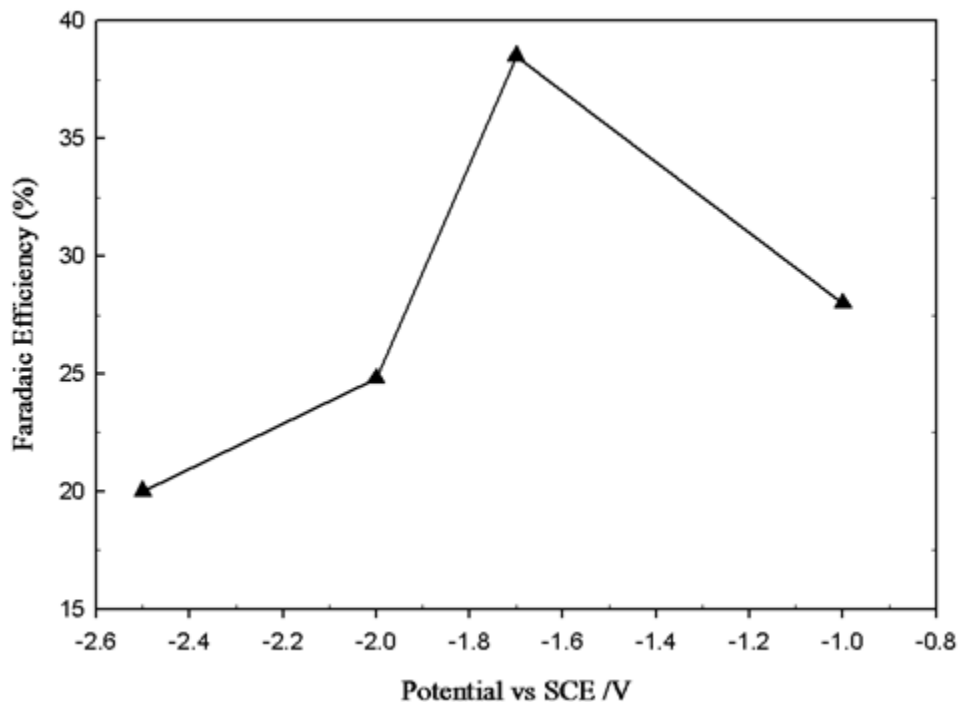
Figure 4-26: Faradaic Efficiency for 20%Cu/CNT for 6000s

Based on the preliminary results from the half cell reaction setup, the catalyst was further evaluated in the fuel cell type reactor setup as explained in the experimental section. For this purpose, 20% Cu on CNT was used as this was found out to be the optimum catalysts. The faradaic efficiency is defined as the portion of the current passing through the cell that goes to the desired product or the charge used for producing the specific product divided by the charge passed through the cell during the experiment [70, 118]. The expression for the faradaic efficiency for the gaseous product can be calculated by the following expression:

$$F.E. = \frac{eFxF_m}{I}$$ ………………………………………………………………… (4.2)

Where

F.E. = Faradaic efficiency, e = no of electron exchanged, F = faraday's constant = 96487

C/mol, x = mol fraction of the gas, F_m= Molar flow rate

$$F_m = \frac{PF_v}{RT}$$ ………………………………………………….……….. (4.3)

P = Pressure, F_v= Volumetric flow rate, R= Gas Constant, T = Temperature in Kelvin

At the end of the experiment the product gas samples were collected and analyzed by using a gas chromatography equipped with two TCD detectors. When the reaction was carried out with membrane electrode assembly i.e. only the cathode and anode catalyst pressed with membrane only H_2 was the product. This observation is consistent to the results reported by Delacourt et. al as well [70]. It was suggested by Delacourt et al that the production of hydrogen was due to water electrolysis. However, when the reaction was carried out in alkaline medium hydrocarbons were produced. Therefore, it was concluded that maintaining near neutral or alkaline environment is essential to produce hydrocarbons [68]. By inserting the fiber glass saturated with sodium bicarbonate solution between the membrane and the cathode catalyst, in addition to H_2 gas CO gas was also obtained, this is very useful product as CO and H_2 is collectively known as synthesis gas or syngas.

Figure 4-26 shows the current density of the reaction at different potential. As the potential was increased to more negative values, the resulting cathodic current also increased. Figure 4-27 shows the faradaic efficiency for the product obtained at different voltages for 20 % Cu/CNT catalyst. Table 4-4 summarizes the products obtained and their faradaic efficiency at different voltages. The reactions have been performed at four different voltages to see the effect of voltage. The faradaic efficiency for methanol increased slightly from -0.5 V to -1.5 V, however, on increasing further towards more negative voltage the efficiency decreased and highest efficiency was found at -1.5 V vs. NHE. The potential of -1.5 V vs. NHE correspond to -1.744 V vs. SCE. The faradaic efficiency for H_2 also increases with increasing the applied voltage but after -1.5 V vs. NHE it starts decreasing. Hydrogen evolution reaction competes with carbon dioxide reduction during electrochemical reaction. Although the hydrogen evolution reaction is not desirable during the course of reaction but the good combination of hydrogen and CO (synthesis gas) is also a useful product and can be used in the petrochemical industry as an intermediate as well. The evolution of hydrogen from the electrochemical carbon dioxide reduction on Cu electrode is evident from the literature [59, 160, 176]. In addition to hydrogen, CO was also observed in this. It is obvious that if the electrodes were to be polarized with more negative potential the product yield could be enhanced but the main motive of this study to get product at low potential as possible. The faradaic efficiency of CO is 12.3% at a potential of -2.5 V vs. NHE while H_2 current efficiency is 80.6% at a metal loading of 4 mg/cm^2. Methanol was produced at low potential and at high potential methanol got converted into H_2 and CO. The efficiency for CO increases with increasing pressure and nanotubes creates high pressure inside the channels due to "nanoeffect".
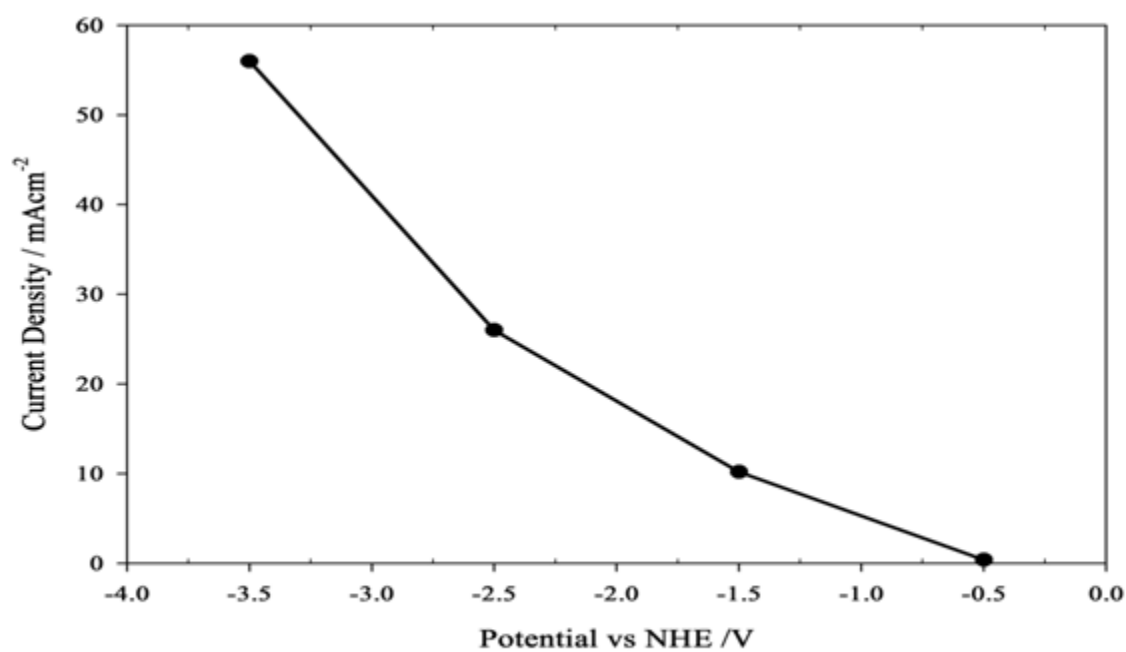
Figure 4-27: Current density at different potential in SPE reactor
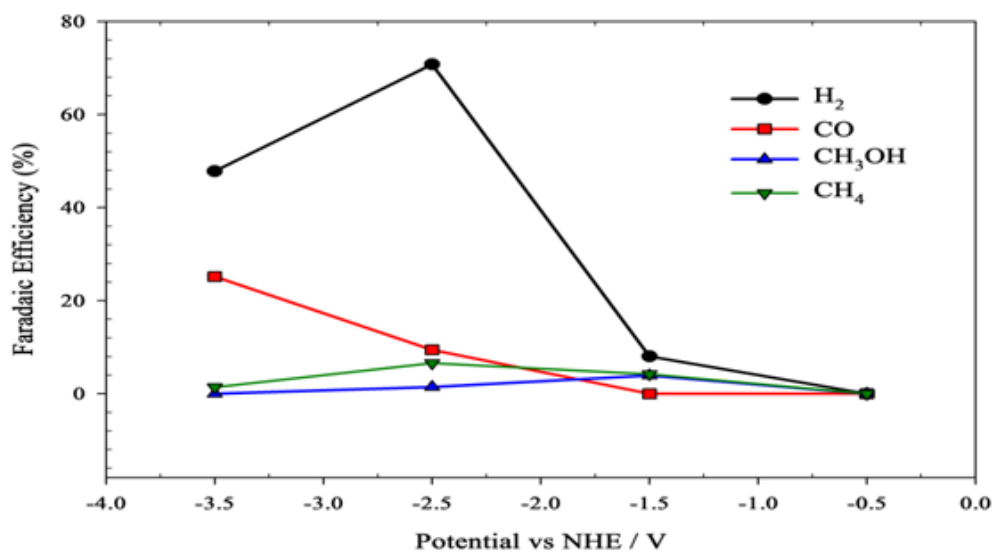
Figure 4-28: Product distribution at different potential in SPE reactor

Table 4-4: Faradaic Efficiency of Products at Different Voltages

Voltage	Faradaic Efficiency (%)				Current density (mA/cm^2)
	Hydrogen	Carbon monoxide	Methanol	Methane	
-0.5	0	0	0	0	0.4
-1.5	8.03	0	3.9174	4.2	5.2
-2.5	70.766	9.43	1.45	6.6	14.4
-3.5	47.83	25.17	0	1.4	40.48

4.1.2 Copper -Iron Supported on CNT

In this section, the effect of incorporating iron on the catalytic activity of the copper supported on CNT has been explored. Iron cathodes have been widely employed for CO_2 electroreduction. Hori et al. found that iron cathodes in neutral and mild acidic solutions yield predominantly hydrogen [50]. Frese and Canfield observed significant amount of CO on Fe electrodes [43]. Hori et al. in 1995, under high pressure conditions (30 atm) at Fe electrode studied the electroreduction of CO_2, and HCOOH was found to be the main product and methane as the side product. Traces of ethane and ethylene were also found [87]. However, the faradaic efficiency was extremely low. Hara et al at high pressure conditions and large current density (120 mA/cm^2) achieved 60% faradaic efficiency for HCOOH formation. By products were long chain hydrocarbons such as 1-butene, trans-2-butene, iso-and n-pentane, with maximum partial current density of ~10 mA/cm^2[105].

In this work, copper and iron are deposited on the high surface area CNTs. It is known in the literature the two metals which are individually active for the ERC. It is anticipated that the two metals together when supported on CNT can provide synergic effect and therefore, may prove to be a better catalyst in comparison with the individual single metal supported on CNT. Apart from the effect of iron incorporation, effect of metal loading on the support was also studied. Three different compositions of Fe and Cu i.e., (5%Cu-5%Fe, 10%Cu-10% Fe, 20%Cu-20%Fe) were synthesized and their electrocatalytic activity tested according to the methodology explained in details in the experimental section. Physical characterization and activity results for these catalysts are given in the following sections.

A.   Physical Characterization

The XRD analysis was carried out to investigate the diffraction structure of the Cu-based catalysts supported on carbon nanotubes (CNTs) for different metal loading conditions. Figures 4-28 through 4-36 show the XRD of the Cu-Fe supported on CNT. For low metal loading as shown in the Figure 4-28, no peak for Cu was visible. This could be due to the fact that copper might have formed well dispersed phase. Characteristic Cu and Fe peaks were evident in the subsequently higher loadings. However, as the metal loading was increased, more intense peaks of copper and iron become evident. This shows that copper and iron particles were successfully loaded on the CNT. Particle sizes decreased as evident from the decrease in the peak width. Peak at 42° was chosen to calculate the crystallite size. Particle size increased from 3 nm for 10% metal total loading to 36.5 nm for 60% total metal loading.
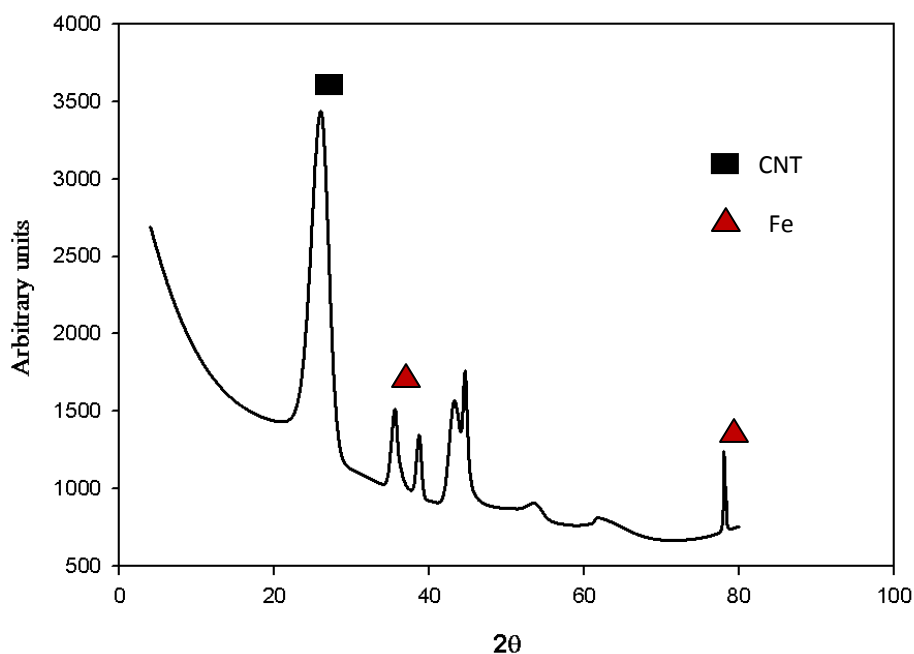
Figure 4-29: Powder XRD Pattern of 5%Cu-5%Fe/CNT

143
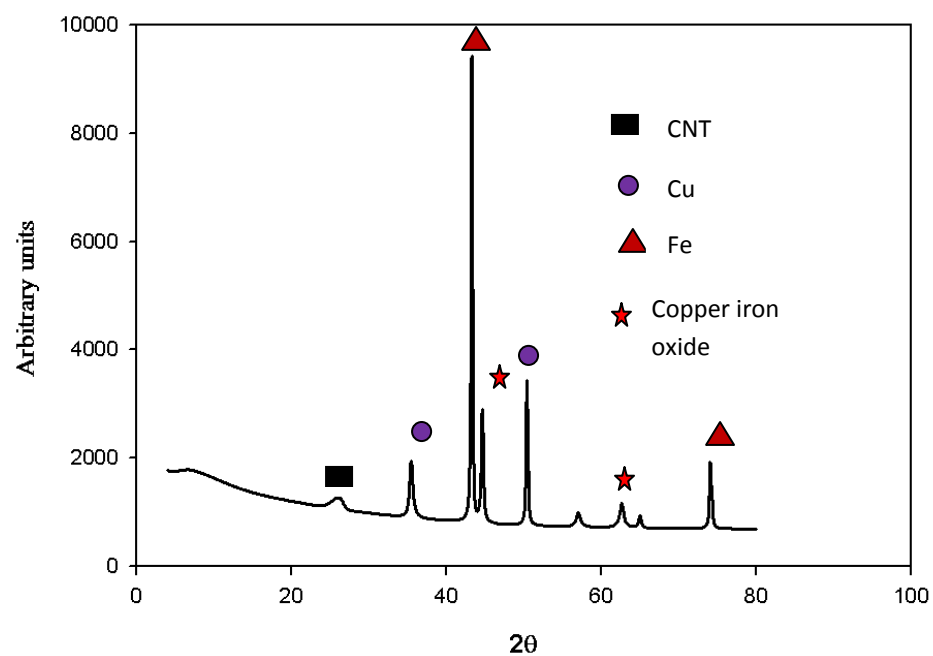
Figure 4-30: Powder XRD Pattern of 10% Cu-10% Fe on CNT
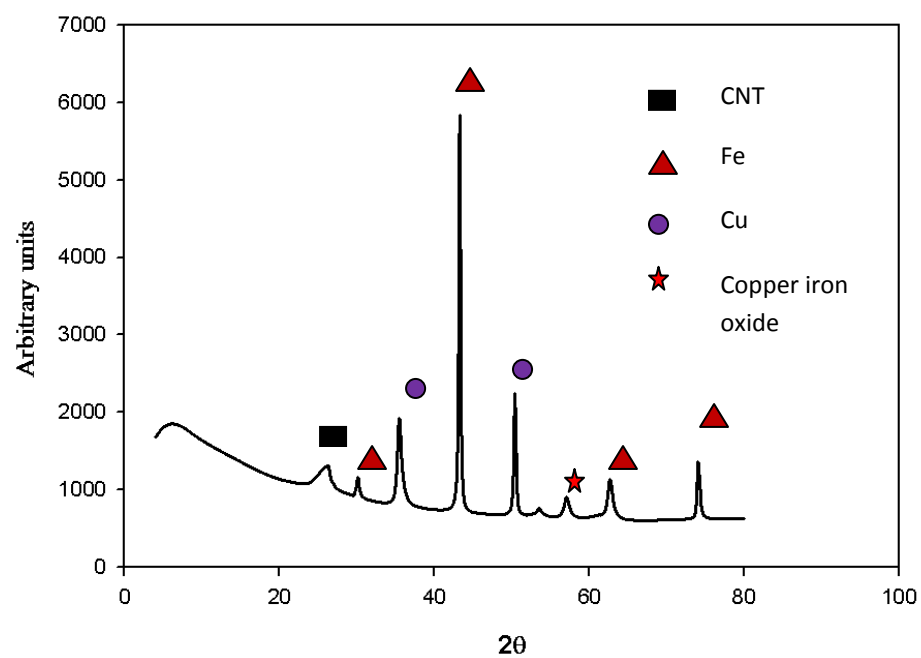
Figure 4-31: Powder XRD Pattern of 20% Cu-20% Fe on CNT
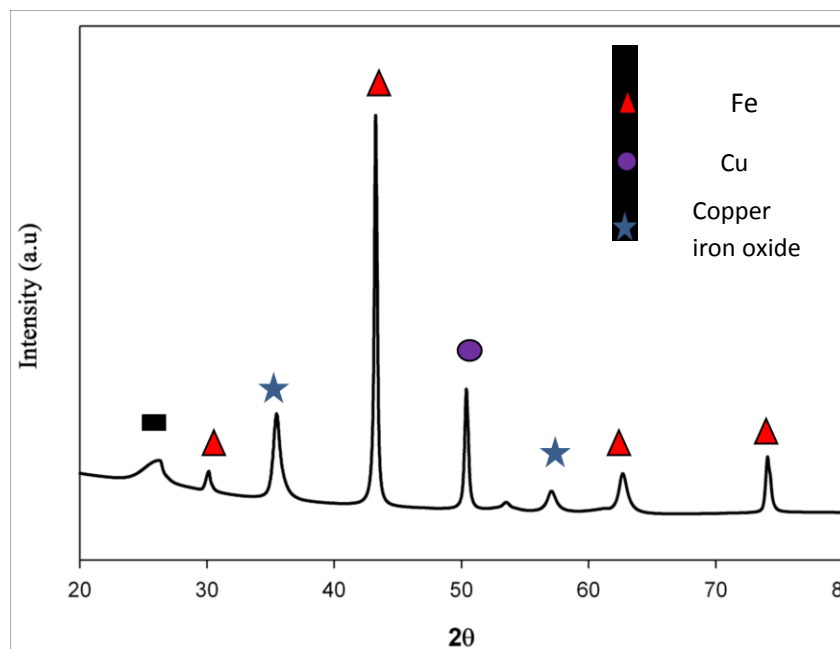
Figure 4-32: Powder XRD Pattern of 30% Cu-30% Fe on CNT

Figures 4-32 through 4-35 show the SEM images obtained for the different metal loadings. It can be observed that all the catalysts have retained the tube like structure of CNTs. This shows that incorporation of copper and iron particles have not distorted the structure of the host CNT. The metal particles are uniformly distributed on the surface of the CNT. With increasing metal loading, more and more agglomerations are found. Figure 4-36 shows the SEM-EDX results for 20% Cu-20% Fe catalyst on CNT. Very strong peak of carbon is observed along with peaks of copper, iron and oxygen was observed. Oxygen peak arises as a result of acid functionalization of the pristine CNT. Therefore, it can be inferred from this observation that acid group was indeed created on the CNT. Presences of copper and iron peaks indicate that copper and iron have been successfully mounted on the CNTs.

145

Fe
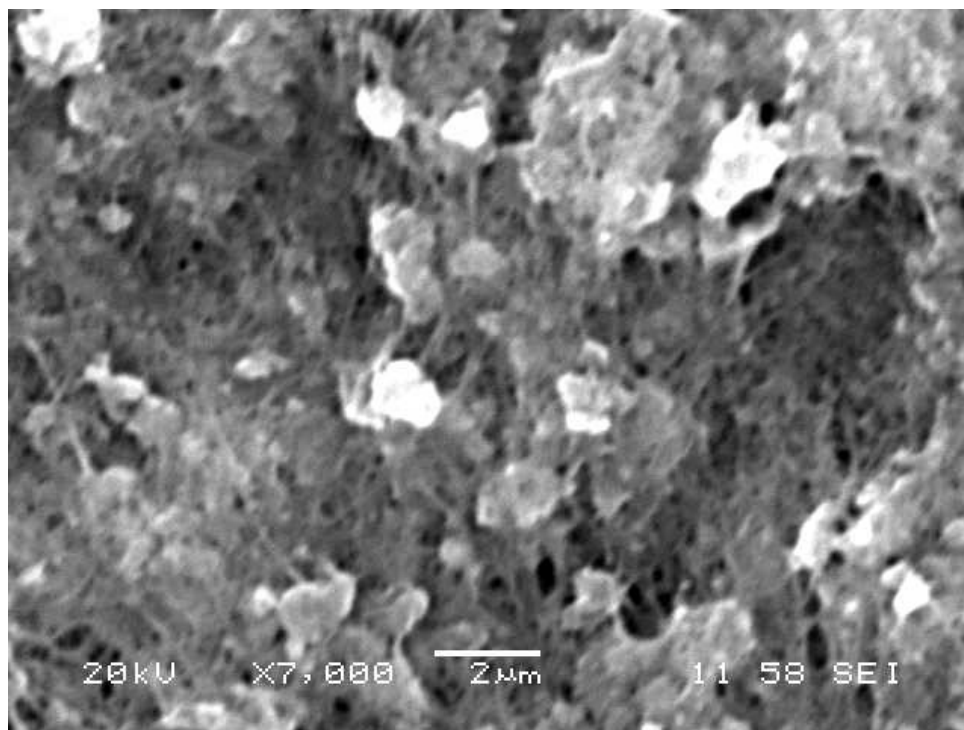
Figure 4-33: SEM micro graph of 5%Cu-5%Fe on CNT
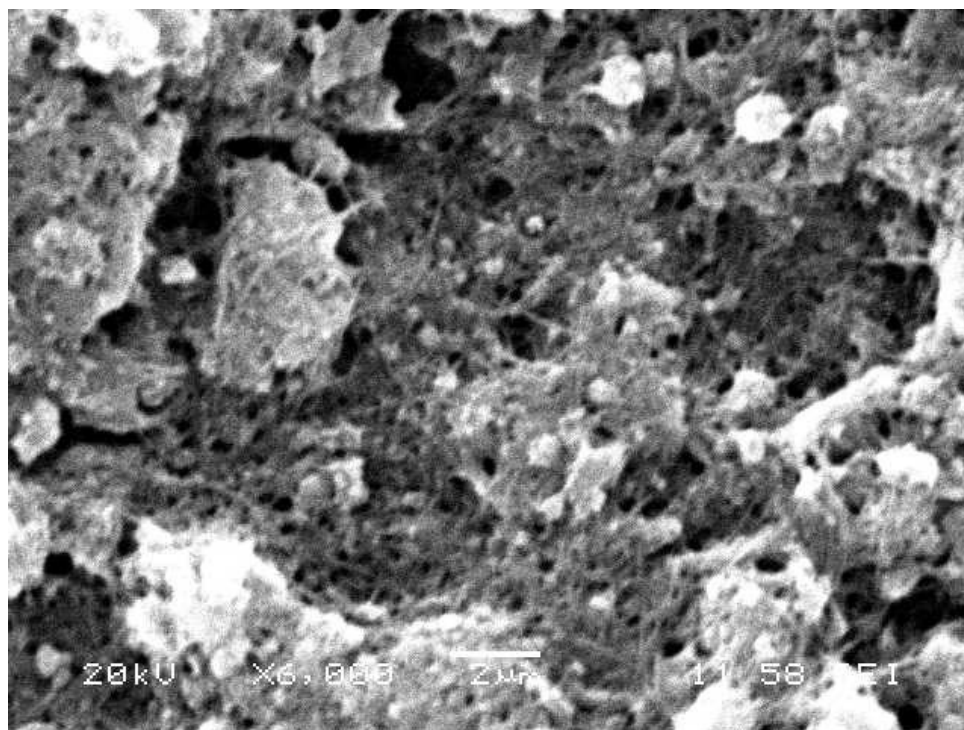
Figure 4-34: SEM micro graph of 10%Cu-10%Fe on CNT

146
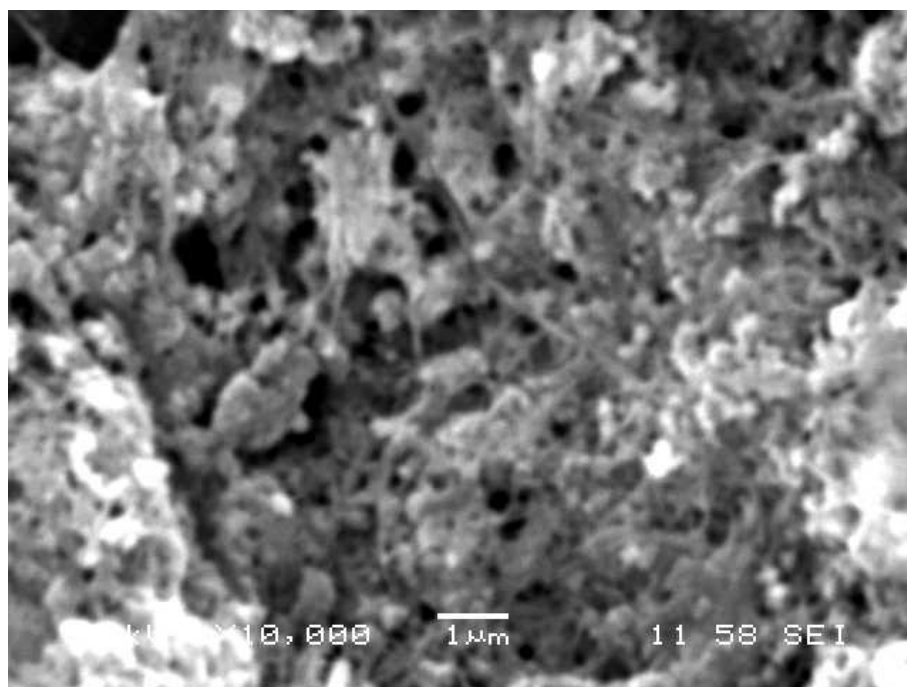
Figure 4-35: SEM micro graph of 20%Cu-20%Fe on CNT
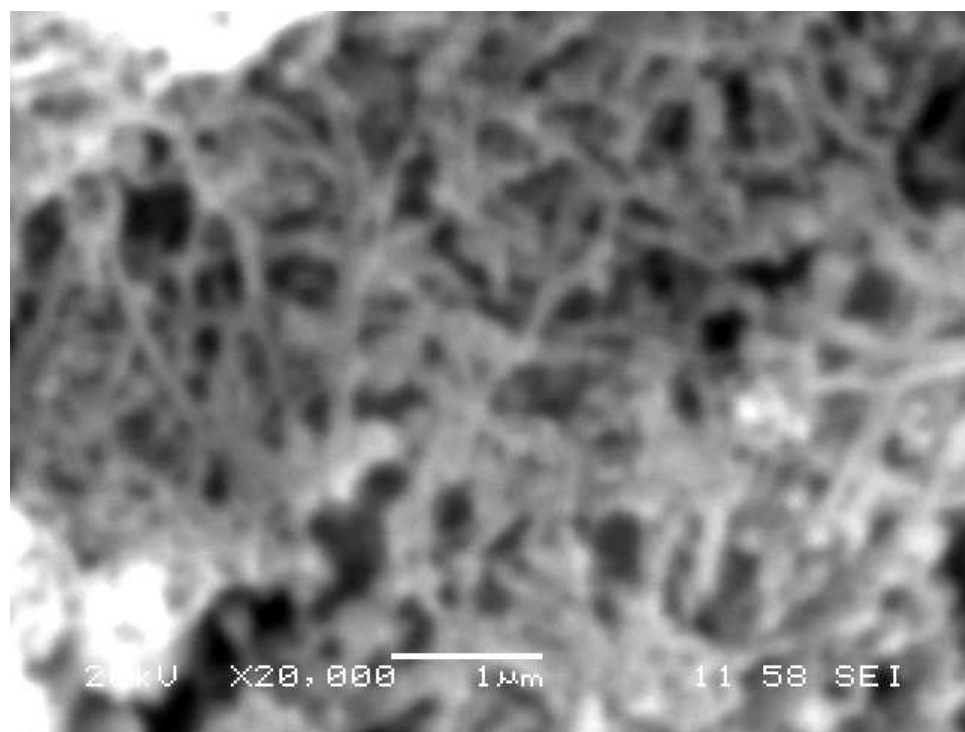
Figure 4-36: SEM micro graph of 30%Cu-30%Fe on CNT
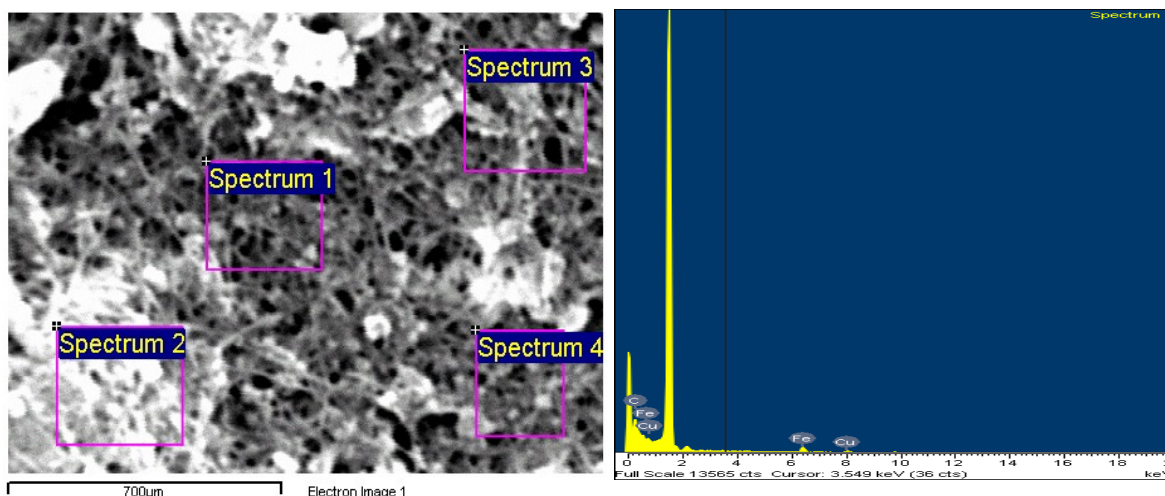
Figure 4-37: EDX results on 20%Cu-20%Fe on CNT

B. Electrochemical Performance

Figure 4-37 shows the effect of copper and iron loading on the current–potential curves. Cathodic current was found to increase with increase in copper loading till 20 %Cu-20% Fe, and with further increase in loading, current, eventually, started decreasing. For example, current density for 10% Cu-10% Fe/CNT at -1.5 V was -7 mA/cm^2. One important observation is that at low potentials e.g., -1.5, there was no effect of changing the metal loading. But at high potential current increased with increased the metal loading till 20%Cu-20%Fe and then decreased with further increase in metal loading. Starting from CNT, effect of adding Cu is manifested in terms of *A*) increased catalytic activity, hence, high current density. This is due to the fact that the fact that effect of adding Cu and iron is masked by the increased particle size and poor distribution of copper in the CNT as shown by SEM and XRD results. Adding iron increased the current density as

compared with the pure copper. This could be due to the favorable effect imparted by the increased amount of iron metal in the catalyst but low surface area and poor distribution of metal prohibits its effective utilization. Similar observation was made by Lee et al. in ERC copper loaded gas diffusion electrode[173]. Therefore, it is concluded that 20% Cu-20%Fe loading on CNT is the optimum loading. Addition of iron in the copper supported on CNT catalysts does not seem to show any advantage in terms of current density. However, the product distribution might be different for copper and iron supported catalysts.

Apart from the activity test, long term performance test of the prepared catalysts were conducted by doing chronoamperometry analysis at -1.7 V for 100 minutes. Figure 4-38 shows the chronoamperometry results for the electrocatalysts. It can be observed that the catalysts are fairly stable at the potential for 100 min. Trends for chronoamperometry results are in accordance with linear sweep results. It was
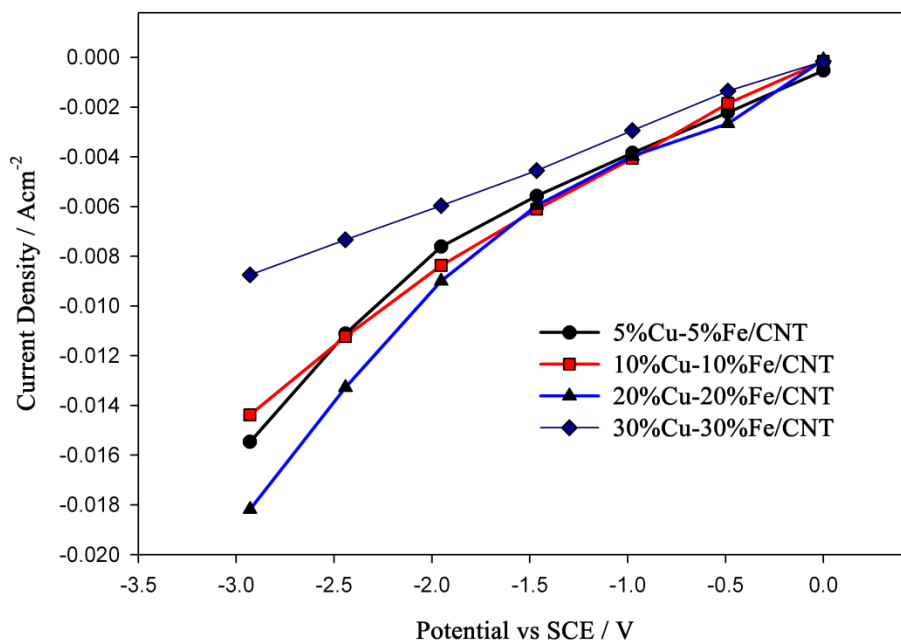
Figure 4-38: Linear sweep voltammetry results for Cu-Fe supported on CNT in CO2 saturated electrolyte
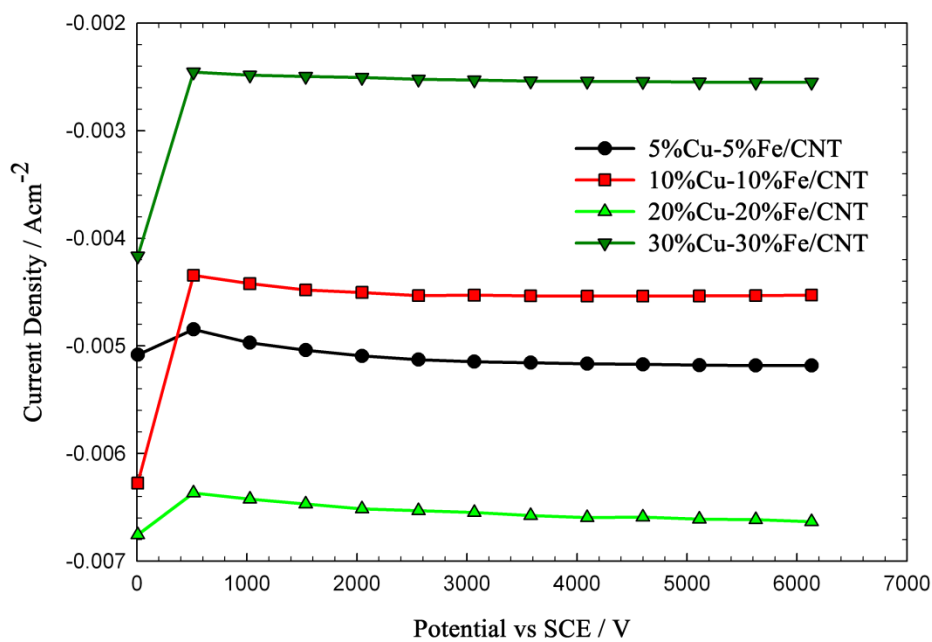
Figure 4-39: Chronoamperometry of Cu-Fe supported on CNT

150

4.1.3   Copper-Ruthenium Supported on CNT

A.   Physical Characterization

Ruthenium and copper binary catalysts were prepared to investigate the effect of addition of ruthenium on copper supported on CNT catalysts Figures 4-39 through 4-42 show the XRD of the copper and ruthenium supported on CNT catalysts. The obtained XRD patterns are similar to that of the host CNT. In Figure 4-39, no peak for Cu was visible. The Cu–Ru/CNTs show only the peaks corresponding to copper metal, and no peak corresponding to ruthenium metal was detected. This can be ascribed to the occurrence of highly dispersed Ru species in which the Ru^{3+} cations selectively replace surface copper atoms, especially the active sites (defects, vacancies, *etc.*), resulting in discontinuous Ru metal species. It is reasonable to speculate that the Ru metal species should be selectively located on the surface of Cu metal nanoparticles to generate tiny Ru clusters. This could be due to the fact that copper might have formed well dispersed phase instead alloy CuRu was formed. Characteristic Cu and Ru peaks were evident in the subsequent loadings. For example, as shown in Figure 4-41 which shows the XRD pattern for 20% Cu-20% Ru loaded on CNT, peaks at 38.88°, 58.56° and 69.80° belong to ruthenium phase whereas 43.22° and 50.5° peaks are assigned to copper. It is evident from the XRD patterns that no alloy formation took place in case of Cu-Ru/CNT. The particles were very small as the peaks were broad. Particle sizes of Cu and Ru were 5 nm and 4 nm respectively. As the metal loading increased, particle sizes increased as evident from the decrease in the peak width. Peak at 42° was choosen to calculate the particle size of copper. For ruthenium peak at 38.8° was chosen to calculate the ruthenium particle size. Copper particle size increased from 4 nm for 10% Cu-10% Ru to 136.5 nm for 30% Cu-30% Ru.
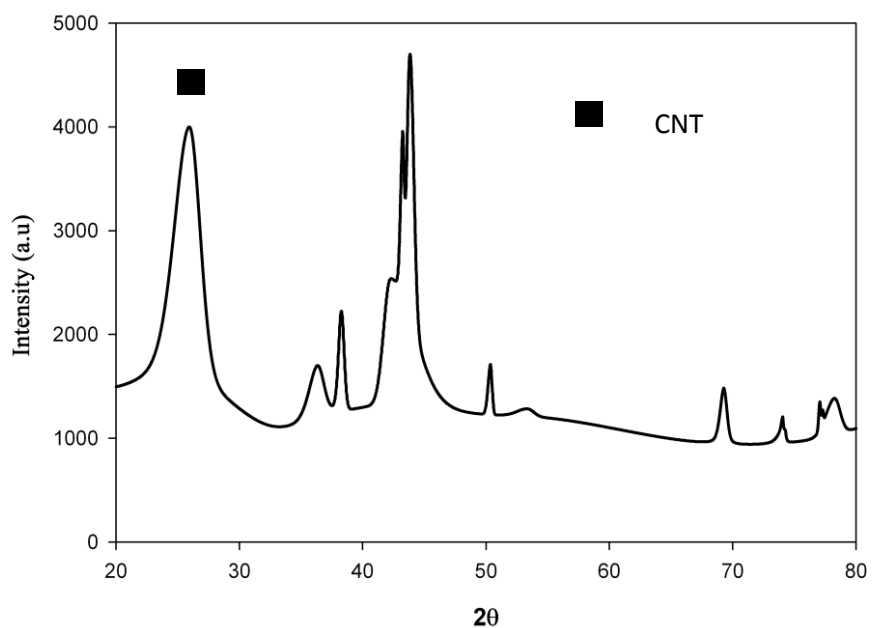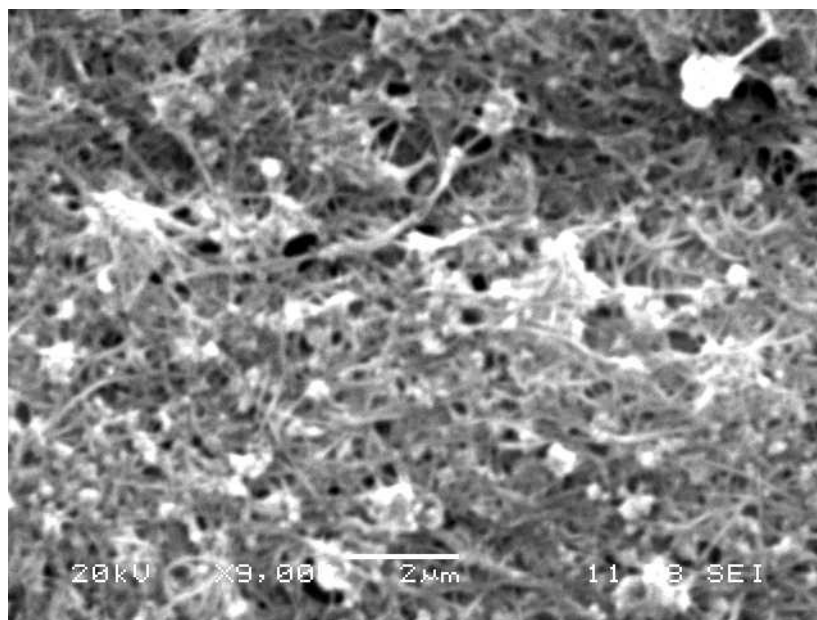
Figure 4-40: XRD Pattern of 5% Cu-5% Ru on CNT
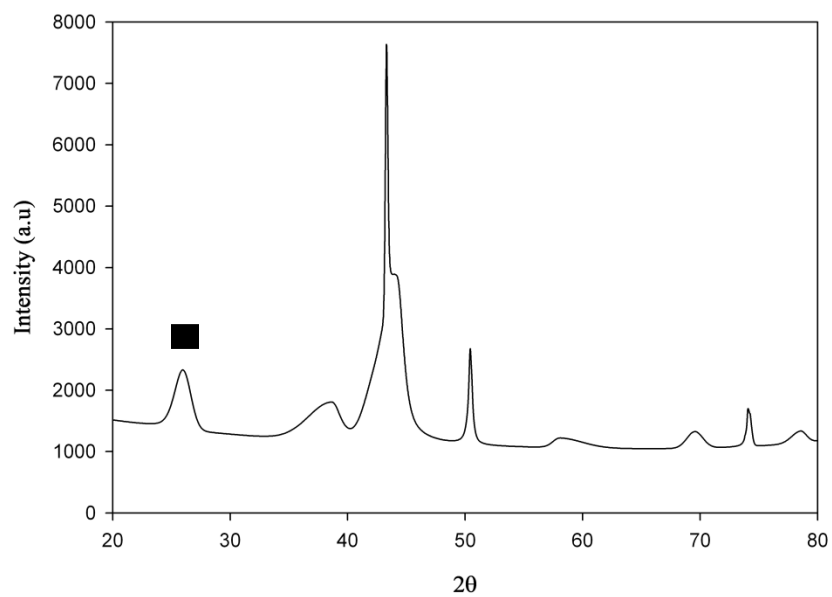
Figure 4-41: Powder XRD Pattern of 10% Cu-10% Ru on CNT
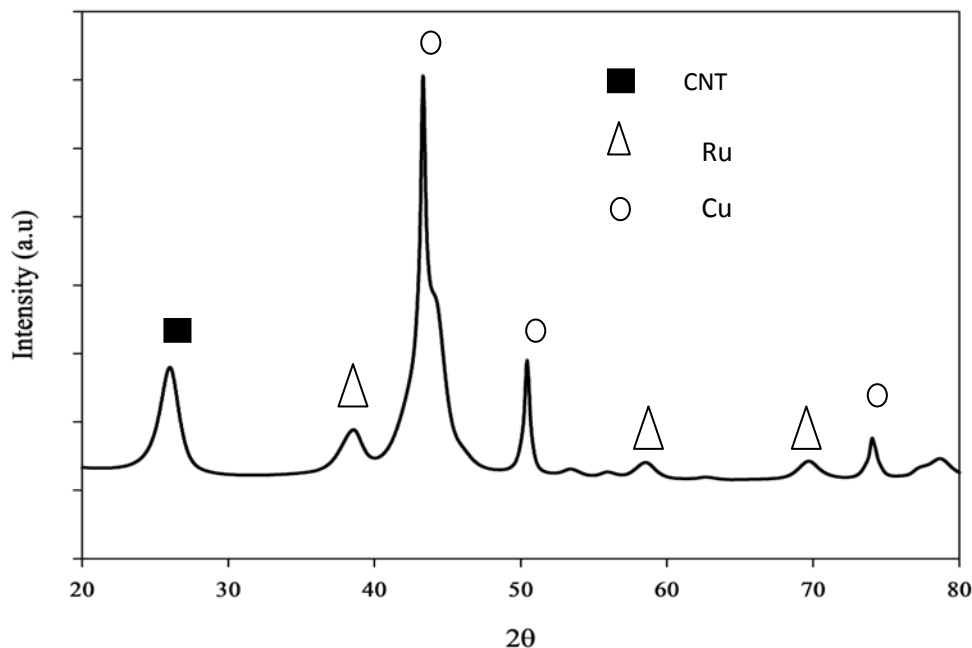
Figure 4-42: XRD Pattern of 20% Cu-20% Ru on CNT

Scanning electron microscopy (SEM) was carried out to ascertain the morphology and dispersion of metals on the support. Figure 4-43 shows the SEM image of the copper and ruthenium supported on CNT. Characteristic uniform tubular nanostructure of the CNT can be observed in the micrograph. Average diameters of the nanotubes are found to be in few nanometers and length up to few microns. There are large empty spaces in between the entangled tubes. Furthermore, copper and ruthenium metals were deposited on the surface of CNT. Figures 4-42 through 4-44 show the SEM images of the prepared catalysts. It is evident that the metal particles were homogenously dispersed on the surface of CNT. However, with very high metal loading agglomeration were evident. Figure 4-45 shows the SEM-EDX results for 20% Cu-20% Ru catalyst on CNT. Very strong peak of carbon is observed along with peaks of copper, iron and oxygen was observed. Oxygen peak arises as a result of acid functionalization of the pristine CNT. Therefore, it can be inferred from this observation that acid group was indeed created on

153

the CNT. Presences of copper and ruthenium peaks indicate that copper and ruthenium have been successfully mounted on the CNTs.

Figure 4-43: Powder XRD Pattern of 5% Cu-5% Ru on CNT
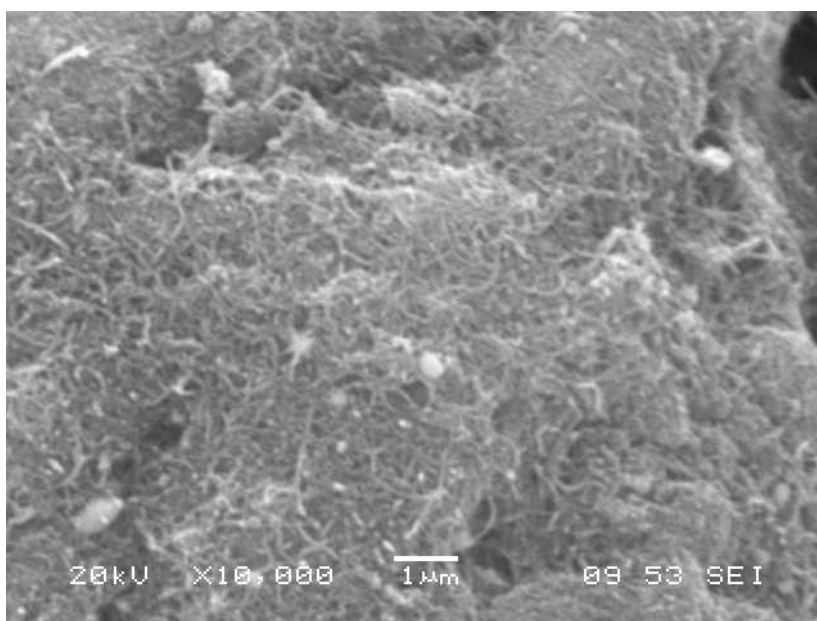
Figure 4-44: Powder XRD Pattern of 10% Cu-10% Ru on CNT
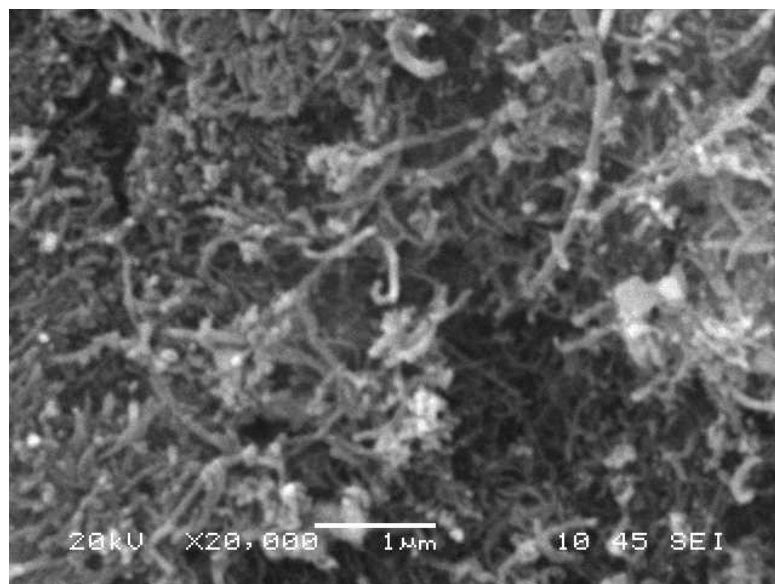
Figure 4-45: SEM image of 20% Cu-20% Ru on CNT
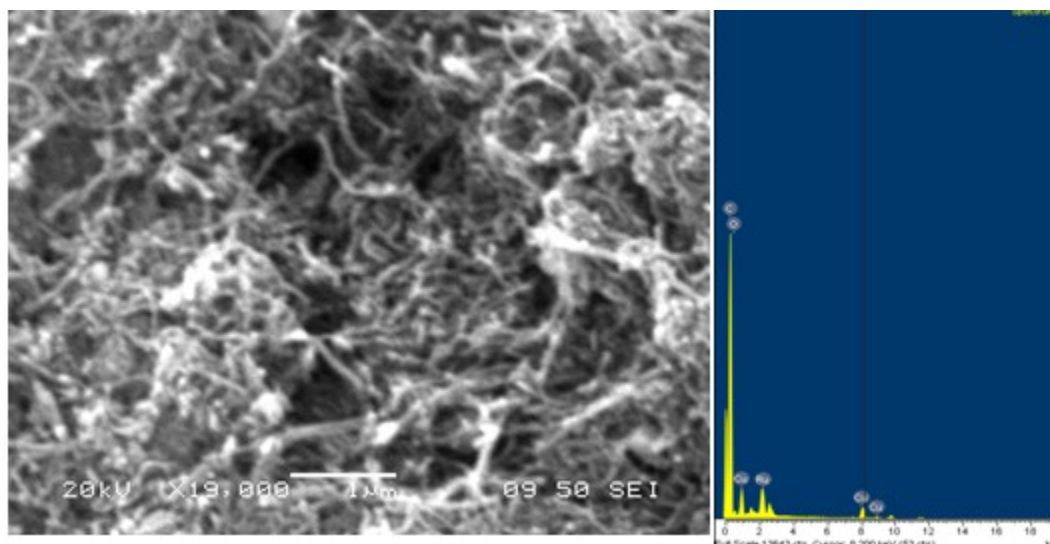
Figure 4-46: EDX spectrum of 20%Cu-20%Ru on CNT

Figure 4-46 shows the transmission electron microscope (TEM) images of the metal catalysts supported on CNT. For calculating size of the particles 300 particles were taken. Most of the Ru, Cu and Cu–Ru alloyed particles are located on the external surface of the

CNTs without incorporating clusters into the pores. Metal particles were mostly spherical in shape. Figure 4-47 shows the TEM at high magnification. It is evident that spherical metal particles are homogenously distributed on the surface of the CNT and their mean particle size was 3-4 nm. This is in agreement with the results obtained from the XRD analysis.
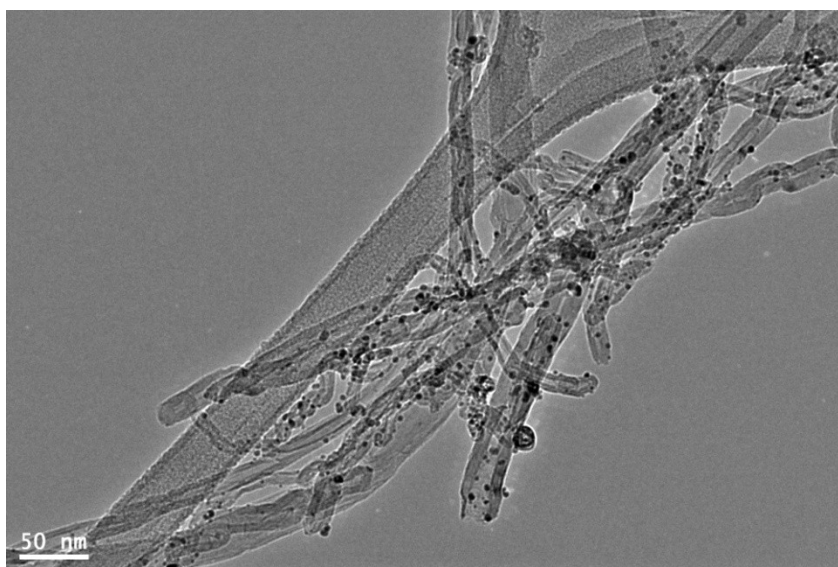
Figure 4-47: TEM image of 10%Cu-10%Ru supported on CNT
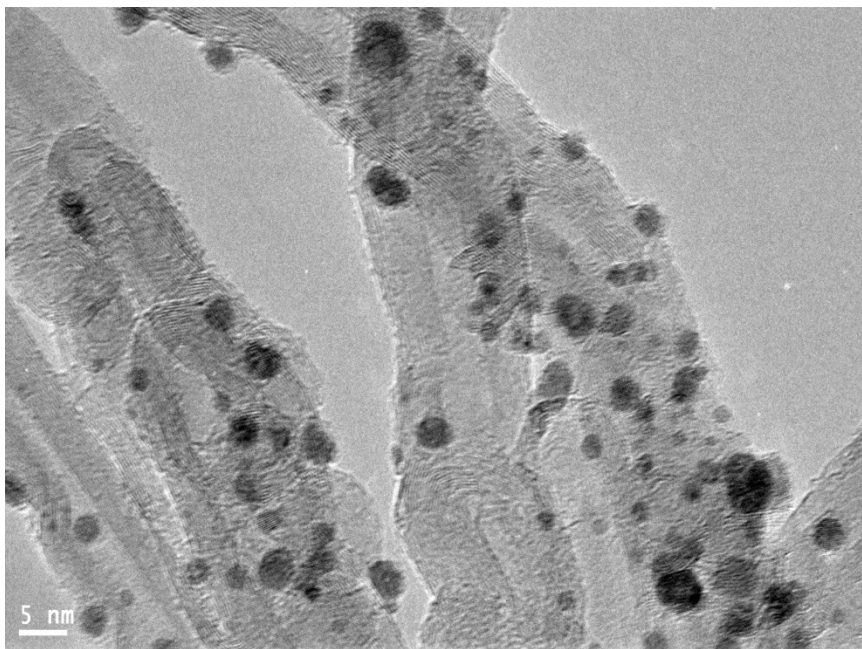
Figure 4-48: TEM image of 10%Cu-10%Ru supported on CNT at high magnification

B.   Electrochemical Performance

Linear sweep voltammetry (LSV) was employed to study the activity of the as prepared

Cu-Ru supported on CNT catalysts. Figure 4-48 shows the LSV curves for

electrochemical reduction of carbon dioxide for the prepared catalysts in 0.5 M $NaHCO_3$

solution saturated with CO_2. It is evident that Cu-Ru deposited on CNT shows more

activity for any other catalyst. For example, the current density for 20%Cu-20%Ru on

CNT at -1.5 V is 12.5 mA /cm^2.Similar amount of current is shown by 10%Cu-10%Ru on

CNT catalysts. However, at potentials greater than -2 V, 20%Cu-20%Ru showed higher

current density compared with 10% Cu-10% Ru catalyst. Electrocatalyst with 30%Cu-

30%Ru showed less current density. This could be due to the fact that surface area of the

157

catalyst decreases drastically for total metal loading more than 40%. The addition of ruthenium does not bring about any apparent change in the current density in comparison with copper coated on CNT. Moreover, particle size increases due to agglomeration as shown by the XRD and SEM results. However, it is anticipated that addition of ruthenium may have positive effect on the product distribution

Apart from the activity test, long term performance test of the prepared catalysts were conducted by doing chronoamperometry analysis at -1.7 V for 100 minutes. Figure 4-50 shows the chronoamperometry results for the electrocatalysts. It can be observed that the catalysts are fairly stable at the potential for 100 min. Trends for chronoamperometry results are in accordance with linear sweep results.
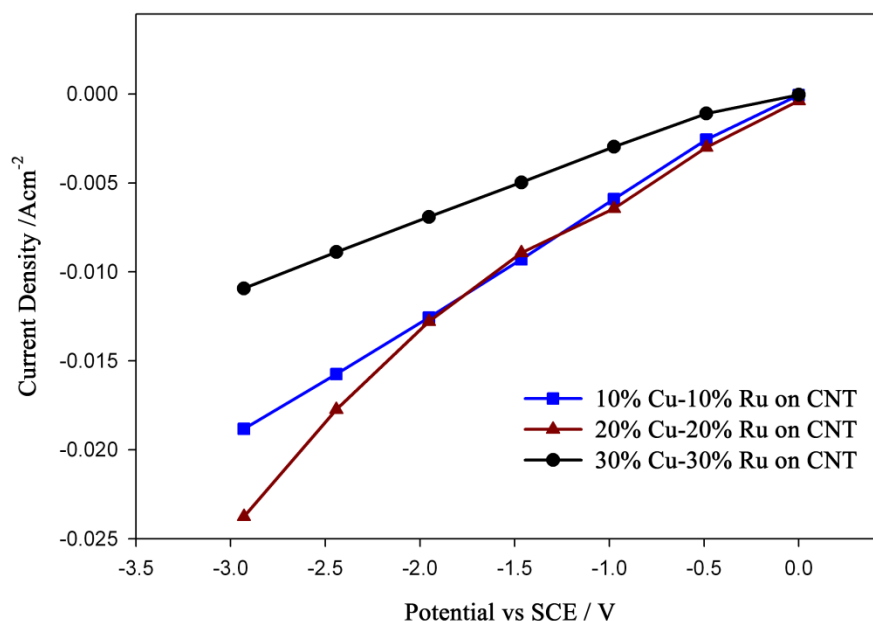
Figure 4-49: Linear sweep voltammetry results for Cu-Ru supported on CNT in CO2 saturated electrolyte
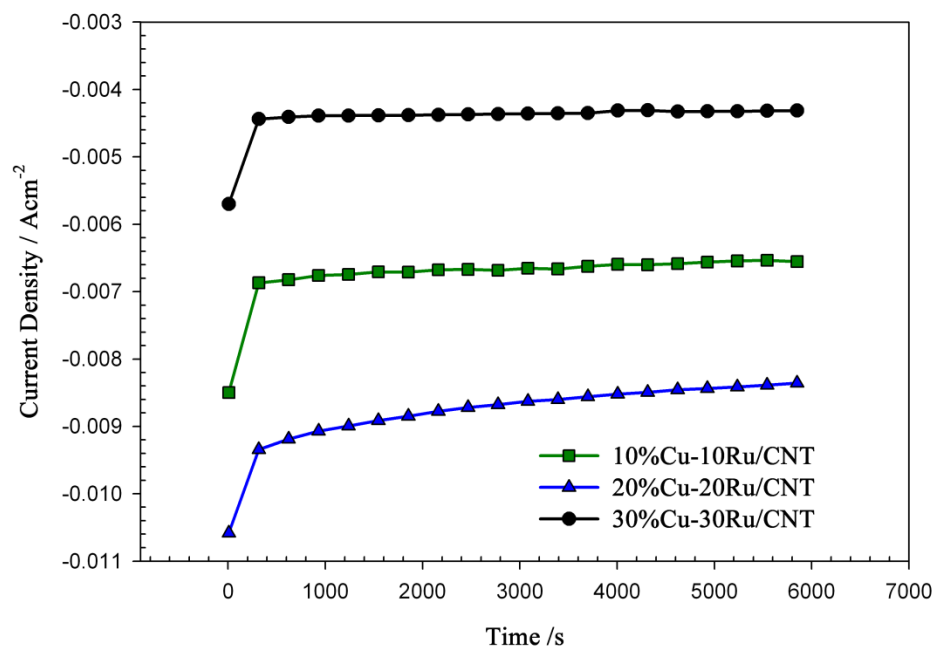
Figure 4-50: Chronoamperometry of Cu-Ru supported on CNT

The optimum catalyst, that is, 20% Cu-20% Ru supported on CNT was used to prepare MEA and tested in the SPE. Figure 4-50 shows the effect of potential on the product distribution. The figure shows that for Cu-Ru supported on CNT catalysts, no methane or any other hydrocarbon were detected. However, methanol and CO were produced. Highest faradaic efficiency for methanol was obtained at -1.5 V. This faradaic efficiency is much higher than with copper deposited on CNT. With increase in potential, CO increased along with H_2. Overall, the performance of copper and ruthenium deposited on CNT was better than with copper only.
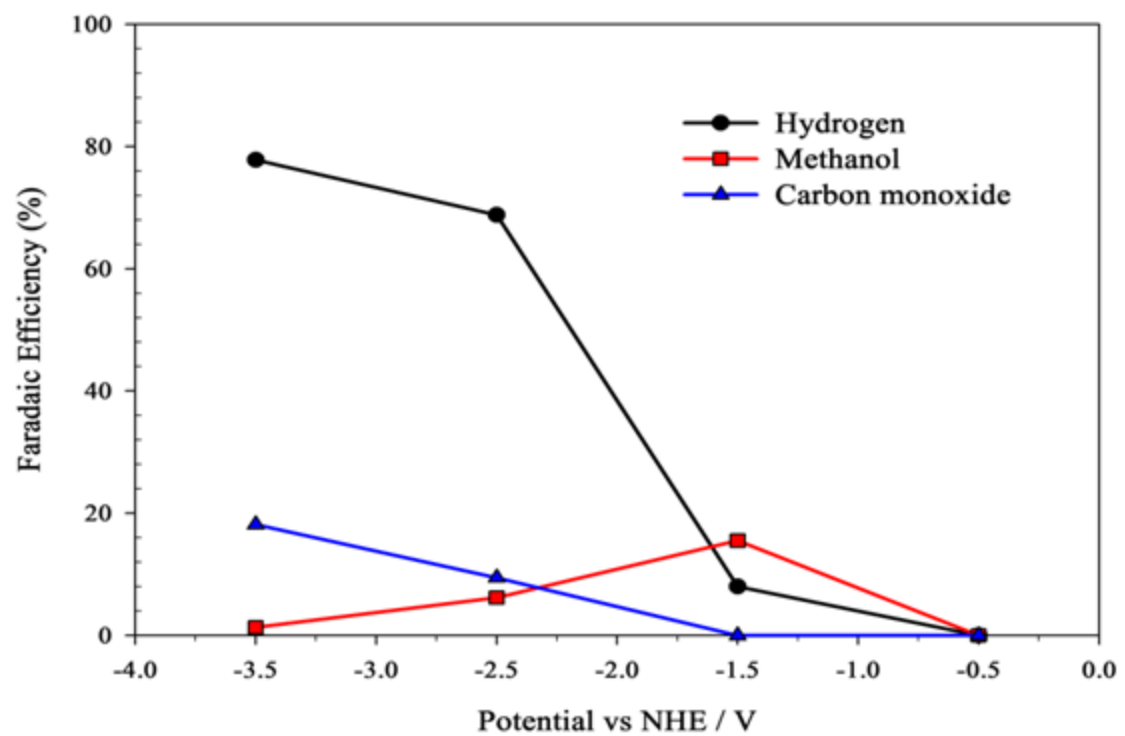
Figure 4-51: Product distribution at different potential in SPE reactor for Cu-Ru/CNT

4.1.4   Copper-Palladium Supported on CNT

Palladium and copper binary catalysts were prepared to investigate the effect of addition of palladium on copper supported on CNT catalysts.

Figures 4-51through 4-53 show the XRD of the Cu-Pd supported on CNT. The XRD patterns are somewhat similar to that of the host CNT with the additional peak arising due to coating of the copper and palladium and their possible alloy formation. In Figure 4-51, in addition to the characteristic peaks of Cu, additional peaks at 26.1°, 41.57°, 48.55° and 71.29° occur. These peaks are due to the phase Cu_3Pd with particle size 4.1nm. Similar features were found in catalysts with higher loading. For 20% Cu-20% Pd, the particle size was calculated to be 5.1 nm. For 30% Cu-30% Pd supported CNT, the mean particle size was 4.9 nm. Therefore, it was observed that increasing the metal loading did not show any growth in particle size.
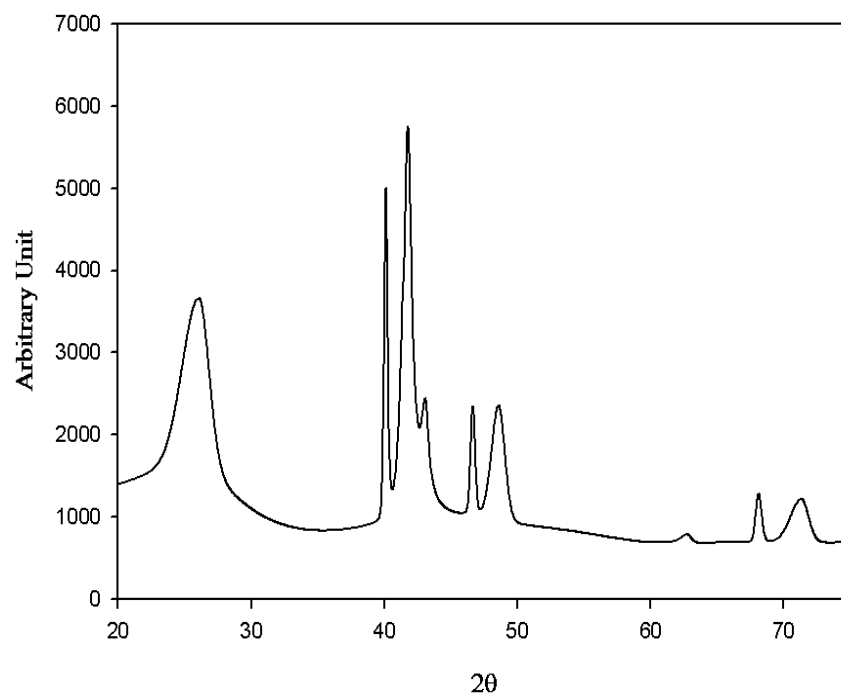
Figure 4-52: Powder XRD Pattern of 5%Cu-5%Pd/CNT
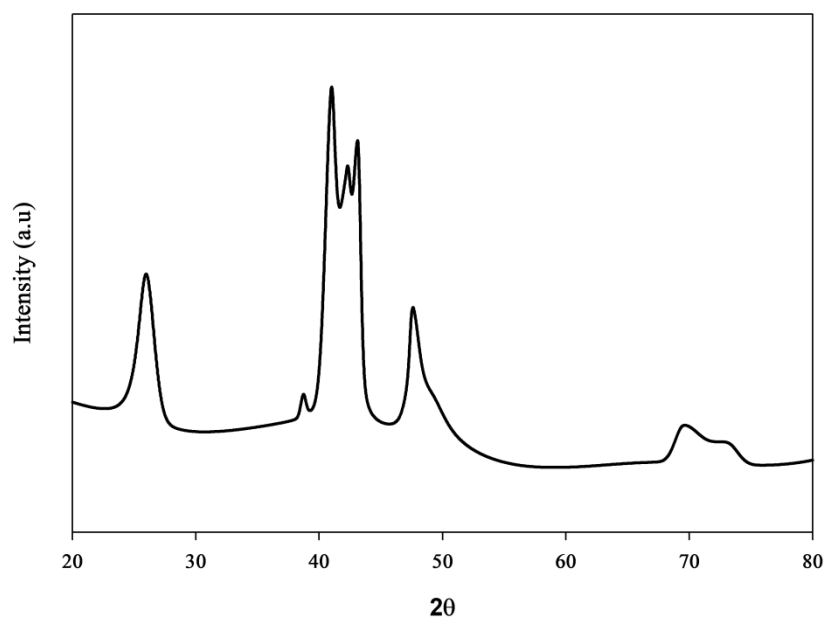
Figure 4-53: Powder XRD Pattern of 10%Cu-10%Pd /CNT

162
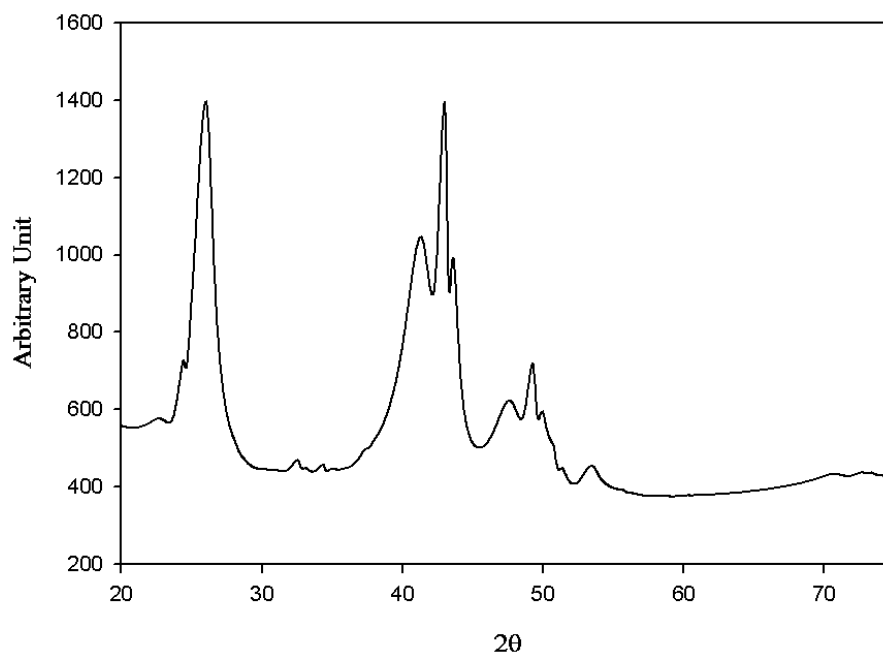
Figure 4-54: Powder XRD Pattern of 20%Cu-20% Pd/CNT

SEM results of the catalyst are shown in Figure 4-54 through 4-57. The figures show that metals were deposited homogenously on the surface of the CNT. There are empty spaces in the catalyst at low loading and homogenous deposition is achieved. However, at high loading particles tend to form agglomeration and with empty spaces largely taken by the metal particles. In any case, the original structure of the CNTs remained intact. Figure 4-59 shows that SEM-EDX of the catalyst. It is evident that the copper and palladium are successfully deposited on CNT.
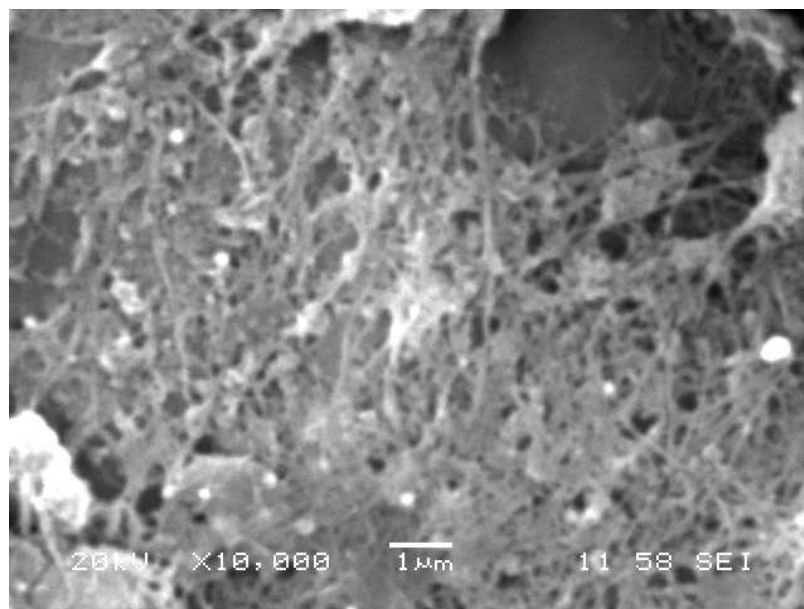
Figure 4-55: SEM micrograph for 5%Cu-5%Pd/CNT
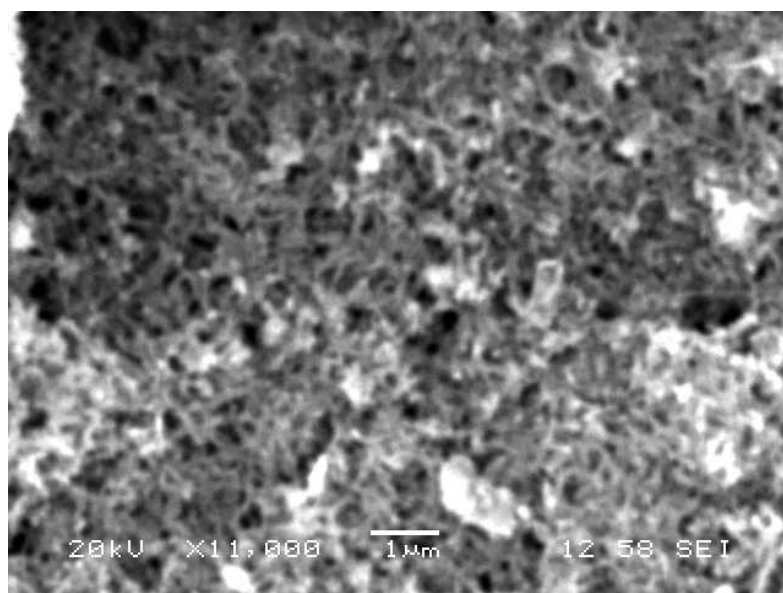
Figure 4-56: SEM image of 10%Cu-10%Pd/CNT
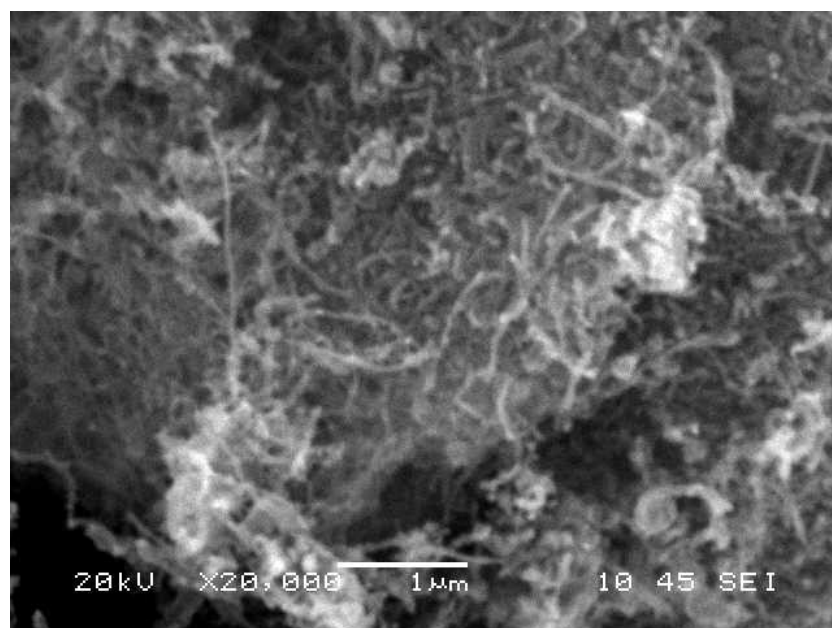
Figure 4-57: SEM image of 20%Cu-20%Pd/CNT
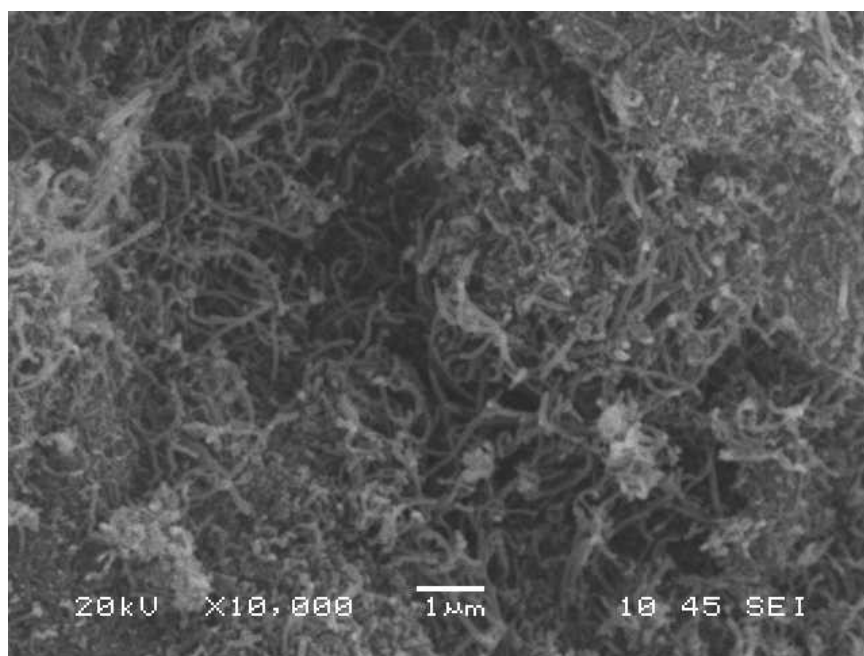
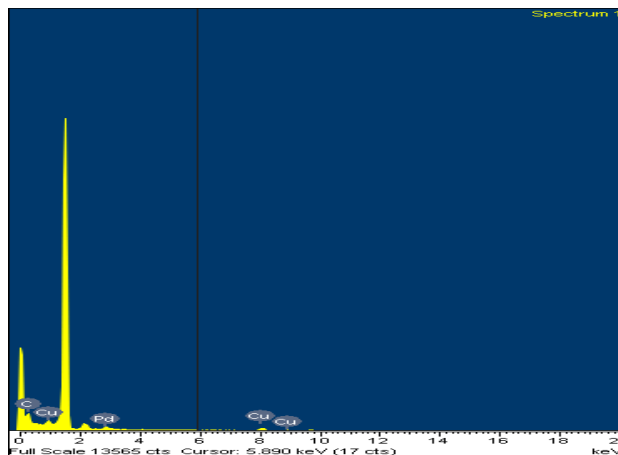Figure 4-58: SEM image of 30%Cu-30%Pd/CNT

Figure 4-59: EDX spectra for 30%Cu-30%Pd on CNT

Figure 4-59 shows the transmission electron microscope (TEM) images of the support and metal catalysts. Most of the Ru, Cu and Cu–Ru particles are located on the external surface of the MWCNTs without incorporating clusters into the pores of MWCNTs. Figure 4-60 shows the TEM at high magnification. It is evident that spherical metal particles are well distributed on the surface of the CNT and their mean particle size is 2-4 nm.
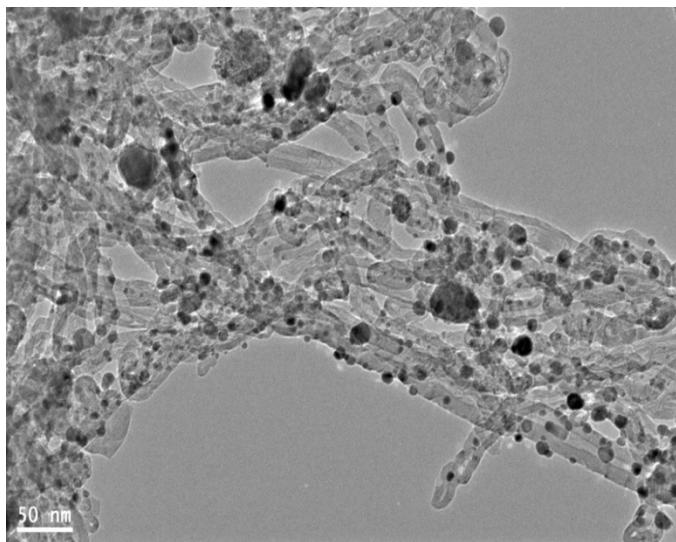
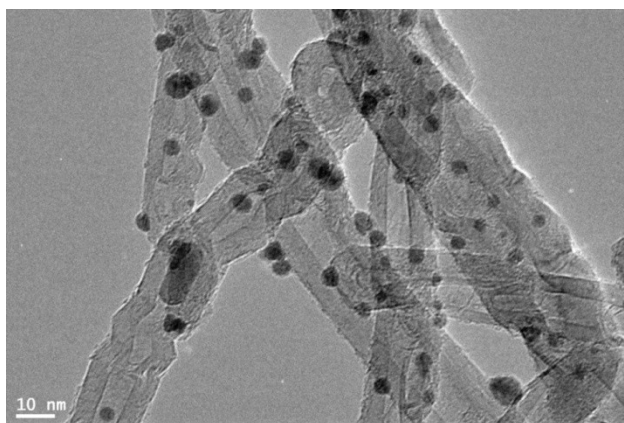Figure 4-60: TEM image of 30%Cu-30%Pd on CNT

Figure 4-61: TEM image of 30%Cu-30%Pd on CNT at high magnification

Linear sweep voltammetry (LSV) was employed to study the activity of the as prepared Cu-Ru supported on CNT catalysts. Figure 4-61 shows the LSV curves for

electrochemical reduction of carbon dioxide for the prepared catalysts in 0.5M NaHCO$_3$ solution saturated with CO$_2$. It is evident that Cu-Pd deposited on CNT shows more activity for any other catalyst. For example, the current density for 20% Cu-20% Pd on CNT at -1.5 V is 12 mA /cm^2. Current density increased until 20%Cu-20%Pd loading and with further increase in metal loading to 30%Cu-30%Ru, the current density, in fact, decreased. This could be due to the fact that surface area of the catalyst decreases drastically for total metal loading more than 40%. Moreover, particle size increases due to agglomeration as shown by the XRD and SEM results.

Apart from the activity test, long term performance test of the prepared catalysts were conducted by doing chronoamperometry analysis at -1.7 V for 100 mins. Figure 4-62 shows the chronoamperometry results for the electrocatalysts. It can be observed that the catalysts are fairly stable at the potential for 100 min. Trends for chronoamperometry results are in accordance with linear sweep results.
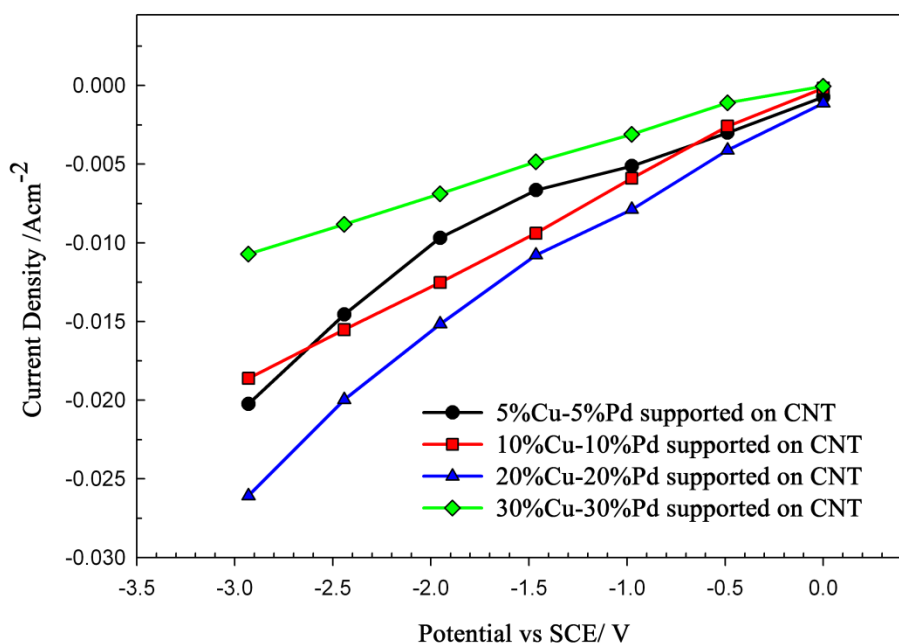

Figure 4-62: Linear sweep voltammetry results for Cu-Pd supported on CNT in CO$_2$ saturated electrolyte
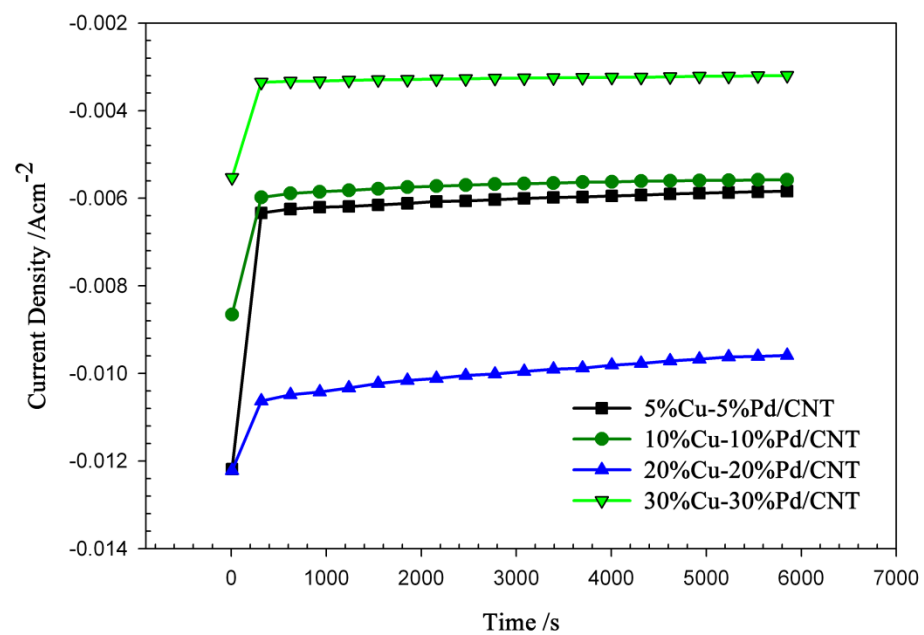
Figure 4-63: Chronoamperometry of Cu-Pd supported on CNT

4.2   Titania Nanotubes (TNTs) Supported Catalysts

In this section, physical characterization results of the electrocatalysts based on Cu, Fe, Pd, & Ru supported on titania nanotubes (TNTs) are presented and discussed, and later, their catalytic activities are discussed.

4.2.1   Copper supported on TNT

Figure 4-64 is a typical X-ray diffraction (XRD) data taken from the TiO_2 nanotube samples. The strong diffraction peak at 2θ angles of $25.0°$, $37.4°$ and $48.5°$ may correspond to the spacing of (1 0 1), (0 0 4) and (2 0 0) of the anatase (tetragonal) phase, two diffraction peaks at 2θ angles of $27.4°$, $36.3°$ may correspond to the spacing of (1 1 1), (1 0 1) of the rutile phase. Because the nanotubes may form by rolling up the two-dimensional sheets of TiO_2 structure, some diffraction peaks of rutile phase TiO_2 may not appear in the XRD pattern.
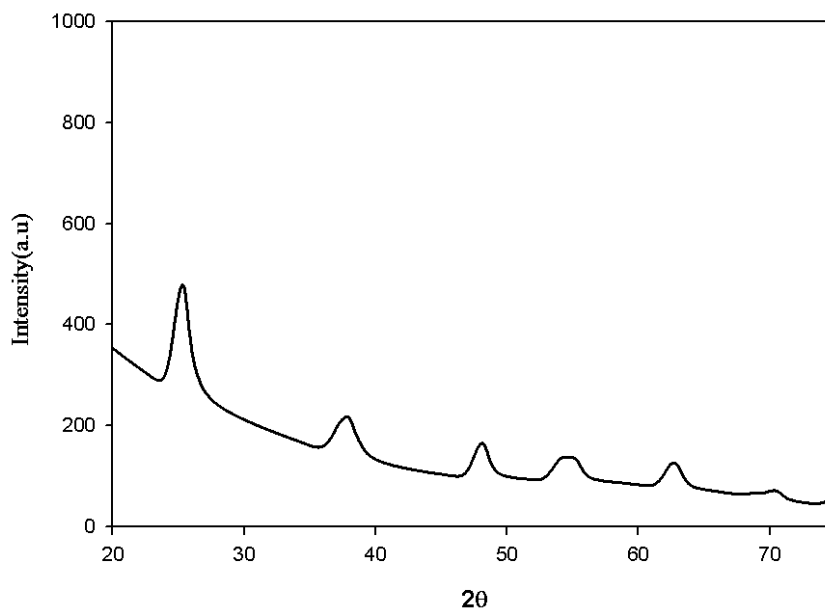
Figure 4-64: XRD spectra of Titania Nano Tubes

In Figure 4-65, XRD pattern for 5% Cu deposited on TNT is given. It is evident that only copper oxide peak at 35.48° is visible. Crystallite size of the copper oxide was calculated to be 7.6 nm. All other peaks correspond to anatase. Similar peak was found for 10 % copper loading with crystallite size 2.2 nm. For 20% Cu on TNT, the crystallite size was 18 nm. It is concluded that for copper was successfully deposited on TNTs with nano size.
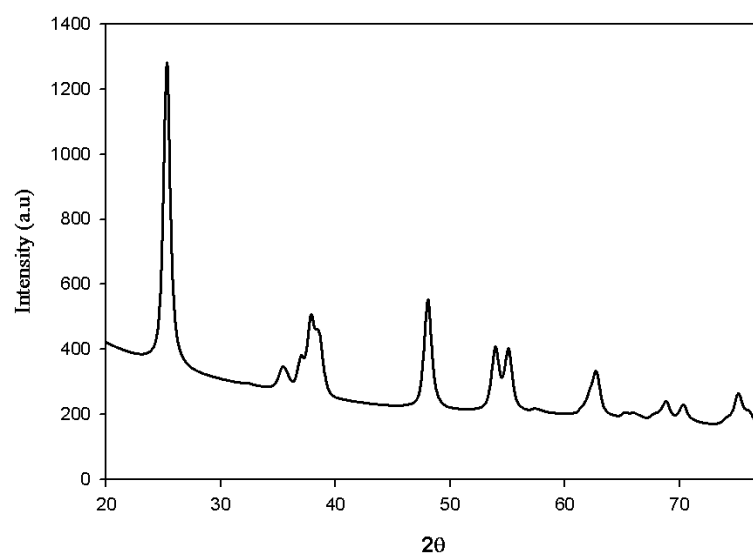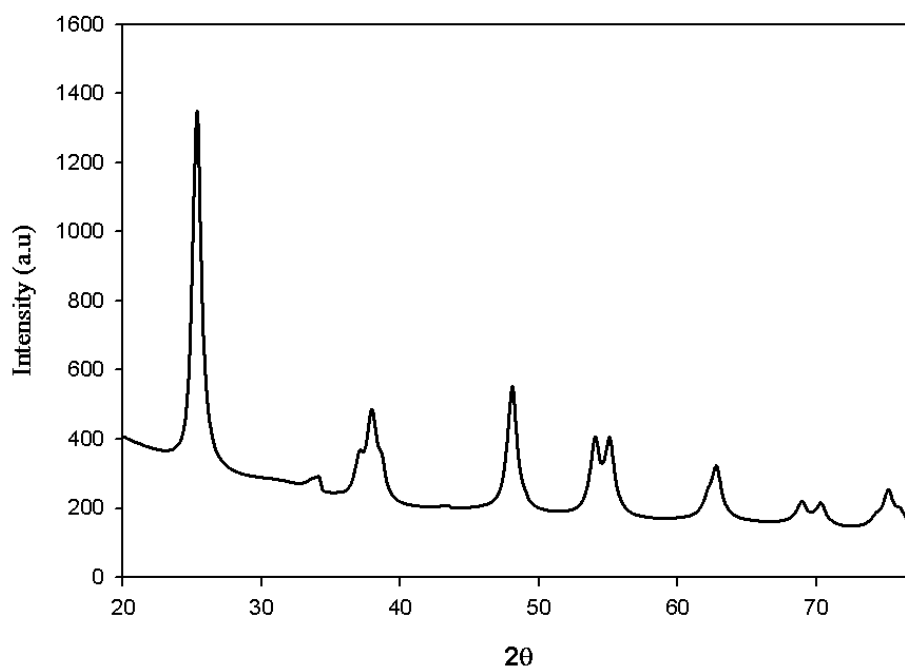
Figure 4-65: XRD spectra of 5%Cu/TNT

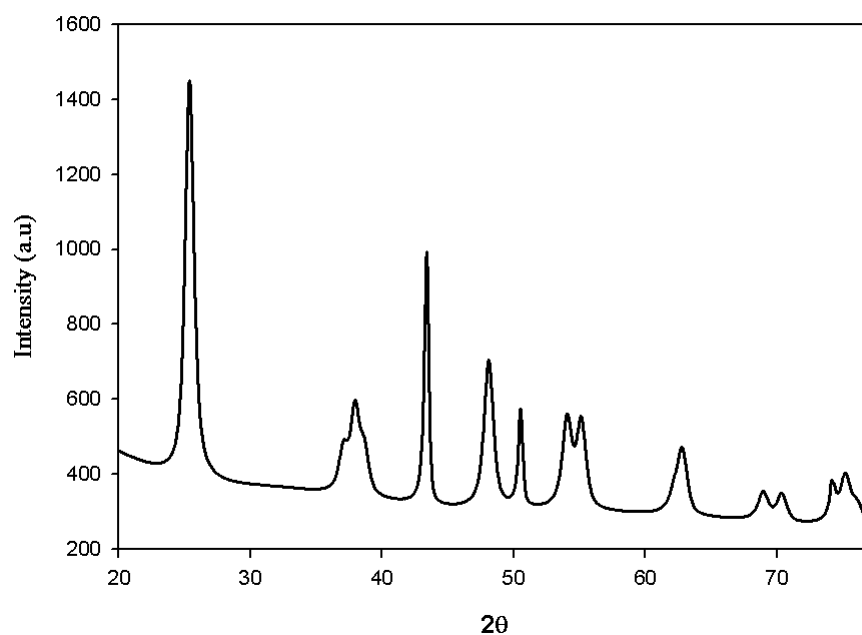**Figure 4-66: XRD spectra of 10%Cu/TNT**

172

Figure 4-67: XRD spectra for 20%Cu/TNT

Figure 4-79 shows the SEM image of pure TNT. The tube like structure was obvious from the figure with lots of empty spaces. This shows the successful preparation of tube like structure. When copper was deposited, the metal was deposited on the surface of the TNTs and the empty space is filled up as shown in figure 4-81. As the loading of copper increased, the empty spaces started to be filled up with copper metal and agglomerations are visible. However, the even after deposition of Cu, the original structure remain intact.
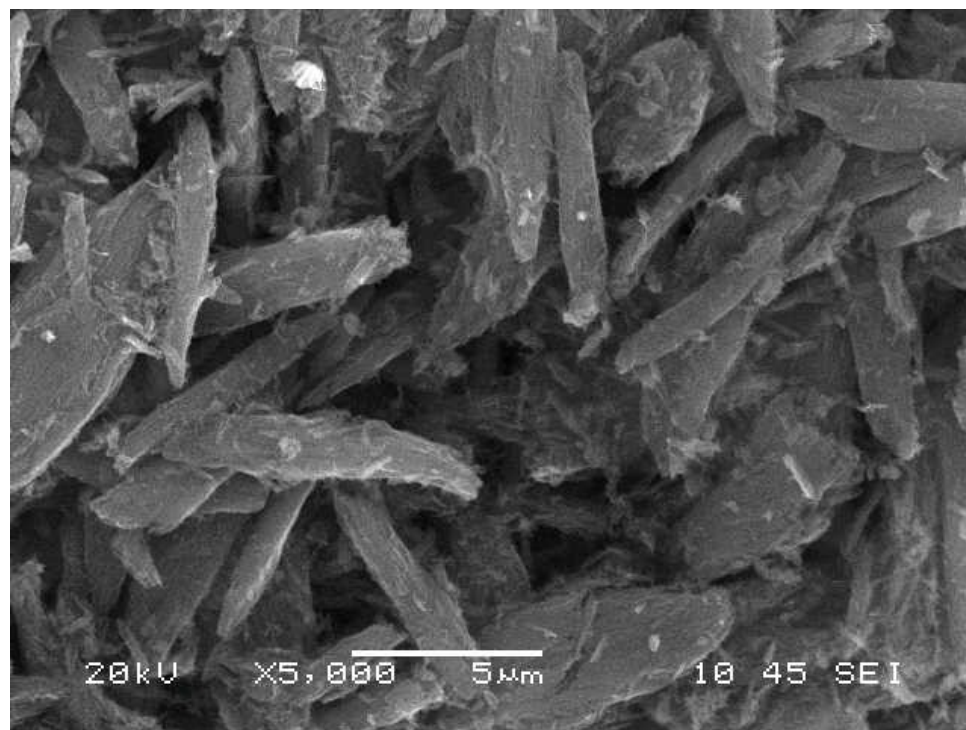
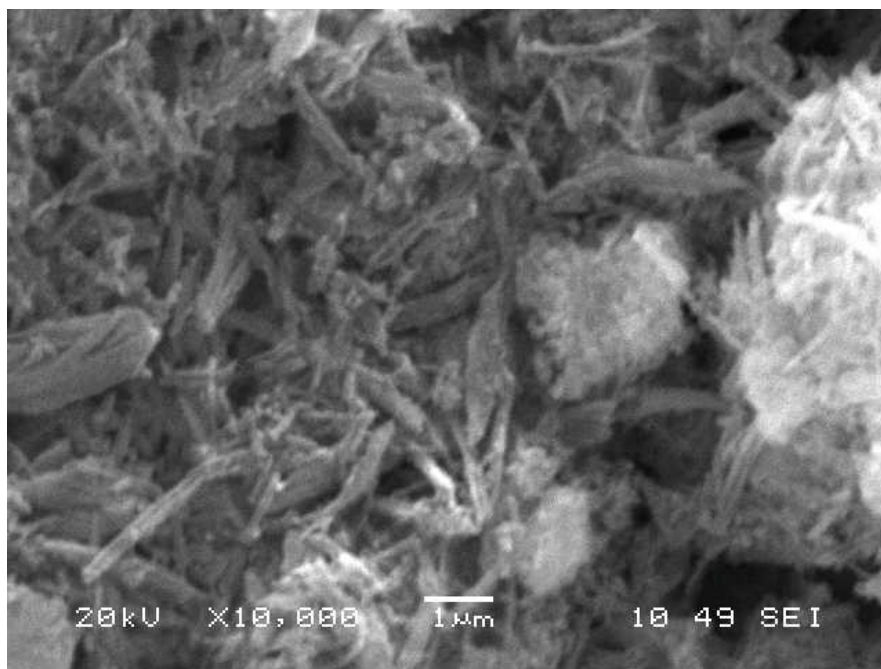Figure 4-68: SEM image of pure TNT
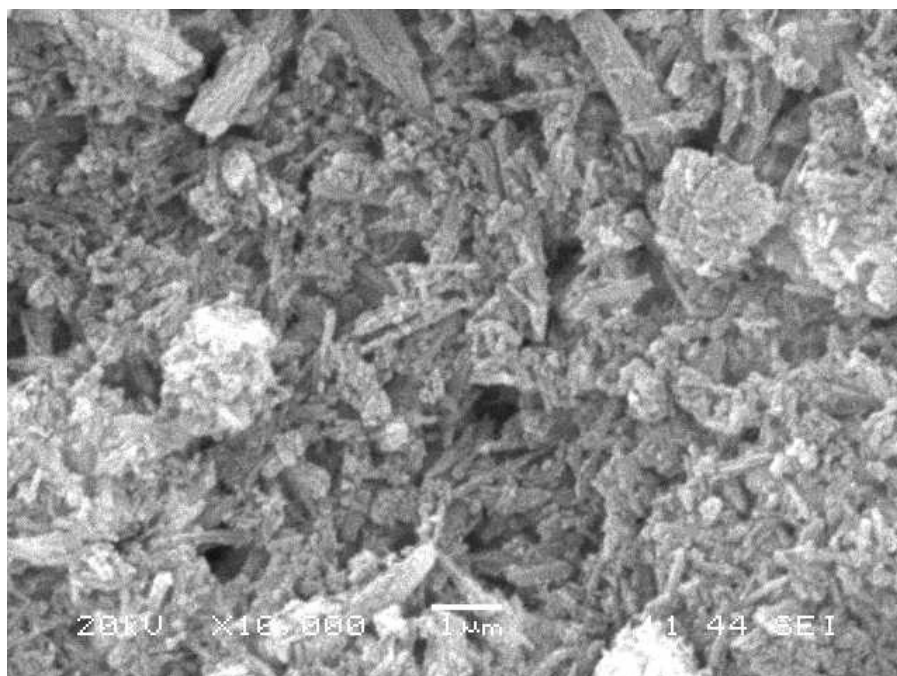

Figure 4-69: SEM image of 5%Cu/TNT

Figure 4-70: SEM image of 10% Cu/TNT
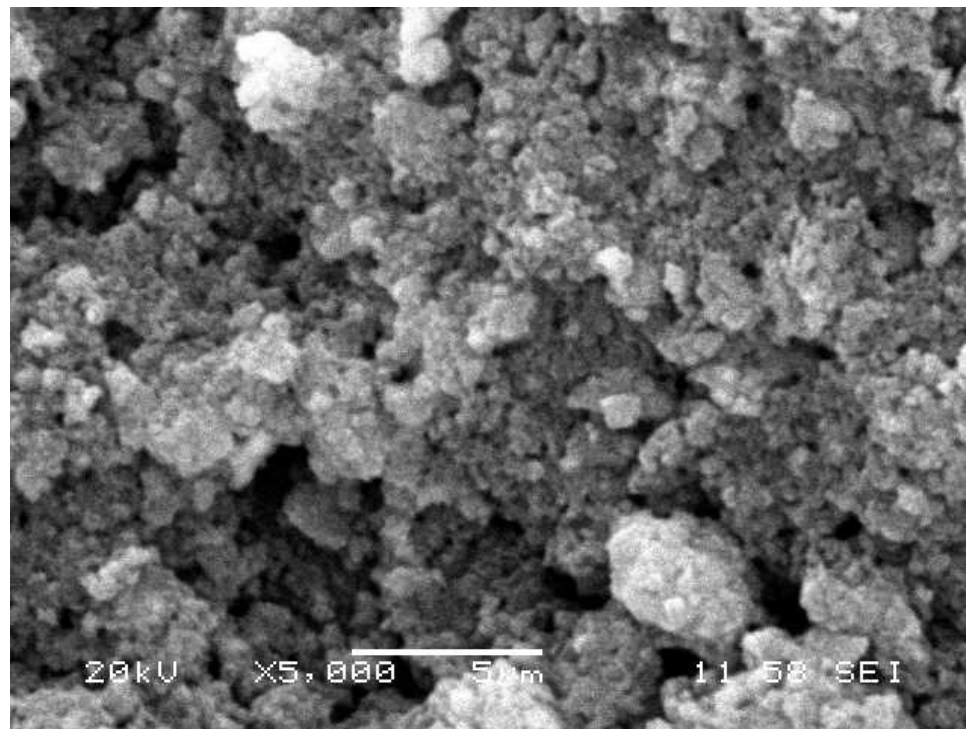
Figure 4-71: SEM micrograph for 20% Cu/TNT

175

Figure 4-72 shows the transmission electron microscope (TEM) images of the support and metal catalysts. Well developed and distinct nanotubes of 5-8 nm diameters are visible from the TEM image. Figure 4-84 shows the TEM image for 5% Cu loading. Most of Cu particles are located on the external surface of the MWCNTs without incorporating clusters into the pores of TNTs. It is evident that spherical metal particles are well distributed on the surface of the TNT and their mean particle size is 10 nm.

Figure 4-72: TEM image of pure TNTs
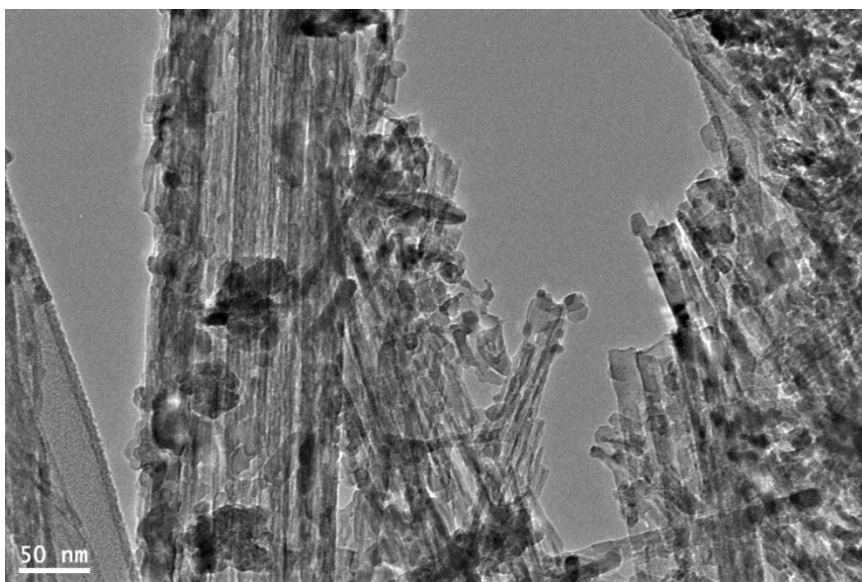
Figure 4-73: TEM image of 5% Cu/TNT

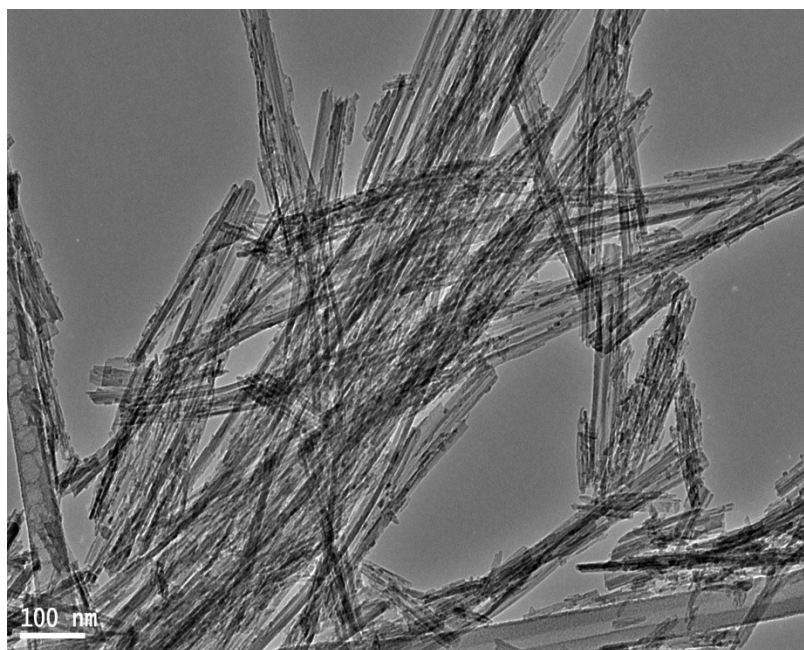Linear sweep voltammetry (LSV) was employed to study the activity of the as prepared Cu-Ru supported on CNT catalysts. Figure 4-74 shows the LSV curves for electrochemical reduction of carbon dioxide for the prepared catalysts in 0.5 $MNaHCO_3$ solution saturated with CO_2. It is evident that Cu deposited on TNT shows activity. For example, the current density for 20% Cu on TNT at -1.5 V is 12 mA /cm^2. Current density increased until with increasing metal loading.

Apart from the activity test, long term performance test of the prepared catalysts were conducted by doing chronoamperometry analysis at -1.7 V for 100 mins. Figure 4-81 shows the chronoamperometry results for the electrocatalysts. It can be observed that the catalysts are fairly stable at the potential for 100 min. Trends for chronoamperometry results are in accordance with linear sweep results
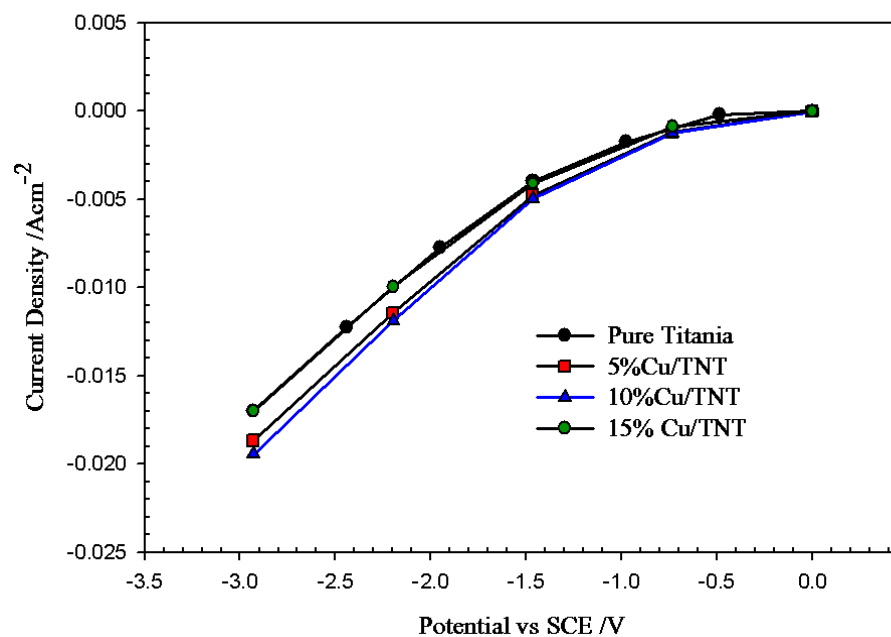
Figure 4-74: Linear sweep of copper supported on TNT in CO2 saturated electrolyte
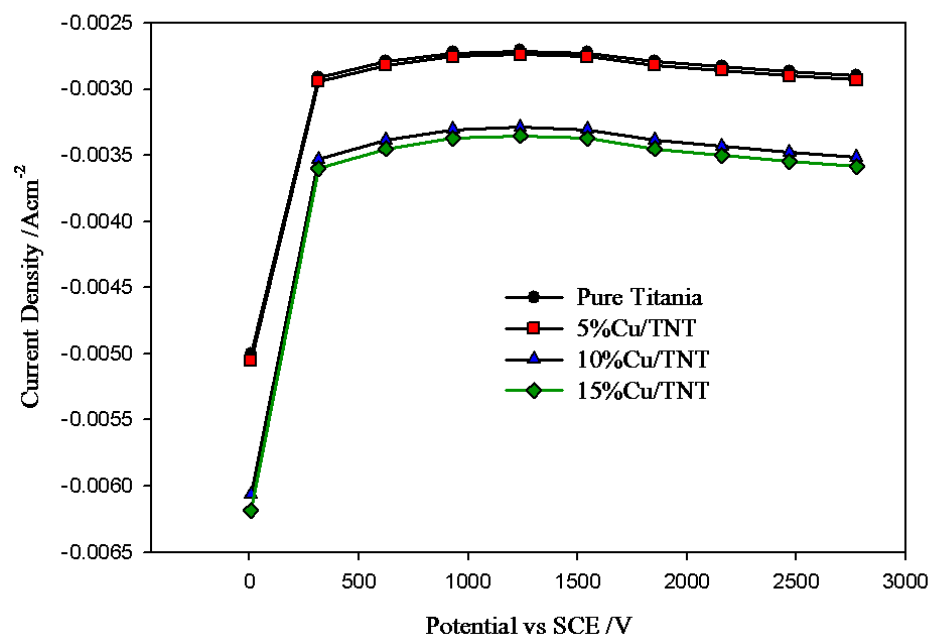
Figure 4-75: Chronoamperometry of copper supported on TNT

178

4.2.2 Copper-Ruthenium Supported on TNT

Ruthenium and copper binary catalysts were prepared to investigate the effect of addition of ruthenium on copper supported on CNT catalysts.

In figure 4-76, XRD pattern for 5% Cu -5%Ru deposited on TNT is given. No peaks corresponding to the characteristic peaks of copper or ruthenium was obtained for 5% Cu -5% Ru supported on TNT. This shows that at this loading metals were homogenously dispersed on the surface of the TNT. At higher loading, as Figure 4-88, XRD shows peaks of Ru at 38.5°, 63.4° and 70.4°.The crystallite size was calculated to be 6.7 nm. In addition, XRD did not reveal any formation of new crystalline species during catalyst preparation. Based on the results obtained from XRD patterns, we conclude that a homogeneous surface dispersion of Cu and Ru was achieved for all doped samples.
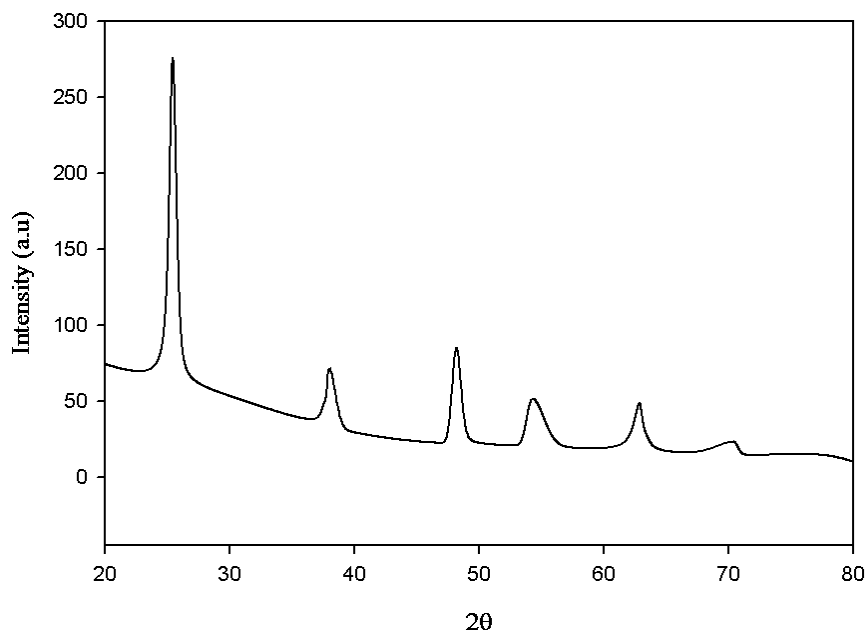
Figure 4-76:XRD spectra of 5%Cu-5%Ru/TNT
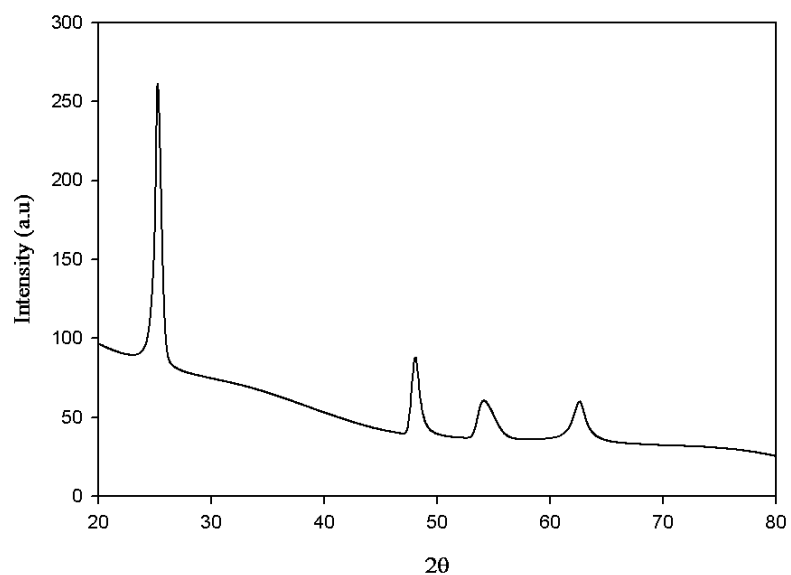
Figure 4-77: XRD spectra of 10%Cu-10%Ru/TNT
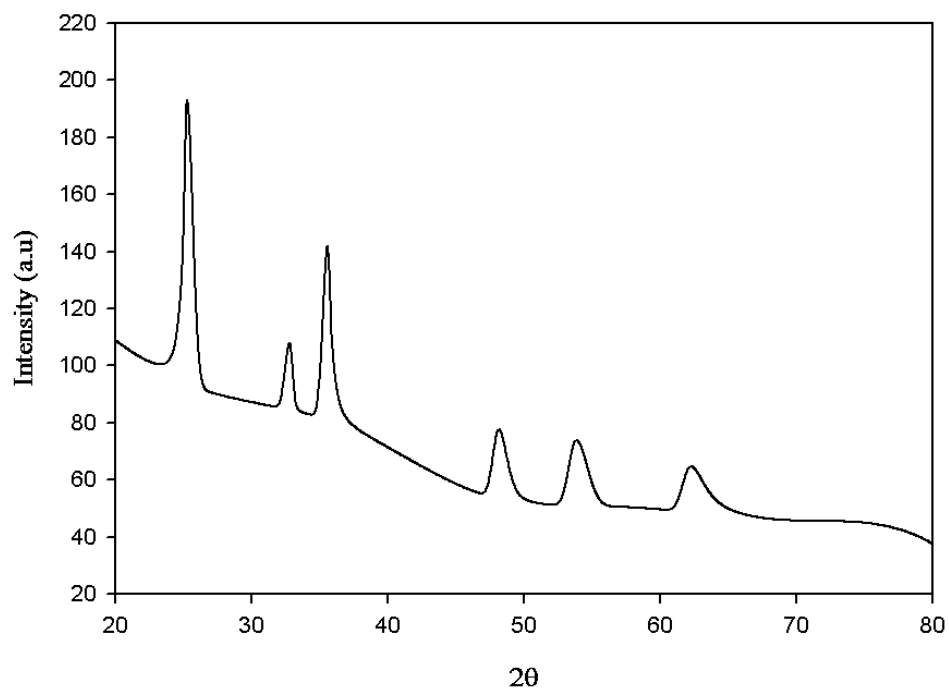
Figure 4-78: XRD spectra of 20%Cu-20%Ru/TNT

Scanning electron microscopy (SEM) results shown in Figure 4-79 and 4-80 were very much consistent with the XRD plots. As the metal oxide content was increased the

180

crystalline size increases and as a result the dispersion went down. SEM was carried out with magnification x14000 at 1µm scale. The SEM pictures show that the metal occupies the vacant space in the TNT.
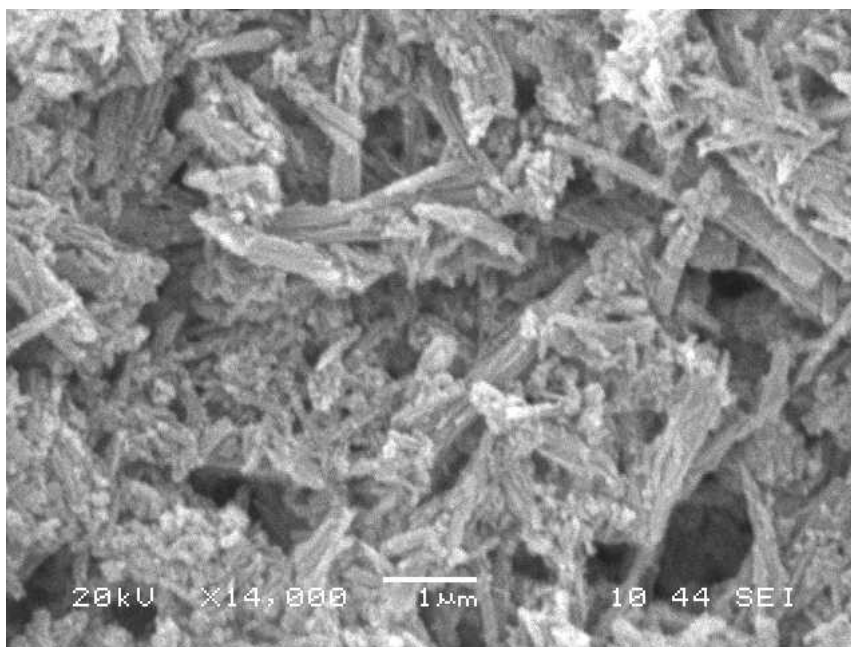
Figure 4-79: SEM image of 5%Cu-5% Ru/TNT
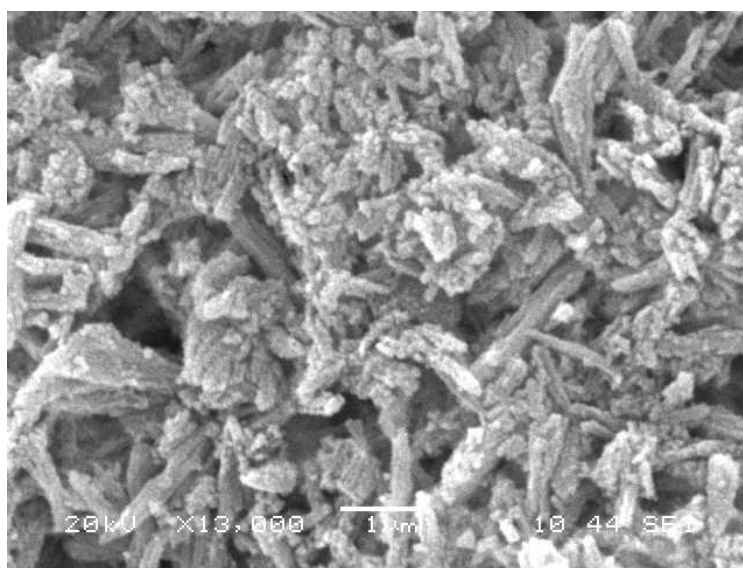
Figure 4-80: SEM image of 20%Cu-20%Ru/TNT

Figure 4-81 show the TEM image of 10%Cu-10% Ru deposited on TNT. It is clearly seen that the metal particles of sizes 6-10 nm were finely dispersed over the surface of the TNT. Figure 4-82 shows the TEM image for 20%Cu-20% Ru deposited on TNT. The particles were well dispersed on TNT as inferred from XRD and SEM
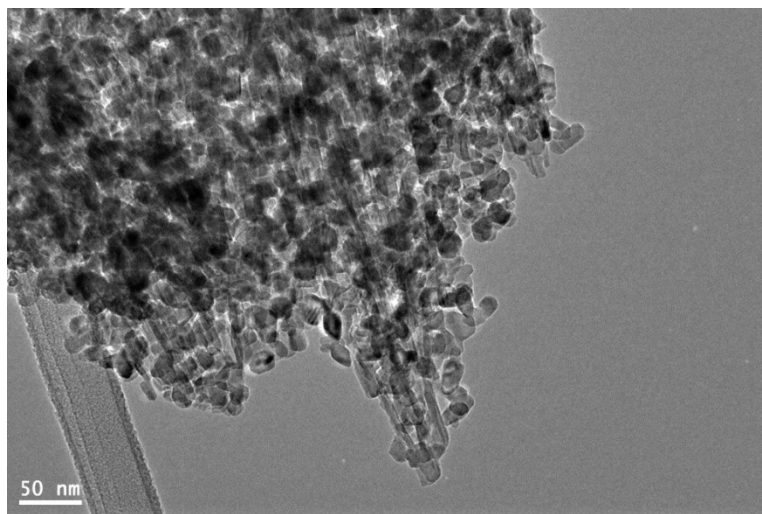
Figure 4-81: TEM image of 10%Cu-10%Ru/TNT
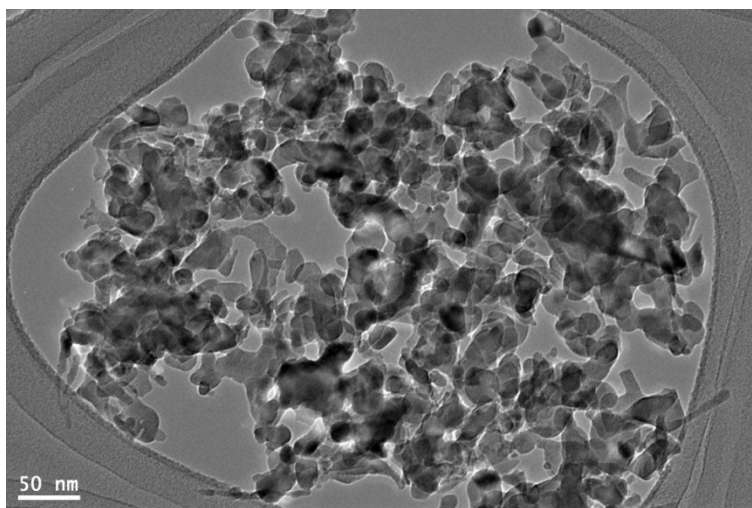
Figure 4-82: TEM image of 20%Cu-20%Ru/TNT
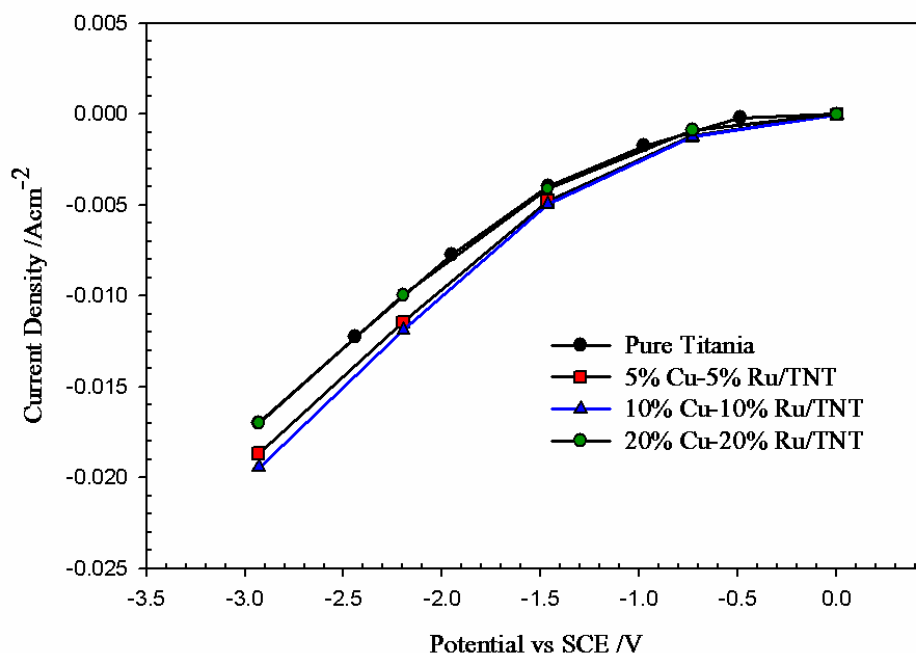
Figure 4-83: Linear sweep of copper & Ru supported on TNT in CO2 saturated electrolyte

Linear sweep voltammetry (LSV) was employed to study the activity of the as prepared Cu-Ru supported on TNT catalysts. Figure 4-83 shows the LSV curves for electrochemical reduction of carbon dioxide for the prepared catalysts in 0.5M $NaHCO_3$ solution saturated with CO_2. It is evident that Cu-Ru deposited on TNT showed good activity. For example, the current density for 10%Cu-10%Ru on TNT at -1.5 V is 8 mA /cm^2. Current density increased until 10%Cu-10%Ru loading, and further increase in the metal loading leads to the decrease in current density.

Table 4-3 shows the faradaic efficiency for the product obtained at different voltages for 20 % Cu-20% Ru/TNT catalyst. The reactions have been performed at four different voltages to see the effect of voltage. The potential are vs. Normal Hydrogen Electrode (NHE). Maximum faradaic efficiency of methanol (12.6%) formation was obtained at -

183

1.5 V. Apart from methanol, hydrogen and carbon monoxide are also produce.

Table 4-5: Effect of potential on the product distribution

Potential vs NHE	F.E for H_2	F.E for CH_3OH	F.E for CO
-0.5	0	0	0
-1.5	5.3	12.2	2.8
-2.5	67.2	9.6	7.2
-3.5	77.4	8.8	13.2

4.2.3   Copper-Palladium Supported on TNT

In figure 4-84, XRD pattern for 5% Cu -5% Pd deposited on TNT is given. No peaks corresponding to the characteristic peaks of copper or palladium was obtained for 5% Cu -5% Pd. This shows that at this loading metals were homogenously dispersed on the surface of the TNT. At higher loading, as figure 4-98, XRD shows peak of Pd at 41.4°.The crystallite size was calculated to be 4.7 nm. In addition, XRD did not reveal any formation of new crystalline species during catalyst preparation. Based on the results obtained from XRD patterns, scanning electron microscopy and EDX studies, we conclude that a homogeneous surface dispersion of Cu was achieved for all doped samples.
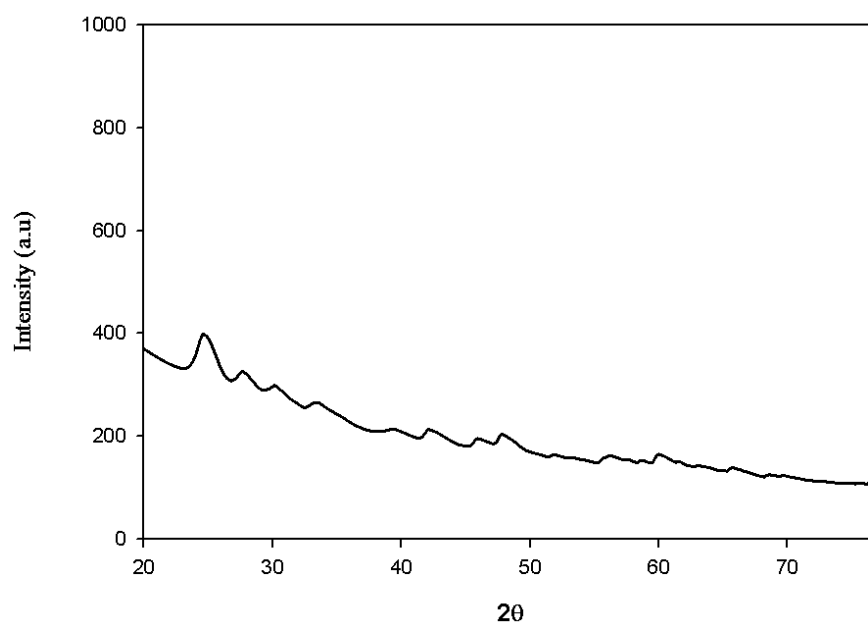
Figure 4-84: XRD spectrum of 5%Cu-5%Pd on TNT
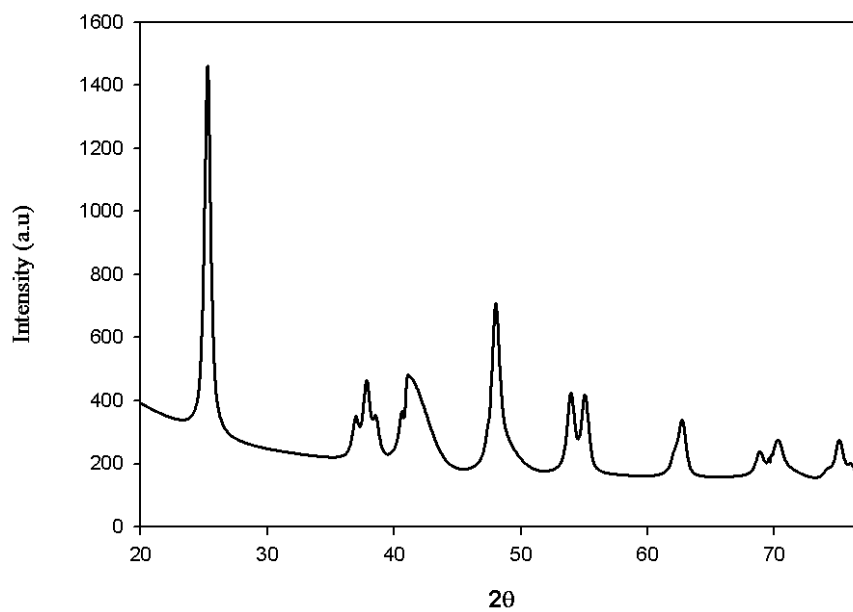
Figure 4-85: XRD spectrum of 10%Cu-10%Pd on TNT
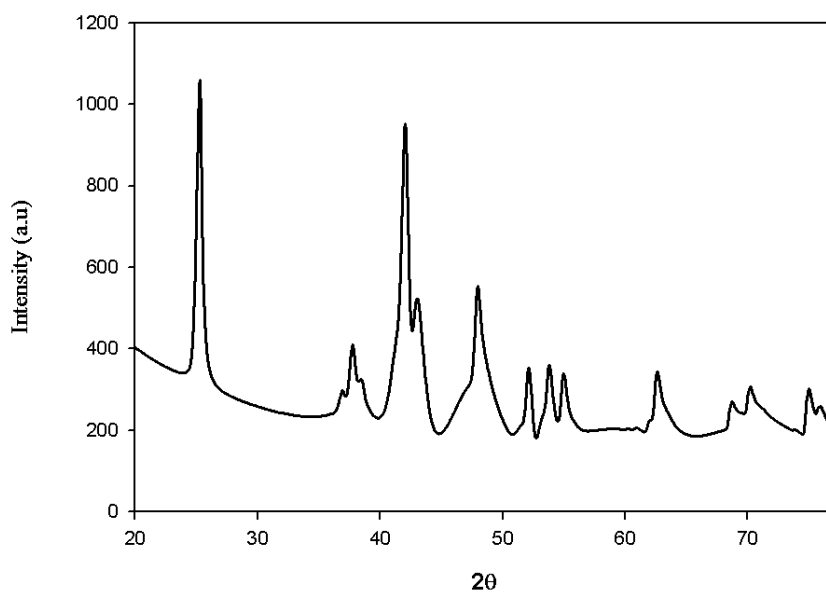
Figure 4-86: XRD spectrum of 20%Cu-20%Pd on TNT

Figure 4-97 shows the SEM image of Cu and Pd supported TNT. The tube like structure was obvious from the figure with the original empty spaces taken up by the metals. The impregnated metals were finely coated on the surface of the TNTs. As the loading of metal was increased, the empty spaces started to be filled up with copper metal and agglomerations are visible. However, the even after deposition of Cu, the original structure remain intact. It is evident from the SEM that the metals were homogenously dispersed over the surface of TNTs.

186
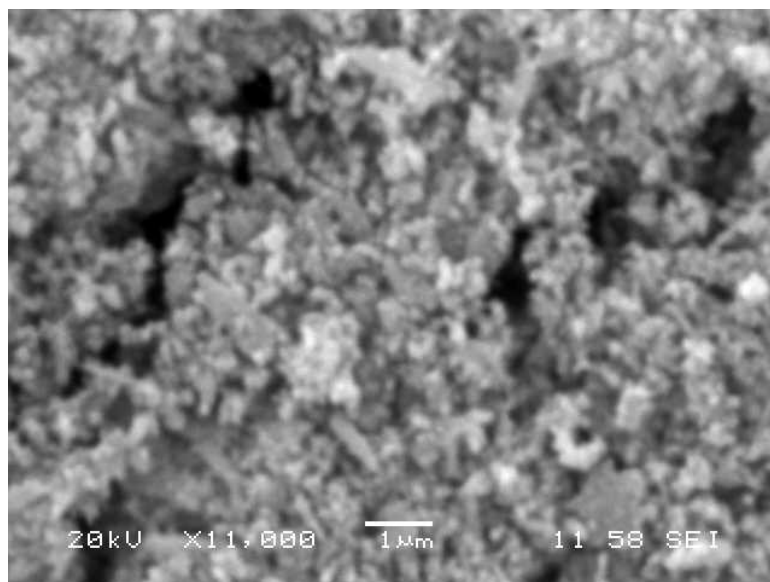
Figure 4-87: SEM image of 20%Cu-20%Pd on TNT

Figure 4-88 shows the TEM image of 10%Cu-10% Pd deposited on TNT. It is clearly seen that the metal particles of sizes 8-10 nm were finely dispersed over the surface of the TNT. Figure 4-89 shows the high magnification image of the same catalyst. Figure 4-90 shows the TEM image for 20%Cu-20% Pd deposited on TNT. The particles were well dispersed on TNT as inferred from XRD and SEM.
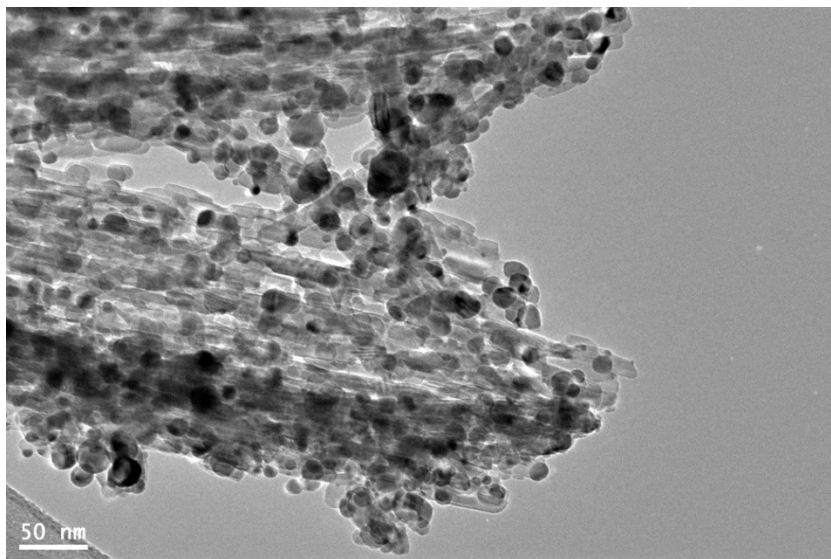
Figure 4-88: TEM image of 10%Cu-10%Pd on TNT
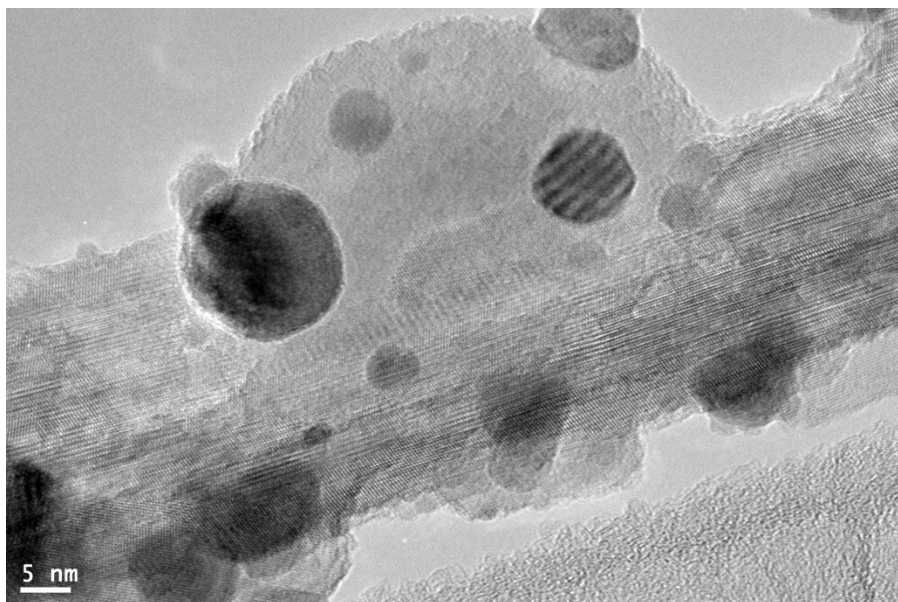
Figure 4-89: TEM image of 10%Cu-10%Pd on TNT at high magnification
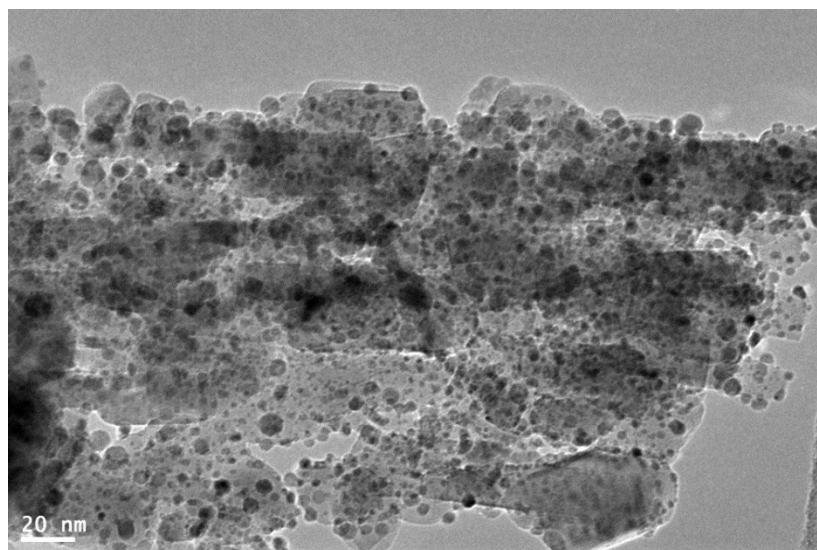
Figure 4-90: TEM image of 20%Cu-20%Pd on TNT

Linear sweep voltammetry (LSV) was employed to study the activity of the as prepared Cu-Pd supported on TNT catalysts. Figure 4-91 shows the LSV curves for electrochemical reduction of carbon dioxide for the prepared catalysts in 0.5M $NaHCO_3$ solution saturated with CO_2. It is evident that Cu-Pd deposited on TNT showed good activity. For example, the current density for 20%Cu-20%Pd on TNT at -1.5 V is 10 mA /cm^2. Current density increased until 20%Cu-20%Pd loading and with further increase in the current density. This could be due to the fact that adding more active material helped in getting more current density.

Apart from the activity test, long term performance test of the prepared catalysts were conducted by doing chronoamperometry analysis at -1.7 V for 100 mins. Figure 4-92 shows the chronoamperometry results for the electrocatalysts. It can be observed that the catalysts are fairly stable at the potential for 100 min. Trends for chronoamperometry results are in accordance with linear sweep results
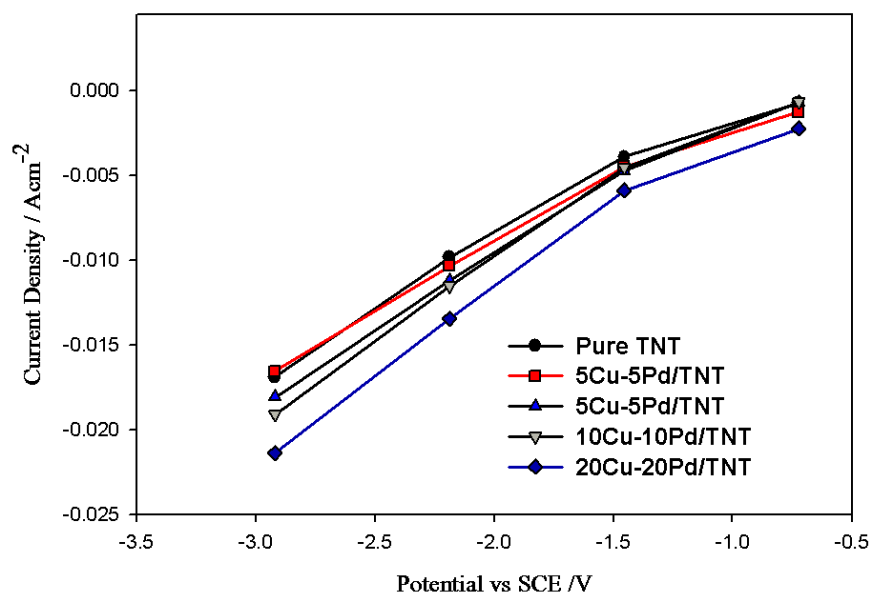
Figure 4-91: Linear sweep voltammetry for copper & palladium supported on TNT
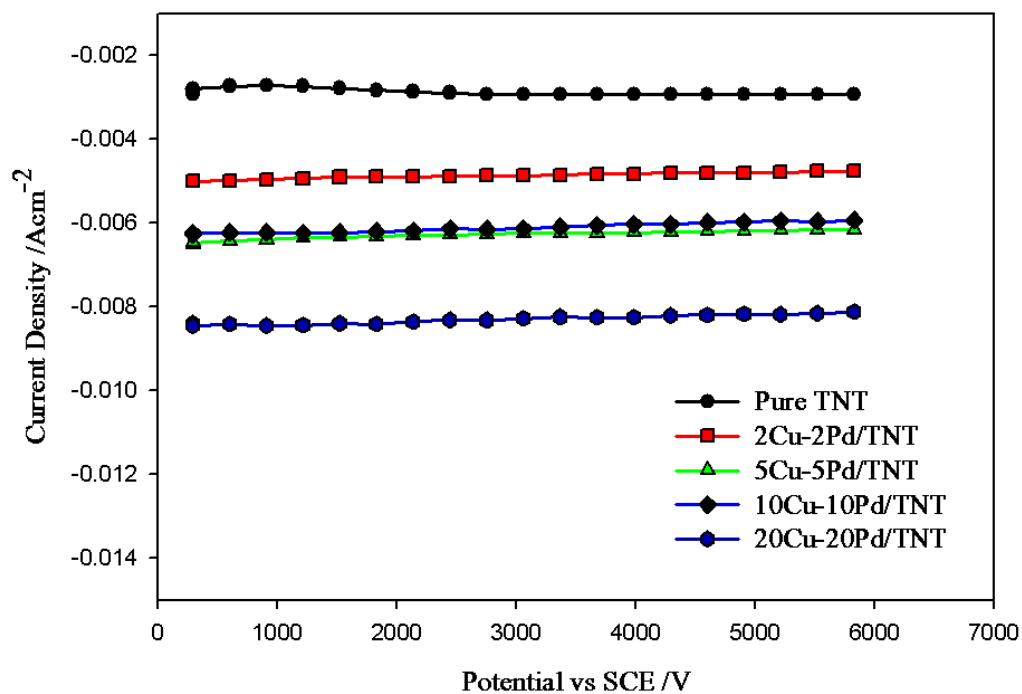
Figure 4-92: Chronoamperometry for copper & palladium supported on TNT

CHAPTER 5

CONCLUSION

In this work, several catalyst systems for electrochemical reduction of carbon dioxide were synthesized, characterized and their activity tested. Carbon nanotubes (CNTs) and Titania nanotubes (TNT s) were investigated for their suitability as catalyst support. Copper, iron, ruthenium and palladium were investigated for their activity for reducing carbon dioxide.

Copper was loaded on CNT by homogeneous deposition-precipitation method. The characterization results showed that copper was deposited on the CNT in the nano form. Copper modified CNT reduced CO_2 with high current density. Of all the loading used, 20% Cu loading gave highest current density. Methanol was found to be the major product with current efficiency of 38.2%.

Binary metals Cu-Fe, Cu-Ru, Cu-Pd supported on CNTs were also synthesized to investigate the effect of other metals on the performance of the catalyst. Low metal loading catalysts were prepared by incipient impregnation method whereas high loading catalysts were synthesisized by homogeneous deposition-precipitation method. Catalysts with well dispersed metal particles of few nanometer sizes were achieved. Cu-Ru and Cu-Pd showed higher current density compared with Cu supported on CNT whereas Cu-Fe showed less current density. All the prepared catalysts showed reasonable activity and stability. Thus, the prepared catalysts have potential to be used for the electrochemical

191

reduction of carbon dioxide. Hydrogen, methanol, methane, and carbon monoxide were the reduction products in the SPE reactor. Copper ruthenium supported on CNT showed highest faradaic efficiency for methanol production. Iron and Pd increased the faradaic efficiency for hydrogen evolution. The current density of the SPE was much higher than the half. Thus, it justifies the use of SPE.

In the second part of this work, Titania nanotubes (TNTs) were first synthesized and then utilized as support material for the active metals (Cu, Ru, Fe, and Pd). From the characterization results, very high surface area (395 m^2/g) titania nanotubes with diameter 2-4 nm. Copper deposited TNTs were prepared and tested. The results show that Cu/TNT catalyses the reaction but the current density was low compared to CNT. Similarly, Cu-Ru and Cu-Pd were tested. All the catalysts showed reasonable catalytic activity and stability. With Cu-Ru loaded on TNT, the main product in continuous reactor was methanol and showed good faradaic efficiency.

REFERENCES

[1]   Song C, Gaffney AM, Fujimoto K, "CO$_2$ Conversion and Utilization ":An American Chemical Society Publication.(2002)

[2]   Agency IE (2011) CO2 emissions from fuel combustion.

[3]   IPCC (2007) Fourth Assessment on Climate Change :Climate Change 2007: Synthesis Report In: RK Pachauri, A Reisinger (eds).

[4]   Centi G, Perathoner S, Opportunities and prospects in the chemical recycling of carbon dioxide to fuels, Catalysis Today 2009; 148(3-4): 191-205

[5]   Braasch G, "Earth under fire : how global warming is changing the world":University of California Press.(2009)

[6]   Ball M, Wietschel M, The future of hydrogen-Opportunities and challenges, International Journal of Hydrogen Energy 2009; 34(615-27

[7]   EPA US (2009) Report number. EPA 430-R-09-004.

[8]   Centi G, Perathoner S, Problems and perspectives in nanostructured carbon-based electrodes for clean and sustainable energy, Catalysis Today 2010; 150(1-2): 151-62

[9]   Scibioh AM, Vishwanathan B, Electrochemical reduction of carbon dioxide - Status report, Proceedings of Indian National Science Academy 2004; 70A(3): 407-62

[10]   (1998) Kyoto Prtocol.

[11]   M.M.Hallmann, Steinberg M (1999) Greenhouse Gas Carbon dioxide Mitigation Science and Technology Boca Raton,Fl: Lewis Publishers.

[12]   Centi G, Van Santen RA (eds.) (2007) Catalysis for Renewables. Weinham,

Germany: Wiley VCH Publications.

[13]   Wilson E, Gerard D (eds.) (2007) Carbon Capture and Sequestration Integrating

Technology, Monitoring, Regulation Ames, USA: Blackwell Publishing.

[14]   Song SQ, Liang ZX, Zhou WJ, Sun GQ, Xin Q, Stergiopoulos V, et al., Direct

methanol fuel cells: The effect of electrode fabrication procedure on MEAs

structural properties and cell performance, Journal of Power Sources 2005;

145(2): 495-501

[15]   Benson EE, Kubiak CP, Sathrum AJ, Smieja JM, Electrocatalytic and

homogeneous approaches to conversion of CO_2 to liquid fuels, Chemical Society

Reviews 2009; 38(89-99

[16]   Gattrell M, Gupta N, Co A, Electrochemical reduction of CO_2 to hydrocarbons to

store renewable electrical energy and upgrade biogas, Energy Conversion and

Management 2007; 48(4): 1255-65

[17]   Bandi A, Specht M, Weimer T, Schaber K, Electrochemical Reduction of Carbon

dioxide, Energy Conversion and Management 1995; 36(6): 899-907

[18]   K. W. Frese, Jr., Leach S, Electrochemical Reduction of Carbon Dioxide to

Methane, Methanol, and CO on Ru Electrodes, Journal of The Electrochemical

Society 1985; 132(1): 259-60

[19]   Seshan K, Lercher JA, Carbon Dioxide Chemistry: Environmental Issues, The

Royal Society of Chemistry 1994; 12(12-29

[20]   Jitaru M, Electrochemical carbon dioxide reduction- fundamental and applied

topics (Reviews), Journal of the University of Chemical Technology and

Metallurgy 2007; 42(4): 333-44

[21]   Li H (2006) Development of a continuous reactor for the electrochemical

reduction of carbon dioxide. Chemical & Biological engineering, p. 156: University of british coloumbia.

[22] Fujiwara M, Kieffer R, Ando H, Xu Q, Souma Y, Change of catalytic properties of FeZnO/zeolite composite catalyst in the hydrogenation of carbon dioxide, Applied Catalysis A: General 1997; 154(1-2): 87-101

[23] Fan M-S, Abdullah AZ, Bhatia S, Hydrogen production from carbon dioxide reforming of methane over Niā€"Co/MgOā€"ZrO2 catalyst: Process optimization, International Journal of Hydrogen Energy 2011; 36(8): 4875-86

[24] Wu JCS, Lin H-M, Lai C-L, Photo reduction of CO2 to methanol using optical-fiber photoreactor, Applied Catalysis A: General 2005; 296(2): 194-200

[25] Adachi K, Ohta K, Mizuno T, Photocatalytic reduction of carbon dioxide to hydrocarbon using copper-loaded titanium dioxide, Solar Energy 1994; 53(2): 187-90

[26] Kaneco S, Katsumata H, Suzuki T, Ohta K, Photoelectrocatalytic reduction of CO2 in LiOH/methanol at metal-modified p-InP electrodes, Applied Catalysis B: Environmental 2006; 64(1-2): 139-45

[27] Cook RL, Robert CM, Anthony FS, Photoelectrochemical Carbon Dioxide Reduction to Hydrocarbons at Ambient Temperature and Pressure, Journal of The Electrochemical Society 1988; 135(12): 3069-70

[28] Lin CC, Liu SK, Chen YS, Li HF, Jing Chie L, Lee SL, et al., Photo-Electrochemical Reduction of Carbon Dioxide on the Self-organized TiO[sub 2] Nanotube Layers, ECS Transactions 2010; 25(24): 123-34

[29] Kaneco S, Ueno Y, Katsumata H, Suzuki T, Ohta K, Photoelectrochemical reduction of CO2 at p-InP electrode in copper particle-suspended methanol,

Chemical Engineering Journal 2009; 148(1): 57-62

[30]   Aurian-Blajeni B, Halmann M, Manassen J, Photoreduction of carbon dioxide and

water into formaldehyde and methanol on semiconductor materials, Solar Energy

1980; 25(2): 165-70

[31]   Tseng IH, Chang W-C, Wu JCS, Photoreduction of CO_2 using sol-gel derived

titania and titania-supported copper catalysts, Applied Catalysis B: Environmental

2002; 37(1): 37-48

[32] Hori Y (2008) Electrochemical CO_2 Reduction on Metal Electrodes. In: CG

Vayenas, RE White, ME Gamboa-Aldeco (eds). Modern Aspects of

Electrochemistry. New York: Springer.

[33]   Tryk DA, Yamamoto V, Kokubun M, Hirota K, Hashimoto K, Okawa M, et al.,

Recent developments in electrochemical and photoelectrochemical CO2

reduction:involvement of the $(CO2)_2^-$ dimer radical anion, Journal of

Organometallic Chemistry 2001; 15(113-20

[34]   Centi G, Perathoner S, Wine G, Gangeri M, Electrocatalytic conversion of CO2 to

long carbon-chain hydrocarbons, Green Chemistry 2007; 9(6): 671-8

[35]   Chang T-Y, Liang R-M, Wu P-W, Chen J-Y, Hsieh Y-C, Electrochemical

reduction of CO2 by Cu2O-catalyzed carbon clothes, Materials Letters 2009;

63(12): 1001-3

[36]   Jitaru M, Lowly DA, Toma T, Toma BC, Oniciu L, Electrochemical reduction of

carbon dioxide on flat metallic cathodes, Journal of Applied Electrochemistry

1997; 27(45): 875-89

[37]   Hori Y, Konishi H, Futamura T, Murata A, Koga O, Sakurai H, et al.,

Deactivation of copper electrode in electrochemical reduction of CO2,

Electrochimica Acta 2005; 50(27): 5354-69

[38]   Hori Y, K.Ketshuei, A.Murata, S.Suzuki, Production of methane and ethylene in Electrochemical reduction of carbon dioxide in the aqueous hydrogen carbonate solution, Chemistry Letters 1986: 897-8

[39]   Hara K, Kudo A, Sakata T, Electrochemical reduction of carbon dioxide under high pressure on various electrodes in an aqueous electrolyte, Journal of Electroanalytical Chemistry 1995; 391(1-2): 141-7

[40]   Gattrell M, Gupta N, Co A, A review of the aqueous electrochemical reduction of CO2 to hydrocarbons at copper, Journal of Electroanalytical Chemistry 2006; 594(1): 1-19

[41]   Fu LJ, Gao J, Zhang T, Cao Q, Yang LC, Wu YP, et al., Effect of Cu2O coating on graphite as anode material of lithium ion battery in PC-based electrolyte, Journal of Power Sources 2007; 171(2): 904-7

[42]   Frese KW, Electrochemical reduction of CO2 at intentionally oxidezed copper electrodes, Journal of Ectrochemical Society 1991; 138(11): 3338-44

[43]   Frese Karl W, Summers David P (1988) Electrochemical Reduction of Aqueous Carbon Dioxide at Electroplated Ru Electrodes. Catalytic Activation of Carbon Dioxide, pp. 155-70. Washington, DC: American Chemical Society.

[44]   DuBois DL, "Electrochemical Reactions of Carbon Dioxide":Wiley-VCH Verlag GmbH & Co. KGaA.(2007)

[45]   Cook RL, MacDuff RC, Sammells AF, Gas-Phase CO_2 Reduction to Hydrocarbons at Metal/Solid Polymer Electrolyte Interface, Journal of Ectrochemical Society 1990; 137(1): 187-9

[46]   Cook RL, MacDuff RC, Sammells AF, Electrochemcial Reduction of carbon

dioxide to methane at high current densities, Journal of Ectrochemical Society 1987; 134(1873-4

[47]   Brisard GM, Camargo APM, Nart FC, Iwasita T, On-line mass spectrometry investigation of the reduction of carbon dioxide in acidic media on polycrystalline Pt, Electrochemistry Communications 2001; 3(11): 603-7

[48]   Whipple DT, Kenis PJA, Prospects of CO2 Utilization via Direct Heterogeneous Electrochemical Reduction, The Journal of Physical Chemistry Letters 2010: 3451-8

[49]   Hernandez RM, Marquez J, Marquez OP, Choy M, Ovalles C, Garcia JJ, et al., Reduction of Carbon Dioxide on Modified Glassy Carbon Electrodes, Journal of The Electrochemical Society 1999; 146(11): 4131-6

[50]   Hori Y, A.Murata, R.Takahashi, Formation of Hydrocarbons in the Electrochemical Reduction of Carbon Dioxide at a Copper Electrode in Aqueous Solution, Journal of the Chemical Society, Faraday Transactions 1: Physical Chemistry in Condensed Phases 1989; 85(8): 2309-26

[51]   Flannery BP, Carbon Management: Implications for R&D in the Chemical Sciences and Technology, A Workshop Report to the Chemical Sciences Roundtable 2000: 44-59

[52]   Bandi A, Kühne HM, Electrochemical Reduction of Carbon Dioxide in Water: Analysis of Reaction Mechanism on Ruthenium-Titanium-Oxide Journal of Ectrochemical Society 1992; 139(6): 1605-10

[53]   Yamamoto T, Tryk DA, Hashimoto K, Fujishima A, Okawa M, Electrochemical Reduction of CO2 in the Micropores of Activated Carbon Fibers, Journal of The Electrochemical Society 2000; 147(9): 3393-4000

[54] Chaplin RPS, Wragg AA, Effects of process conditions and electrode material on reaction pathways for carbon dioxide electroreduction with particular reference to formate formation, Journal of Applied Electrochemistry 2003; 33(52): 1107-23

[55] B.P.Suvillan, Krist K, Guard HE (eds.) (1993) Electrochemical and Electrocatalytic Reactions of Carbo Dioxide. Amsterdam: Elseevier.

[56] Friebe P, Bogdanoff P, Alonso-Vante N, Tributsch H, A Real-Time Mass Spectroscopy Study of the (Electro)chemical Factors Affecting CO_2 Reduction at Copper, Journal of Catalysis 1997; 168(2): 374-85

[57] Azuma M, Hashimoto K, Hiramoto M, Watanabe M, Sakata T, Electrochemical Reduction of Carbon Dioxide on Various Metal Electrodes in Low-Temperature Aqueous KHCO3 Media Journal of Ectrochemical Society 1990; 137(6): 1772-8

[58] Aydin R, Kleli F, Electrocatalytic conversion of CO2 on a polypyrrole electrode under high pressure in methanol, Synthetic Metals 2004; 144(1): 75-80

[59] Aresta M, Dibenedetto A, Utilisation of CO2 as a chemical feedstock: opportunities and challenges, Dalton Transactions 2007; 28): 2975-92

[60] Dubé P, Brisard GM, Influence of adsorption processes on the CO2 electroreduction: An electrochemical mass spectrometry study, Journal of Electroanalytical Chemistry 2005; 582(1-2): 230-40

[61] Ito K, Ikeda S, Electrochemical reduction of CO2 on Indium electrodes, Bulletin of Chemical Society of Japan 1987; 60(2517-21

[62] Frese JKW, Leach S, Electrochemical Reduction of Carbon Dioxide to Methane, Methanol, and CO on Ru Electrodes, Journal of The Electrochemical Society 1985; 132(1): 259-60

[63] Gupta N, Gattrell M, MacDougall B, Calculation for the cathode surface

concentrations in the electrochemical reduction of CO2 in KHCO3 solutions
Journal of Applied Electrochemistry 2006; 36(2): 161-72

[64]   Oloman C, Li H, Electrochemical Processing of Carbon Dioxide, ChemSusChem
        2008; 1(5): 385-91

[65]   Ohta K, Hasimoto A, Mizuno T, Electrochemical reduction of carbon dioxide by
        the use of copper tube electrode, Energy Conversion and Management 1995;
        36(6-9): 625-8

[66]   Mizuno T, Naitoh A, Ohta K, Electrochemical reduction of CO_2 in methanol at -
        30°C, Journal of Electroanalytical Chemistry 1995; 391(1-2): 199-201

[67]   Mizuno T, Kawamoto M, Kaneco S, Ohta K, Electrochemical reduction of carbon
        dioxide at Ti and hydrogen-storing Ti electrodes in KOH-methanol,
        Electrochimica Acta 1998; 43(8): 899-907

[68]   Delacourt C, Ridgway LP, John BK, Newman J, Design of an Electrochemical
        Cell Making Syngas ($CO + H_2$) from CO_2 and H_2O Reduction at Room
        Temperature, Journal of The Electrochemical Society 2008; 155(1): B42-B9

[69]   Mahmood MN, Masheder D, Harty CJ, Use of gas-diffusion electrodes for high-
        rate electrochemical reduction of carbon dioxide. I. Reduction at lead, indium-
        and tin-impregnated electrodes Journal of Applied Electrochemistry 1987; 17(6):
        1159-70

[70]   Kyriacou G, Anagnostopoulos A, Electrochemical reduction of CO2 at Cu + Au
        electrodes, Journal of Electroanalytical Chemistry 1992; 328(1-2): 233-43

[71]   Yano H, Shirai F, Nakayama M, Ogura K, Electrochemical reduction of CO2 at
        three-phase (gas | liquid | solid) and two-phase (liquid | solid) interfaces on Ag
        electrodes, Journal of Electroanalytical Chemistry 2002; 533(1-2): 113-8

[72]   Akhori Y, Iwanaga N, Kato Y, Kamamoto O, Electrochemical reduction of carbon dioxide, Electrochemistry Communications 2004; 72(4): 266-72

[73]   Li H, Oloman C, The electro-reduction of carbon dioxide in a continuous reactor, Journal of Applied Electrochemistry 2005; 35(955-65

[74]   Weimer T, Schaber K, Specht M, Bandi A, Methanol from atmospheric carbon dioxide: A liquid zero emission fuel for the future, Energy Conversion and Management 1996; 37(6-8): 1351-6

[75]   Watanabe M, Shibata M, Kato A, Azuma M, Sakata T, Design of alloy electrocatalysts for CO2 reduction, Journal of Ectrochemical Society 1991; 138(11): 3382-9

[76]   Tomita Y, Teruya S, Koga O, Hori Y, Electrochemical Reduction of Carbon Dioxide at a Platinum Electrode in Acetonitrile-Water Mixtures, Journal of The Electrochemical Society 2000; 147(11): 4164-7

[77]   Terunuma Y, Saitoh A, Momose Y, Relationship between hydrocarbon production in the electrochemical reduction of CO2 and the characteristics of the Cu electrode, Journal of Electroanalytical Chemistry 1997; 434(1-2): 69-75

[78]   Spataru N, Tokuhiro K, Terashima C, Rao TN, Electrochemical reduction of carbon dioxide at ruthenium dioxide deposited on boron-doped diamond, Journal of applied electrochemistry 2003; 33(1205-10

[79]   Seshadri G, Lin C, Bocarsly AB, A new homogeneous electrocatalyst for the reduction of carbon dioxide to methanol at low overpotential, Journal of Electroanalytical Chemistry 1994; 372(1-2): 145-50

[80]   Schrebler R, Cury P, Herrera F, Gomez H, Cordova R, Study of the electrochemical reduction of CO2 on electrodeposited rhenium electrodes

inmethanol media, Journal of Electroanalytical Chemistry 2001; 516(1): 23-30

[81]   Sánchez-Sánchez CM, Montiel V, Tryk DA, Aldaz A, Fujishima A, Electrochemical approaches to alleviation of the problem of carbon dioxide accumulation, Pure and Apllied Chemistry 2001; 73(12): 1917–27

[82]   A.Coehn, S.Jahn, Electrolytic Reduction of carbon dioxide, Berichte der Deutschen Chemischen Gesellschaft 1904; 37(

[83]   F.Fischer, O.Prziza, Electrolytic Reduction of Carbon Oxides Dissolved Under Pressure., Berichte der Deutschen Chemischen Gesellschaft 1914; 47(

[84]   Paik W, Andersen TN, Eyring H, Kinetic studies of the electrolytic reduction of carbon dioxide on the mercury electrode, Electrochimica Acta 1969; 14(12): 1217-32

[85]   Udupa KS, Subramanian GS, Udupa HVK, The electrolytic reduction of carbon dioxide to formic acid, Electrochimica Acta 1971; 16(9): 1593-8

[86]   Russell PG, Kovac N, Srinivasan S, Steinberg M, The Electrochemical Reduction of Carbon Dioxide, Formic Acid, and Formaldehyde, Journal of The Electrochemical Society 1977; 124(9): 1329-38

[87]   Hori Y, K.Ketshuei, A.Murata, S.Suzuki, Electrochemical reduction of carbon monoxide to hydrocarbons at various metal elctrodes inaqoues solution, Chemistry Letters 1985: 1695-8

[88]   Canfield D, K. W. Frese, Jr., Reduction of Carbon Dioxide to Methanol on n- and p-GaAs and p-InP. Effect of Crystal Face, Electrolyte and Current Density, Journal of The Electrochemical Society 1983; 130(8): 1772-3

[89]   Summers DP, Leach S, Frese Jr KW, The electrochemical reduction of aqueous carbon dioxide to methanol at molybdenum electrodes with low overpotentials,

Journal of Electroanalytical Chemistry and Interfacial Electrochemistry 1986; 205(1-2): 219-32

[90]   Bandi A, Kuhne HM, Electrochemical Reduction of Carbon Dioxide in Water: Analysis of Reaction Mechanism on Ruthenium-Titanium-Oxide, Journal of The Electrochemical Society 1992; 139(6): 1605-10

[91]   K. W. Frese, Jr., Canfield D, Reduction of CO[sub 2] on n-GaAs Electrodes and Selective Methanol Synthesis, Journal of The Electrochemical Society 1984; 131(11): 2518-22

[92]   Kaneco S, Iiba K, Hiei N-h, Ohta K, Mizuno T, Suzuki T, Electrochemical Reduction of Carbon Dioxide to Hydrocarbons with High Faradaic Efficiency in LiOH/Methanol, Journal of Physical Chemsitry 1999; 103(7456-60

[93]   Kaneco S, Iiba K, Katsumata H, Suzuki T, Ohta K, Effect of sodium cation on the electrochemical reduction of CO2 at a copper electrode in methanol, Journal of solid state electrochemistry 2007; 11(4): 490-5

[94]   Kaneco S, Iiba K, Ohta K, Mizuno T, Electrochemical reduction of carbon dioxide on copper in methanol with various potassium supporting electrolytes at low temperature, Journal of solid state electrochemistry 1999; 3(7): 424-8

[95]   Kaneco S, Iiba K, Ohta K, Mizuno T, Reduction of carbon dioxide to petrochemical intermediates, Energy Sources 2000; 22(127-35

[96]   Kaneco S, Iiba K, Ohta K, Mizuno T, Saji A, Electrochemical reduction of CO2 at an Ag electrode in KOH-methanol at low temperature, Electrochimica Acta 1998; 44(4): 573-8

[97]   Kaneco S, Iiba K, Ohta K, Mizuno T, Saji A, Electrochemical reduction of CO2

on Au in KOH + methanol at low temperature, Journal of Electroanalytical Chemistry 1998; 441(1-2): 215-20

[98]   Kaneco S, Iiba K, Yabuuchi M, Nishio N, Ohnishi H, Katsumata H, et al., High Efficiency Electrochemical CO2-to-Methane Conversion Method Using Methanol with Lithium Supporting Electrolytes, Industrial & Engineering Chemistry Research 2002; 41(21): 5165-70

[99]   Kaneco S, Iwao R, Iiba K, Ohta K, Mizuno T, Electrochemical conversion of carbon dioxide to formic acid on Pb in KOH/methanol electrolyte at ambient temperature and pressure, Energy 1998; 23(12): 1107-12

[100] Kaneco S, Katsumata H, Suzuki T, Ohta K, Electrochemical Reduction of CO2 to Methane at the Cu Electrode in Methanol with Sodium Supporting Salts and Its Comparison with Other Alkaline Salts, Energy & Fuels 2005; 20(1): 409-14

[101] Kaneco S, Katsumata H, Suzuki T, Ohta K, Electrochemical reduction of carbon dioxide to ethylene at a copper electrode in methanol using potassium hydroxide and rubidium hydroxide supporting electrolytes, Electrochimica Acta 2006; 51(16): 3316-21

[102] Kaneco S, Ueno Y, Katsumata H, Suzuki T, Ohta K, Electrochemical reduction of CO2 in copper particle-suspended methanol, Chemical Engineering Journal 2006; 119(2-3): 107-12

[103] Ohya S, Kaneco S, Katsumata H, Suzuki T, Ohta K, Electrochemical reduction of CO2 in methanol with aid of CuO and Cu2O, Catalysis Today 2009; 148(3-4): 329-34

[104] Bidrawn F, Kim G, Corre G, Irvine JTS, Vohs JM, Gorte RJ, Efficient Reduction of CO[sub 2] in a Solid Oxide Electrolyzer, Electrochemical and Solid-State

Letters 2008; 11(9): B167-B70

[105]   Hara K, Kudo A, Sakata T, Watanabe M, High Efficiency Electrochemical

Reduction of Carbon Dioxide under High Pressure on a Gas Diffusion Electrode

Containing Pt Catalysts, Journal of The Electrochemical Society 1995; 142(4):

L57-L9

[106]   Gonēalves MCMR, Condeēo JAD, Pardal TCD, Roncero DM, Santos DMF,

Sequeirac CAC, Electrochemical Reduction of Carbon Dioxide for Fuel Cell

Utilisation, ECS Transactions 2007; 3(18): 49-56

[107]   Gonēalves MR, Gomes A, Condeēo J, Fernandes R, Pardal T, Sequeira CAC, et

al., Selective electrochemical conversion of CO2 to C2 hydrocarbons, Energy

Conversion and Management 2010; 51(1): 30-2

[108]   Lee J, Tak Y, Electrocatalytic activity of Cu electrode in electroreduction of CO2,

Electrochimica Acta 2001; 46(19): 3015-22

[109]   Komatsu S, Tanaka M, Okumura A, Kungi A, Preparation of cu-solid polymer

electrolyte composite electrodes and application to gas-phase electrochemical

reduction of CO2, Electrochimica Acta 1995; 40(6): 745-53

[110]   Qu J, Zhang X, Wang Y, Xie C, Electrochemical reduction of CO2 on

RuO2/TiO2 nanotubes composite modified Pt electrode, Electrochimica Acta

2005; 50(16-17): 3576-80

[111]   Mitrovski S, Nakano A, "Synthesis and Characterization of Tin-Modified Gold

Catalysts for the Electrochemical Carbon-Dioxide Reduction ":American

Chemical Society.(2009)

[112]   Yamamoto T, Tryk DA, Fujishima A, Ohata H, Production of syngas plus oxygen

from CO2 in a gas-diffusion electrode-based electrolytic cell, Electrochimica Acta

2002; 47(20): 3327-34

[113]   Whipple DT, Finke EC, Kenis PJA, Microfluidic Reactor for the Electrochemical
         Reduction of Carbon Dioxide: The Effect of pH, Electrochemical and Solid-State
         Letters 2010; 13(9): B109-B11

[114]   Gangeri M, Perathoner S, Caudo S, Centi G, Amadou J, Bégin D, et al., Fe and Pt
         carbon nanotubes for the electrocatalytic conversion of carbon dioxide to
         oxygenates, Catalysis Today 2009; 143(1-2): 57-63

[115]   Subramanian K, Asokan K, Jeevarathnam D, Chandrashekaran M,
         Electrochemical membrane reactor for the reduction of carbon dioxide to formate,
         Journal of Applied Electrochemistry 2006; 37(255-60

[116]   Narayanan SR, Haines B, Soler J, Valdez TI, Electrochemical Conversion of
         Carbon Dioxide to Formate in Alkaline Polymer Electrolyte Membrane Cells,
         Journal of The Electrochemical Society 2011; 158(2): A167-A73

[117]   Rodrĳ-guez-Reinoso F, The role of carbon materials in heterogeneous catalysis,
         Carbon 1998; 36(3): 159-75

[118]   R. Schlögl i, "Preparation of Solid Catalysts":Wiley-VCH.(1999)

[119]   Iijima S, Helical microtubules of graphitic carbon, Nature 1991; 354(6348): 56-8

[120]   Coq B, Planeix JM, Brotons V, Fullerene-based materials as new support media
         in heterogeneous catalysis by metals, Applied Catalysis A: General 1998; 173(2):
         175-83

[121]   De Jong KP, Synthesis of supported catalysts, Current Opinion in Solid State and
         Materials Science 1999; 4(1): 55-62

[122]   Shao Y, Liu J, Wang Y, Lin Y, Novel catalyst support materials for PEM fuel
         cells: current status and future prospects, Journal of Materials Chemistry 2009;

19(1): 46-59

[123]   Moy D, Hoch R (2002) to Hyperion Catalysis. In: E Patent (ed).

[124]   Fischer JE, Johnson AT, Electronic properties of carbon nanotubes, Current Opinion in Solid State and Materials Science 1999; 4(1): 28-33

[125]   J.-P. Issi, J.-C. Charlier, "The Science and Technology of CarbonNanotubes":Elsevier.(1999)

[126]   Charlier JC, Defects in carbon nanotubes, Accounts of Chemical Research 2002; 35(12): 1063-9

[127]   Menon M, Andriotis AN, Froudakis GE, Curvature dependence of the metal catalyst atom interaction with carbon nanotubes walls, Chemical Physics Letters 2000; 320(5-6): 425-34

[128]   P.J..F.Harris, "Carbon Nanotubes and Related Structures":Cambridge University Pres.(2003)

[129]   Serp P, Corrias M, Kalck P, Carbon nanotubes and nanofibers in catalysis, Applied Catalysis A: General 2003; 253(2): 337-58

[130]   Ma Y, Lin Y, Xiao X, Zhou X, Li X, Sonicationā€"hydrothermal combination technique for the synthesis of titanate nanotubes from commercially available precursors, Materials Research Bulletin 2006; 41(2): 237-43

[131]   Yuan Z-Y, Su B-L, Titanium oxide nanotubes, nanofibers and nanowires, Colloids and Surfaces A: Physicochemical and Engineering Aspects 2004; 241(1-3): 173-83

[132]   Garcia T, Solsona B, Taylor SH, The oxidative destruction of hydrocarbon volatile organic compounds using palladium-vanadia-titania catalysts, Catalysis Letters 2004; 97(1-2): 99-103

[133] Zhu H, Qin Z, Shan W, Shen W, Wang J, Pd/CeO2-TiO2 catalyst for CO oxidation at low temperature: A TPR study with H2 and CO as reducing agents, Journal of Catalysis 2004; 225(2): 267-77

[134] Ivanovskaya VV, Enyashin AN, Ivanovskii AL, Electronic structure of single-walled TiO2 and VO2 nanotubes, Mendeleev Communications 2003; 13(1): 5-7

[135] Roderick EF, Brenda LG, John WW, Effect of Titanium Dioxide Supports on the Activity of Pt-Ru toward Electrochemical Oxidation of Methanol, Journal of The Electrochemical Society 2011; 158(5): B461-B6

[136] Huang S-Y, Ganesan P, Popov BN, Electrocatalytic activity and stability of niobium-doped titanium oxide supported platinum catalyst for polymer electrolyte membrane fuel cells, Applied Catalysis B: Environmental 2010; 96(1-2): 224-31

[137] Billik P, Plesch G, Mechanochemical synthesis of nanocrystalline TiO2 from liquid TiCl4, Scripta Materialia 2007; 56(11): 979-82

[138] Hoyer P, Formation of a Titanium Dioxide Nanotube Array, Langmuir 1996; 12(6): 1411-3

[139] Imai H, Takei Y, Shimizu K, Matsuda M, Hirashima H, Direct preparation of anatase TiO2 nanotubes in porous alumina membranes, Journal of Materials Chemistry 1999; 9(12): 2971-2

[140] Kasuga T, Hiramatsu M, Hoson A, Sekino T, Niihara K, Formation of Titanium Oxide Nanotube, Langmuir 1998; 14(12): 3160-3

[141] Kasuga T, Hiramatsu M, Hoson A, Sekino T, Niihara K, Titania Nanotubes Prepared by Chemical Processing, Advanced Materials 1999; 11(15): 1307-11

[142] Hori Y, Takahashi I, Koga O, Hoshi N, Electrochemical reduction of carbon dioxide at various series of copper single crystal electrodes, Journal of Molecular

Catalysis A: Chemical 2003; 199(1-2): 39-47

[143] Mahmood MN, Masheder D, Harty CJ, Use of gas-diffusion electrodes for high-rate electrochemical reduction of carbon dioxide. I. Reduction at lead, indium- and tin-impregnated electrodes, Journal of applied electrochemistry 1987; 17(6): 1159-70

[144] Mahmood MN, Masheder D, Harty CJ, Use of gas-diffusion electrodes for high-rate electrochemical reduction of carbon dioxide. II. Reduction at metal phthalocyanine-impregnated electrodes, Journal of applied electrochemistry 1987; 17(6): 1223-7

[145] Cook RL, MacDuff RC, Sammells AF, Efficient High Rate Carbon Dioxide Reduction to Methane and Ethylene at in situ Electrodeposited Copper Electrode, Journal of Electrochemical Society 1987:

[146] Furuya N, Yamazaki T, Shibata M, High performance Ru---Pd catalysts for CO2 reduction at gas-diffusion electrodes, Journal of Electroanalytical Chemistry 1997; 431(1): 39-41

[147] Cook R, L., Robert CM, Anthony FS, High Rate Gas Phase CO[sub 2] Reduction to Ethylene and Methane Using Gas Diffusion Electrodes, Journal of The Electrochemical Society 1990; 137(2): 607-8

[148] Michael S, Ronald LC, Victoria MK, Robert CM, Jay P, Anthony FS, Carbon Dioxide Reduction to Alcohols using Perovskite-Type Electrocatalysts, Journal of The Electrochemical Society 1993; 140(3): 614-8

[149] Saeki T, Hashimoto K, Fujishima A, Kimura N, Omata K, Electrochemical Reduction of CO2 with High Current Density in a CO2-Methanol Medium, Journal of Physical Chemsitry 1999; 99(20): 8440-226

[150] Dewulf DW, Bard AJ, The electrochemical reduction of CO2 to CH4 and C2H4 at Cu/Nafion electrodes (solid polymer electrolyte structures), Catalyst Letters 1988; 1(1-3): 73-9

[151] Cook RL, MacDuff RC, Sammells AF, On the Electrochemical Reduction of Carbon Dioxide at In Situ Electrodeposited Copper, Journal of Electrochemical Society 1988; 135(6): 1320-6

[152] Cook RL, MacDuff RC, Sammells AF, Ambient Temperature Gas Phase C02 Reduction to Hydrocarbons at Solid Polymer Electrolyte Cells, Journal of Applied Electrochemistry 1988; 135(6): 1470-1

[153] Maeda M, Kitaguchi Y, Ikeda S, Ito K, Reduction of carbon dioxide on partially-immersed Au plate electrode and Au-SPE electrode, Journal of Electroanalytical Chemistry 1987; 238(1-2): 247-58

[154] Saleem-ur-rahman (1995) Development of Raney-Ni gas diffusion electrodes for fuel cells. Chemical Engineering, p. 106. Dhahran: King Fahd university of petroleum & minerals.

[155] Hara K, Kudo A, Sakata T, Electrochemical CO2 reduction on a glassy carbon electrode under high pressure, Journal of Electroanalytical Chemistry 1997; 421(1-2): 1-4

[156] Koleli F, Balun D, Reduction of CO2 under high pressure and high temperature on Pb-granule electrodes in a fixed-bed reactor in aqueous medium, Applied Catalysis A: General 2004; 274(1-2): 237-42

[157] Yano J, Morita T, Shimano K, Nagami Y, Yamasaki S, Selective ethylene formation by pulse-mode electrochemical reduction of carbon dioxide using copper and copper oxide electrodes, Journal of solid state electrochemistry 2007;

11(554-7

[158] Naitoh A, Ohta K, Mizuno T, Yoshida H, Sakai M, Noda H, Electrochemical reduction of carbon dioxide in methanol at low temperature, Electrochimica Acta 1993; 38(15): 2177-9

[159] Kaneco S, Iiba K, Hiei N-h, Ohta K, Mizuno T, Suzuki T, Electrochemical reduction of carbon dioxide to ethylene with high Faradaic efficiency at a Cu electrode in CsOH/methanol, Electrochimica Acta 1999; 44(26): 4701-6

[160] Ikeda S, Takagi T, Ito K, Slective formation of formic acid,oxalic acid,and carbon monoxide by electrochemical reduction of carbon dioxide, The Chemical Society of Japan 1987; 60(2517-22

[161] Hori Y, K.Ketshuei, A.Murata, S.Suzuki, Electrochemical reduction of carbon monoxide to hydrocarbons at various metal elctrodes inaqoues solution, Chemistry Letters 1987: 1665-8

[162] Hori Y, K.Ketshuei, A.Murata, S.Suzuki, Production of methane and ethylene in Electrochemical reduction of carbon dioxide in the aqueous hydrogen carbonate solution, Chemistry Letters 1985: 897-8

[163] Ryu J, Andersen TN, Erying H, Electrode reduction kinetics of carbon dioxide in aqueous solution, Journal of Physical Chemsitry 1972; 76(22): 3278-86

[164] Chen M, Wang Z-B, Ding Y, Yin G-P, Investigation of the Ptā€"Niā€"Pb/C ternary alloy catalysts for methanol electrooxidation, Electrochemistry Communications 2008; 10(3): 443-6

[165] Xiong L, Manthiram A, High performance membrane-electrode assemblies with ultra-low Pt loading for proton exchange membrane fuel cells, Electrochimica Acta 2005; 50(16-17): 3200-4

211

[166]   Qi Z, Kaufman A, Low Pt loading high performance cathodes for PEM fuel cells, Journal of Power Sources 2003; 113(1): 37-43

[167]   Kim H, Oh J, Kim J, Chang H, Membrane electrode assembly for passive direct methanol fuel cells, Journal of Power Sources 2006; 162(1): 497-501

[168]   Li J, Matsuura A, Kakigi T, Miura T, Oshima A, Washio M, Performance of membrane electrode assemblies based on proton exchange membranes prepared by pre-irradiation induced grafting, Journal of Power Sources 2006; 161(1): 99-105

[169]   Hou P-X, Liu C, Cheng H-M, Purification of carbon nanotubes, Carbon 2008; 46(15): 2003-25

[170]   Branca C, Frusteri F, Magaz^1^ľ V, Mangione A, Characterization of Carbon Nanotubes by TEM and Infrared Spectroscopy, The Journal of Physical Chemistry B 2004; 108(11): 3469-73

[171]   Wang G, Shi C, Zhao N, Du X, Synthesis and characterization of Ag nanoparticles assembled in ordered array pores of porous anodic alumina by chemical deposition, Materials Letters 2007; 61(18): 3795-7

[172]   Bandi A, Electrochemical Reduction of Carbon Dioxide on Conductive Metallic Oxides Journal of Ectrochemical Society 1990; 137(7): 2157-60

[173]   Lee K-R, Lim J-H, Lee J-K, Chun H-S, Reduction of carbon dioxide in 3-dimensional gas diffusion electrodes, Korean Journal of Chemical Engineering 1999; 16(6): 829-36

[174]   Ogura K, Endo N, Electrochemical Reduction of CO_2 with a Functional Gas-Diffusion Electrode in Aqueous Solutions With and Without Propylene Carbonate, Journal of The Electrochemical Society 1999; 146(10): 3736-40

VITAE

Name: Safdar Hossain SK

Father's Name: SK Nooruddin

Mother's Name: Mehmooda khatoon

Place of Birth: Kolkata in INDIA

Date of Birth 10th September 1980

Religion Islam

Nationality Indian

Permanent Address Q-567, S. A. Farooqui Road, Kolkata,

West Bengal, India, PIN: 700024

Phone: 913324893719

Current Address KFUPM P.O.BOX: 853

King Fahd University of Petroleum & Minerals

Dhahran, Kingdom of Saudi Arabia, PIN: 31261

Phone: 966-3-860-4374

Email safdarnoor@gmail.com

Education

Doctor of Philosophy in Chemical Engineering (2011)

King Fahd University of Petroleum & Minerals (KFUPM)

Dhahran, Saudi Arabia

Master of Technology (M. Tech.) in Chemical Engineering (2005)

Indian Institute of Technology (IIT)

Kharagpur, India

Research Interests: Catalysis for environmental applications, electrochemical systems, fuel cells, nanocatalysts synthesis and applications